IMPACT ASSESSMENT OF URBANISATION ON THE GROUNDWATER RECHARGE OF AHMEDABAD DISTRICT USING GEOSPATIAL TECHNIQUES AND HYDROLOGICAL MODELLING

A Thesis submitted to Gujarat Technological University

for the Award of

Doctor of Philosophy

In

Civil Engineering

by

Bhavsar Chaitali Navkar

189999912033

under supervision of

Dr. Mahendrasinh S. Gadhavi

GUJARAT TECHNOLOGICAL UNIVERSITY
AHMEDABAD

August– 2026

IMPACT ASSESSMENT OF URBANISATION ON THE GROUNDWATER RECHARGE OF AHMEDABAD DISTRICT USING GEOSPATIAL TECHNIQUES AND HYDROLOGICAL MODELLING

A Thesis submitted to Gujarat Technological University

for the Award of

Doctor of Philosophy

In

Civil Engineering

by

Bhavsar Chaitali Navkar

189999912033

under supervision of

Dr. Mahendrasinh S. Gadhavi

GUJARAT TECHNOLOGICAL UNIVERSITY
AHMEDABAD

August – 2026

DECLARATION

I declare that the thesis entitled **IMPACT ASSESSMENT OF URBANISATION ON THE GROUNDWATER RECHARGE OF AHMEDABAD DISTRICT USING GEOSPATIAL TECHNIQUES AND HYDROLOGICAL MODELLING** submitted by me for the degree of Doctor of Philosophy is the record of research work carried out by me during the period from June 2019 to June 2026 under the supervision of **Dr. Mahendrasinh S. Gadhavi,** and this has not formed the basis for the award of any degree, diploma, associateship, fellowship, or title in this or any other university or other institution of higher learning.

I further declare that the material obtained from other sources has been duly acknowledged in the thesis. I shall be solely responsible for any plagiarism or other irregularities if noticed in the thesis.

Signature of the Research Scholar: ………………………………Date: 25/08/2026

Name of Research Scholar: Bhavsar Chaitali Navkar

Place: GTU Ahmedabad

CERTIFICATE

I certify that the work incorporated in the thesis **IMPACT ASSESSMENT OF URBANISATION ON THE GROUNDWATER RECHARGE OF AHMEDABAD DISTRICT USING GEOSPATIAL TECHNIQUES AND HYDROLOGICAL MODELLING** submitted by Mrs. Bhavsar Chaitali Navkar was carried out by the candidate under my supervision/guidance. To the best of my knowledge, (i) the candidate has not submitted the same research work to any other institution for any degree/diploma, associateship, fellowship, or other similar title; (ii) the thesis submitted is a record of original research work done by the research scholar during the period of study under my supervision; and (iii) the thesis represents independent research work on the part of the research scholar.

Signature of the Research Supervisor: …………………………… Date: 25|08|2026

Name of Supervisor: **Dr. Mahendrasinh S. Gadhavi**

Place: GTU Ahmedabad

Coursework Completion Certificate

This is to certify that **Mrs. Bhavsar Chaitali Navkar**, enrollment no. **189999912033**, is enrolled for the PhD program in the Civil Engineering branch of Gujarat Technological University, Ahmedabad.

(Please tick the relevant option(s).)

☐ She has been exempted from the coursework (successfully completed during the M.Phil. course).

☐ She has been exempted from the Research Methodology Course only (successfully completed during the M.Phil. Course).

☑ She has successfully completed the PhD coursework for the partial requirement for the award of the PhD degree. His/her performance in the coursework is as follows:

Grade Obtained in Research Methodology [PH 001]	Grade Obtained in Self-Study Course/Contact Program [PH 002]
BB	AB

Supervisor's Sign

(Dr. Mahendrasinh S. Gadhavi)

Originality Report Certificate

It is certified that the PhD thesis titled **IMPACT ASSESSMENT OF URBANISATION ON THE GROUNDWATER RECHARGE OF AHMEDABAD DISTRICT USING GEOSPATIAL TECHNIQUES AND HYDROLOGICAL MODELLING** by **Bhavsar Chaitali Navkar has** been examined by us. We undertake the following:

a) The thesis has significant new work/knowledge as compared to what has already been published or are under consideration to be published elsewhere. No sentence, equation, diagram, table, paragraph, or section has been copied verbatim from previous work unless it is placed under quotation marks and duly referenced.

b) The work presented is original and the author's own work (i.e., there is no plagiarism). No ideas, processes, results, or words of others have been presented as the author's own work.

c) There is no fabrication of data or results that have been compiled/analyzed.

d) There is no falsification by manipulating research materials, equipment, or processes, or changing or omitting data or results such that the research is not accurately represented in the research record.

e) The thesis has been checked using **Turnitin** (copy of originality report attached) and found within limits as per the GTU Plagiarism Policy and instructions issued from time to time (i.e., permitted similarity index <=10%).

Signature of the Research Scholar: Chaitali Date: 25/08/26

Name of the Research Scholar: Bhavsar Chaitali Navkar

Signature of the Research Supervisor: Date: 25/08/26

Name of the Research Supervisor: Dr. Mahendrasinh S. Gadhavi

Chaitali BHAVSAR

ALL CHAPTER

ALL CHAPTER

CHAITALI

Gujarat Technological University

Document Details

Submission ID

trn:oid:::1:3588666678

Submission Date

Jun 7, 2026, 6:15 PM GMT+5:30

Download Date

Jun 8, 2026, 1:06 AM GMT+5:30

File Name

ALL_CHAPTER.docx

File Size

21.9 MB

158 Pages

27,666 Words

172,863 Characters

7% Overall Similarity

The combined total of all matches, including overlapping sources, for each database.

Filtered from the Report

- Bibliography
- Quoted Text
- Cited Text
- Small Matches (less than 15 words)
- Submitted works

Match Groups

116 Not Cited or Quoted 7%
Matches with neither in-text citation nor quotation marks

0 Missing Quotations 0%
Matches that are still very similar to source material

0 Missing Citation 0%
Matches that have quotation marks, but no in-text citation

0 Cited and Quoted 0%
Matches with in-text citation present, but no quotation marks

Top Sources

6% Internet sources

2% Publications

0% Submitted works (Student Papers)

Integrity Flags

0 Integrity Flags for Review

No suspicious text manipulations found.

Our system's algorithms look deeply at a document for any inconsistencies that would set it apart from a normal submission. If we notice something strange, we flag it for you to review.

A Flag is not necessarily an indicator of a problem. However, we'd recommend you focus your attention there for further review.

Ph.D. Thesis Non-Exclusive License to GUJARAT TECHNOLOGICAL UNIVERSITY

In consideration of being a Research Scholar at Gujarat Technological University, and in the interests of the facilitation of research at the University and elsewhere, I, **Bhavsar Chaitali Navkar** (Enrollment No. **189999912033**) hereby grants a non-exclusive, royalty-free, and perpetual license to the University on the following terms:

a. The University is permitted to archive, reproduce and distribute my thesis, in whole or in part, and/or my abstract, in whole or in part (referred to collectively as the "Work") anywhere in the world, for non-commercial purposes, in all forms of media;

b. The University is permitted to authorize, sub-lease, subcontract, or procure any of the acts mentioned in paragraph (a);

c. The University is authorized to submit the Work at any national/international library, under the authority of their "Thesis Non-Exclusive License";

d. The Universal Copyright Notice (©) shall appear on all copies made under the authority of this license;

e. I undertake to submit my thesis, through my university, to any library and archives. Any abstract submitted with the thesis will be considered to form part of the thesis.

f. I represent that my thesis is my original work, does not infringe any rights of others, including privacy rights, and that I have the right to make the grant conferred by this non-exclusive license.

g. If third-party copyrighted material was included in my thesis for which, under the terms of the Copyright Act, written permission from the copyright owners is required, I have obtained such permission from the copyright owners to do the acts mentioned in paragraph (a) above for the full term of copyright protection.

h. I understand that the responsibility for the matter as mentioned in paragraph (g) rests with the authors/me solely. In no case shall GTU have any liability for any acts/ omissions / errors / copyright infringement from the publication of the said thesis or otherwise.

i. I retain copyright ownership and moral rights in my thesis and may deal with the copyright in my thesis in any way consistent with rights granted by me to my university in this non-exclusive license.

j. GTU logo shall not be used/printed in the book (in any manner whatsoever) being published or any promotional or marketing materials or any such similar documents.

k. The following statement shall be included appropriately and displayed prominently in the book or any material being published anywhere: "The content of the published work is part of the thesis submitted in partial fulfillment for the award of the degree of Ph.D. in Civil Engineering of the Gujarat Technological University."

l. I further promise to inform any person to whom I may hereafter assign or license my copyright in my thesis of the rights granted by me to my university in this nonexclusive license. I shall keep GTU indemnified from any and all claims from the publisher(s) or any third parties at all times resulting from or arising from the publishing or use or intended use of the book/such similar document or its contents.

m. I am aware of and agree to accept the conditions and regulations of the Ph.D., including all policy matters related to authorship and plagiarism.

Date: 25/08/2026

Signature of the Research Scholar

Place: Ahmedabad.

Recommendation of the Research Supervisor: **Recommended**

Signature of the Research Supervisor

Thesis Approval Form

The viva-voce of the PhD thesis submitted by **Mrs. Bhavsar Chaitali Navkar** (Enrollment No. **189999912033**) entitled **Impact Assessment of Urbanisation on the Groundwater Recharge of Ahmedabad District using Geospatial Techniques and Hydrological Modelling** was conducted on **Tuesday,25/08/2026** at Gujarat Technological University.

(Please tick any one of the following options.)

- [x] The performance of the candidate was satisfactory. We recommend that he/she be awarded the PhD degree.
- [ ] Any further modifications in research work recommended by the panel after 3 months from the date of the first viva-voce upon request of the supervisor or request of the independent research scholar, after which the viva-voce can be re-conducted by the same panel again.
- [ ] (briefly specify the modifications suggested by the panel)

The performance of the candidate was unsatisfactory. We recommend that he/she should not be awarded the PhD degree.

(The panel must give justifications for rejecting the research work)

Name and Signature of Supervisor with Seal

D. P. Patel

1) (External Examiner 1) Name and Signatu

Prof. Dhruvesh Patel

Anil Kr Mishra

2) (External Examiner 2) Name and Signatu

Prof Anil Kumar Misra
Department of Geology
Sikkim University
Gangtok

ABSTRACT

This study provides insight into urban groundwater recharge of the Ahmedabad district, which happens to be one of the most urbanised cities of India. Urbanization, a dominant global trend of the 21st century, reshapes hydrological dynamics and directly influences groundwater recharge rates. Groundwater is essential to the social and economic well-being of urban populations of the developing world. According to the Central Ground Water Board, India is the world's largest groundwater extractor, with 45–50% of urban water supply dependent on groundwater. Ahmedabad is extracting an enormous amount of available groundwater recharge. Groundwater recharge is one of the most significant hydrological processes that needs thorough analysis during urbanisation. The study was carried out with the objectives of assessing the impact of urbanisation on groundwater recharge by performing statistical analysis of existing hydro-meteorological conditions, detecting changes in land use using geospatial techniques, and hydrological modelling. This work integrates multi-temporal and geospatial analysis with the Soil and Water Assessment Tool (SWAT), which is a semi-distributed hydrological model. The required input data, including hydrometeorological data and spatial maps, have been collected from authentic sources like CWC, SWDC, IMD and satellites. The multi-temporal satellite imagery was imported in ArcGIS to prepare land use maps for each decade. After performing land-use change detection, it is found that the built-up area increased consistently across all decades, with the largest expansion of 7.2% between 2011 and 2020.

The analysis was carried out by the non-parametric Mann-Kendall (MK) test, which was used to examine historical temperature and rainfall time series for temporal trends in order to identify statistically significant changes in climatic variables over the period of 1981 to 2020. Following the hydrological modelling, the analysis part includes the SWAT model, as it is one of the most efficient models in this field. It is made to run using multiple land-use/land-cover scenarios with a Digital Elevation Model (DEM), soil-type data, and climate inputs to simulate hydrological processes. From the existing literature review, it has been observed that out of all the basins available in the study area, Vasna barrage (22.99°N, 72.55°E), located in the heart of the city, is one of the most significant hydraulic structures that contributes to the hydrology of the study area. SWAT model output, i.e., groundwater recharge specifically to the shallow aquifer, was visualized

using a tool named “SWAT output viewer,” which is widely used to represent outputs obtained from SWAT runs.

SWAT-CUP and the SUFI-2 algorithm perform the calibration and validation for 2014-2019 and 2020-2024, respectively. Observed streamflow data from the Vasna barrage were used by identifying the sensitive parameters that affect the value of groundwater recharge considerably. During the calibration and validation periods, model predictions performed well, as shown by the coefficient of determination (R^2) and Nash-Sutcliffe efficiency (NSE) values that significantly exceeded 0.70. During the calibration phase, the coefficient of determination value of 0.74 indicates a highly accurate correlation between the simulated and observed daily discharge. The Nash Sutcliffe coefficients obtained were 0.79 and 0.72 for the calibration and validation period, respectively. After the successful validation, the absolute values of sensitive parameters are incorporated in the SWAT model to replicate the watershed, and analyses suggest the marginal increase in groundwater recharge was 0.58% during 1991-2000 and 1.98% increase during 2001-2010 with the baseline period (1981-1990) due to a relatively higher amount of rainfall, and during 2011-2020 groundwater recharge declined by 5.36% relative to the baseline due to rapid urbanisation.

Future projections were carried out after calibration and validation of the SWAT model, where rainfall and temperature projections are derived from the Coupled Model Intercomparison Project Phase 6 (CMIP6) dataset that represents the latest generation of climatic projections. The CMIP6 provides climate projections from a large number of global climate models (GCMs). In this study, EC-Earth3, one of the CMIP6 models, is used for the Indian monsoon region and provides consistent daily climate variables required for hydrological modelling. Daily precipitation, maximum temperature, and minimum temperature data will be used for future periods under the SSP3-7.0. The coefficient of determination (R^2) between observed and simulated values was found to be 0.96, indicating strong agreement in the model. The model was subsequently used to generate future climate projections up to the year 2050, which shows annual average groundwater recharge decreases up to 11.79%. This trend indicates that Ahmedabad might face groundwater extraction challenges in the near future.

The study shows the significant decadal variability in groundwater recharge, where recharge exhibited an increasing trend during the first two decades but declined in the most recent decade, where urbanisation is one of the dominant driver, but climatic variability may also have played a secondary role.

The integrated GIS and SWAT modelling approach provides a solid framework to understand how urbanization impacts groundwater dynamics and aids in sustainable water resource management and planning in semi-arid regions like Ahmedabad. By analysing land-use change and its impact on groundwater recharge, the study contributes directly to achieving SDG 6 and SDG 11.

Acknowledgement and/or Dedication

I would first like to express my deepest gratitude to the Almighty for His blessings, guidance, and strength throughout this journey. His grace has been my source of perseverance during challenging times and my inspiration in moments of clarity and achievement. Without his divine support, the completion of this work would not have been possible.

I express my deepest gratitude to my supervisor, **Dr. Mahendrasinh S. Gadhavi,** whose guidance, patience, and unwavering support shaped not only this thesis but also my growth as a researcher. Her belief in my work has been invaluable. I also extend my sincere thanks to my doctoral committee members **Dr. Ghanshyam P. Vadodaria and Dr. Shital H. Shukla** for their thoughtful suggestions, encouragement, and time.

I would like to express my deepest and most sincere gratitude to my friend Dr. Mohdzuned Mohmedraffi Shaikh, without whom the completion of this Ph.D. would not have been possible. You have not only supported me, but you have truly guided me like a child being held by the finger while learning to walk patiently, gently, and with unwavering faith in every step I took. From the very beginning of this journey to its completion. I will forever remain grateful for the way you shaped my academic journey.

I would like to express my sincere gratitude to Dr. Jalpa P. Modi and Dr. Zarna J. Chovatiya for her valuable guidance, encouragement, and continuous support throughout this research.

I would like to thank Dr. Rajesh Jain, Head of the Civil Engineering Department; Prof. A.M. Malek and Dr. R.B. Khasiya, former heads of the Civil Engineering Department; Dr. M.B. Dholakiya; the late Dr. P.J. Gundaliya; Prof. N.N. Borad; Prof. S.A. Trivedi; Prof. H.M. Gandhi; Prof. V.J. Chitaria; Dr. R.N. Shukla; Prof. Rita Jadav; Dr. N.J. Dalal; Dr. N.G. Raval; Dr. S.L. Panchal; Dr. Z.R. Chhaya; Dr. Pratima Shah; Dr. S.H. Kazi; Prof. P.K. Lalwani; Dr. S.B. Jha; Prof. A.M. Mirza; Dr. U.P. Nigam; and Prof. S.S. Dixit for creating an environment filled with motivation, learning, and constant support.

I would like to acknowledge Gujarat Technological University for granting access to their resources and facilities for research work. I am also thankful to resource persons from the Ahmedabad Irrigation Department and from the SWDC for providing data.

I would like to express my sincere gratitude to Shri Hardik Patel, Proprietor, DH Geo Consultancy, Ahmedabad, for generously providing access to the ArcGIS software and for their valuable technical support throughout this research. I am truly grateful to the Principal of the L. D. College of Engineering for providing facilities and support for this research.

I would like to express my deepest and most heartfelt gratitude to my husband for his unwavering support, patience, and encouragement throughout my journey. I remain deeply grateful for his invaluable role in this achievement.

I would like to express my deepest and most sincere gratitude to my parents for their constant support and unwavering belief in me throughout my academic journey.

I would like to express my sincere gratitude to my mother-in-law for her constant support and to my late father-in-law, whose values and blessings to inspire and guide me even in his absence.

My son and daughter, despite their young age, have been a great source of strength for me. Their innocent affection and smiles always gave me courage during difficult moments of my research. This achievement is lovingly dedicated to both of them, who are the true joy of my life.

To all my family members, thank you for your blessings, unconditional love, prayers, and belief in me. Your support has been the foundation on which I built my dreams.

Finally, I am profoundly grateful to everyone who, in one way or another, stood by me throughout these long, transformative chapters of life. Each of you has contributed to this thesis in ways big and small, and I carry this achievement in your honour.

Dedicated to

My husband

Mr. Navkar Bhavsar

My Parents

Shri Girish Shah, Smt. Kalaben Shah

&

My in-laws

Late Shri Sumanbhai Bhavsar,

Smt. Manjulaben Bhavsar

Table of Contents

List of Figures

List of Tables

List of Abbreviations

SDG	Sustainable Development Goal
Avg.	Average
km	Kilometre
max	Maximum
min	Minimum
mm	Millimetre
RS	Remote Sensing
ArcGIS	Aeronautical Reconnaissance Coverage Geographic Information System
LANDSAT	Land-Use Satellite
LULC	Land Use Land Cover
SWAT	Soil and Water Assessment Tool
DEM	Digital Elevation Model
ArcSWAT	ArcGIS interface Soil and Water Assessment Tool
HRU	Hydrologic Response Unit
TMP	Temperature
CWC	Central Water Commission
IMD	India Meteorological Department
SWDC	State Water Data Centre
CMIP6	Coupled Model Intercomparison Project-6
SSP	Shared Socioeconomic Pathways
ISIMIP	Inter-Sectoral Impact Model Intercomparison Project

List of Appendices

CHAPTER 1
INTRODUCTION

1.1 General

Globally, groundwater is the most widely available source of accessible freshwater and is essential for human consumption, agricultural production, and industrial activities. Groundwater has more stability and drought resilience than surface water, characterized by lower evaporative losses and seasonal variation, thereby serving as a crucial buffer against climate variability.

However, this hidden resource is under increasing threats from unsustainable extraction, alterations in land use, and the rapid expansion of urban impermeable surfaces. The transformation of natural permeable areas such as agricultural fields, grasslands, and open green spaces into concrete-dominated urban landscapes modifies the hydrological cycle by reducing infiltration, increasing surface runoff, and reducing the natural replenishment of aquifers. Especially in semi-arid regions where surface water resources are limited, the degradation of the groundwater recharge system profoundly impacts water security.

1.2 Global scenario of groundwater depletion

Groundwater accounts for approximately 30% of the total global freshwater. It supplies drinking water to almost fifty percent of the global population (UNESCO, 2022). Groundwater is extensively used to meet the irrigation, industrial production, thermal power generation, mining, and urban water supply systems in addition to drinking uses.

However, rapid urbanisation, industrialisation, population growth, and climate change have increased the stress on groundwater resources worldwide significantly. Groundwater depletion (Wada et al., 2010) has been documented for many regions in Asia, North America, the Middle East, and Africa, where high groundwater extraction and declining recharge conditions have been observed. Climate change also intensifies groundwater stress by changes in precipitation patterns, prolonged periods of drought, increased rates of evapotranspiration, and reduced opportunities for natural recharge. Therefore, sustainable groundwater management has become a major global environmental challenge.

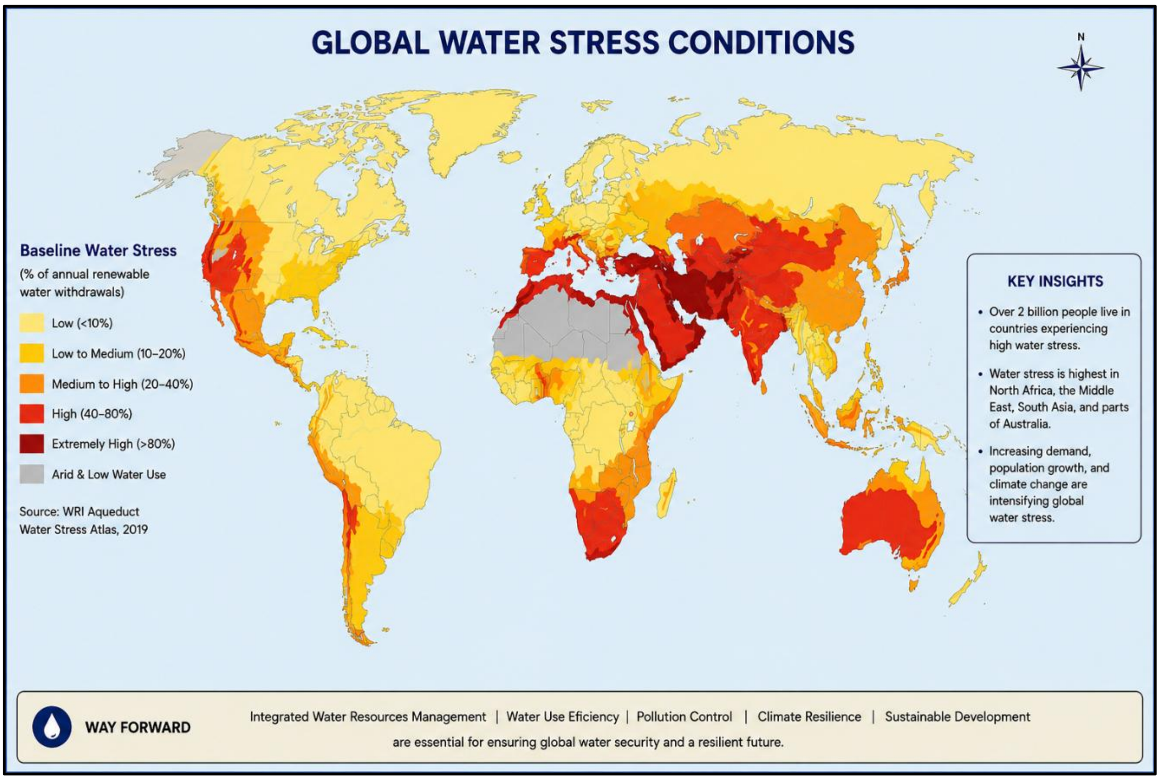

Figure 1.1 Global Distribution of Water Stress Conditions

Source: World Resources Institute (WRI) Aqueduct Water Risk Atlas (2019)

Figure 1.1 shows the worldwide distribution of water stress conditions. indicates substantial spatial variability in the availability and utilization of freshwater resources across different regions of the world. Areas such as North Africa, the Middle East, South Asia, and parts of Australia experience high-to-extremely-high levels of water stress. The observed pattern highlights the combined influence of population growth, urbanisation, agricultural expansion, industrial development, and climate variability on water resource availability. Increasing pressure on freshwater systems in highly stressed regions underscores the need for sustainable water management practices, improved water-use efficiency, and demand management to ensure long-term water security. (WRI, 2019).

1.3 The Indian groundwater crisis

India is one of the greatest groundwater-dependent countries in the world, where groundwater plays an important role for domestic water supply, agricultural irrigation, and industrial development. Approximately 85% of rural potable water supply, 50% of urban water needs, and nearly 60–65% of irrigation requirements in the country are fulfilled through groundwater resources (CGWB, 2022). The Central Ground Water Board (CGWB) has assessed the total annual groundwater extraction for all uses in India for the year 2025 at 247.22 BCM, with a Stage of Extraction (SoE) of 60.63%—meaning that more than 60% of the nation's annual replenishable groundwater is being withdrawn.

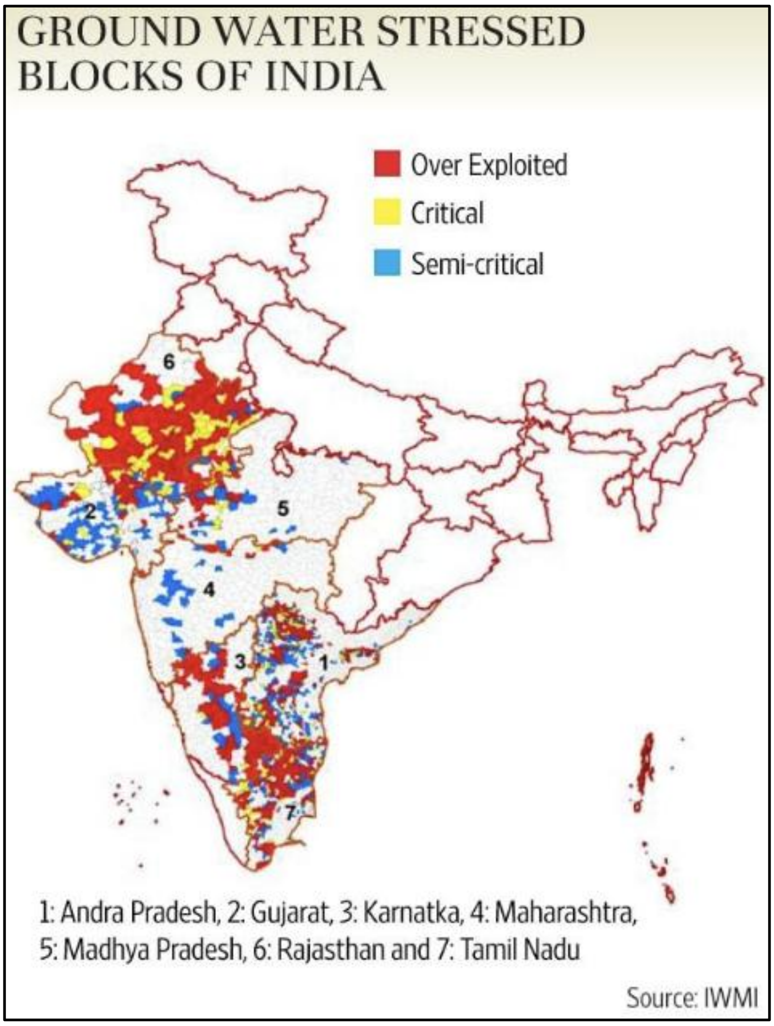

Figure 1.2 Groundwater-stressed blocks and over-exploited regions in India

Figure 1.2 illustrates the spatial distribution of groundwater-stressed blocks across India, categorised into over-exploited, critical, and semi-critical groundwater regions.

The over-exploited regions shown in red represent areas where groundwater withdrawal is substantially higher than annual replenishable groundwater resources, leading to continuous groundwater depletion and declining water table conditions. Critical regions shown in yellow indicate areas approaching unsustainable groundwater extraction levels, while semi-critical regions shown in blue represent moderately stressed groundwater zones. The figure highlights that states such as Punjab, Rajasthan, Gujarat, Karnataka, Maharashtra, Andhra Pradesh, Madhya Pradesh, and Tamil Nadu contain a large number of groundwater-stressed blocks due to intensive agricultural activities, rapid urbanization, industrial development, and increased domestic water demand.

1.4 Groundwater scenario in Ahmedabad

Ahmedabad district, situated in the central part of Gujarat, is one of the fastest-growing urban and industrial regions in western India. In recent decades, rapid urbanisation, industrial growth, and increasing freshwater demand have increased pressure on the groundwater resources of Ahmedabad District. The ongoing extraction of groundwater and alterations in land use have profoundly affected groundwater availability and natural recharge processes in the region.

Consequently, evaluating groundwater recharge conditions and utilization patterns is crucial for sustainable groundwater resource management and long-term water security in the district.

1.4.1 Groundwater scenario and recharge status

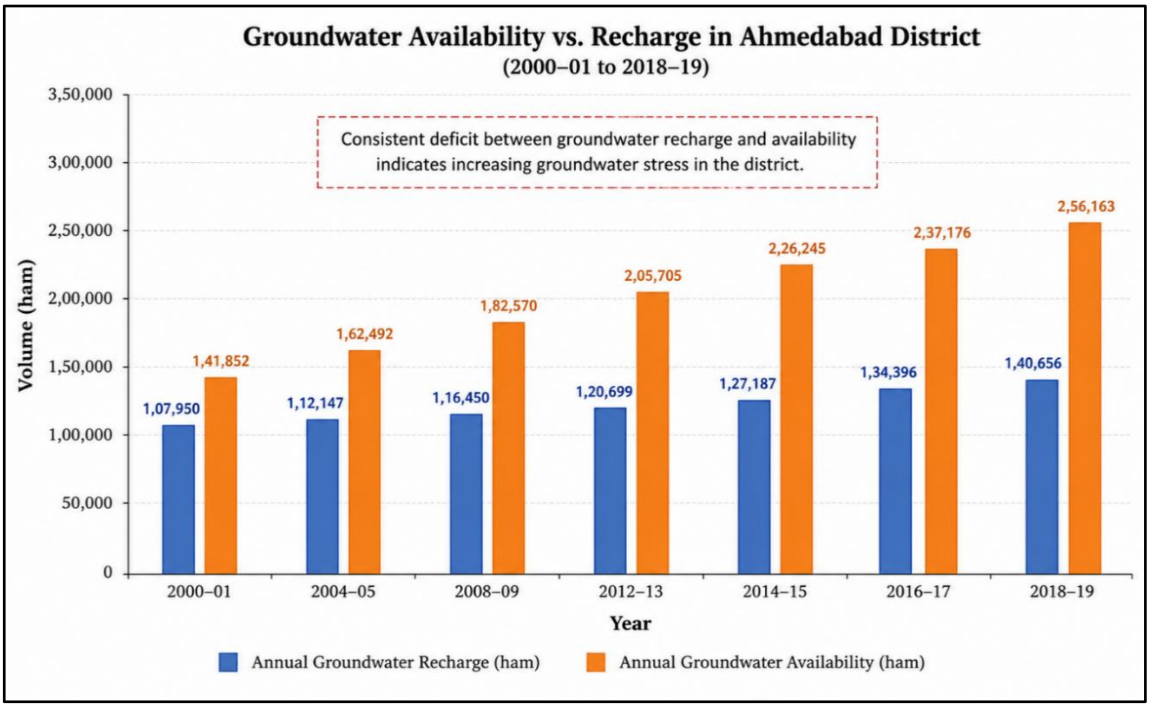

Figure 1.3 Groundwater scenario and recharge status of study area

Source: Reports of the Central Ground Water Board (CGWB), Government of India, and Gujarat State Water Resources Department (2000–2019)

Figure 1.3 shows the comparative trend of annual groundwater recharge and groundwater availability in the Ahmedabad district (2000-01 to 2018-19). The analysis indicates a consistent increase in groundwater use and freshwater demand in the study period, which is mainly attributed to rapid urbanization, industrialization, population growth, and increasing demand for agricultural water. Though there is a progressive increase in groundwater recharge, overall demand and extraction pressure on groundwater increased at a relatively higher rate.

1.4.2 The dual pressures of over-extraction and rapid urbanisation

- **Over-extraction crisis**

Groundwater extraction (19,423.60 ham) exceeds net annual recharge (13,381.73 ham) by 52%, resulting in a 152% utilization rate. The Central Ground Water Board has classified Ahmedabad as "overexploited."

• A supply-side crisis

The conversion of permeable surfaces (agricultural land, bare areas, vegetation) into impermeable, built-up areas prevents rainwater from seeping and percolating down to the water table. The effect is a reduction in the volume of recharge but also a change in the nature of the recharge mechanism.

Therefore, estimation of groundwater recharge in the Ahmedabad region is important for evaluating the impact of urbanization on groundwater replenishment, analysing the long-term hydrological changes, and enabling sustainable management of urban water resources. The scientific assessment of groundwater recharge using geospatial techniques and hydrological modelling (including the SWAT model) provides a robust base for the analysis of recharge dynamics in changing environmental scenarios and for sustainable watershed planning in the district.

1.5 Sustainable development goals (SDGs)

The UN ratified the 2030 Agenda for Sustainable Development in September 2015, with 169 targets aimed at fulfilling 17 sustainable development goals.

This research is grounded on SDG 6 (Clean Water and Sanitation) and SDG 11 (Sustainable Cities and Communities).

1.5.1 SDG 6: Clean water and sanitation

The Sustainable Development Goal 6 (SDG 6) objective is to ensure the availability and sustainable management of all water and sanitation resources by 2030. The goal highlights the importance of safe drinking water, groundwater conservation, sanitation facilities, and protection of water-related ecosystems. SDG 6 also emphasises sustainable freshwater withdrawal and efficient water resource management to reduce water stress conditions worldwide.

Table 1.1 Targets and indicators of sustainable development goal 6 (SDG 6)

Targets	Indicators	Relevance to present study
6.4: By 2030, enhance water-use efficiency and guarantee sustainable extraction and provision of freshwater resources to mitigate water scarcity.	**6.4.2:** Water stress level: freshwater extraction relative to available freshwater resources	The present study assesses groundwater recharge dynamics, groundwater stress, and sustainable groundwater resource management under urbanisation and climatic variability conditions in the Ahmedabad district.
6.6: By 2030, safeguard and rehabilitate aquatic ecosystems, encompassing aquifers, rivers, wetlands, lakes, and watersheds.	**6.6.1:** Temporal alterations in the scope of water-related ecosystems	The study evaluates the influence of urbanisation and land use/land cover (LULC) change on watershed hydrology, groundwater recharge, and aquifer sustainability using geospatial techniques and SWAT modelling.

Source: United Nations Sustainable Development Goals (UN SDGs), 2015

In 2015, the United Nations established the Sustainable Development Goals (SDGs) as a component of the 2030 Agenda for Sustainable Development to tackle global environmental, social, and economic issues. Among these goals, SDG 6 aims to ensure the availability and sustainable management of water and sanitation resources for all by 2030. Since 2015, increased groundwater extraction, rapid urbanization, climatic variability, and declining recharge conditions have intensified groundwater stresses across many parts of the world.

Achieving SDG 6 targets by 2030 requires significant improvement in groundwater conservation, recharge enhancement, integrated watershed management, and sustainable urban planning practices.

1.5.2 SDG 11: Sustainable cities and communities

Sustainable Development Goal 11 (SDG 11) seeks to ensure that urban areas and human settlements are inclusive, secure, resilient, and sustainable by the year 2030. Accelerated urbanization, demographic expansion, enlarged developed areas, and heightened strain on natural resources have collectively engendered significant environmental and water resource concerns in urban locales globally.

Table 1.2 SDG 11 Targets and indicators relevant to urbanisation and groundwater recharge assessment

Target	Indicator	Relevance to present study
11.3: By 2030, improve inclusive and sustainable urbanization and the capacity for participative, integrated, and sustainable human settlement planning and management.	**11.3.1** – Proportion of land consumption rate to population growth rate	The study evaluates urban expansion and Land Use/Land Cover (LULC) changes affecting groundwater recharge and watershed hydrology within the Ahmedabad district.
11.6: By 2030, mitigate the negative environmental effects of urban areas through sustainable resource management and environmental planning.	**11.6.1** – Reduction in environmental impacts of urban areas	The assessment of groundwater recharge decline due to urbanisation supports sustainable urban environmental management and groundwater conservation planning.

*Source**:** United Nations Sustainable Development Goals (UN SDGs), 2015*

Goal 11 highlights the necessity of sustainable urban development and environmentally resilient cities in an era of increased urbanisation and climate stress. Between 2011 and 2025, rapid urban growth and expansion of impervious surfaces have significantly altered natural hydrological systems and reduced groundwater recharge opportunities in many urban regions worldwide. The United Nations projects that by 2030, sustainable urban planning and integrated environmental management will become increasingly important for reducing urban environmental effects and ensuring sustainable water security.

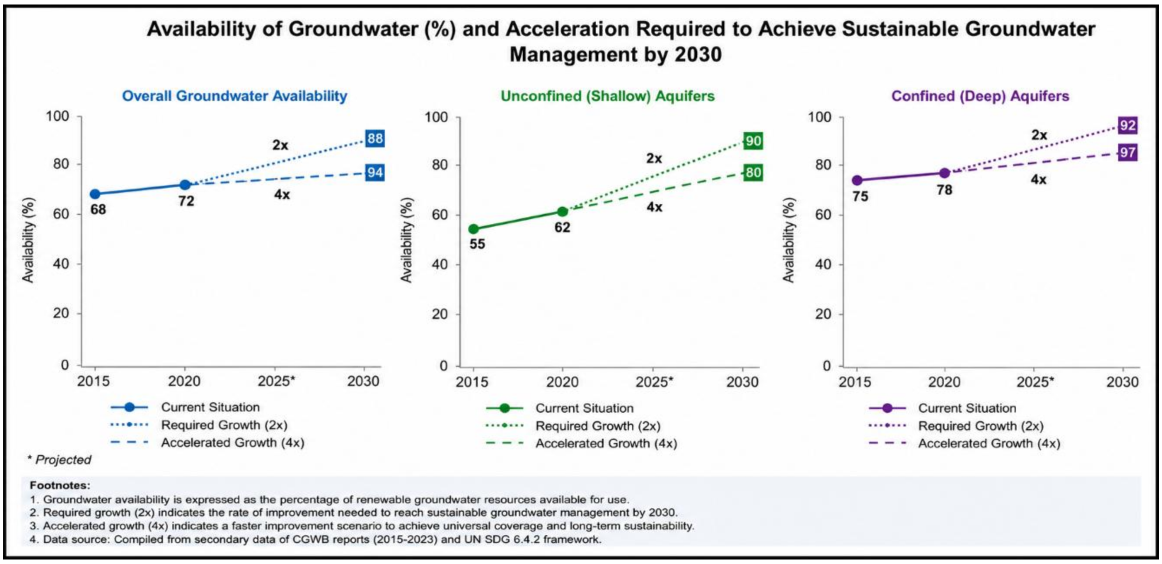

Figure 1.4 Conceptual representation of groundwater availability trends and the requirement for sustainable groundwater management toward 2030

Source: CGWB reports (2015–2023) and the SDG 6.4 framework.

Figure 1.4 illustrates the changing availability of groundwater resources and the level of improvement required to achieve sustainable groundwater management by 2030. The graph illustrates that groundwater availability is being increasingly stressed by rapid population growth, urbanisation, industrialisation and increasing demand for fresh water. It also brings out the fact that the existing status of groundwater is not sufficient for long-term sustainability unless we improve groundwater recharge and conservation significantly.

The 'Required Growth' and 'Accelerated Growth' scenarios point to the need for better practices for groundwater recharge management, watershed conservation, sustainable urban planning and scientific assessment of groundwater resources. Thus, the figure contributes directly to the present study, which aims to assess the impacts of urbanisation and climate variability on groundwater recharge.

- Groundwater availability saw a small increase from 68% in 2015 to 72% in 2020, indicating a limited improvement in groundwater resource conditions.
- The dotted projection line is an indication of the pace of improvements needed to attain sustainable groundwater management by 2030, which is twice as fast, resulting in an increase in groundwater availability to almost 88%.
- The dashed projection line represents an accelerated management scenario requiring approximately 4 times faster intervention, leading to projected groundwater availability of around 94% by 2030.
- Availability of shallow aquifer groundwater increased from 55% in 2015 to approximately 62% in 2020.
- Under the required improvement scenario (2x growth), groundwater availability may increase to around 90% by 2030.
- Under accelerated groundwater management practices (4x growth), groundwater availability is projected to reach approximately 80% by 2030.

The figure highlights that current groundwater management practices are insufficient to achieve sustainable groundwater availability targets by 2030 without a significant improvement in recharge and conservation measures.

1.6 Government initiatives

(a) Government initiatives related to SDG 6 – Clean Water and Sanitation

The Government of India has instituted many programs and policy efforts to enhance sustainable water resource management, groundwater conservation, rainwater harvesting, and aquifer recharge in alignment with SDG 6 objectives.

Major initiatives such as

Jal Shakti Abhiyan

The Jal Shakti Abhiyan is a national initiative for water conservation initiated by the Government of India to promote rainwater harvesting, groundwater recharge, and sustainable water management practices. The programme focuses on the restoration of water bodies, watershed development, and efficient utilisation of freshwater resources in water-stressed regions.

Atal Bhujal Yojana

ATAL JAL (Atal Bhujal Yojana) is a groundwater management scheme implemented to improve groundwater sustainability in water-scarce areas of India. The programme focuses on scientific groundwater monitoring, aquifer management, community-based water budgeting and improvement of groundwater recharge.

Jal Jeevan Mission

The Jal Jeevan Mission is an initiative by the Government of India designed to ensure safe and sufficient drinking water supplies to all rural families via operational tap water connections.

(b) Government initiatives related to SDG 11 – Sustainable Cities and Communities

Smart Cities Mission

The Smart Cities Mission is an initiative of the Government of India to drive economic growth and improve people's quality of life by enabling local area development and harnessing technology to create smart outcomes for citizens.

AMRUT 2.0 (Atal Mission for Rejuvenation and Urban Transformation)

AMRUT 2.0 aims to improve urban water supply, wastewater, stormwater drainage, and rejuvenation of urban water bodies. The mission supports sustainable urban infrastructure and water-wise urban development.

The present study provides a scientific basis to understand the impact of rapid urbanisation and climatic variability on the groundwater recharge dynamics in the Ahmedabad district. The study contributes to sustainable groundwater resource management and evidence-based urban planning through the integration of geospatial techniques, land use/land cover (LULC) analysis, hydroclimatic assessment and SWAT hydrological modelling.

The study contributes to the Sustainable Development Goal 6 on groundwater recharge and sustainable management of freshwater and to Goal 11 by assessing the impacts of urban expansion on hydrological systems.

1.7 Necessity of groundwater recharge estimation

Groundwater recharge estimation is a crucial element of sustainable water resource management because it provides scientific understanding regarding the quantity of water replenishing underground aquifers through natural and artificial processes. Estimation of recharge helps in evaluating the balance between groundwater extraction and aquifer replenishment, which is necessary for ensuring long-term groundwater sustainability (Healy, 2010). Accurate groundwater recharge estimation supports groundwater budgeting, watershed management, irrigation planning, drought mitigation, urban water management, and formulation of groundwater conservation strategies (Scanlon et al., 2002).

Globally, increasing population growth, rapid urbanisation, industrialisation, and agricultural expansion have significantly increased groundwater demand and extraction pressure. Simultaneously, climate variability, irregular precipitation patterns, increasing temperature, and prolonged drought conditions have altered natural hydrological processes and affected groundwater recharge dynamics (IPCC, 2021). Excessive groundwater withdrawal beyond natural recharge capacity may result in groundwater depletion, declining water table conditions, deterioration of groundwater quality, reduction in baseflow contribution, and long-term water scarcity problems (Todd and Mays, 2005).

Groundwater recharge estimation is particularly important in urban regions where increasing impervious surface coverage reduces infiltration opportunities and enhances surface runoff generation. Urbanisation significantly modifies the hydrological cycle by transforming permeable land surfaces into roadways, pavements, residential infrastructure, and industrial areas, thereby limiting groundwater replenishment potential (Shuster et al., 2005). Therefore, scientific estimation of groundwater recharge has become increasingly important under changing climatic and land use conditions.

In the context of Ahmedabad, groundwater recharge estimation is highly necessary due to rapid urban expansion, industrial development, increasing population pressure, and growing groundwater demand. Ahmedabad district falls within the semi-arid climatic region of Gujarat, where groundwater recharge largely depends on monsoon rainfall and infiltration processes. According to the Central Ground Water Board (CGWB), groundwater resources in the Ahmedabad district are experiencing increased stress due to excessive groundwater extraction and declining recharge opportunities associated with urbanisation and changing land use patterns (CGWB, 2023).

1.8 Objectives

- To perform land use change detection using geospatial techniques.
- Statistical analysis of existing hydrometeorological conditions.
- Impact assessment of urbanisation on groundwater recharge using hydrological modelling.
- To model the groundwater recharge using future projections.

1.9 Scope of the work

Following is the scope of the present study:

- Decadal land use and land cover maps are generated utilizing satellite imagery to examine spatial and temporal changes in urban expansion.
- To identify trends in hydro-meteorological variables the Mann–Kendall test is used.
- The SWAT model is utilised to simulate watershed hydrology and estimate groundwater recharge using the SWAT output viewer. Input datasets such as DEM, soil maps, weather data, and LULC are integrated within a GIS environment.
- Sensitivity analysis is conducted to determine the hydrological parameters most influential on groundwater recharge utilizing the SWAT-CUP and SUFI-2 algorithms.
- SWAT model is calibrated using observed data to adjust sensitive parameters and improve simulation accuracy. Statistical indicators such as Nash-Sutcliffe Efficiency (NSE) and R^2 are employed to evaluate model performance.

- Model is validated with an independent dataset to test its reliability.
- Spatial and temporal variations in groundwater recharge are estimated under existing land use conditions.
- Future climate projections from CMIP6 (Coupled Model Intercomparison Project Phase 6) using the EC-Earth3 under selected SSP scenarios are used.
- Future groundwater recharge is estimated under projected climate scenarios to assess the impact of urbanization on groundwater sustainability.

1.10 Methodology

Figure 1.5 presents the entire research methodology used in this work. The methodology was systematically developed to analyse hydroclimatic variations, land use changes and groundwater recharge dynamics under historical and future climatic conditions.

The first conceptual phase involved a thorough literature review, identification of the research gap, development of the research topic and establishment of research objectives related to the assessment of groundwater recharge and urbanisation impacts. Thereafter, various datasets required for hydrological modelling and geospatial analysis were collected from various government and scientific sources.

The data collection phase involved the collection of spatial data such as Digital Elevation Model (DEM), Land Use/Land Cover (LULC) data and soil data. Hydro-meteorological datasets such as rainfall and temperature data were collected for the purpose of hydro-climatic analysis and SWAT model simulation. Hydrological data such as observed streamflow records were collected for model calibration and validation. Furthermore, datasets for projecting future climate, such as CMIP6 climate data and shared socioeconomic pathways (SSPs) scenarios, were collected to simulate future groundwater recharge and to evaluate climate impacts.

The collected datasets were further subjected to data preprocessing procedures such as DEM processing, projection and clipping, LULC classification, accuracy assessment and soil and slope preparation using GIS and remote sensing techniques. The hydro-climatic trends of long-term variability of rainfall and temperature in the study area were analysed using statistical methods like the Mann-Kendall trend test and Sen’s slope estimator.

Following data preparation and trend analysis, the SWAT hydrological model was developed through watershed delineation, stream network generation, Hydrological

Response Unit (HRU) generation, weather data integration, and simulation period definition. A sensitivity analysis was conducted to determine the most significant hydrological parameters influencing streamflow modelling using t-statistics and p-value analyses.

The SWAT model underwent calibration and validation with observed and simulated streamflow data to improve model performance and reliability. Model performance was evaluated using statistical indicators such as the coefficient of determination (R^2) and Nash–Sutcliffe efficiency (NSE), along with 95PPU uncertainty analysis during validation.

After successful calibration and validation, groundwater recharge (GW_RCHG) values were extracted from the SWAT output viewer for annual and decadal groundwater recharge estimation.

Furthermore, urbanisation impact assessments were conducted via LULC change detection and a comparison of groundwater recharge variations with precipitation patterns. Finally, future projection analysis for the period 2021–2050 was performed using CMIP6 climate projection datasets integrated within the SWAT modelling framework to estimate future groundwater recharge conditions and analyse long-term hydrological trends under changing climatic and urbanisation scenarios.

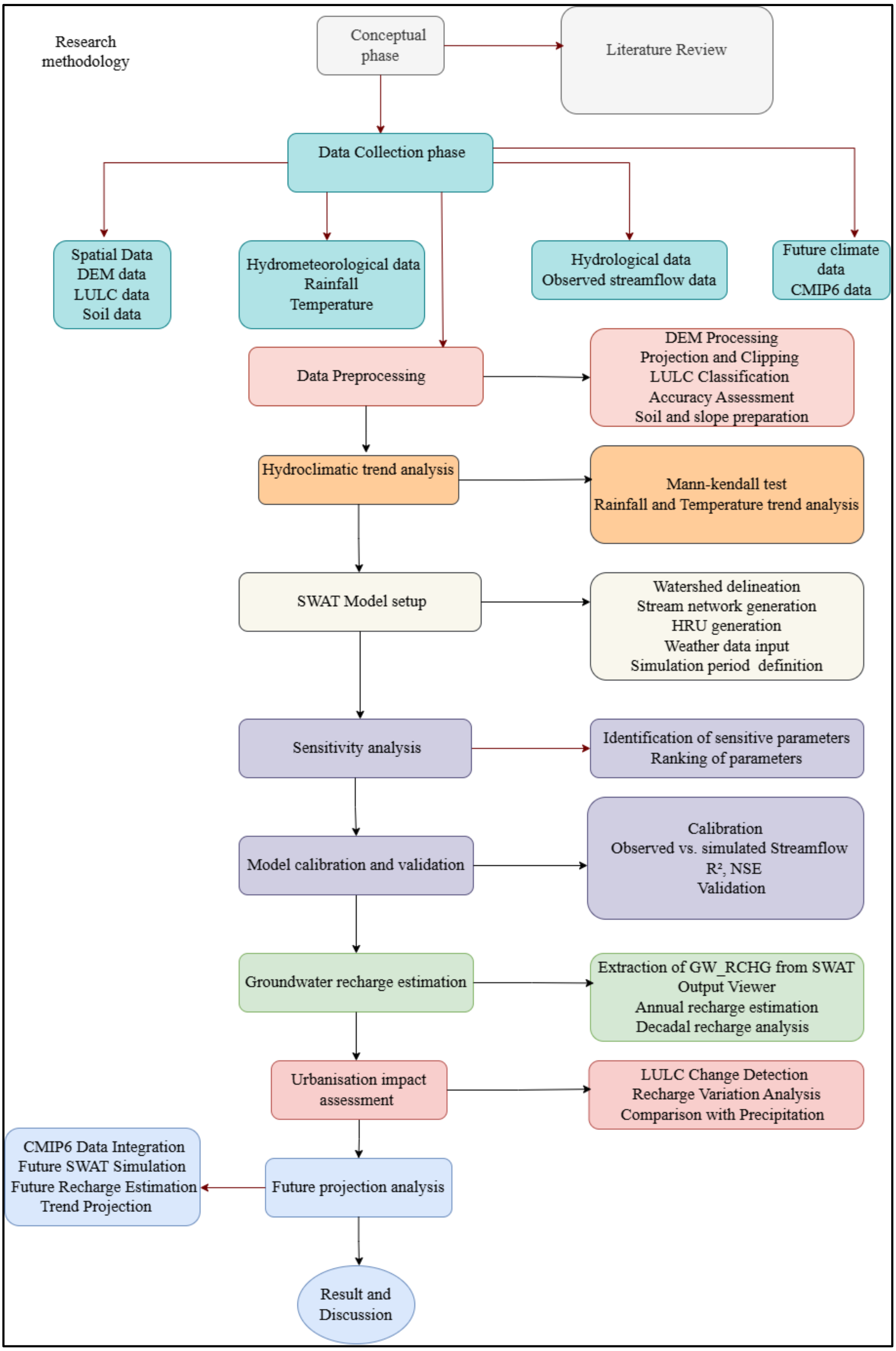

Figure 1.5 Flowchart of research approach

The integrated methodological framework, therefore, provides a comprehensive approach to understanding the influence of urbanisation and climate variability on groundwater recharge dynamics and supports sustainable groundwater resource management within the study area.

1.11 Organization of the thesis

The thesis is organized as follows:

Chapter 1: Introduction

The background of the study is included in this chapter, providing global to regional groundwater scenarios, the problem statement, the objectives of the study, the necessity of groundwater recharge assessment, and the significance of urbanisation impact analysis. The chapter also includes the study area overview and organisation of the thesis.

Chapter 2: Literature review

This chapter provides a detailed review of previous studies related to groundwater recharge estimation, trend analysis, urbanisation impact assessments, geospatial techniques, hydrological modelling, and climate change impact studies.

Chapter 3: Study area and data collection

This module delineates the geographical, climatic, hydrological, and environmental characteristics of the Ahmedabad district and the Vasna Barrage watershed selected as a hydrological monitoring point. The chapter also includes details of spatial, hydro-meteorological, hydrological, and future climate datasets utilised for SWAT modelling and geospatial analysis. The study also discusses the data sources, preprocessing techniques, and software tools used.

Chapter 4: Trend analysis

This chapter presents hydro-climatic trend analysis of rainfall and temperature variables within the study area. Statistical techniques, including the Mann–Kendall trend test and Sen’s slope estimator, are utilised to analyse long-term temporal variations and trends in climatic parameters. The chapter assists in understanding climatic variability and its influence on groundwater recharge conditions.

Chapter 5: Land Use Land Cover (LULC) Mapping and Change Detection

This chapter emphasizes the preparation of land use/land cover maps utilising remote sensing and GIS techniques. Multi-temporal satellite imagery is utilised LULC classification and urban expansion analysis within the Ahmedabad district. The chapter also presents an LULC change detection analysis to evaluate temporal changes in built-up areas, vegetation, agricultural land, and water bodies and their influence on groundwater recharge dynamics.

Chapter 6: Hydrological modelling

This chapter explains the setup and application of the SWAT hydrological model for watershed simulation and groundwater recharge estimation. The chapter includes watershed delineation, Hydrological Response Unit (HRU) generation, sensitivity analysis, calibration, validation, and groundwater recharge simulation. Future groundwater recharge projection using CMIP6 climate data under the SSP3-7.0 scenario is also presented.

Chapter 7: Results and Discussion

This chapter presents and discusses the findings obtained from hydroclimatic trend analysis, LULC change detection, SWAT model calibration and validation, groundwater recharge estimation, urbanisation impact assessment, and future groundwater recharge projection analysis. Spatial and statistical interpretations of the obtained results are discussed in detail.

Chapter 8: Conclusions and Future Scope

This chapter encapsulates the principal findings and conclusions generated from the current investigation. This chapter outlines future research directions.

CHAPTER 2
LITERATURE REVIEW

2.1 General

Groundwater is one of the most important freshwater resources supporting domestic, agricultural, and industrial activities throughout the world. Increased population, rapid urbanisation, industrial expansion, and climatic variability have considerably affected groundwater availability and recharge conditions in many urban and semi-urban regions. In developing countries like India, groundwater is essential for meeting urban water demands and enhancing agricultural output. However, continuous extraction of groundwater beyond the recharge capacity has resulted in declining groundwater levels, increasing water stress, and hydrological imbalance in several regions. The United Nations and UNESCO water assessment reports indicate that increasing urban expansion combined with climate variability has become a significant factor contributing to groundwater depletion and declining recharge potential in rapidly developing cities.

Urbanisation is one of the most significant demographic and socioeconomic trends of the twenty-first century, with projections indicating that over 68% of the global population will inhabit urban areas by 2050**.** The natural water cycle is being drastically altered by the quick growth of metropolitan areas, which is putting increasing strain on freshwater resources across the globe. Particularly susceptible to these changes is groundwater, which supplies about 50% of the world's irrigation demands and makes up almost 97% of the planet's liquid freshwater. (USGS**)**

India has experienced remarkable urban growth in recent decades as a result of economic development and migration from rural to urban areas. One of the main effects of India's urbanization is environmental stress. In addition to changing local hydrology and increasing surface imperviousness, the transformation of natural and agricultural landscapes into urban environments can lead to groundwater depletion and water scarcity when municipal systems are unable to keep up with the increasing demand. (World Bank, 2018; IPCC, 2022; CGWB, 2023). Urban growth frequently involves the transformation of permeable natural surfaces into impervious artificial environments. Urbanization significantly alters patterns of land use and land cover (LULC) by replacing vegetative and permeable surfaces with impermeable structures such as highways, buildings, and pavements. Nath et al. (2021).

The amount of rainwater that seeps into groundwater reserves may decrease as a result of this loss of natural recharge zones since there may be less natural infiltration and greater surface runoff (Weatherl et al., 2021). India's yearly groundwater recharge is estimated to be around 448.52 billion cubic meters, while total extraction is still high at about 247.22 billion cubic meters (with extraction at about 60.63% of recharge), according to the most recent Dynamic Groundwater Resources assessment (CGWB-2025). This indicates continuous pressures on the aquifer systems. Rapid urban growth, changing LULC patterns, and increasing water demand are all contributing factors to the severe strain on groundwater systems in metropolitan India. The combined effects of rapid urban expansion, changing LULC patterns, and increasing water demand have placed significant stress on groundwater systems in urban India (Parween et al., 2026).

Water is a vulnerable and valuable natural resource. According to the United Nations Development Program (UNDP, 2007), Asia is the most vulnerable area and has the scarcest freshwater resources in the world. More than half of the world's population lives in urban areas, a proportion that is expected to increase in the next decades (McDonald et al., 2014). Global urbanization projections indicate that by 2050, 60 to 90% of the global population will reside in cities (Ritchie, 2022). This rapid surge in urbanization driven by population growth and socioeconomic conditions has heightened the demand for water, thereby straining both surface and subsurface water resources (Nasiri, S. 2020). In many cities in the world, urbanization changes the land use practice, usually by reducing the natural land area and increasing the impervious cover area (Murakami et al., 2005). Assessing the impact of land-use change on hydrological parameters is considered an important step in water resources management and a prerequisite for ecological restoration as well as for their sustainable management. Groundwater is not only the primary source of drinking water for half of the world's population but also sustains ecosystems by providing water, nutrients, and a relatively stable temperature (Tharme et al., 2003). The increase of groundwater abstraction to meet the water supply demand of a growing urban population is one of the causes of groundwater depletion in megacities (Naik and Tambe, 2008). Land use changes and anthropogenic activities such as surface sealing due to streets and buildings, flood control, forest management, and irrigation modify the infiltration and movement of water (Baillieux et al., 2015).

The Rapid Land Use/Land Cover (LULC) transformation resulting from urbanszation significantly modifies the natural hydrological cycle by increasing impervious surfaces, reducing infiltration, and enhancing surface runoff generation. These modifications directly affect groundwater recharge processes and watershed hydrology. Therefore, understanding the interaction between urbanisation, climatic variability, and groundwater recharge dynamics has become crucial for sustainable water resource management and watershed planning (Shuster et al., 2005).

In recent decades, the Ahmedabad district has experienced rapid urbanization, industrial growth, and population increases that have led to significant changes in land cover and increased pressure on groundwater resources. Simultaneously, variability in rainfall distribution and climatic conditions further increases groundwater stress and hydrological vulnerability within the region. Therefore, the identification and assessment of groundwater recharge conditions have become increasingly important for understanding the impacts of urbanisation and climatic variability on watershed hydrology and groundwater sustainability.

Remote sensing (RS), Geographic Information System (GIS), and hydrological modelling techniques are widely used for analysing watershed hydrology, groundwater recharge potential, and climate change impacts on water resources. Hydrological models such as the Soil and Water Assessment Tool (SWAT) provide an efficient platform for simulating watershed response under different land use and climatic conditions (Arnold et al., 1998; Sharannya, 2025). Similarly, climate projection datasets developed under the Coupled Model Intercomparison Project Phase 6 (CMIP6) and ISIMIP frameworks are increasingly used for assessing the impacts of future climate.

This chapter provides in-depth studies related to urbanisation, LULC change analysis, trend analysis, hydrological modelling, SWAT modelling, groundwater recharge assessment, and future climate projections using CMIP6 datasets. The references provided are in the form of research publications, reports, and website blogs followed by the critical analysis and identification of research gaps.

2.2 Literature review on trend analysis

The identification of trends in hydro-meteorological time series is an essential component of climate change research and water resource management. Understanding historical changes in rainfall, temperature, and related variables provides essential context for evaluating the vulnerability of water systems and for developing adaptation strategies. In the Ahmedabad district, where groundwater recharge is under stress from both urban expansion and climate variability, trend analysis serves as the essential first step in separating these two factors.

Indrani Pal (2009) shows the socio-economic impacts associated with extreme climatic events influenced by climate change. The study highlighted that predicting the exact occurrence of such events remains challenging because of their random and uncertain nature. The impacts of extreme weather events can be substantial, affecting both human and environmental systems. The research identified an increasing tendency of extreme rainfall occurrences during the monsoon season across central India, a region that shares several climatic characteristics with Gujarat. Furthermore, the study highlighted that high-intensity rainfall events corresponding to moderate to long return periods have been recorded in regions such as Kerala, demonstrating that extreme precipitation events are not restricted to traditionally high-rainfall areas but may occur across a wide range of climatic settings.

Jain (2012) conducted a comprehensive analysis of many research concerning long-term trends in rainfall, rainy days, and temperature throughout India, utilizing datasets from station level to river basin scale. The review highlighted considerable regional variability in climatic trends and showed the importance of long-term climate analysis for water resource management. The study also identified the Mann–Kendall test and Sen's slope estimator as reliable and widely used methods for detecting and quantifying hydro-climatic trends, providing a strong methodological basis for subsequent climate trend assessments.

Rapid urbanization draws numerous individuals to metropolitan areas for diverse reasons, including employment, education, healthcare, and business opportunities. The United Nations Department of Economic and Social Affairs (2019) reported that in 2018, the global rate of urbanization reached 55%, and it is projected that 68% of the world's population will live in urban areas by 2050. Climatic conditions of metropolitan cities tend to change over time due to global climate change and localized anthropogenic activities such as urbanization, industrialization, pollution, rapid population growth, etc. (Kumar, 2021). Such activities alter land surface characteristics, increase heat absorption, and reduce evapotranspiration, contributing to the urban heat island (UHI) effect, which raises local temperatures, especially during nights (Nichol, 2005). The prolonged high temperature will lead to a heatwave, and heavy rainfall in a short span of time leads to urban floods, and short rainfall leads to water crises and increased dry periods; these events are often occurring in these metropolitan cities and affecting the day-to-day life of people (Matthews *et al.,* 2017). Analysing the long-term climatic pattern is very important for monitoring climate and policymaking (Murugan & Santhoshkumar, 2025*)*.

Yue and Wang (2004) highlighted that the MK test is reliable for analysing hydrological time-series data affected by serial correlation and climatic variability. Gocic and Trajkovic (2013) applied the MK test along with Sen's slope estimator to evaluate long-term trends in meteorological parameters and reported significant seasonal variability in rainfall and temperature conditions. Similarly, Tabari et al. (2011) identified increasing temperature trends and irregular precipitation patterns using the Mann–Kendall approach in semi-arid climatic regions.

Table 2.1 Summary of key findings

Authors & Year	**Study focus**	**Method**	**Key findings**
Indrani Pal (2009)	Socio-economic impacts of extreme climatic events	Analysis of extreme rainfall events and climatic variability	Reported an increasing occurrence of extreme monsoon events over central India and highlighted the severe socio-economic impacts associated with stochastic climatic extremes. The study observed rainfall events with return periods of 10–50 years in climatically diverse regions such as Kerala.
Jain, S. K. (2012)	Rainfall, rainy days, and temperature trend analysis across India	Literature review using the Mann–Kendall test and Sen's slope estimator	Identified significant spatial and temporal variability in rainfall and temperature trends across India. The study highlighted the widespread application of Mann–Kendall and Sen's slope methods for hydro-climatological trend analysis.
Gupta (2025)	Global urbanisation and climatic challenges	Urbanisation trend analysis	Reported that global urbanisation reached approximately 55% in 2018 and projected that nearly 68% of the global population will reside in urban areas by 2050, increasing

			environmental and hydrological stress in metropolitan regions.
Kumar (2021)	Impact of urbanisation on metropolitan climatic conditions	Urban climate variability analysis	Observed that rapid urbanisation, industrialisation, and anthropogenic activities significantly alter local climatic conditions by modifying land surface characteristics and increasing thermal stress within metropolitan regions.
Nichol (2005)	Urban Heat Island (UHI) effect in urban environments	Remote sensing and urban climatic analysis	Reported that urban expansion and impervious surfaces increase heat absorption and reduce evapotranspiration, intensifying the Urban Heat Island effect and increasing nighttime temperatures in metropolitan cities.
Matthews et al. (2017)	Urban climatic hazards and environmental stress	Climate impact and urban hazard assessment	Identified increasing frequency of heatwaves, urban flooding, prolonged dry periods, and water scarcity in metropolitan regions due to climatic variability and rapid urban development.
Santhoshkumar et al. (2024)	Long-term climatic pattern analysis	Climatic trend and environmental monitoring studies	Emphasised the importance of long-term climatic trend analysis for climate monitoring, urban environmental management, and policy formulation.
Yue and Wang (2004)	Hydrological trend analysis under serial correlation	Modified Mann–Kendall trend analysis	Demonstrated that the Mann–Kendall test is reliable for analysing hydrological time-series data influenced by serial correlation and climatic variability.

Gocic and Trajkovic (2013)	Meteorological trend analysis	Mann–Kendall test with Sen's slope estimator	Identified significant seasonal variability in rainfall and temperature patterns and confirmed the effectiveness of MK analysis for climatic trend assessment.
Tabari et al. (2011)	Temperature and precipitation variability in semi-arid regions	Mann–Kendall trend analysis and Sen's slope estimation	Reported increasing temperature trends and irregular precipitation patterns associated with climate variability in semi-arid climatic regions.

The reviewed literature indicates that previous studies have extensively investigated climate variability, urbanisation, and hydrological changes using statistical methods and hydrological models. However, limited research has comprehensively examined the combined effects of long-term climate trends, land use/land cover (LULC) changes, and future climate scenarios on groundwater recharge in rapidly urbanising regions such as Ahmedabad.

2.3 Literature review on land use and land cover (LULC) mapping and change detection

Land use has a direct impact on a nation's economic growth. As a result, land use patterns are essential and need to be examined closely. Land use and land cover change (LULCC) are seen as an important tool to assess global change in different spatiotemporal scales (Lambin, 1997). LULC is changing rapidly due to rapid urban settlements and overpopulation (Sikarwar & Chattopadhyay, 2016). During the 20th century, urbanization, deforestation, extreme weather events, and increasing demands from livestock and agricultural output, including overgrazing and forest conversion, caused land degradation (AbdelRahman, 2023). All activities are significantly impacted by land use and land cover change (LULCC). In addition, it is unavoidable and unstoppable due to economic development and population growth. Land Use and Land Cover (LULC) mapping is one of the most important applications of Remote Sensing (RS) and Geographic Information System (GIS) techniques for analysing spatial and temporal changes occurring on the Earth's surface. Remote sensing technology has become highly effective for preparing multi-temporal LULC maps because satellite imagery provides repetitive, synoptic, and spatially distributed information over large geographical regions. Anderson et al. (1976) developed one of the earliest standardised land use classification systems for remote sensing applications and emphasised the importance of hierarchical classification for land resource studies. Subsequently, Lillesand and Kiefer (2000) explained that satellite image classification techniques are highly useful for identifying spatial land cover variability and monitoring environmental transformation over time.

Supervised classification is one of the most commonly utilised image classification approaches in LULC mapping studies. In supervised classification, representative training samples are selected for known land cover classes, and spectral signatures are employed to classify the remaining image pixels into predefined categories. The method provides comparatively higher classification accuracy because the analyst controls training sample selection based on field knowledge and image classification. Common supervised classification algorithms include Maximum Likelihood Classification (MLC). According to Jensen (2005), supervised classification methods provide reliable results for urban and environmental studies when researchers use appropriate training samples and classification schemes. Similarly, Singh (1989) highlighted that change detection analysis utilising classified satellite images is highly effective for identifying land transformation patterns and environmental change over time.

Dewan and Yamaguchi (2009) identify urban expansion and land transformation in developing metropolitan regions using supervised classification techniques and report a substantial rise in built-up land at the expense of agricultural and vegetation-covered areas. Similarly, Rawat and Kumar (2015) observed substantial urban expansion and reduction in natural land cover classes using multi-temporal satellite imagery and GIS-based change detection analysis.

LULC mapping plays a critical role in hydrological and groundwater studies, as land cover characteristics directly affect infiltration, evapotranspiration, runoff generation, and groundwater recharge potential. Agricultural land, grassland, scrubland, and forest areas generally support infiltration and recharge processes, whereas urban built-up surfaces restrict groundwater recharge due to increased imperviousness (Shuster et al., 2005; Scanlon et al., 2006). Fohrer et al. (2001) identify that land cover changes significantly alter watershed hydrological response and water balance conditions.

Accuracy assessment and Kappa coefficient analysis are used in validating the reliability of Land Use/Land Cover (LULC) classification results derived from remote sensing data. Accuracy assessment is considered an important step in supervised classification because it quantitatively evaluates the agreement between classified outputs and reference or ground truth data. Congalton and Green (2019) examined that confusion matrix analysis, overall accuracy, producer's accuracy, user's accuracy, and the Kappa coefficient are among the most widely used statistical measures for evaluating classification performance in remote sensing applications. Phiri and Morgenroth (2017) show that supervised classification methods integrated with high-quality training samples and validation datasets can achieve classification accuracies greater than 85%, which is typically considered acceptable for land cover studies.

Belgiu and Drăguţ (2016) indicated that Kappa coefficient values exceeding 0.80 represent strong agreement between classified imagery and reference observations, confirming satisfactory classification reliability

Table 2.1 Summary of findings

Authors & Year	**Study focus**	**Method**	**Key findings**
Lambin (1997)	Global Land Use and Land Cover Change (LULCC) assessment	Multi-scale LULCC analysis	Identified LULCC as an important indicator for assessing global environmental change at different spatial and temporal scales.
Ankit Sikarwar et al. (2016)	Urbanisation and rapid LULC transformation	Remote sensing and GIS-based analysis	Reported that rapid urban settlements and population growth significantly accelerate changes in land use and land cover patterns.
AbdelRahman (2023)	Land degradation and environmental stress	Environmental and land degradation assessment	Observed that urbanisation, deforestation, extreme climatic events, and agricultural pressure intensify land degradation processes.
Anderson et al. (1976)	Development of a standard LULC classification system.	Hierarchical land use classification framework	Developed one of the earliest standardised land use classification systems for remote

			sensing-based land resource studies.
Lillesand and Kiefer (2000)	Remote sensing applications in LULC mapping	Satellite image interpretation and classification	Reported that remote sensing techniques are highly effective for identifying spatial land cover variability and monitoring environmental changes over time.
Singh (1989)	Change detection analysis using satellite imagery	Multi-temporal image classification and change detection	Demonstrated that classified satellite imagery effectively identifies land transformation patterns and environmental changes.
Jensen (2005)	Supervised image classification in remote sensing	Supervised classification techniques	Reported that supervised classification methods provide reliable results for urban and environmental studies when appropriate training samples are used.
Dewan and Yamaguchi (2009)	Urban expansion and land transformation	GIS and supervised classification-based change detection	Identified significant increase in built-up land and decline in vegetation and agricultural land in developing metropolitan regions.
Rawat and Kumar (2015)	Urbanisation and environmental change	Multi-temporal LULC mapping and GIS analysis	Observed substantial urban expansion and reduction in natural land cover classes using satellite imagery and change detection techniques.
Fohrer et al. (2001)	Impact of LULC changes on watershed hydrology	Hydrological and GIS-based watershed analysis	Demonstrated that LULC changes significantly influence infiltration, runoff generation, evapotranspiration, and groundwater recharge conditions.

Congalton and Green (2019)	Accuracy assessment of LULC classification	Confusion matrix and Kappa coefficient analysis	Highlighted that overall accuracy, producer's accuracy, user's accuracy, and Kappa coefficient are essential for validating classification reliability.
Phiri and Morgenroth (2017)	Evaluation of supervised classification accuracy	Supervised classification with validation datasets	Reported that supervised classification techniques can achieve classification accuracies greater than 85% when high-quality training samples are used.
Belgiu and Drăguţ (2016)	Reliability of image classification techniques	Kappa coefficient and classification assessment	Indicated that Kappa coefficient values above 0.80 represent strong agreement between classified imagery and reference observations.

The reviewed studies demonstrate that remote sensing and GIS techniques have been extensively applied for land use/land cover (LULC) mapping, change detection, and urban expansion analysis. Although previous studies have successfully quantified historical LULC changes and their environmental implications, relatively few have integrated multi-temporal LULC analysis with watershed-scale hydrological modelling and future climate change assessment to evaluate groundwater recharge in rapidly urbanising regions.

2.4 Literature review on Hydrological modelling

Hydrological models are simplified representations of the real-world hydrological cycle that allow researchers and water managers to simulate, understand, and predict the movement, distribution, and quality of water across the landscape. These models serve as vital tools for addressing a wide range of water resource challenges, including flood forecasting, drought assessment, water quality management, climate change impact analysis, and groundwater recharge estimation. The fundamental basis of hydrological modelling is that, while a complete physical representation of catchment hydrology is impossible due to the complexity of natural systems, simplified models can capture essential processes with adequate accuracy for practical decision-making.

Hydrological models are commonly classified based on the manner in which they represent watershed characteristics and hydrological processes. Among these, according to Chow et al. (1988) and Singh and Woolhiser (2002), lumped models treat the entire catchment as a single unit, assuming uniform conditions throughout the watershed and employing average parameter values to simulate the overall hydrological response. According to Beven (2012) and Singh and Woolhiser (2002), distributed hydrological models divide the catchment into grid cells, facilitating spatial variations in inputs, parameters, and outputs. Semi-distributed models represent an intermediate approach, dividing the catchment into sub-basins or hydrological response units that are assumed to be homogeneous while allowing heterogeneity between units.

The Soil and Water Assessment Tool (SWAT) is a physically based, semi-distributed hydrological model developed by the United States Department of Agriculture–Agricultural Research Service (USDA-ARS) to simulate watershed processes under varying environmental and land management conditions (Arnold et al., 1998). The model is designed to assess both surface water and groundwater components of the hydrological cycle at the watershed scale and operates on a continuous daily time. Due to its ability to simulate long-term hydrological responses across extended periods, SWAT has been widely used in studies related to water resources management, land use change assessment, climate change impacts, and groundwater recharge evaluation (Arnold et al., 1998, and Neitsch et al., 2011).

SWAT has been continuously refined and updated since its initial release. Several versions of the model have been introduced over time, each incorporating advancements in hydrological process representation, model structure, computational performance, and user accessibility (Arnold et al., 2012). Due to its open-source characteristics, comprehensive documentation, and continuous support from the global SWAT research community, the model has become one of the most widely applied tools for watershed management, climate change assessment, land use analysis, and groundwater recharge studies globally (Arnold et al., 2012; Bieger et al., 2017).

Gassman et al. (2007) conducted an extensive study of SWAT applications, detailing the model's history, capabilities, and limitations. The review noted that SWAT had been applied in over 500 peer-reviewed studies across the globe. Arnold et al. (1998) described the early development of SWAT and its integration with ArcGIS, which significantly enhanced the model's accessibility for researchers and practitioners. Neitsch et al. (2011) produced the definitive theoretical documentation of the SWAT model, which serves as the primary source for understanding the model's process algorithms and parameter requirements. Arnold et al. (2012) provided an updated review of SWAT applications and model enhancements, documenting the model's evolution through the SWAT2012 version. The SWAT model operates on a daily time step and simulates the hydrological cycle using the water balance equation. The model delineates a watershed into sub-basins based on topographic analysis of a digital elevation model (DEM). Each sub-basin is further subdivided into Hydrological Response Units (HRUs), which are unique combinations of land use, soil type, and slope class. This HRU methodology enables the SWAT model to capture spatial variability in hydrological processes without requiring computationally intensive grid-based calculations.

The hydrological cycle simulated by the SWAT model has the following principal components as documented by Neitsch et al. (2011):

Precipitation serves as the principal input driving the hydrological system. Daily precipitation data can be presented as actual observation or synthetic stochastic generation.

Evapotranspiration represents the combined loss of water through soil evaporation and plant transpiration. SWAT offers three methodologies to determine potential evapotranspiration: Penman-Monteith (recommended for most applications), Priestley-Taylor (appropriate for humid regions), and Hargreaves (suitable for data-sparse areas). The Penman-Monteith method requires solar radiation, air temperature, relative humidity, and wind speed data.

Surface runoff is assessed with either the SCS Curve Number method or the Green-Ampt infiltration method. The SCS Curve Number method, established by the USDA Soil Conservation Service, is the default approach and is widely used for its simplicity and reasonable accuracy. The method requires daily rainfall and a curve number parameter that varies with land use, soil type, and antecedent moisture conditions.

Lateral flow refers to the subsurface movement of water through the soil profile that occurs when the moisture content of a soil layer exceeds field capacity. Lateral flow is computed simultaneously with percolation and is significant in sloping areas with permeable soils.

Percolation is the downward movement of water through the soil column, calculated when the water content of a soil layer surpasses its capacity. Water percolates to the next layer until it either reaches the shallow aquifer or is removed by evapotranspiration or lateral flow.

Groundwater recharge is the amount of water that reaches the shallow aquifer. In SWAT, recharge is calculated as the water that percolates past the root zone and enters the shallow aquifer system. The delay between percolation and aquifer recharge is represented by the groundwater delay parameter (GW_DELAY), which accounts for the travel time through the vadose zone.

Return flow (baseflow) is the contribution of groundwater to streamflow. SWAT conceptualises the shallow aquifer as a linear reservoir, with return flow calculated as a function of aquifer water content and the baseflow alpha factor (ALPHA_BF).

Santhi et al. (2001) applied SWAT to the Bosque River watershed in Texas and demonstrated the importance of proper groundwater parameter calibration for accurate streamflow simulation. The study found that the groundwater delay parameter (GW_DELAY) and the baseflow alpha factor (ALPHA_BF) were among the most sensitive parameters in the model. Van Liew et al. (2003) assessed the performance of SWAT for three watersheds across the United States and concluded that the model's groundwater representation was satisfactory for most applications.

Using the SUFI-2 algorithm, Kim et al. (2008) evaluated the uncertainty in SWAT groundwater parameters and found that parameter uncertainty could significantly affect model predictions of baseflow and groundwater recharge. The study recommended the use of uncertainty analysis techniques to characterise the reliability of SWAT groundwater simulations. Abbaspour (2015) presented a comprehensive overview of SWAT-CUP (Calibration and Uncertainty Programs), which includes the SUFI-2 algorithm for parameter calibration and uncertainty analysis.

2.5 SWAT calibration and validation

Calibration and validation are essential steps in SWAT applications to ensure that the model adequately represents the hydrological behaviour of the study catchment. Calibration involves adjusting model parameters within reasonable ranges to minimise the discrepancy between simulated and observed outputs (typically streamflow or groundwater levels). Validation involves running the calibrated model over an independent time period and comparing simulated outputs with observed data without further parameter adjustment.

The Sequential Uncertainty Fitting (SUFI-2) algorithm within SWAT-CUP is one of the most widely used methods for SWAT calibration. Abbaspour et al. (2004) first described the SUFI-2 algorithm and its application to SWAT calibration. The algorithm simultaneously calibrates multiple parameters while quantifying parameter values and prediction uncertainty. Yang et al. (2008) evaluated different calibration techniques for

SWAT, including SUFI-2, GLUE, ParaSol, and found that SUFI-2 performed well for calibration efficiency and uncertainty quantification.

The effectiveness of model calibration and validation is commonly assessed using statistical performance indicators that quantify the agreement between observed and simulated values. Moriasi et al. (2007) proposed widely accepted performance evaluation criteria for hydrological models and suggested that models producing acceptable statistical agreement, Nash-Sutcliffe Efficiency (NSE) values >0.5 can be considered suitable for watershed applications. Subsequently, Moriasi et al. (2015) revised these evaluation guidelines by providing precise performance thresholds and recommendations related to different hydrological variables and modelling objectives. These criteria have been extensively adopted in SWAT-based studies for assessing model reliability and ensuring the robustness of simulation results.

2.5.1 Global applications of SWAT for groundwater recharge studies

Aduah et al. (2017) applied SWAT to the Vea catchment in Ghana to estimate groundwater recharge, using 36 years of climate data from 11 gridded climate stations. The model was calibrated and validated with observed streamflow data, achieving NSE of 0.888 and R^2 of 0.960. The study found that annual recharge in the catchment ranged from 0.6% to 20.4% (mean = 10.26%) of rainfall, with rainfall amounts ranging between 747.1 and 1,174.4 mm/year (mean = 963 mm/year). The study employed the water table fluctuation (WTF) technique to validate the SWAT recharge estimates, finding that WTF estimates confirmed the SWAT results, establishing a strong exponential relationship between recharge and precipitation with R^2 of 0.98.

Setegn et al. (2008) applied SWAT to the Lake Tana Basin in Ethiopia to assess hydrological processes and water balance components. The study achieved satisfactory calibration and validation results and demonstrated the model's utility for water resource planning in data-scarce regions. Schuol et al. (2008) applied SWAT to West Africa, calibrating the model for 118 river basins across the region. The study demonstrated that SWAT could be successfully applied at continental scales, providing insights into regional water balance patterns.

Gassman et al. (2007) reviewed SWAT applications worldwide, documenting over 500 peer-reviewed studies across diverse geographical settings. The review found that SWAT had been applied on all continents except Antarctica and had been used for a wide range of purposes, including climate change impact assessment, land use change analysis, water quality modelling, and groundwater recharge estimation. Bressiani et al. (2015**)** reviewed SWAT applications in Brazil, documenting the model's growing adoption in South America and highlighting the importance of proper calibration and validation for tropical catchments.

The SWAT model simulates groundwater recharge as the amount of water that percolates past the root zone and reaches the shallow aquifer. The water balance equation (Neitsch et al., 2011) that represents the hydrologic cycle simulated in SWAT is expressed as:

$SWt = SW + \Sigma (R_{it} - Q_i - ET_i - P_i - QR)$ **2.1**

Where,

SWt = soil water content at time step.

SW = the final soil water content,

R = daily precipitation,

Q = runoff.

ET = evapotranspiration.

P = percolation, and

QR = groundwater flow.

This water balance approach, implemented at the HRU level, enables the quantification of recharge as a residual component of the hydrological cycle.

Sulistani et al. (2025) performed an integrated assessment of groundwater recharge in Surakarta City, Indonesia, using SWAT in combination with Cellular Automata-Artificial Neural Network (CA-ANN) based land use and land cover and climate projections from five Regional Climate Models (RCMs) under SSP2-4.5 and SSP5-8.5 scenarios.

Jagadish and Hemalatha (2024) employed the SWAT model to analyse groundwater recharge in the Bahuda watershed of Chittoor District, India. The study used the SWAT model to analyse various recharge components through a water balance approach, helping to identify areas with high recharge potential and those requiring intervention. The findings formed the basis for formulating strategies for optimal restoration of surface and groundwater resources, including the construction of rainwater harvesting systems, improvement of soil moisture, and alteration of land use practices.

Devika et al. (2020) evaluated the long-term impact of LULC changes on groundwater recharge in the Periyar River watershed in the Ernakulam district, Kerala, India, using SWAT The study analysed LULC changes over four decades (1992-2019) and simulated groundwater recharge corresponding to different LULC scenarios. The comparative analysis between simulated recharge corresponding to initial and subsequent LULC depictions showed an overall decline in groundwater recharge from 1992 to 2019. Statistical analysis revealed that a maximum of 45% decrease in groundwater recharge was observed in 12 sub-basins, while a minimum of 10% reduction was observed in another ten sub-basins among the total 52 sub-basins. The study identified the expansion of built-up land coupled with a decrease in agricultural land and barren land as the primary contributors to the reduction in groundwater recharge. The findings highlight the significant variability in long-term groundwater recharge resulting from temporal changes in LULC and point to the need for regulations in anthropogenic activities to address critical land resource management issues.

2.6 Literature review on future climate projections using CMIP6

The assessment of future climate conditions and their potential impacts on hydrological systems have become an indispensable component of contemporary water resource research, particularly in regions facing rapid urbanisation and groundwater depletion. The Coupled Model Intercomparison Project Phase 6 (CMIP6), which forms the scientific backbone of the Intergovernmental Panel on Climate Change (IPCC) Sixth Assessment Report (AR6), represents the most advanced generation of global climate models (GCMs) available to date (Eyring et al., 2016).

The Coupled Model Intercomparison Project Phase 6 (CMIP6) represents the latest and most advanced generation of global climate models (GCMs) used to inform the Intergovernmental Panel on Climate Change (IPCC) Sixth Assessment Report (AR6).

The SSP framework consists of five distinct pathways. SSP1-1.9 and SSP1-2.6 represent low-emission, sustainability-oriented scenarios. SSP2-4.5 represents a middle-of-the-road scenario with moderate challenges to mitigation and adaptation. SSP3-7.0 is a medium-high emission pathway characterised by regional rivalry and high challenges to both mitigation and adaptation. SSP5-8.5 represents the highest emission scenario, driven by fossil-fueled development (O'Neill et al., 2017; Riahi et al., 2017). For the present study, the SSP3-7.0 scenario is particularly relevant, as it has been widely used in regional precipitation and impact assessment studies for semi-arid regions.

The Inter-Sectoral Impact Model Intercomparison Project (ISIMIP) provides a standardised framework for bias-correcting and downscaling CMIP6 climate model outputs for use in impact models. The Inter-Sectoral Impact Model Intercomparison Project (ISIMIP) provides a standardised framework for bias-correcting CMIP6 outputs using empirical quantile mapping, which preserves long-term climate change signals while correcting mean biases and variability (Lange, 2019; Warszawski et al., 2014). Mishra et al. (2020) developed a bias-corrected CMIP6 climate model dataset of precipitation, maximum temperature, and minimum temperature for six countries in South Asia, including India. The dataset includes 13 CMIP6 models, with each model including five scenarios: historical, SSP1-2.6, SSP2-4.5, SSP3-7.0, and SSP5-8. 5. The bias correction method employed was empirical quantile mapping (EQM), which corrects mean biases and variability while preserving the long-term climate change signal.

Mishra et al. (2020) conducted a comprehensive evaluation of 13 bias-corrected CMIP6 GCMs for Indian conditions. Table 2.1 presents these models along with their spatial resolutions.

The EC-Earth3 model is a state-of-the-art Earth system model developed by the EC-Earth consortium, a collaboration of European research centres (Döscher et al., 2022). Several recent evaluations of CMIP6 climate models have demonstrated that EC-Earth3 performs reliably in reproducing precipitation and temperature patterns across different regions of India.

Table 2-2 CMIP6 GCMs available for Indian climate studies

Sr. no.	Model name	Type	Latitude resolution (°)	Longitude resolution (°)
1	ACCESS-CM2	Bias corrected	1.25	1.875
2	ACCESS ESM1-5	Bias corrected	1.25	1.875
3	BCC-CSM2MR	Bias corrected	1.1215	1.125
4	CanESM5	Bias corrected	2.7906	2.8125
5	EC-Earth3	Bias corrected	0.7018	0.703125
6	EC-Earth3-Veg	Bias corrected	0.7018	0.703125
7	INM-CM4-8	Bias corrected	1.5	2
8	INM-CM5-0	Bias corrected	1.5	2
9	MPI-ESM1-2-HR	Bias corrected	0.9351	0.9375
10	MPI-ESM1-2-LR	Bias corrected	1.8653	1.875
11	MRI-ESM2-0	Bias corrected	1.1215	1.125
12	NorESM2-LM	Bias corrected	1.8947	2.5
13	NorESM2-MM	Bias corrected	0.9424	1.25

Source: Mishra et al. (2020), as presented in IWA Publishing

EC-Earth3 is one of the better-performing models for simulating precipitation in India, making it appropriate for regional hydrological applications (Vinod & Agilan, 2024). The model's comparatively finer spatial resolution and improved representation of atmospheric processes make it particularly useful for hydrological investigations that require realistic simulation of local climatic variability (Hazeleger et al., 2022; Maity et al., 2025). Considering its demonstrated performance in previous studies and the availability of bias-corrected climate projections through the ISIMIP framework, EC-Earth3 was selected for the present study to assess future climate impacts on groundwater recharge and watershed hydrology (Eyring et al., 2016; Döscher et al., 2022; Lange, 2019).

Table 2.3 Summary of Findings

Category	Key Findings / Model features	Key references
Hydrological model classification	Lumped (homogeneous catchment), Distributed (grid cells), Semi-distributed (sub-basins/HRUs)	General literature
SWAT model overview	Semi-distributed, physically based, daily time step, simulates water quantity & quality at the watershed scale	Gassman et al. (2007); Arnold et al. (1998); Neitsch et al. (2011); Arnold et al. (2012)
SWAT hydrological components	Precipitation, Evapotranspiration (Penman-Monteith, Priestley-Taylor, Hargreaves), Surface Runoff (SCS Curve Number / Green-Ampt), Lateral Flow, Percolation, Groundwater Recharge, Return Flow (Baseflow)	Neitsch et al. (2011)
Groundwater parameters	GW_DELAY (groundwater delay), ALPHA_BF (baseflow alpha factor), RCHRG_DP (deep aquifer percolation fraction)	Santhi et al. (2001); Van Liew et al. (2003); Kim et al. (2008)
Calibration & Validation	SUFI-2 algorithm in SWAT-CUP; NSE > 0.5 satisfactory (monthly); R^2, PBIAS, RSR	Abbaspour et al. (2004, 2015); Yang et al. (2008); Moriasi et al. (2007, 2015)
Global SWAT applications	>500 peer-reviewed studies across all continents; recharge ranging 0.6-20.4% of rainfall; NSE up to 0.888	Gassman et al. (2007); Aduah et al. (2017); Setegn et al. (2008); Schuol et al. (2008); Bressiani et al. (2015)

District-level SWAT Studies	Clipping sub-basins to administrative boundaries; recharge declines of 10-45% due to LULC changes	Debnath et al. (2022); Devika et al. (2020); Jagadish & Hemalatha (2024); Sulistani et al. (2025)
CMIP6 overview	Latest GCM generation for IPCC AR6; Shared Socioeconomic Pathways (SSPs)	IPCC AR6
ISIMIP Bias correction	Empirical Quantile Mapping (EQM); bias-corrected data for 13 CMIP6 models over South Asia	Mishra et al. (2020)
CMIP6 models for India	13 models, including EC-Earth3, EC-Earth3-Veg, MPI-ESM1-2-HR, INM-CM5-0, etc.	Mishra et al. (2020)
EC-Earth3 model	Resolution ~0.7°; top-performing for Indian precipitation; ranked among top 10 models	Eyring et al. (2016); Döscher et al., (2022); Lange (2019)
SSP3-7.0 projections	Medium-high emission; increased rainfall intensity, reduced rainy days; pre-monsoon warming of 1.2-1.8°C by 2050	Suthinkumar et al. (2024); Mizan et al. (2025)

The SWAT model has been widely applied for watershed hydrology, streamflow simulation, climate change impact assessment, and groundwater recharge estimation in different regions worldwide, its application for evaluating the combined impacts of long-term climate variability, urbanisation, projected land use/land cover (LULC) change, and future CMIP6 climate scenarios on groundwater recharge remains relatively limited, particularly for rapidly urbanising watersheds such as Ahmedabad.

Overall Research Gap

Based on the literature reviewed, the following research gaps have been identified:

Previous studies have primarily investigated the impacts of climate variability, land use/land cover (LULC) change, or groundwater recharge independently, whereas studies integrating all these components within a single framework are limited. Most groundwater recharge studies have focused on historical conditions, with comparatively fewer investigations evaluating future groundwater recharge under projected climate and urbanisation scenarios.

Although the SWAT model has been widely applied for watershed hydrology, limited studies have integrated SWAT, future LULC simulation, and CMIP6 climate projections to assess long-term groundwater recharge in rapidly urbanising watersheds.

Previous LULC studies have mainly concentrated on mapping and change detection, while relatively few have quantified the hydrological implications of future urban expansion on groundwater recharge. Limited research has incorporated bias-corrected CMIP6 climate datasets together with projected LULC scenarios to evaluate the combined effects of climate change and urbanisation on groundwater recharge.

Therefore, the present study addresses these gaps by developing an integrated framework combining climate trend analysis, remote sensing, GIS, SWAT hydrological modelling and bias-corrected CMIP6 climate projections to evaluate historical and future groundwater recharge, thereby providing scientific support for sustainable groundwater management and climate-resilient urban planning.

2.7 Summary

The literature review demonstrates that urbanisation significantly reduces groundwater recharge, with built-up expansion causing recharge declines. For trend analysis, the Mann-Kendall test with Sen's slope estimator is the conventional non-parametric method for detecting changes in rainfall and temperature. Remote sensing and GIS, particularly supervised classification of Landsat data, effectively measure decadal land use and land cover changes. The Soil and Water Assessment Tool (SWAT) is a well-validated, semi-distributed hydrological model capable of simulating groundwater recharge at watershed and district scales using established calibration protocols such as SUFI-2.. For future projections, the CMIP6 EC-Earth3 model, bias-corrected via the ISIMIP framework, performs reliably for Indian climatic conditions and, under the SSP3-7.0 scenario, projects increased rainfall intensity and reduced rainy days. SWAT modelling calibrated at the Vasna Barrage outlet, and CMIP6 EC-EARTH3 future projections to assess the impact of urbanisation on groundwater recharge specifically for the study area. The present study directly addresses this by creating an integrated geospatial-hydrological modelling framework to quantify historical recharge decline and project future changes under combined urbanisation and climate pressures, thus offering evidence-based support for sustainable groundwater management in one of India's fastest-growing metropolitan regions.

CHAPTER 3
STUDY AREA AND DATA COLLECTION

3.1 General

In this study, Ahmedabad was selected due to its rapid urbanization, semi-arid climate and groundwater resources. The study area represents a typical urban system of India where the combined effects of land use change and weather variability influence the hydrological processes.

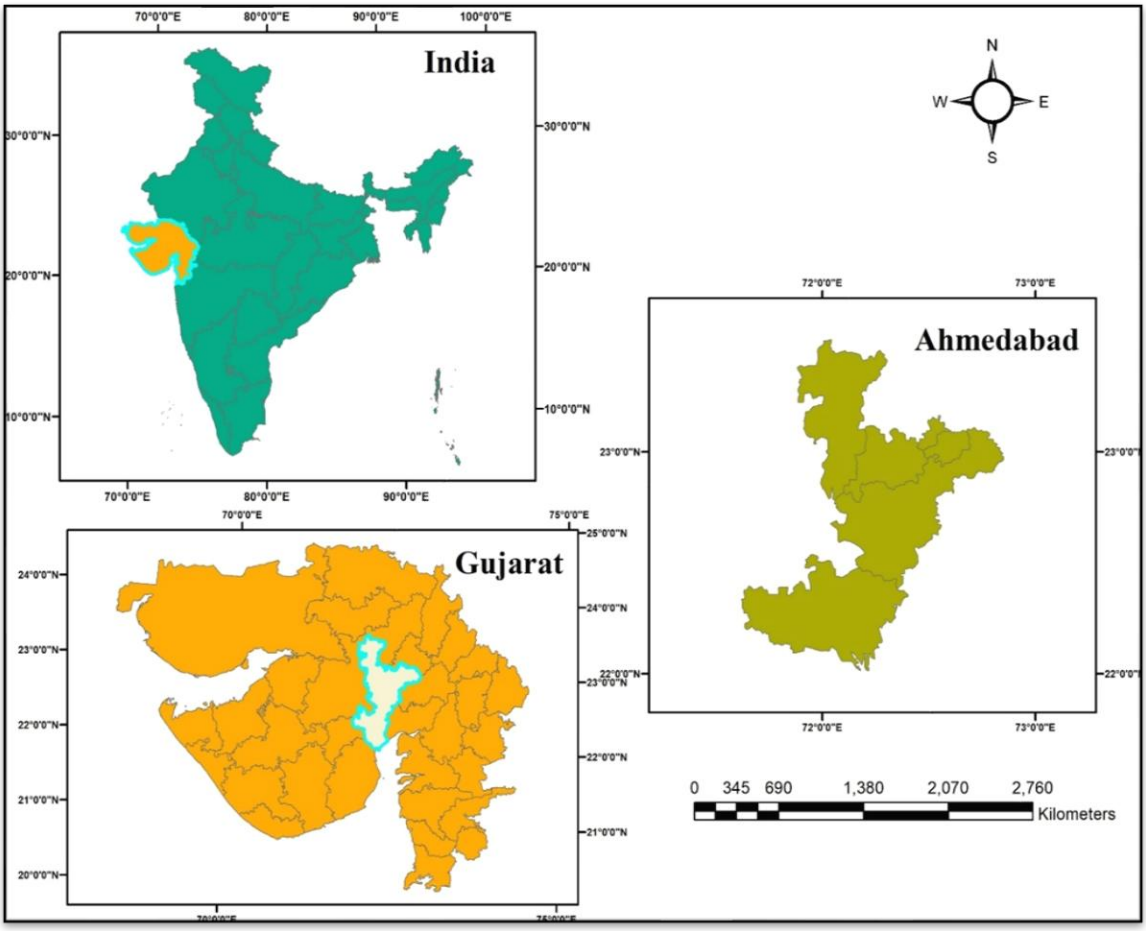

Figure 3.1 Study area map, Ahmedabad

3.2 Study Area

The Ahmedabad district is located in the central part of Gujarat State, western India, between 22°30′ N and 23°46′ N latitude and 72°02′ E and 72°58′ E longitude, as shown in *Figure 3.1*. It is situated on the banks of the Sabarmati River, which flows from north to south and greatly impacts the regional hydrological system.

3.2.1 Physiography

The research area's physiography features primarily flat to gently undulating topography, including a segment of the vast alluvial plains of western India.

3.2.2 Climate

The climate of the study area is characterized by hot summers and overall aridity, except for the southwest monsoon seasons. The year is partitioned into four distinct seasons. The interval from March to May constitutes the hot season (summer), succeeded by the southwest monsoon from June to September. October and November represent the post-monsoon or receding monsoon period.

Based on available rainfall data, Ahmedabad has a moderate amount of precipitation, averaging 715 mm of rainfall annually. *Figure 3.2* shows the average monthly rainfall.

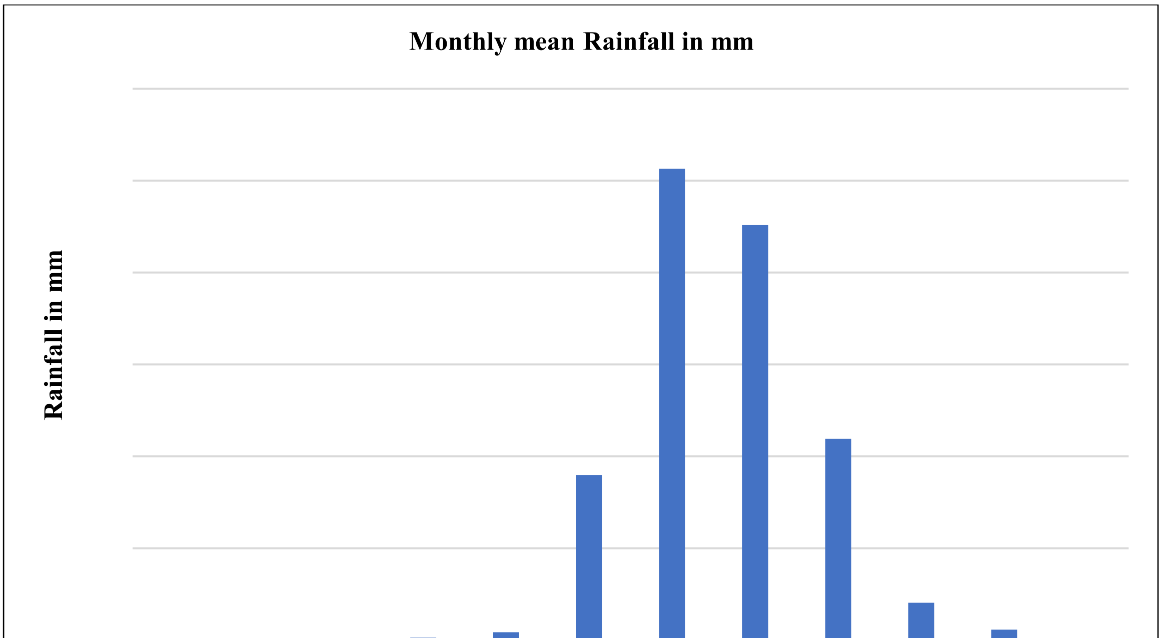

	JAN	FEB	MARCH	APRIL	MAY	JUNE	JULY	AUG	SEPT	OCT	NOV	DEC
Series1	0.6035	0.10175	0.42175	1.38275	4.2805	89.845	256.51	225.7695	109.46575	20.2755	5.61525	0.7235

Figure 3.2 Mean monthly precipitation (mm) of the study area

3.2.3 Temperature

The research area experiences semi-arid climatic conditions, resulting in severe temperature levels. *Figures 3.3* and *3.4* illustrate that December and January were the coldest months, with low temperatures of 9.11°C and 7.85°C, while April and May were the hottest, with maximum temperatures of 46.27°C and 45.03°C, respectively.

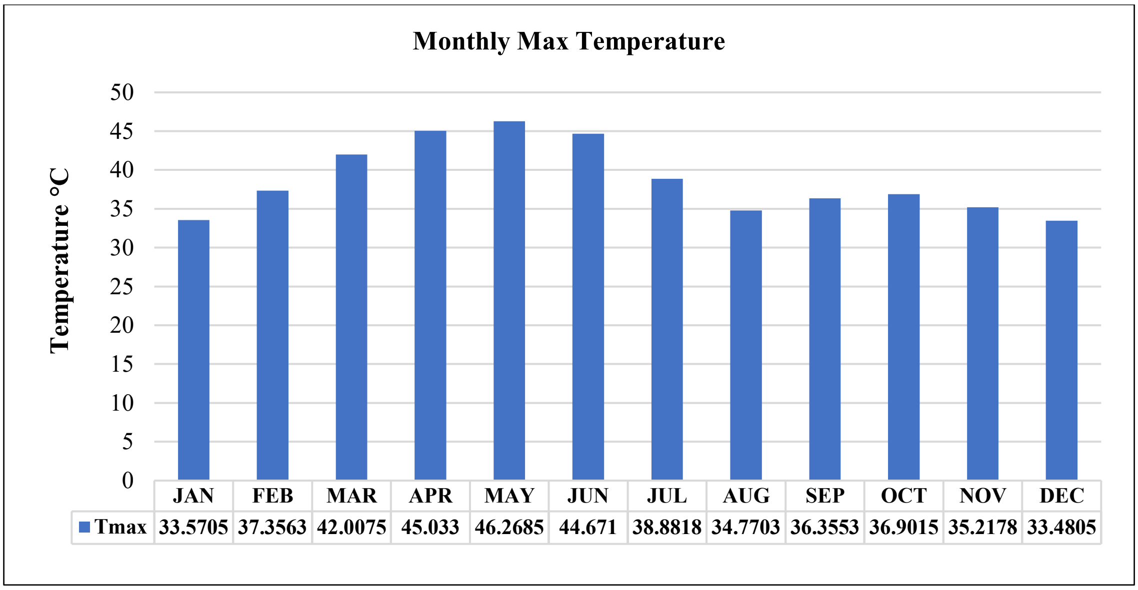

Figure 3.3 Average month-wise distribution of maximum temperature

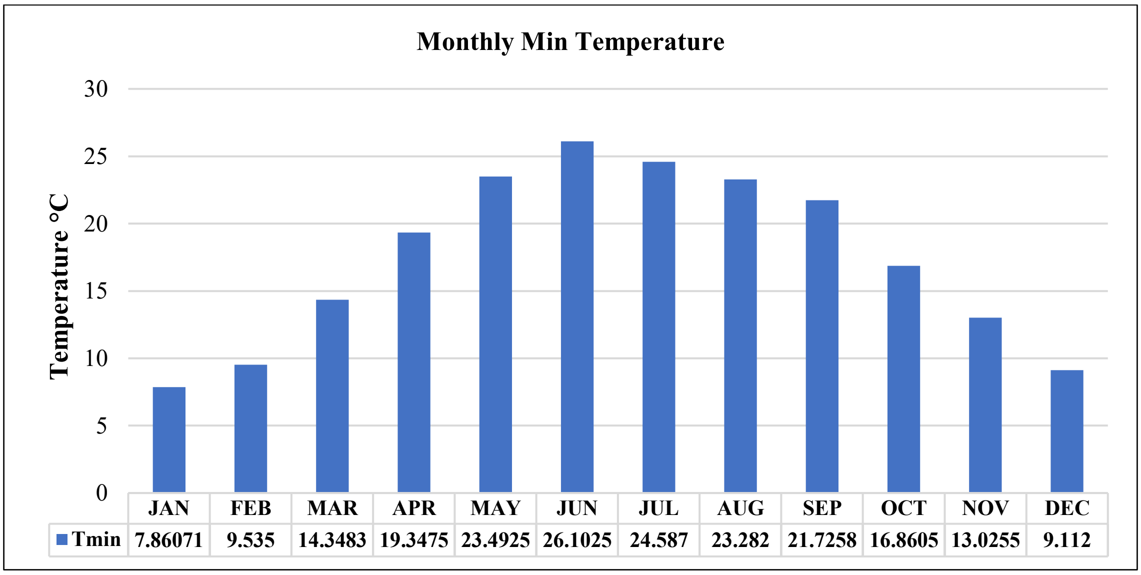

Figure 3.4 Average monthly distribution of minimum temperature

3.2.4 Wind

Between May and September, approximately 70–75% of days in Ahmedabad exhibit significant wind activity, with average wind speeds typically exceeding those of the remainder of the year. Depending on the watershed delineation used for hydrological modelling, the study area may also spatially extend to the surrounding regions.

The above-mentioned conditions correspond to the windier season from late April to August, when average wind speeds exceed ~8–11 mph (≈13–18 km/h), with June being the month with the highest wind intensity. (WeatherSpark, 2024). Typical Meteorological Conditions (Ahmedabad.)

3.2.5 Relative Humidity

Relative humidity is often high during the southwest monsoon season, which spans from June to September. and generally, varies between 70% and 85%. During the summer or pre-monsoon period, the relative humidity is lower, ranging between 20% and 40%. This is due to the high temperature and dry atmosphere. The winter season has moderate humidity levels. It is normally between 40% and 60%. This shows reasonably stable and cooler atmospheric conditions.

3.2.6 Soil Type

The study area is covered by alluvial soils that are deposited by the sedimentary action by the fluvial process associated with the Sabarmati River. These soils typically are a mixture of sand, silt, and clay in varying proportions. The textural classification of soils in this area varies widely. Soil properties are important parameters for the SWAT model as they control the infiltration, percolation, water retention capacity and runoff production. Soil information for the study area was obtained from the Food and Agriculture Organization (FAO) Digital Soil Map of the World. as depicted in Table 3.1 and Figure 3.6.

Table 3.1 Major soil types of Ahmedabad

Soil Type	Approximate Area (%)
Sandy Loam	45–50%
Loam	25–30%
Clay Loam	20–25%

.

3.2.7 Specific contributions of the present research to the study area

1. **Estimate** the reduction of groundwater recharge due to the observed land use and land cover change 2011–2020 using the physically based representation of infiltration, percolation and aquifers by the SWAT model.
2. **Integrate** geospatial methods (LULC classification, DEM analysis and soil mapping) with hydrological modelling in a single framework, away from the descriptive or correlative studies that have dominated the literature for the region.
3. **Scenario-based assessment with climate projections from CMIP6** The contribution of this thesis is substantial and unique in that it simulates future climatic scenarios to evaluate the interaction between anticipated changes in precipitation and temperature and the effect of continued urbanization on groundwater recharge. The project will use the latest advances in climate science, in particular the Coupled Model Intercomparison Project Phase 6 (CMIP6). This framework provides the latest

standardized climate projections and is important for assessing projected hydrological impacts under different global development pathways and greenhouse gas emission scenarios. Through the Inter-Sectoral Impact Model Intercomparison Project (ISIMIP), the research will draw on the latest advances in climate science.

The bias-adjusted data, produced by a trend-preserving method, provide reliable local hydrological forecasts. This study will decouple the effects of climate change and urban land cover change by comparing projected recharge under different scenarios to historical baselines. This early-stage assessment provides immediate evidence-based adaptation planning for water resource challenges in Ahmedabad.

3.2.8 Summary of the rationale

In summary, Ahmedabad is a case of urgent hydrological stress (152% groundwater utilisation) superimposed on a rapidly changing land surface. A changing rainfall regime, more intense monsoon rainfall within a shorter window, further amplifies runoff responses from impervious surfaces. Previous modelling efforts in the Sabarmati basin have demonstrated the suitability of SWAT for capturing regional hydrology, but none have applied the model to isolate the impact of urbanisation on groundwater recharge within the Ahmedabad urban area. This research fills that gap by providing the first integrated, process-based, spatially explicit quantification of how urban land-cover change reduces natural groundwater replenishment in one of India's fastest-growing metropolitan regions.

3.3 Data collection

3.3.1 Meteorological data

Meteorological data necessary for the current investigation were obtained from credible national and international sources to guarantee precision and uniformity. Daily precipitation data were acquired from the Central Water Commission, India-WRIS using the geographical coordinates (latitude and longitude) corresponding to the study area. Daily temperature data were sourced from the NASA POWER database.

3.3.2 Spatial data

Various thematic maps, Digital Elevation Model (DEM), land use/land cover, and soil maps utilizing CARTOSAT and BHUVAN satellite data, preparations have been conducted in ArcGIS for the study area. The Digital Elevation Model (DEM) was obtained with a spatial resolution of 30 meters, which is widely used for watershed-scale hydrological modelling and has been successfully applied in numerous SWAT studies and appropriate for urban-scale hydrological modelling after requisite sink filling and reprojection to UTM Zone 43N.

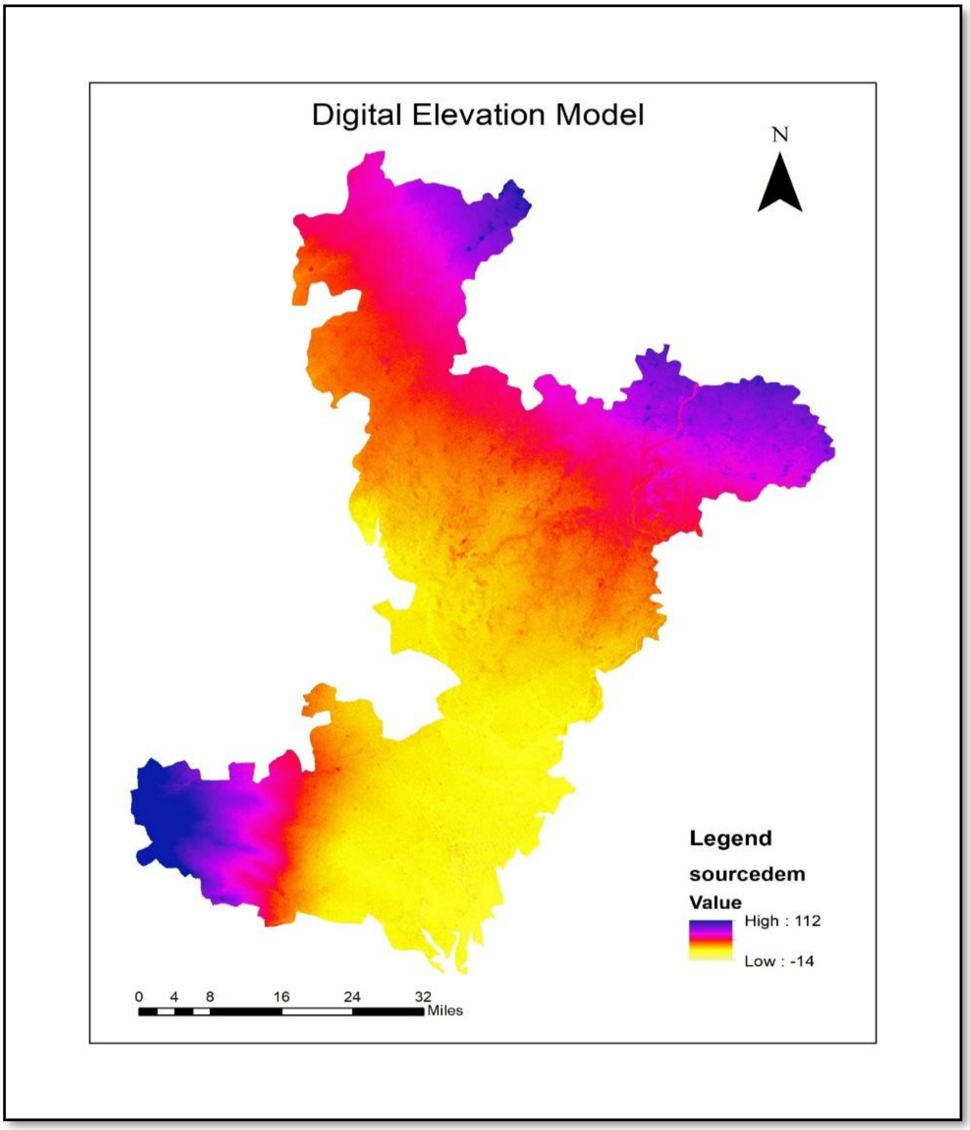

Figure 3.5 Digital elevation model of the study area

The elevation of the study area ranges from –14 m to 114 m above mean sea level. The minimum elevation (–14 m) occurs in only two raster cells, indicating an isolated DEM data uncertainty rather than an actual topographic depression. As these cells represent a negligible portion of the study area, they are not expected to significantly affect the watershed representation or the SWAT model simulations

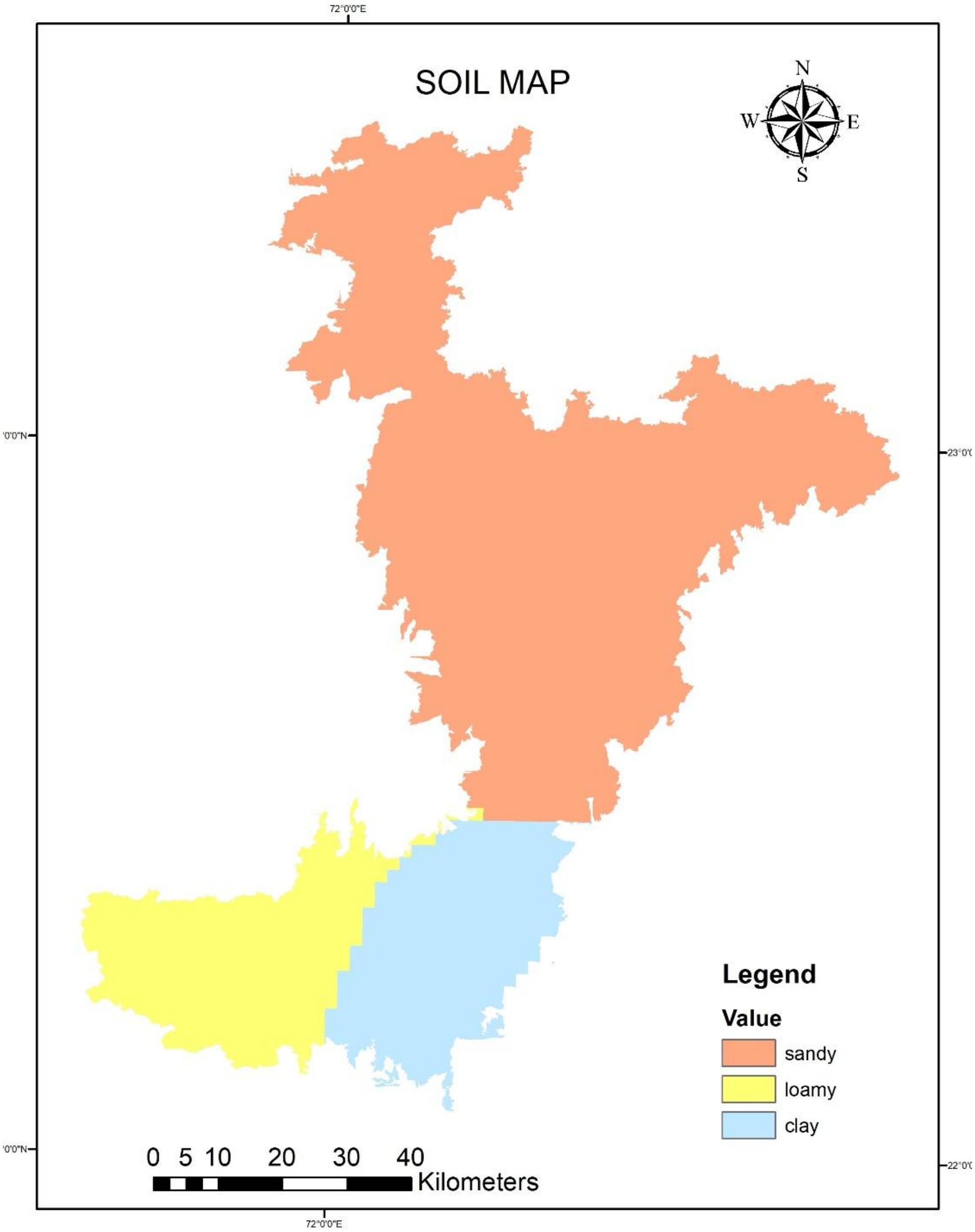

Figure 3.6 Soil map of the study area

3.3.3 Land use land cover (LULC) decadal maps.

Land Use Land Cover (LULC) data is an important type of spatial data used in hydrological modelling. The study generated decadal land use and land cover maps of the Ahmedabad district for four different time intervals, i.e. 1985, 1990, 2005, and 2017. The selected time points were selected to represent the peak period of urban expansion in the district which started in the late 1990s and intensified post 2010. The decadal intervals provide significant comparison of landscape change rates and provide essential input data to the SWAT model across different LULC scenarios.

The primary data source for LULC mapping in this study was the Landsat satellite data archive, which offers the most comprehensive continuous space-based record of the Earth's land surface. Landsat data are globally consistent, freely available, and possess a spatial resolution of 30 meters, rendering them appropriate for regional hydrological study. *Table 3.2* delineates the specific Landsat sensors employed during each decade.

Table 3.2 Detailed information about the satellite data used in this study

Satellite	**Sensor**	**Acquisition date**	**Spatial resolution (m)**	**Spectral band(s)**
Landsat -8	OLI/TIRS	26/03/2017	30	B1 (Blue): 0.45–0.52 B2 (Green): 0.53–0.59 B3 (Red): 0.60–0.69, B4 (NIR): 0.76–0.90
Landsat-5	TM	08/02/1995	30	B1 (Blue): 0.45–0.52 B2 (Green): 0.53–0.59 B3 (Red): 0.60–0.69 B4 (NIR): 0.76–0.90
Landsat-5	TM	25/04/2005	30	B1 (Blue): 0.45–0.52 B2 (Green): 0.53–0.59 B3 (Red): 0.60–0.69 B4 (NIR): 0.76–0.90

3.4 Hydrological monitoring station (Vasna Barrage)

The hydrological response of the study area was evaluated using observed streamflow data obtained from the Vasna barrage hydrological monitoring station. The watershed draining towards the Vasna barrage on the Sabarmati River was selected for hydrological modelling and groundwater recharge assessment using the SWAT model. The Vasna barrage was considered the outlet point of the watershed for streamflow simulation, model calibration, and validation based on observed discharge data availability.

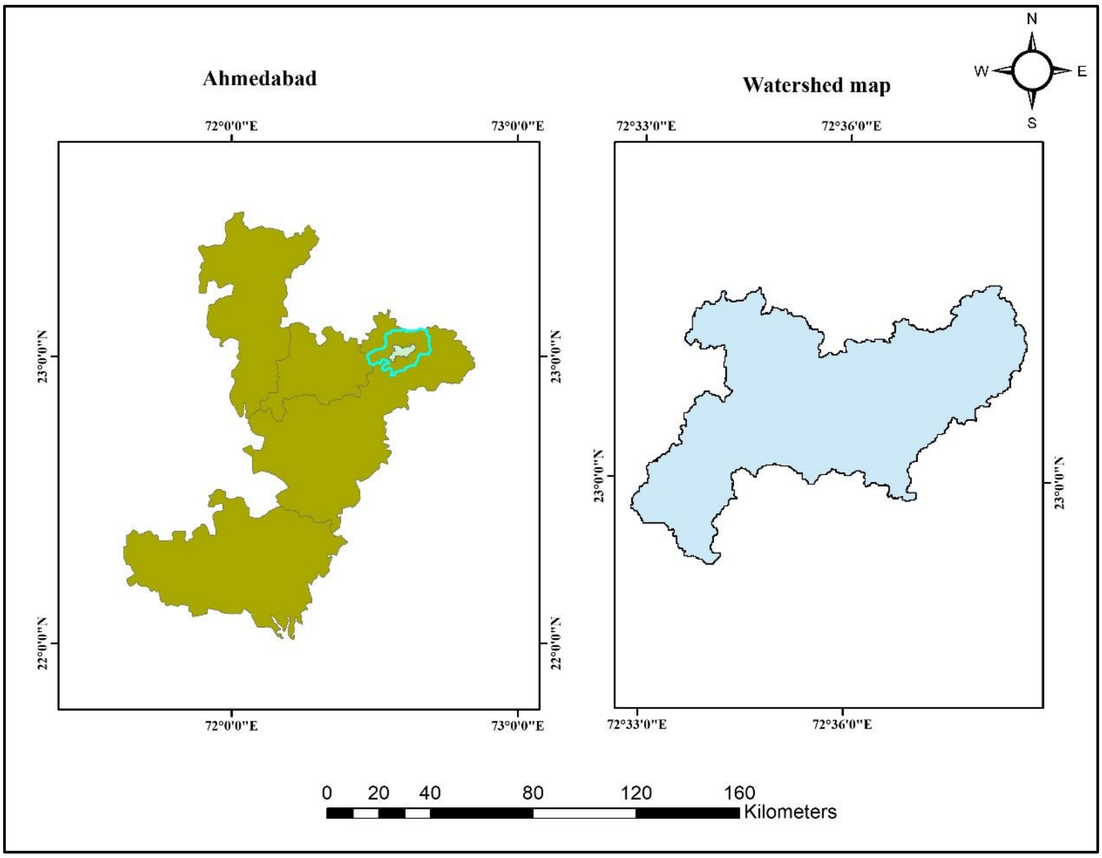

Figure 3.7 Hydrological monitoring point at Vasna Barrage within the study area

Figure 3.7 illustrates the location of the Vasna Barrage hydrological monitoring station within Ahmedabad district. The watershed was delineated using DEM data by considering Vasna barrage as the outlet point of the basin. The watershed represents the hydrological catchment contributing runoff and recharge towards the Sabarmati River in Ahmedabad district. The station is situated along the Sabarmati River and represents the primary monitoring point used for obtaining observed discharge data for the watershed. The delineated watershed therefore forms the basis for streamflow simulation, model calibration, validation, and groundwater recharge estimation in the study.

3.5 Hydrological data

Hydrological data comprising observed streamflow records from Vasna Barrage were obtained from the Ahmedabad Irrigation Department, Government of Gujarat, covering the duration from 2014 to 2024. The discharge data collected was in the form of daily streamflow data, which was later converted to monthly and annual flow series for hydrological analysis.

The observed streamflow data illustrates the hydrological response of the watershed discharging into Vasna Barrage across the Sabarmati River basin, which is used to evaluate the performance and accuracy assessment of the SWAT model under different hydrological conditions.

3.6 Future climate data

Future hydrological conditions of the study area were assessed using climate projection data obtained from the Coupled Model Intercomparison Project Phase 6 (CMIP6) database through the Inter-Sectoral Impact Model Intercomparison Project (ISIMIP) platform (ISIMIP, 2023).

This study used the Shared Socioeconomic Pathway scenario SSP3-7.0 for future hydrological simulations and groundwater recharge evaluations from 2021 to 2050. The SSP3 -7.0 scenario delineates a medium-to-high greenhouse gas emission trajectory denoted by regional competition, intensifying socioeconomic difficulties, and comparatively elevated radiative forcing conditions (O'Neill et al., 2017).

Table 3.3 Details of CMIP6 climate projection data used in the study

Data type	Climate model source	Scenario used	Variables used	Time period	Purpose
Future climate projection data	CMIP6 dataset obtained from the Inter-Sectoral Impact Model Intercomparison Project (ISIMIP)	SSP3 -7.0	Precipitation and Temperature	2021-2050	Future groundwater recharge and hydrological simulation using the SWAT model

Table 3.3 presents the details of CMIP6 climate projection datasets utilised in the present study for future hydrological simulation and groundwater recharge assessment.

3.7 Software and tools used

Table 3.4 Software and tools utilized in the study

Software	Purpose
ArcGIS 10.3	Spatial analysis, watershed delineation, map preparation
ArcSWAT 2012	Hydrological modelling
SWAT-CUP 2012	Calibration, validation, sensitivity analysis
SWAT Output Viewer 0.1.3.0	Visualization and analysis of SWAT model outputs

Table 3.4 presents the software and analytical tools utilised in the present study for geospatial analysis, hydrological modelling, calibration, validation, and graphical

representation of results. ArcGIS and ArcSWAT were primarily used for spatial data processing, watershed delineation, Hydrological Response Unit (HRU) generation, and SWAT model setup. SWAT-CUP was utilised for sensitivity analysis, model calibration, and validation using observed streamflow data. Additional statistical analysis, graphical representation, and data processing were carried out using Microsoft Excel and other supporting software tools.

3.8 Coordinate system and projection system

All spatial datasets utilised in the present study were projected into a common coordinate reference system to ensure spatial consistency during GIS analysis and SWAT model simulation. The datasets were processed using the World Geodetic System (WGS 84) coordinate system and appropriate Universal Transverse Mercator (UTM) projection zone for the Ahmedabad district.

3.9 Summary

The study area of this research is Ahmedabad. Ahmedabad is the largest city of Gujarat, western India. It is situated along the banks of the Sabarmati River. The city mostly lies on the level alluvial plains, with the Sabarmati River serving as the central drainage. The changing rainfall regime of the region, with more intense monsoon rainfall within a shorter window, further amplifies the runoff response of expanding impervious surfaces. These qualities make Ahmedabad an ideal example to evaluate the impact of urbanisation on groundwater recharge.

To this end, a wide range of datasets was compiled, including a 30 m SRTM DEM, multi-temporal Landsat 8 data for LULC, soil data from FAO, historical meteorological data (1981–2020) and future climate projections from the ISIMIP3b bias-adjusted CMIP6 dataset under the SSP scenario centered on 2050. The stream flow data of Ahmedabad irrigation department were used for calibration and validation of the model. All datasets were pre-processed into SWAT compatible formats to allow quantification of historical (1981–2020) and projected (2050) changes in groundwater recharge under different urbanisation and climate scenarios, directly addressing the objectives identified in the study area.

CHAPTER 4
TREND ANALYSIS

4.1 General

In India, rainfall and temperature patterns have exhibited noticeable changes over recent decades due to climate variability and increasing anthropogenic influences. These climatic variables play a critical role in regulating the hydrological cycle, particularly processes such as infiltration, evapotranspiration, and groundwater recharge (Freeze & Cherry, 1979). Over the past few decades, Ahmedabad has experienced significant urban growth, which has led to extensive modifications in land use and land cover. The replacement of natural surfaces with impervious structures has reduced the capacity of the land to absorb rainfall, consequently reduces groundwater replenishment. However, modifications in recharge patterns cannot be attributed only by urbanisation, as climatic variability also plays a crucial role. Therefore, this study analyses long-term trends in rainfall and temperature to better understand the combined and individual impacts of climate variability and urban development on groundwater systems (Kundzewicz & Robson, 2004). To carry out this assessment, Initially, a linear trend line was fitted to the time series data to provide a visual representation of the direction of change over the study period. This graphical method helps in identifying general increasing or decreasing patterns in the dataset. To determine the statistical significance of the observed trend, historical climatic records were analysed over a prolonged period, incorporating both annual and seasonal variations. The Mann–Kendall (MK) test was applied to find the presence of statistically significant trends in the time series data.

The research work is initiated by collecting the observed weather data of 40 years for the said study area and statistical analysis is performed. This method determines the trend of rainfall and temperature over time variation.

4.2 Rainfall analysis

The average annual rainfall for the period 1981–2020 was conducted to understand long-term trend in the study area. The India Meteorological Department, SWDC, CWC, provides historical climatic data for a duration of forty years. A linear trend line was fitted to the rainfall time series to find the direction of change over the study period. This graphical analysis provides an initial understanding of rainfall patterns supported by statistical analysis using the Mann–Kendall test.

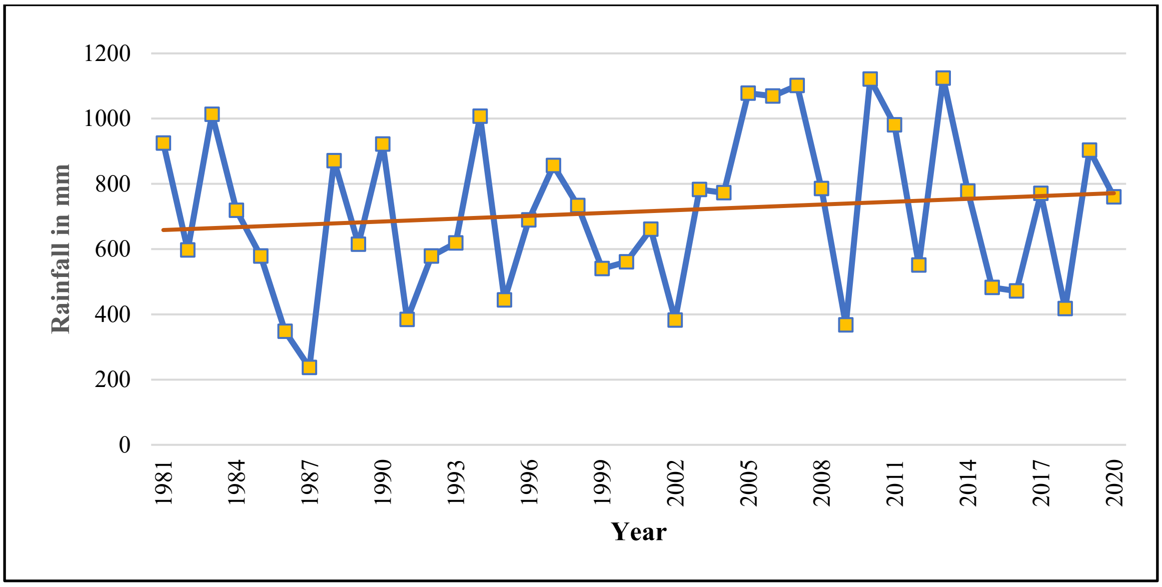

Figure 4.1Annual average rainfall of 1981-2020

Figure 4.1 represents the yearly rainfall measurements in mm for the study area. A linear trend line was fitted to the annual rainfall data to assess the direction of change. The trend equation has a slope of 2.89 mm/yr, indicating an upward trend in rainfall during the study period.

To examine intra-seasonal variability within the monsoon period, a month-wise trend analysis was carried out for June, July, August, and September for the period 1981–2020 in the study area.as shown in figure 4.2 (a) to 4.2(d).

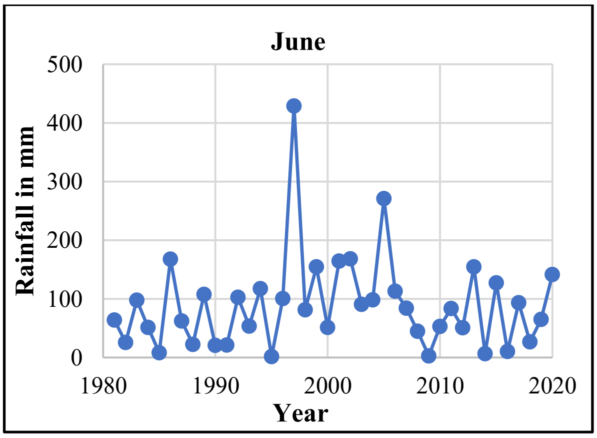

Figure 4.2(a)

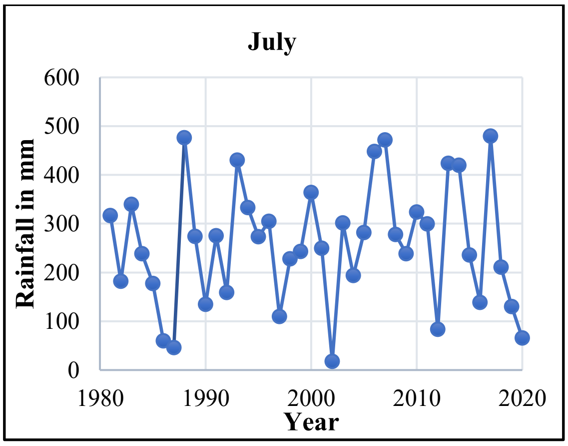

Figure:4.2(b)

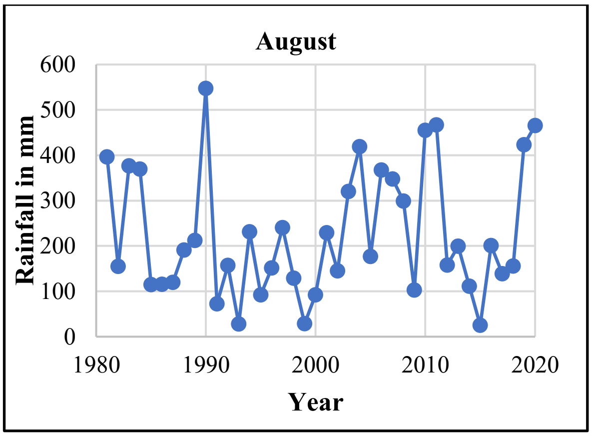

Figure 4.2(c)

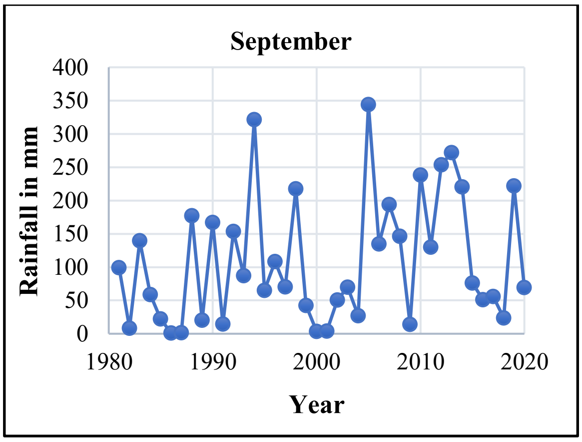

Figure:4.2(d)

Figure 4.2 (a to d) Time series analysis of rainfall for individual monsoon months (June, July, August, and September) from 1981 to 2020

4.3 Temperature analysis

The long-term variation in temperature was analysed for the period 1981–2020 to understand climatic changes in the study area. Annual average values of maximum and minimum temperature were computed and plotted against time.

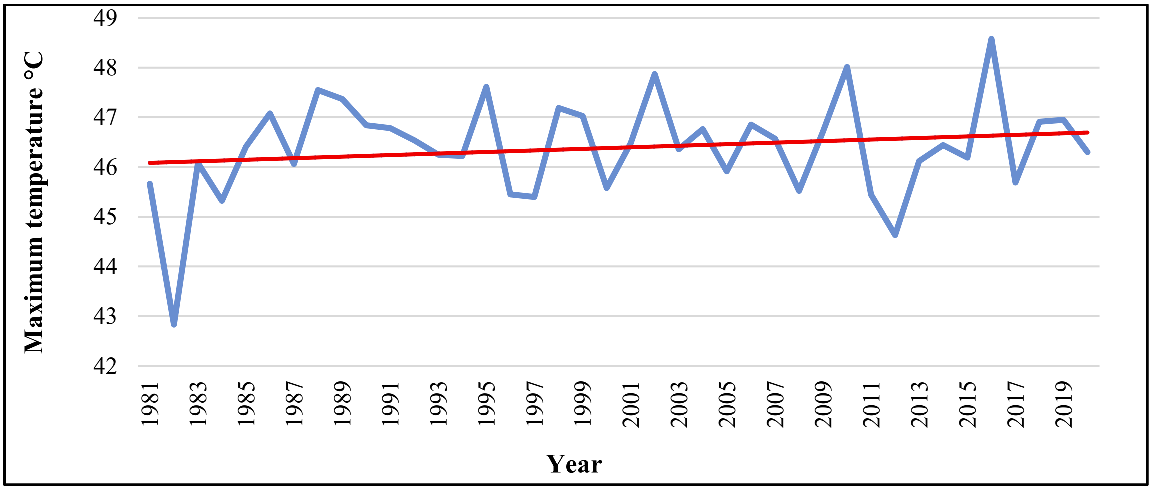

Figure 4.3 Longterm trend in the annual maximum temperature, from 1981 to 2020

The long-term trend in annual maximum temperature, as illustrated in Figure 4-3, indicates a rising tendency. The average annual maximum temperature was highest in the year 2016, i.e., 48.58 °C.

Similarly, average annual minimum temperature, as shown in Figure 4.4, is highest in the year 2009 and lowest in the year 1991. The observed variability in temperature may result from atmospheric circulation patterns, increasing greenhouse gas concentrations, and land use modifications, all of which contribute to alterations in local climatic conditions. Both the time series of minimum and maximum temperature show a significant upward trend. The Mann–Kendall test further supports the linear trend line's confirmation of an increasing tendency.

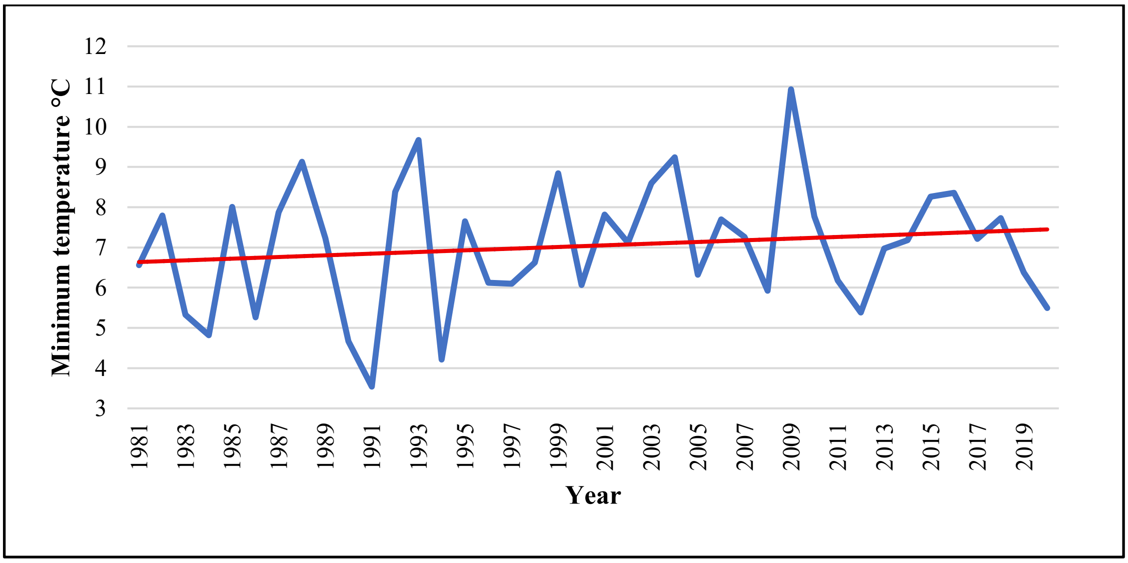

Figure 4.4 Longterm trend in the annual minimum temperature from 1981 to 2020

The linear trend analysis provides a preliminary understanding of the trend in the time series data. To obtain a statistically robust assessment of the trends, the Mann–Kendall (M–K) test, which is a non-parametric method, was applied.

4.4 Trend analysis using the Mann–Kendall test method

The Mann–Kendall (MK) test is a widely used nonparametric method to detect trends in time series data (Mann, 1945). Unlike parametric tests, the MK test does not assume any particular distribution of the data. Instead, it relies on rank correlation, evaluating whether values tend to increase or decrease consistently over time. The test statistic is calculated by comparing all possible data pairs in the series. A positive value indicates an upward trend, while a negative value indicates a downward trend. Two hypothesis tests have to be tested in the MK: The null hypothesis is denoted as H_0, while the alternative hypothesis is denoted as H_a. The null hypothesis defines that there is no trend in the concerned time series, and in the alternative hypothesis there is a significant trend in the time series. The MK test does not require the assumption of normality and indicates both the direction and the magnitude of significant trends. The Mann-Kendall test measures values (Xj-Xk) for cases where j is greater than k, and the test statistic S is computed using a specific formula.

$$S = \sum_{k=1}^{n-1} \sum_{j=k+1}^{n} \operatorname{sgn}(Xj - Xk) \quad \textbf{4.1}$$

In this context, Xj and Xk represent the annual values for the years j and k, where j is greater than k.

$$\operatorname{sgn}(Xj - Xk) = \begin{cases} 1 & \text{if } Xj - Xk > 0 \\ 0 & \text{if } Xj - Xk = 0 \\ -1 & \text{if } Xj - Xk < 0 \end{cases} \qquad \textbf{4.2}$$

The test statistics τ can be computed as

$$\tau = \frac{S}{n(n-1)/2} \qquad \textbf{4.3}$$

It is necessary to compute the probability associated with S and the sample size n to statistically quantify the significance of the trend. The calculating formula of variance S is denominated as;

$$VAR(S) = \frac{1}{18}\left[n(n-1)(2n+5) - \sum_{p=1}^{q} t\,p(tp-1)(2tp+5)\right] \qquad \textbf{4.4}$$

Where q is defined as the number of tied groups and tp is the number of data in the p^{th} group. The values of S and VAR(S) are used to calculate the test statistic Z, which is the following:

$$Z = \begin{cases} \frac{S-1}{\sqrt{VAR(S)}} & \text{if } S > 0 \\ 0 & \text{if } S = 0 \\ \frac{S+1}{\sqrt{VAR(S)}} & \text{if } S < 0 \end{cases} \qquad \textbf{4.5}$$

Z scores follow a normal distribution. If Z is negative and its absolute value is greater than the significance level, the trend is decreasing; if Z is positive and greater than the significance level, it is increasing.

The present research work begins with the collection of long-term observed weather data for the study area of Ahmedabad. The India Meteorological Department, CWC, and SWDC provide historical climatic data spanning forty years. This research utilizes its results to create scenarios in hydrological modelling (ArcSWAT) by identifying the trends of temperature and rainfall over temporal variation. The combined impact of rainfall and temperature modifies the hydrological regime.

A detailed trend analysis of long-term rainfall and temperature data was carried out using the non-parametric Mann–Kendall (MK) test for a period of four decades. The Mann–Kendall test is widely used in hydro-climatic studies because of its suitability for analysing time-series data that do not necessarily follow a normal distribution and are often influenced by extreme values. The analysis was performed to evaluate the temporal variations in rainfall and temperature to identify whether these parameters show increasing or decreasing trends. The results of the detailed trend analysis (presented in Appendix-A) clearly indicate noticeable changes in rainfall and temperature over the study period. These trends were further utilised to develop different climatic scenarios, which were incorporated into the hydrological modelling process to assess their impact on groundwater recharge under rapidly urbanising conditions.

4.5 Summary of trend analysis

Trend analysis using the non-parametric Mann–Kendall (MK) test is carried out to determine the significance of trends in maximum temperature, minimum temperature, and rainfall over a defined period in the study area. The detailed trend analysis clearly indicates noticeable temporal changes in rainfall and temperature. These findings are directly influencing the hydrological characteristics of the region. The observed trends were further utilized to develop different climatic scenarios, and their impact on key hydrological parameters, such as groundwater recharge, is analysed using hydrological modelling.

The monthly trend analysis of maximum and minimum temperature was performed to understand seasonal variations and the direction of temperature change across different months.

Table 4.1 Summary of trend analysis (Temperature)

Month 1981-2020	Mann–Kendall Z-statistic (Maximum Temperature)	Mann–Kendall Z-statistic (Minimum Temperature)
January	-1.73	0.07
February	0.79	0.44
March	0.74	0.08
April	1.21	2.56
May	0.16	2.46
June	-0.73	0.92
July	-1.34	1.14
August	-0.34	0.43
September	-2.34	-1.41
October	-1.97	-1.10
November	-1.97	1.89
December	-1.64	-0.50

Table 4.1 shows Mann–Kendall Z-statistics, which are used to identify both the direction and statistical significance of temperature trends. A positive Z-statistic indicates an increasing trend, whereas a negative Z-statistic indicates a decreasing trend. Above summarised value suggesting the increasing trend is more pronounced during the summer months. The minimum temperature for most of the month also shows an increasing trend. This trend suggests a reduction in diurnal temperature variation and is consistent with observed warming patterns in semi-arid regions.

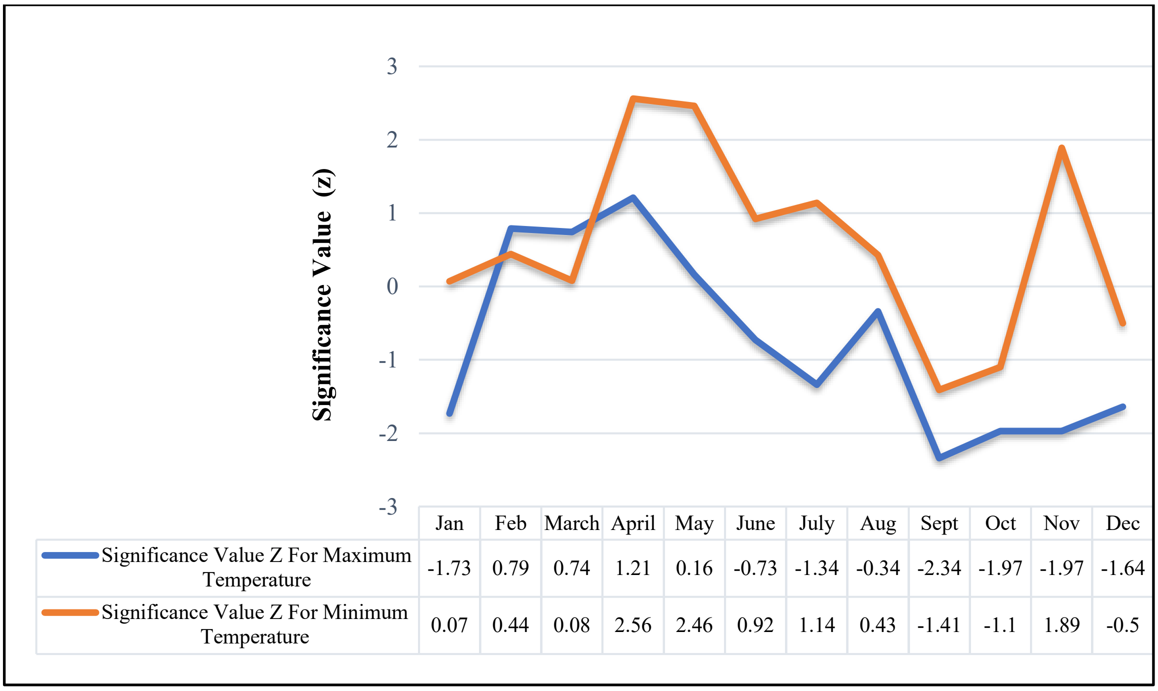

	Jan	Feb	March	April	May	June	July	Aug	Sept	Oct	Nov	Dec
Significance Value Z For Maximum Temperature	-1.73	0.79	0.74	1.21	0.16	-0.73	-1.34	-0.34	-2.34	-1.97	-1.97	-1.64
Significance Value Z For Minimum Temperature	0.07	0.44	0.08	2.56	2.46	0.92	1.14	0.43	-1.41	-1.1	1.89	-0.5

Figure 4.5 Significance values of maximum and minimum temperature from trend analysis

The rainfall analysis was performed for annual and monthly as well as seasonal rainfall, including monsoon, post-monsoon, and winter periods. Table 4.2 displays the results of the rainfall trend analysis. The annual monsoon and premonsoon rainfall analysis shows an upward trend. For the post-monsoon season, it indicates a decreasing trend. Overall, as indicated in Table 4.2, the rainfall trends vary across different seasons, with the monsoon season having the most significant influence on annual rainfall variability. The graphical representation of significance value of rainfall from trend analysis is shown in Figure 4.6.

Table 4.2 Summary of trend analysis (Rainfall)

Month (1981-1920)	Z	Trend
January	-1.06	-Ve
February	-0.43	-Ve
March	0.31	+Ve
April	0.13	+Ve
May	-0.54	-Ve
June	0.36	+Ve
July	0.15	+Ve
August	0.71	+Ve
September	1.60	+Ve
October	-0.34	-Ve
November	-0.38	-Ve
December	0.81	+Ve
Annual	0.81	+Ve
Monsoon	0.87	+Ve
Premonsoon	0.22	+Ve
Post-monsoon	-0.44	-Ve

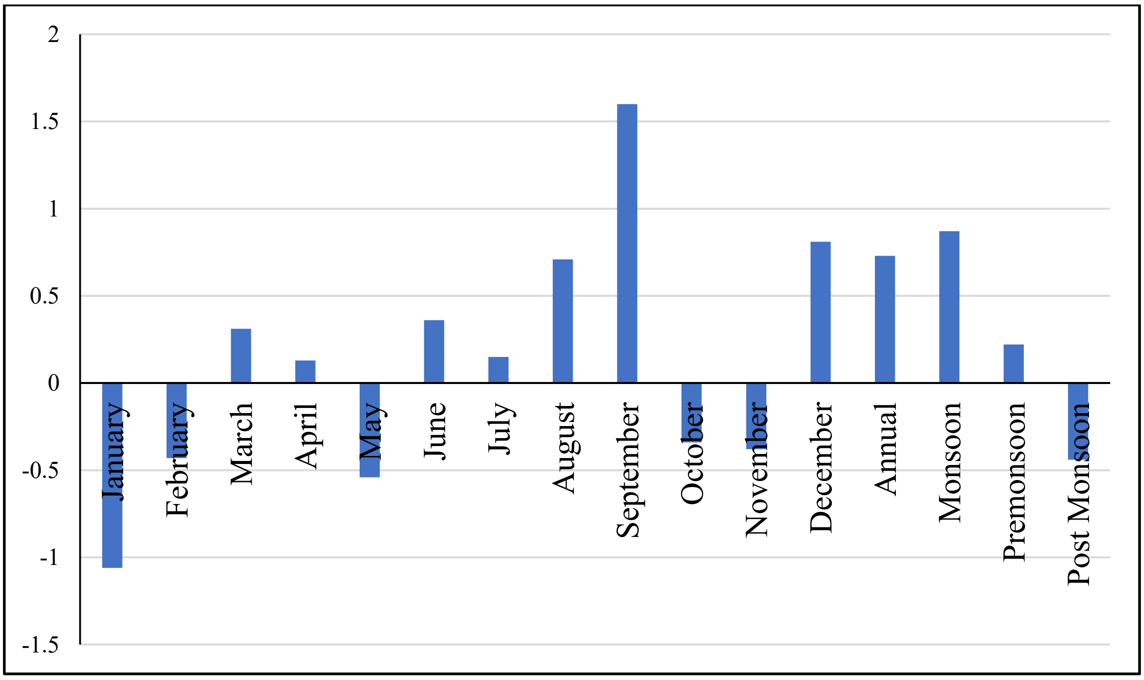

Figure 4.6 Significance values of rainfall from trend analysis

Following the presentation of the Mann–Kendall (MK) test results, a graphical representation has been included to further illustrate the observed rainfall trends in the study area. Figure 4.7 presents the temporal variation of monsoon rainfall over the study period. As the monsoon period contributes the largest share of annual rainfall and plays a crucial role among the different seasonal analyses carried out, only the rainfall graph for the monsoon season is presented here. The scattered data points represent the observed rainfall values for individual years. Several years exhibit relatively high rainfall events, while others reflect below-average precipitation, highlighting the irregular nature of monsoon behaviour. Figure 4.8 to 4.10 shows rainfall trend analysis of post monsoon, Pré monsoon and winter months using the Mann-Kendall test.

All monthly datasets were uniformly processed and the results were presented in Appendix A.

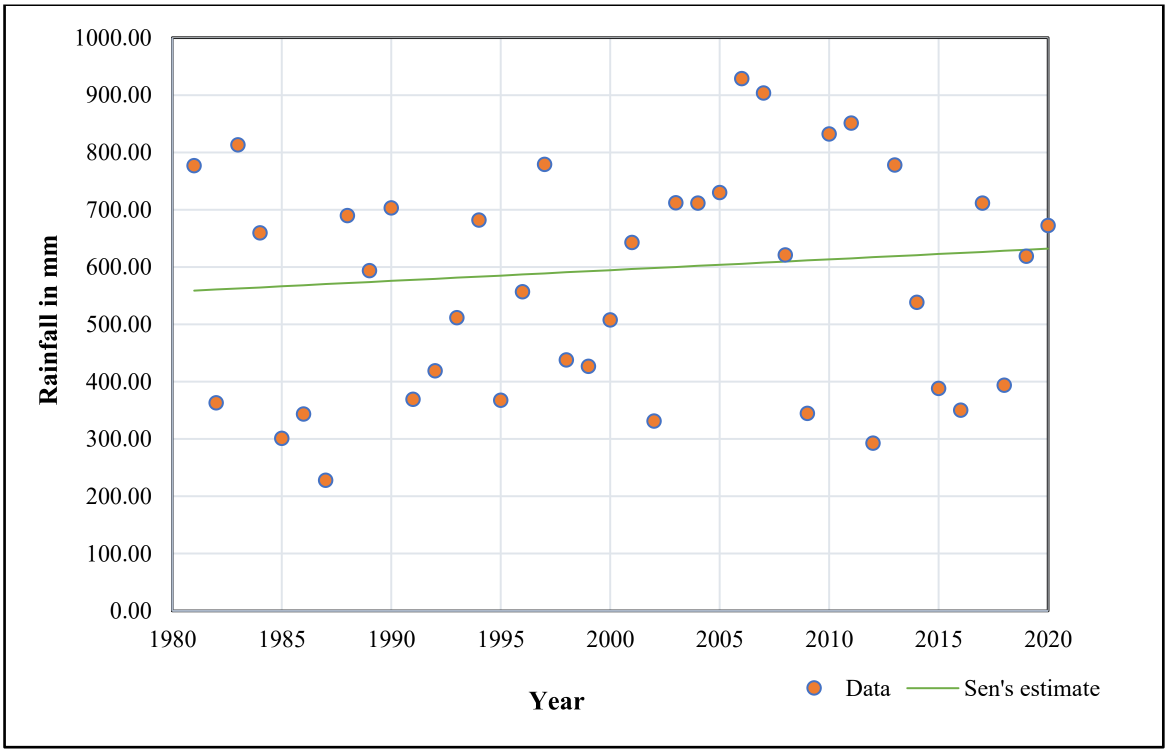

Figure 4.7 Trend analysis of monsoon month rainfall using the Mann–Kendall test

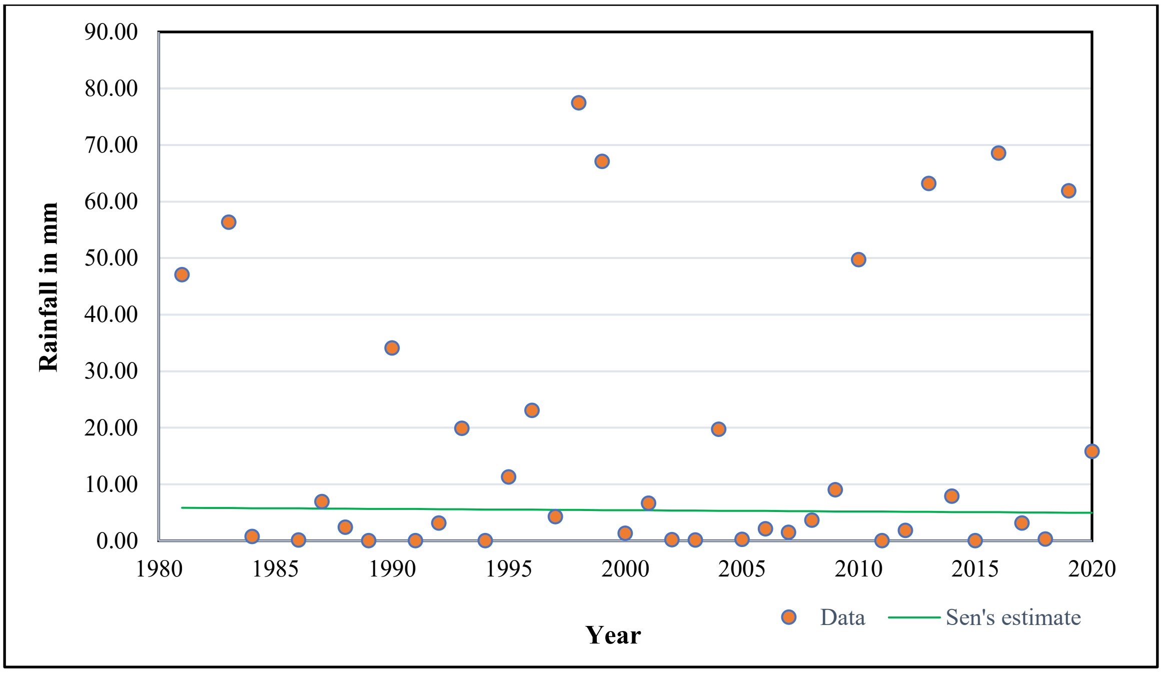

Figure 4.8 Trend analysis of post-monsoon month rainfall using the Mann–Kendall test

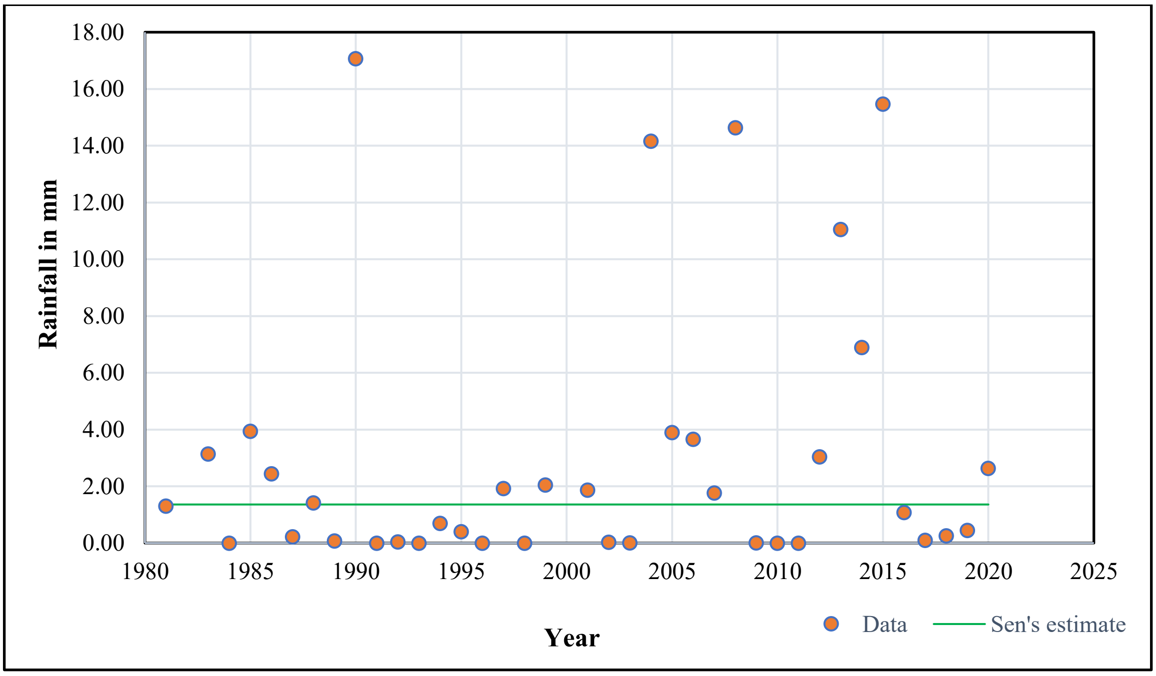

Figure 4.9 Trend analysis of pre-monsoon month rainfall using the Mann–Kendall test

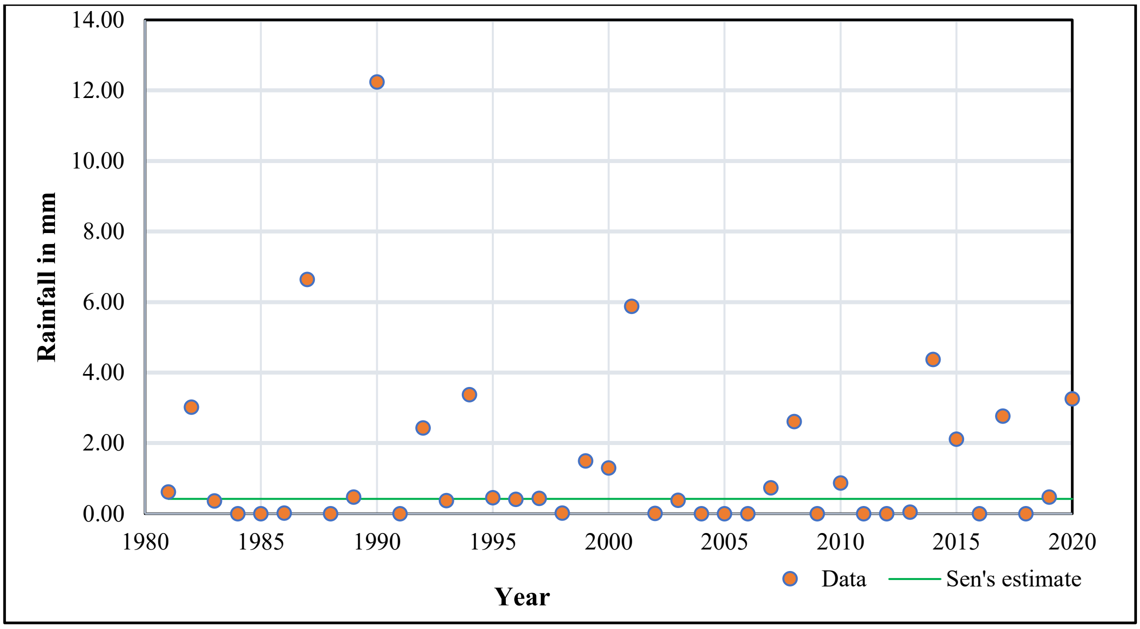

Figure 4.10 Trend analysis of winter month rainfall using the Mann–Kendall test

The trend analysis shows that for most of the months positive Z values were observed, with the monsoon *(Z = 0.87)* and annual *(Z = 0.81)* periods, which indicate a general increasing tendency in rainfall, but negative Z values in a certain month and during winter show minor decreasing tendencies. This indicates that rainfall variability, rather than a sustained trend, is the preliminary climatic feature in the study area. Such findings are essential for hydrological and groundwater recharge assessments.

The positive trend for maximum temperature ranging from *0.16 to 1.21* for February to May, and the negative trend from June to January ranging from *-0.34 to -1.97*.

For minimum temperature, most of the month shows the positive trend ranging from *0.07 to 2.5*.

The above results shows that rainfall trends remain largely insignificant with high variability on both seasonal and monthly basis, the increasing temperature trend may significantly influence hydrological processes such as groundwater recharge in the study area.

This chapter focused on the analysis of long-term variability of rainfall and temperature in the study area using statistical trend analysis techniques. The Mann–Kendall (M–K) test and Sen's slope estimator were used to assess temporal trends in hydro-climatic parameters on annual, seasonal, and monthly basis. However, climatic variability alone does not entirely control hydrological response. Anthropogenic factors like land use modification significantly alter natural hydrological systems.

The subsequent chapter focuses on Land Use/Land Cover (LULC) mapping and change detection analysis using remote sensing and GIS techniques to further understand the spatial and temporal changes occurring within the study area. The next chapter aims to evaluate the extent of urban expansion and land use transformation over different decades and assess their potential impact on hydrology and groundwater recharge dynamics within the study area.

CHAPTER 5
LAND USE LAND COVER (LULC) MAPPING AND CHANGE DETECTION

5.1 General

Land Use/Land Cover (LULC) mapping and change detection are the principal component of this research, as urbanisation is one of the anthropogenic factors altering groundwater recharge mechanisms in the study area. Quantifying the spatial extent and pattern of LULC modifications over time is essential for understanding how urban expansion has progressively reduced the natural infiltration, thereby affecting aquifer replenishment (Garg & Singh, 2010; Jensen, 2005). Remote sensing and Geographic Information System (GIS) techniques provide effective tools for multi-temporal LULC mapping and spatial analysis.

This chapter shows the results of the Land Use/Land Cover (LULC) classification for the years 1985, 1995, 2005, and 2017 prepared by supervised classification using the Maximum Likelihood Classification (MLC) technique in ArcGIS 10.3. The spatial distribution and temporal variations in land use and land cover (LULC) classes are examined and interpreted to understand landscape dynamics during the study period.

Satellite imagery from 1985, 1995, 2005, and 2017 was obtained from the USGS Earth Explorer online site and the Esri Sentinel-2 Land Cover, focusing on March, April and May to enhance the probability of obtaining cloud-free images. Landsat datasets were obtained at no cost from the USGS Earth Explorer online archive. The data were downloaded in GeoTIFF format and presented as grayscale photographs of the research area.

5.2 Methodology

This analysis, as shown in Figure 5.1 used supervised classification to categorize the LULC classifications derived from satellite imagery. Designated training sites, representative of known land cover types, are utilized to assign numerical values to different land cover types according to their spectral properties. The Maximum Likelihood (ML) approach, utilized in supervised classification, relies on probability functions and presumes that the training data for each class adhere to a normal distribution throughout each spectral band. The ArcMap 10.3 software is used for the analysis and classification of satellite imagery.

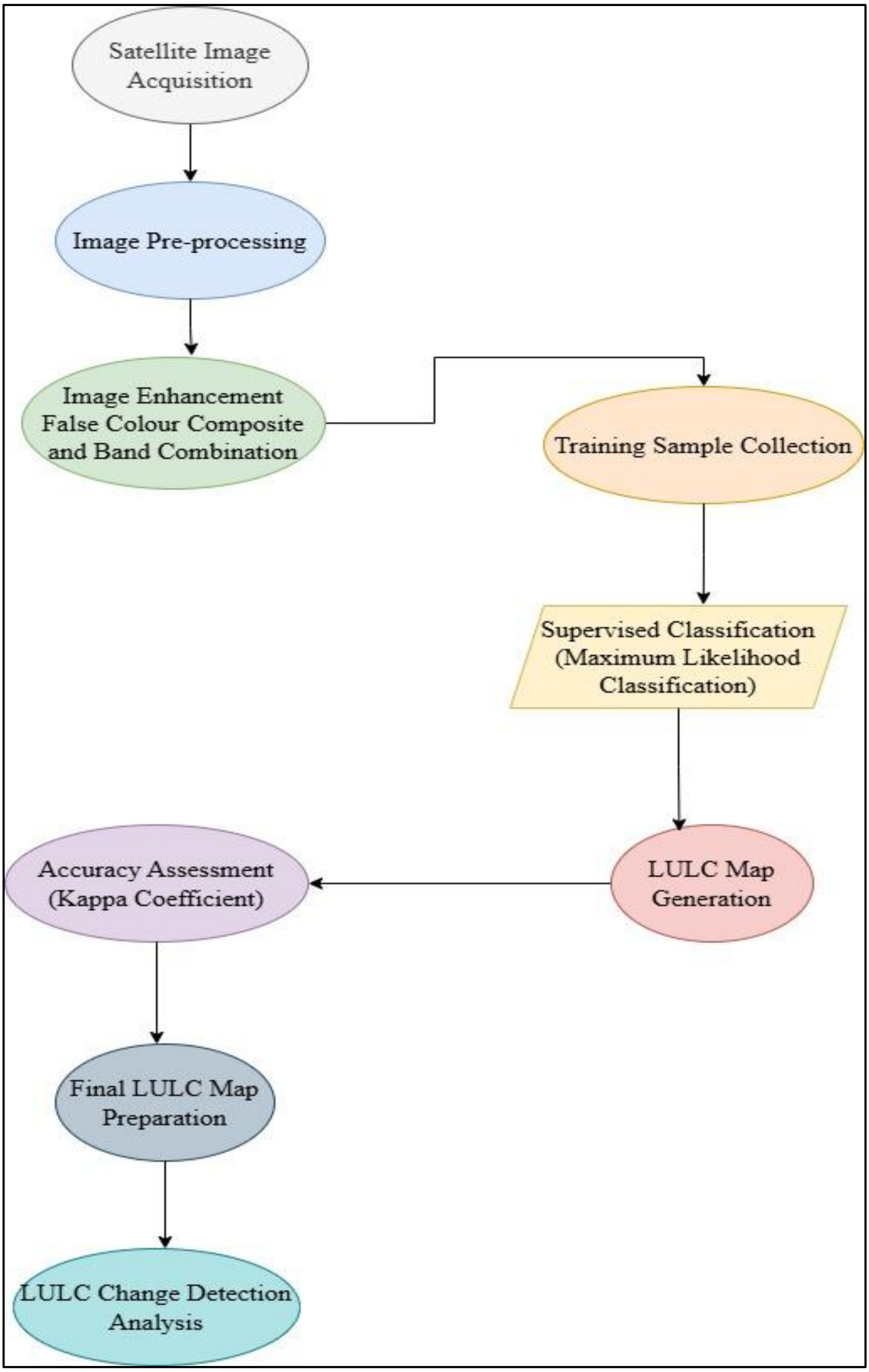

Figure 5.1 Methodological framework for Land use/Land cover (LULC) map preparation and change detection

5.2.1 Data preparation and image preprocessing

Landsat 5 TM images from 1985, 1995, and 2005 are utilized due to their appropriate spatial resolution of 30 meters. whereas Sentinel 2 imagery from 2017 was employed for the most recent time. The files are imported into ArcMap software 10.3 to produce false colour composites (FCC). The USGS Earth Explorer and Sentinel Browser provide satellite imagery free of cost. The datasets are extracted from compressed files after being downloaded in TIF format. The collected images undergo initial processing to improve their quality and spatial accuracy. A natural colour composite (NCC) was generated utilizing the red, green, and blue bands to improve the visual differentiation of various land cover characteristics. Later, all images are projected onto the WGS 1984 coordinate system to ensure spatial consistency. Thereafter, the composite image was cropped to focus particularly on the study area, thus enhancing image processing and analysis with the Extract by Mask tool in the GIS environment.

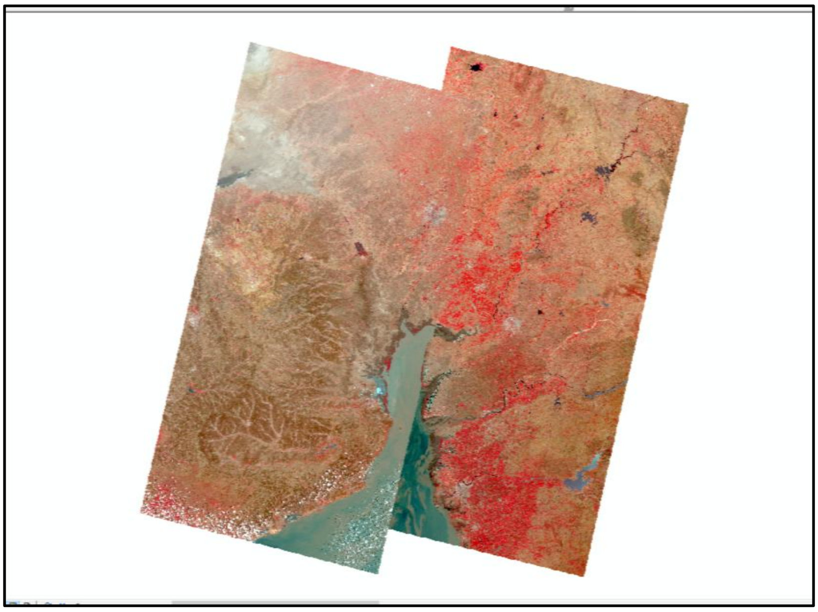

Figure 5.2 Use of mosaic function in preprocessing using ArcMap 10.3

Figure 5.2 shows the utilisation of the Mosaic function during image preprocessing in ArcMap 10.3. The mosaic process was performed to combine multiple satellite image tiles into a single continuous raster dataset covering the entire study area. The generated image was subsequently utilised for image enhancement, clipping of the study area boundary, supervised classification, and Land Use/Land Cover (LULC) mapping.

Following the pre-processing phase, supervised classification was conducted to categorize the satellite images. Through the analysis of both true colour and false colour composites, various categories such as built-up land, wasteland, cropland, waterbodies, shrubland, fallow land and grassland were classified. The study area was extracted from the composite band using the study area shapefile prepared in ArcGIS, and the clipping was performed with ArcGIS tool. The maximum likelihood approach was subsequently employed to categorize the pixels into various land cover classifications based on their spectral attributes. The classification methodology consists of three primary steps: (i) selection of training samples (ii) classification, and (iii) evaluation or accuracy assessment. Training sites were created within the imagery by creating polygons and stored as signature files. Subsequently, these signature files were utilized in the supervised image classification process to produce the LULC map.

5.3 Classification framework for land use and land cover

The Land Use/Land Cover (LULC) classification framework used in this study was developed according to the standard classification framework established by the National Remote Sensing Centre (NRSC), ISRO. The NRSC classification framework is widely used in India for watershed management, environmental assessment, urban planning, and natural resource analysis due to its systematic and regionally suitable classification approach. The original NRSC classification framework (Table 5.1) was referred to and modified based on the dominant land cover characteristics (Table 5.2). The study area was classified into seven major LULC categories, including built-up land, cropland, fallow land, shrubland, grassland, water bodies, and wasteland.

Table 5.1NRSC-based land use and land cover classification

LULC Class Used in Study	Corresponding NRSC Category	Meaning / Description	Hydrological Significance
Built-up land	Built-up land → Urban Area	Areas occupied by residential, commercial, and industrial structures, roads, and urban infrastructure.	Increases impervious surfaces, reduces infiltration, and enhances surface runoff.
Cropland	Agricultural Land → Cropland	Land actively used for cultivation and crop production	Influences infiltration, evapotranspiration, and seasonal groundwater recharge
Fallow land	Agricultural Land → Fallow Land	Agricultural land left uncultivated for a temporary period.	Moderate infiltration potential depending on soil and vegetation conditions
Shrubland	Forest → Scrub Forest	Areas covered with shrubs, bushes, and sparse woody vegetation	Supports infiltration and reduces soil erosion

Grassland	Grass/Grazing Land → Grassland	Land dominated by grasses and herbaceous vegetation cover	Enhances infiltration and groundwater recharge potential
Water bodies	Water Bodies → Rivers/Lakes/Reservoirs	Surface water features including rivers, lakes, reservoirs, ponds, and canals	Contributes to surface storage and groundwater interaction processes
Wasteland	Wasteland → Scrub Land/Barren Land	Unproductive or barren land with sparse vegetation and exposed soil.	Low recharge capacity and limited vegetation cover

Source: National Remote Sensing Centre (NRSC), Indian Space Research Organisation (ISRO), Government of India

.

Table 5.2 Classification scheme for land use/land cover (LULC) utilized in the present study

LULC class	Description	Hydrological Significance
Built-up land	Urban settlements, roads, commercial and industrial infrastructure	Reduces infiltration and increases surface runoff generation
Water bodies	Rivers, lakes, reservoirs, ponds, and canals	Contributes to surface water storage and groundwater interaction
Wasteland	Barren and uncultivated land with sparse vegetation cover	Low infiltration capacity and limited groundwater recharge
Cropland	Agricultural land under active cultivation	Influences evapotranspiration and seasonal recharge processes
Fallow land	Temporarily uncultivated agricultural land	Moderate infiltration potential depending on soil conditions
Shrubland	Areas covered with shrubs and sparse woody vegetation	Supports infiltration and reduces soil erosion
Grassland	Land covered predominantly by grasses and herbaceous vegetation	Enhances infiltration and groundwater recharge potential

Source: Prepared based on the National Remote Sensing Centre (NRSC) Land Use/Land Cover classification framework and satellite image interpretation.

Each LULC category has unique hydrological characteristics. The prepared LULC maps were subsequently integrated with soil, slope, and climatic datasets within the SWAT model to evaluate the impacts of urbanisation and land cover modification on groundwater recharge dynamics in the study area.

5.3.1 Land use and land cover classification for the year 1985

The 1985 LULC map, illustrated in Figure 5.3, represents the baseline condition of the study area. The classification results indicate that agricultural land was the predominant land use category among the entire geographical area.

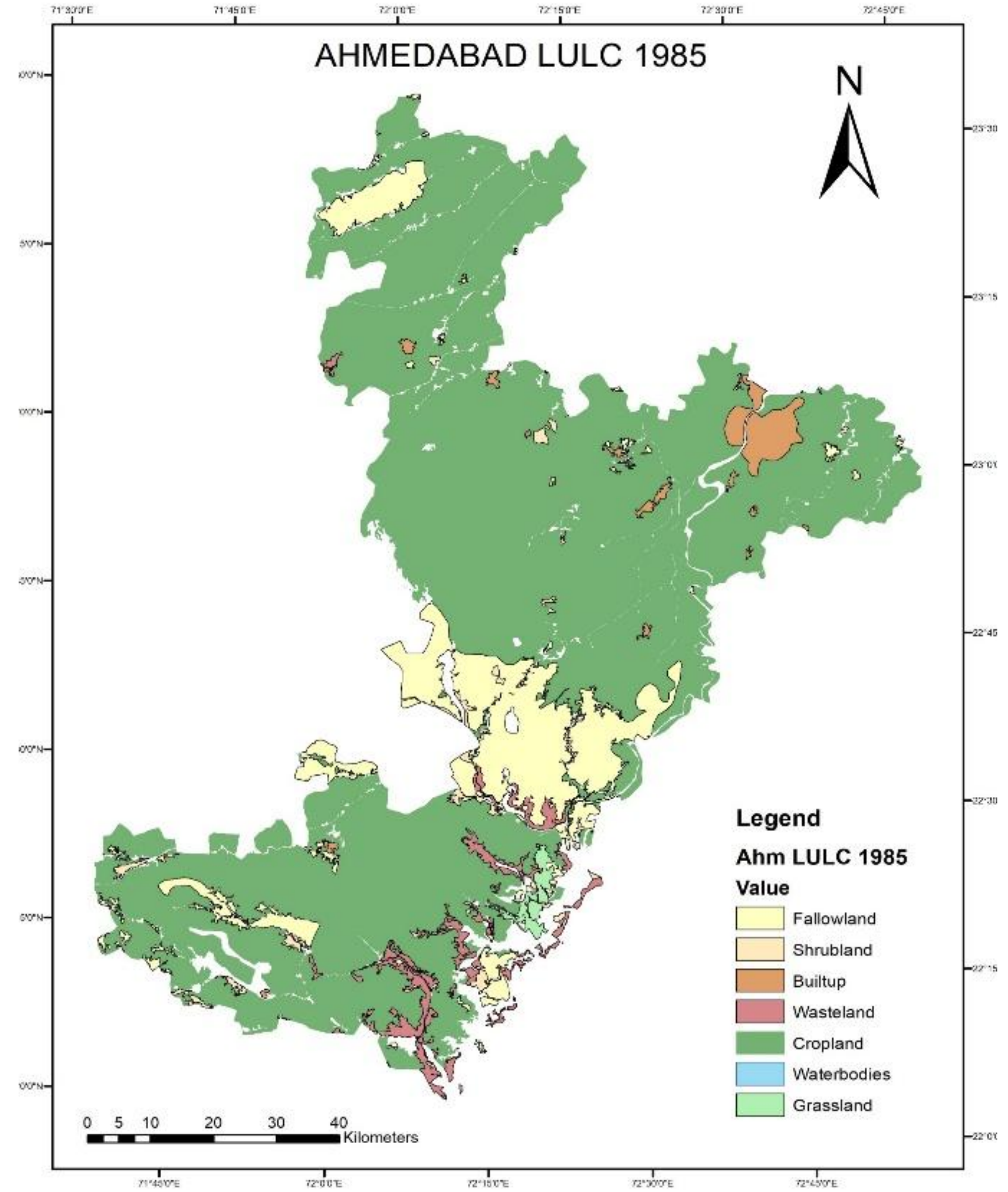

Figure 5.3 LULC map of 1985

5.3.2 Land use and land cover classification for the year 1995

The LULC map for the year 1995, as shown in Figure 5.4, noticeable changes in land use patterns had begun to commence in the Ahmedabad district. Agricultural land remained dominant, but wasteland increased, possibly due to land degradation or fallow agricultural practices.

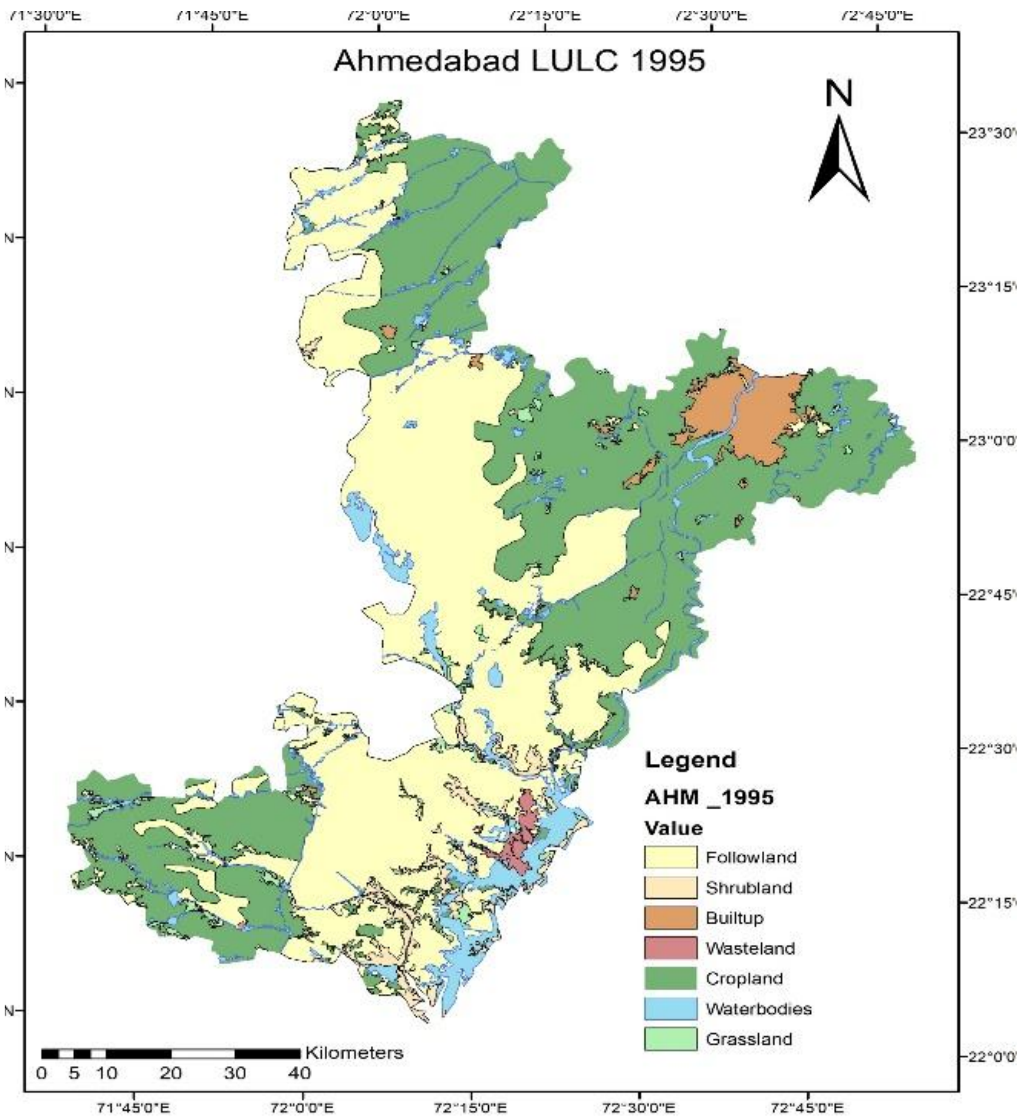

Figure 5.4 LULC map of 1995

5.3.3 Land use and land cover classification for the year 2005

The Land use and land cover map of 2005, as shown in Figure 5.5, shows significant transformations in the Ahmedabad district. Built-up land increased substantially, driven by rapid urbanization

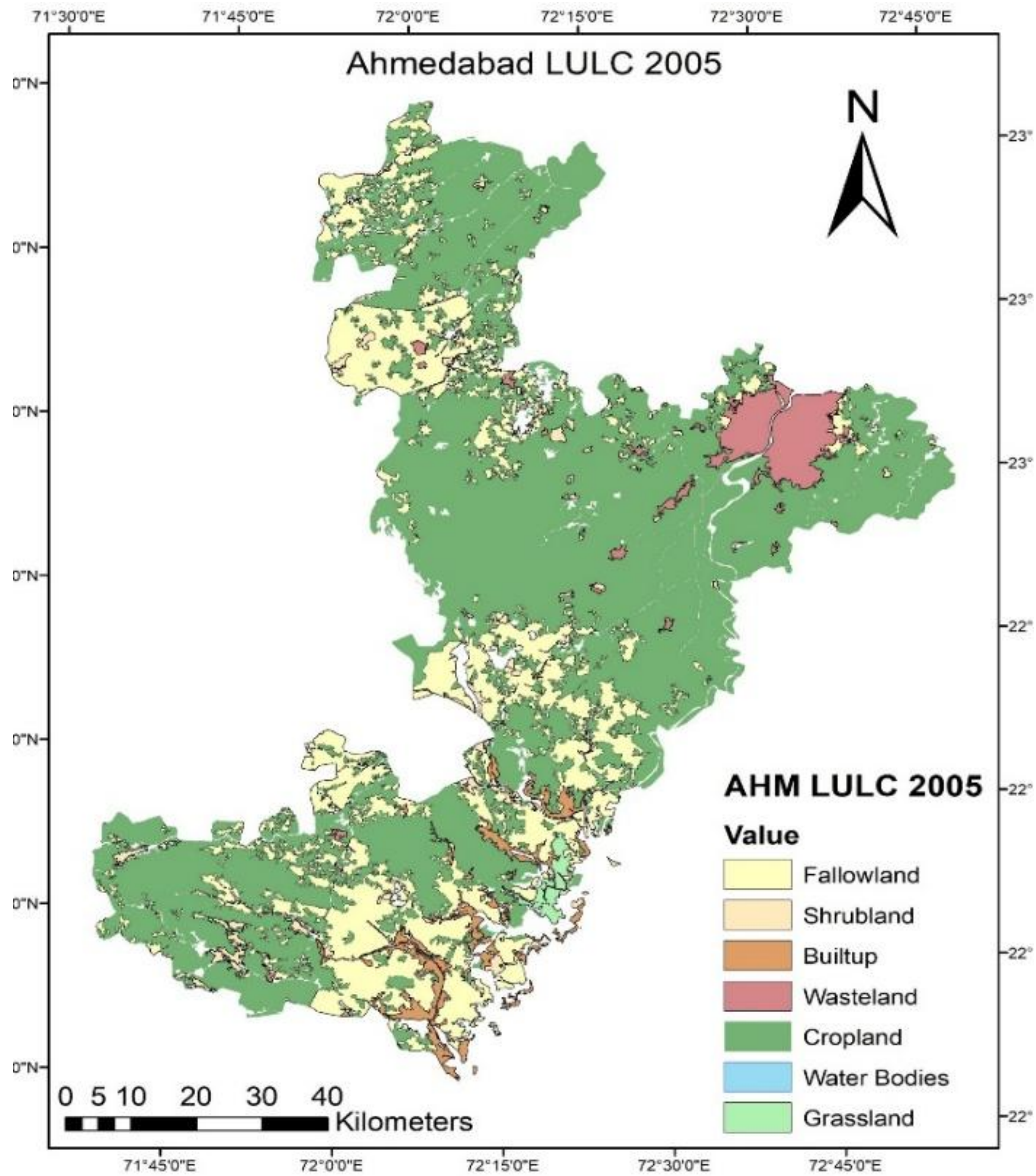

Figure 5.5 LULC map of 2005

5.3.4 Land use and land cover classification for the year 2017

The Land Use and Land Cover map of 2017, as shown in Figure 5.6, highlights extensive land-use changes in the Ahmedabad district. Built-up area expanded significantly and became one of the dominant land use classes. This growth is associated with rapid urbanization. Major developments such as industrial estates and urban infrastructure projects contributed to this expansion. The 2017 LULC map was selected as the final land use dataset because it was the most recent land cover available when this research was initiated in 2018.

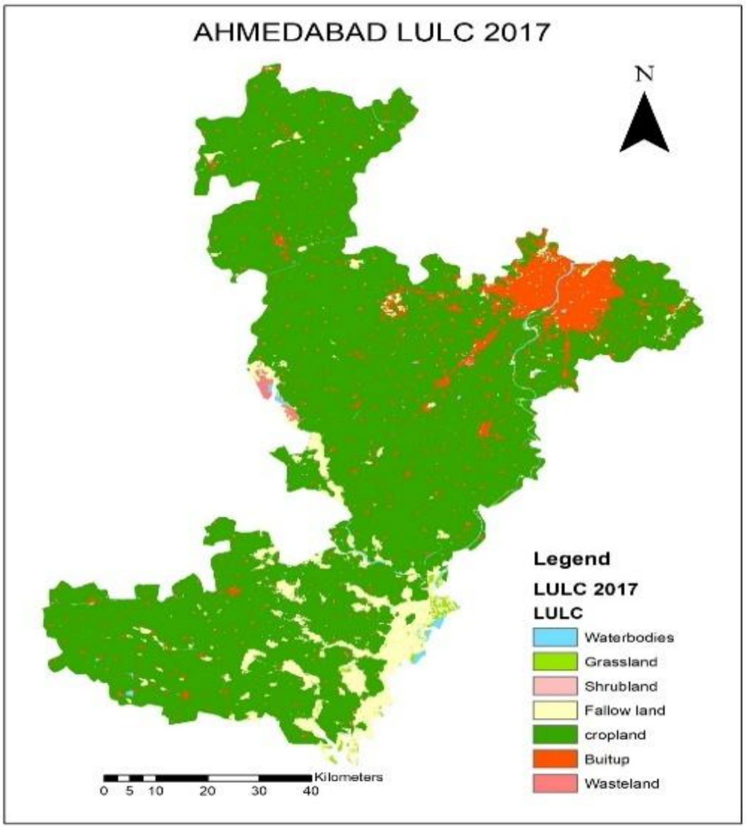

Figure 5.6 LULC Map of 2017

5.4 Accuracy assessment

Accuracy evaluation is an essential phase in land use and land cover (LULC) mapping that measures the agreement between the classified map and the actual land cover as shown by independent reference data (Congalton & Green, 2019).

An accuracy assessment was conducted for the 2017 land use land cover map using high-resolution reference imagery obtained from Google Earth Pro. A stratified random sampling method was employed for the 2017 LULC map in ARCGIS 10.3; 250 points were randomly selected (Table 5.3), with around 34 points allocated to each class. Reference data required for validation were obtained from Google Earth. The points were subsequently superimposed on the classed LULC map, and the associated class values were retrieved via the “Extract Values to Points” tool. Each sample point thus contained both the classified value and the reference (actual) value. Based on these values, a confusion matrix was prepared, where rows represent the classified data and columns represent the reference data. The overall accuracy was calculated as the ratio of the total number of correctly classified samples to the total number of reference samples, represented as a percentage. In this study, LULC exhibited a notable accuracy of 92.8% and a Kappa coefficient of 0.89. Cohen categorized Kappa statistics between 0.2 and 1 for strength of accuracy assessments (Table 5.4).

Table 5.3 Confusion matrix for 2017 LULC classification

Classified data	Built-up land	Cropland	Fallow land	Scrubland	Grassland	Water bodies	Wasteland	Row Total
Built-up land	34	1	0	0	0	0	1	36
Cropland	1	34	1	0	0	0	0	36
Fallow Land	0	1	34	1	0	0	0	36
Scrubland	0	0	1	34	1	0	0	36
Grassland	0	0	0	1	34	1	0	36
Water bodies	0	0	0	0	1	34	1	36
Wasteland	1	0	0	0	0	1	28	34
Column Total	36	36	36	36	36	36	30	250

Table 5.4 Strength accuracy of KAPPA statistics

Sr. no.	Kappa statistics	Strength of accuracy
1	*0.2-0.40*	*Fair*
2	*0.41-0.60*	*Moderate*
3	*0.61-0.80*	*substantial*
4	*0.80-1.00*	*Almost perfect*

Source: https://en.wikipedis.org/wiki/Cohen%27s_kappa

The accuracy assessment results shown in the confusion matrix demonstrate a robust concordance between the categorized Land Use/Land Cover (LULC) map and the reference data utilized for validation. A total of 250 reference samples were utilized for accuracy assessment, of which 232 samples were accurately categorized. The classified LULC map attained an overall classification accuracy of 92.8%, indicating an adequate thematic representation of the land cover categories in the research area.

The calculated Kappa coefficient further indicates a high level of statistical reliability and consistency in the classification results. The obtained accuracy values suggest that the supervised classification approach adopted in the present study is suitable for identifying major land cover classes and analysing spatial land cover dynamics within the watershed. Therefore, the validated LULC maps were subsequently utilized for hydrological modelling, urbanisation assessment, and groundwater recharge analysed using the SWAT modelling framework.

5.5 Detection of land use and land cover changes from 1981 to 2020

Change detection methods employing remote sensing and GIS are preferred for their cost-effectiveness and high temporal resolution. The post-classification comparison methodology, utilizing maximum likelihood supervised classification, is widely employed for detecting alterations in land use and land cover (LULC). Table 5.5 provides an overview of the area changes and percentage of Land Use Land Cover (LULC) classes from 1981 to 2020. A slight increase in the water body area between 1985 and 2017 is attributed to the improved spatial resolution of the 2017 satellite imagery.

Table 5.5 LULC class areas (km²) and percentages

	Area (Km^2)				% of Total area			
LULC Classes	1985	1995	2005	2017	1985	1995	2005	2017
Cropland	6060	3441	4828	5763	77	43.7	61.3	73.2
Fallow land	175	178	169	402	2.2	2.3	2.1	5.1
Waterbodies	469	456	496	506	6	5.8	6.3	6.4
Waste land	916	3413	1933	610	11.6	43.4	24.6	7.7
Built-up	129	252	261	569	1.6	3.2	3.3	7.2
Shrubland	80	89	141	10	1	1.1	1.8	0.1
Grassland	43	43	44	12	0.5	0.5	0.6	0.2

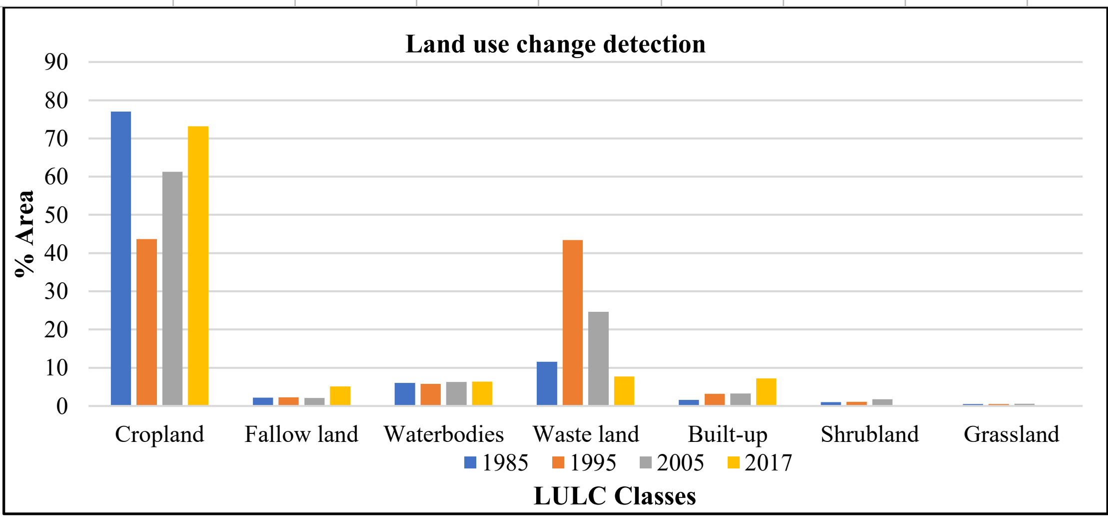

Figure 5.7 Decadal land use change detection

The Land Use/Land Cover (LULC) change detection analysis was carried out to determine the temporal variation in major land cover classes within the study area during the selected study period. Both absolute and relative changes in individual LULC classes were assessed to understand the extent of land transformation, urban expansion, vegetation alteration, and changes in surface water distribution.

Table 5.6 Absolute and relative changes in LULC classes

LULC class	Absolute change (km²)	Relative Change (%)	Trend direction
Cropland	-297	-4.9	Decrease
Fallow Land	227	129.7	Increase
Waterbodies	37	7.88	Increase
Waste land	-306	-33.40	Decrease
Built-up	440	341.08	Increase
Shrubland	-70	-87.5	Decrease
Grassland	-31	-72.0	Decrease

The absolute and relative changes in LULC as shown in Table 5.6 indicate significant variations among different land cover classes within the study area. The expansion of built-up land reflects rapid urbanisation, whereas variations in cropland, fallow land, and vegetation-related classes indicate changing agricultural and environmental conditions over time. The graphical representation of LULC modifications further emphasizes the extent and direction of land cover changes over the study period.

5.6 Summary

This chapter has presented a comprehensive LULC mapping and change detection analysis for the study area over the period 1981–2020. The key findings are the following:

- Significant urban expansion: The built-up area increased from 129 km² ***(1.6%)*** in 1985 to 569 km² ***(7.2%)*** in 2017, a relative change of 341.08% over 40 years.
- Cropland loss: Cropland decreased from 6060 km² ***(77%)*** to 5763 km² ***(73.2%)***, a loss of 297 km² over the study period.
- Fallow land increase: Fallow land increased from 175 km² ***(2.2%)*** to 402 km² ***(5.1%).***
- Shrubland and wasteland declined over the study period.

- Classification accuracy: The LULC classifications achieved an overall accuracy of ***92.8%*** and Kappa coefficient value of ***0.89***, validating the reliability of the maps for hydrological modelling.
- These LULC maps for 1985, 1995, 2005, and 2017 are essential inputs to the SWAT hydrological model (Chapter 6) for quantifying the impact of urbanisation on groundwater recharge.

CHAPTER 6
HYDROLOGICAL MODELLING

6.1 General

A model is a simplified representation of a real-world system utilized to understand, analyse, and forecast system behaviour under different conditions. In environmental and water resource studies, models are essential tools for integrating complex interactions among various physical, climatic, and anthropogenic factors into a structured analytical framework (Beven, 2012).

Hydrological modelling refers to the application of mathematical and computational methods to simulate the movement, distribution, and storage of water within the hydrological cycle. These models simulate essential processes including precipitation, infiltration, evapotranspiration, surface runoff, and groundwater flow. Hydrological models help to assess water balance components and assess the response of a watershed to both natural variability and human-induced changes (Chow et al., 1988). The combined application of hydrological modelling, remote sensing, and geographic information systems offers an effective method for the assessment of watershed processes and supporting sustainable water resource management. (Jensen, 2005; Arnold et al., 1998). Remote sensing provides spatially distributed information on land surface characteristics, while GIS provides efficient integration and analysis of spatial datasets. When combined with hydrological models, these technologies enable a comprehensive assessment of watershed behaviour, water availability, and groundwater recharge dynamics, which provide a scientific basis for water resource planning and management (Jensen, 2005; Arnold et al., 1998).

6.2 Introduction to the SWAT model

The Soil and Water Assessment Tool (SWAT) is a semi-distributed, physically-based hydrological model developed by the United States Department of Agriculture (USDA), to simulate watershed-scale hydrological processes under varying land use, soil, and climatic conditions (Arnold et al., 1998). The model is capable of representing key components of the hydrological cycle, including surface runoff, infiltration, evapotranspiration, percolation, soil water movement, and groundwater flow over long-term simulation periods. By integrating these interconnected processes, SWAT provides a comprehensive framework for evaluating watershed responses to environmental change and resource management practices. Since groundwater recharge is governed by the interaction of climatic conditions, land surface characteristics, and subsurface water movement, the model has been widely applied for assessing recharge potential and supporting sustainable water resource planning (Arnold et al., 1998; Neitsch et al., 2011). In the model, recharge is defined as the percolation of water from the soil profile into the shallow aquifer, which enhances baseflow and groundwater storage. This feature makes SWAT particularly useful for this study, as it is focused on groundwater dynamics, which allows for the estimation of recharge rates under varying land use and climatic conditions.

SWAT supports scenario analysis, enabling researchers to assess changes in land use and their potential impact on groundwater resources (Neitsch et al., 2011).

SWAT was selected as the framework for the study due to its being available as a free, open-source tool; its active support from developers; its comprehensive documentation; and global testing. The SWAT interface was created as an ArcGIS plug-in, which is reportedly the most advanced SWAT module currently in use. ArcGIS version 10.3 interfaces with SWAT 2012 and is used for the study.

The Soil and Water Assessment Tool represent groundwater illustrates a conceptual flow of water from the land surface to underground aquifers. Following precipitation, a portion of water infiltrates into the soil profile while the remainder contributes to surface runoff (Arnold et al.). The infiltrated water moves downward through the soil layers as percolation, eventually reaching the shallow aquifer, which serves as the primary source of groundwater storage in SWAT. From the shallow aquifer, water contributes to streamflow in the form of baseflow, sustaining river discharge during dry periods.

Additionally, a fraction of water from the shallow aquifer infiltrates further into the deep aquifer, which serves as long-term storage and is often considered a loss from the system. This sequence of processes illustrates the dynamic interaction between surface water, soil moisture, and groundwater, allowing SWAT to simulate the overall hydrological balance of the watershed (Arnold et al., 1998; Neitsch et al., 2011).

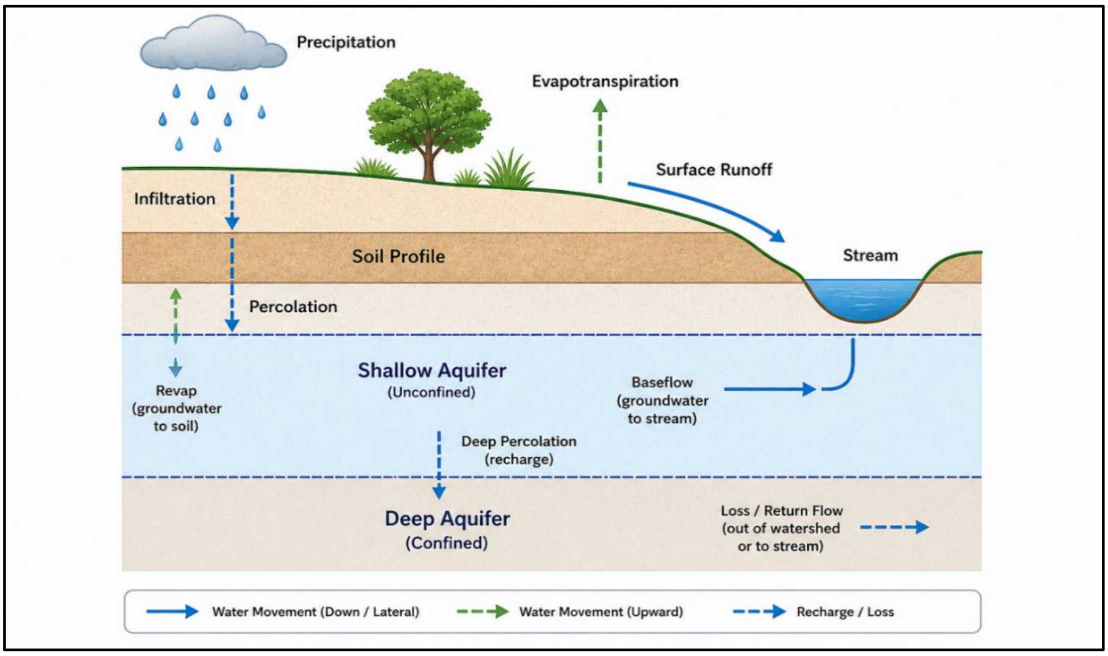

Figure 6.1 Groundwater processes in SWAT

6.3 Critical consideration for multi-decadal simulation

This study will adopt a discrete LULC change approach. The simulation period (1981–2020) is divided into four intervals. The SWAT model will be run sequentially, with the LULC input being updated at the start of each interval.

Interval 1 (1980–1990): Uses LULC 1985

Interval 2 (1991–2000): Uses LULC 1995

Interval 3 (2001–2010): Uses LULC 2005

Interval 4 (2011–2020): Uses LULC 2017

6.4 Model development

For model development, the following processes are required:

1. Watershed delineation

2. HRU (hydrologic response unit) formation

3. Uploading weather data files

4. Writing input tables

5. SWAT Run

6. Model Output

6.4.1 Watershed delineation

This is the initial phase of modelling following to the establishment of the project files. A Digital Elevation Model (DEM) serves as the primary input in a specified unit, format, and projection to delineate the topographic characteristics of the region. Based on a selected threshold value, stream networks and defined outlet points are generated. The watershed boundary was then delineated automatically by the model. The area was further divided into sub-basins.

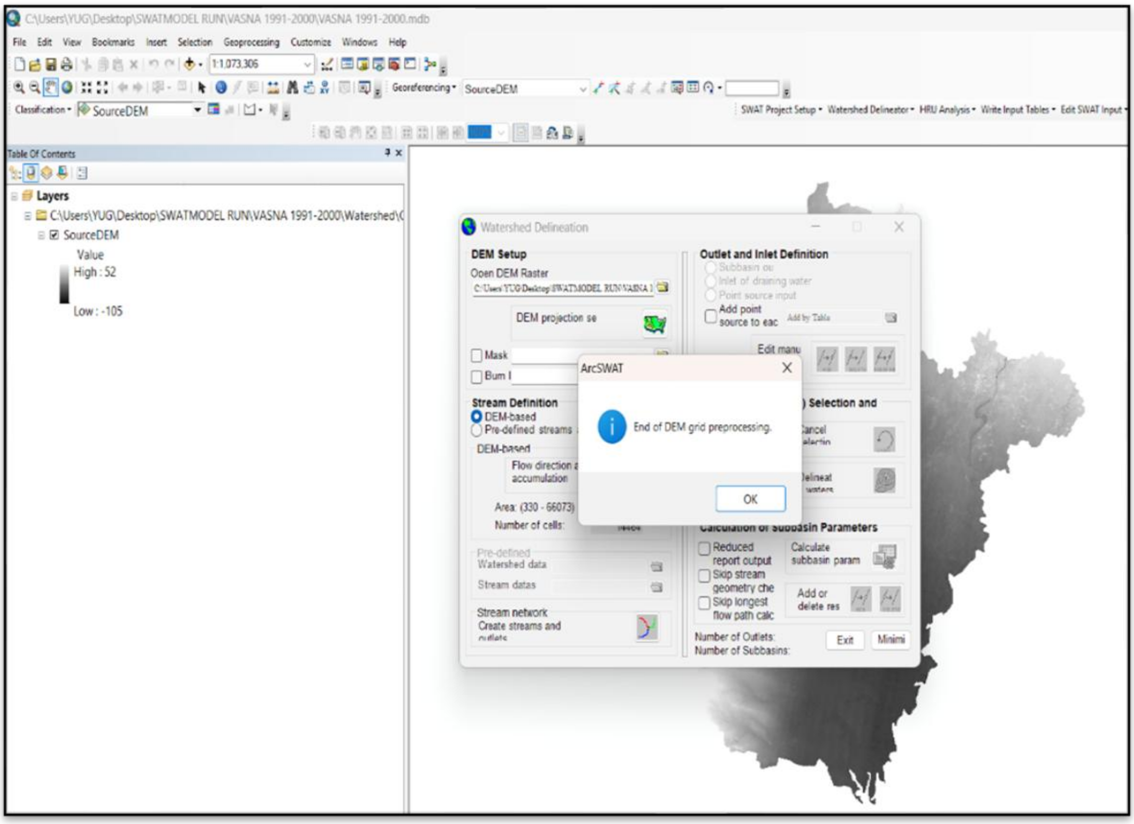

Figure 6.2 Stream network generation using DEM

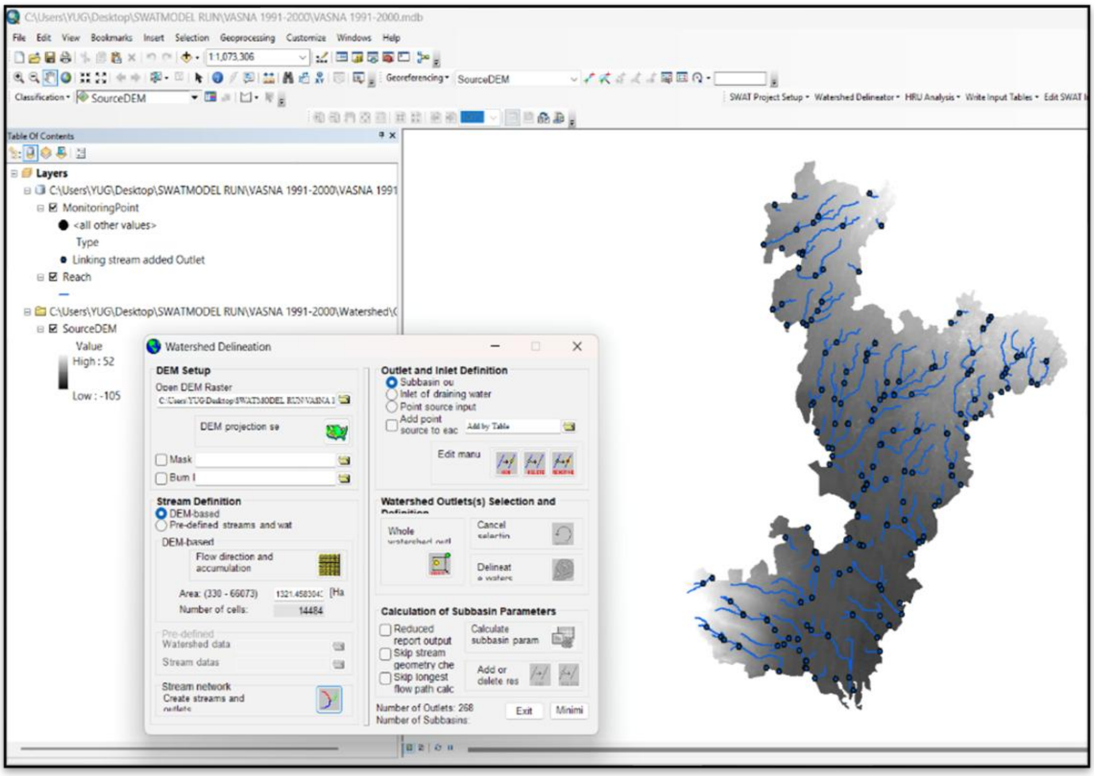

Figure 6.3 Stream network generation using DEM

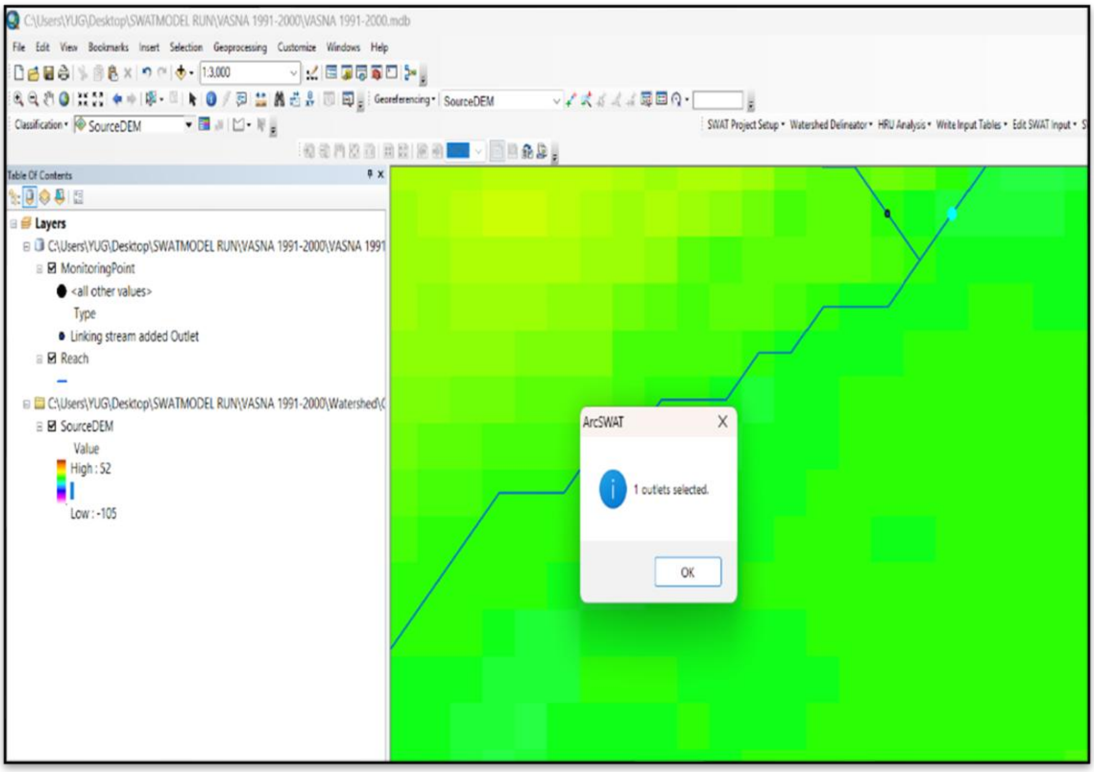

Figure 6.4 Outlet point definition for watershed delineation

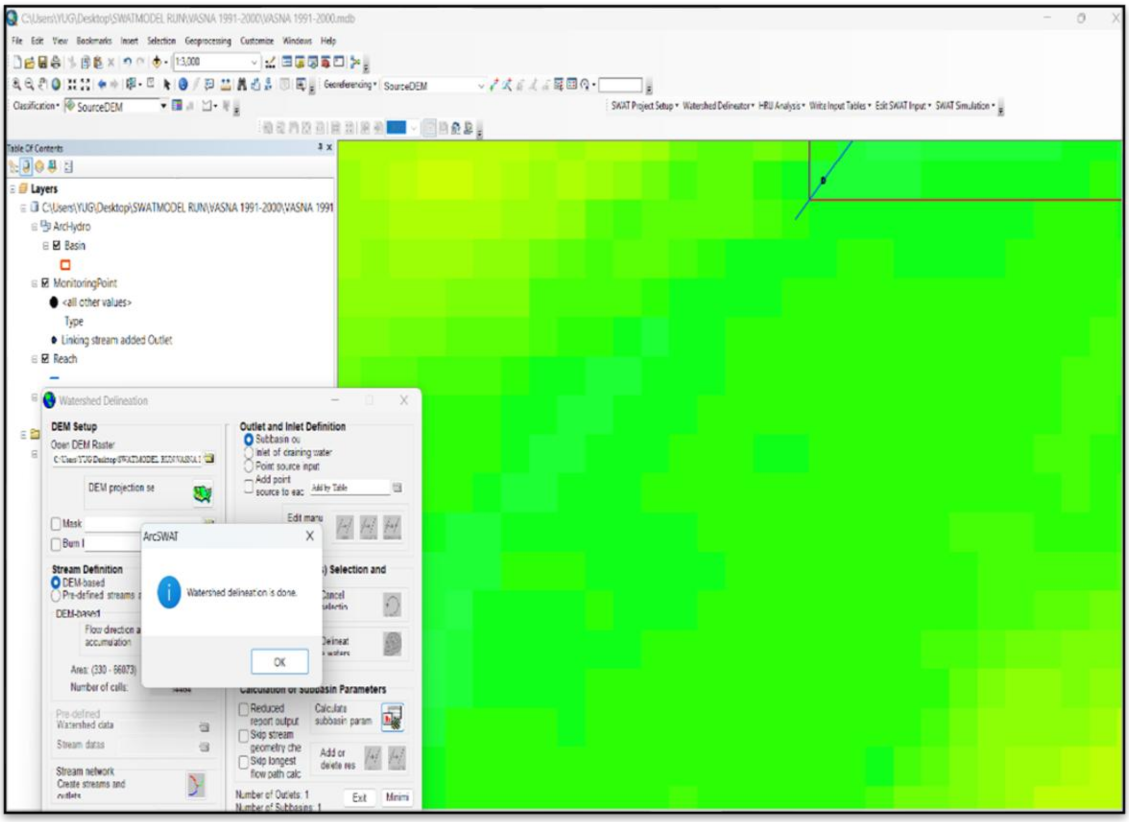

Figure 6.5 Completed watershed delineation

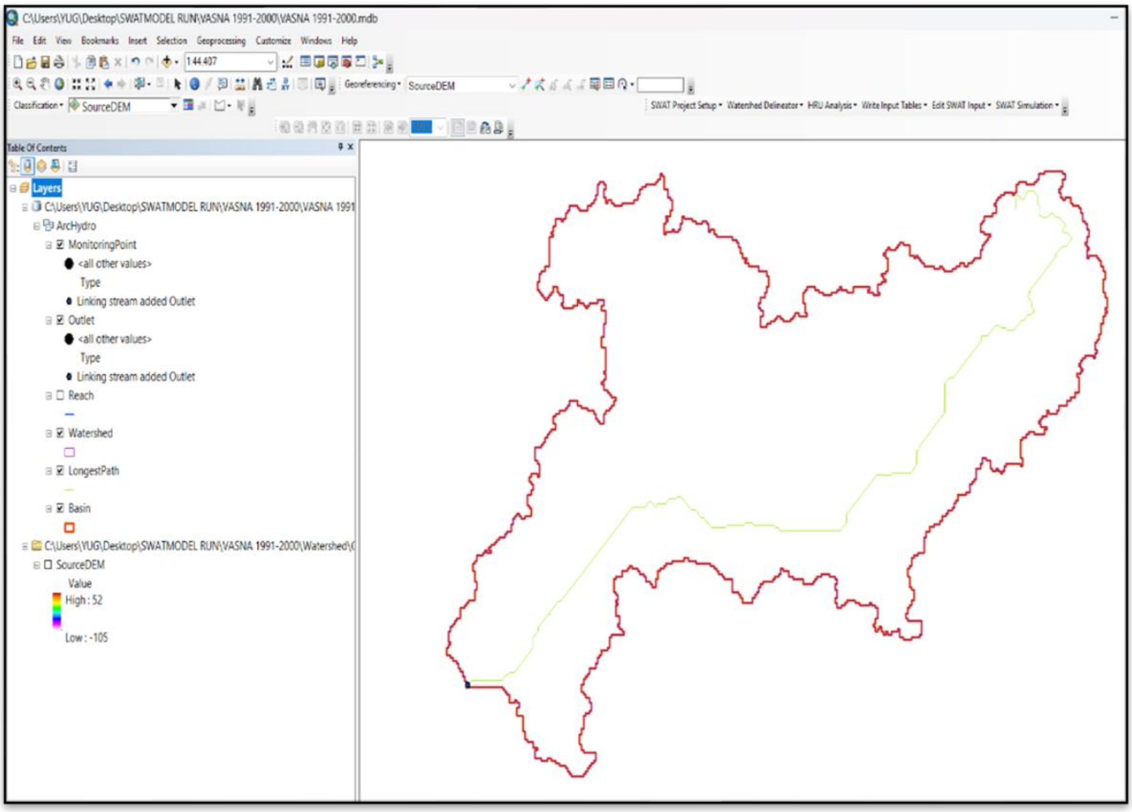

Figure 6.6 Sub-Basin creation and final watershed configuration

Figures 6.2 to 6.6 shows the sequential steps involved in watershed delineation using the SWAT model, including stream network generation, outlet definition, watershed boundary extraction, and sub-basin formation.

Figure 6.7 represents the topographic report of the catchment for the area under study. The analysis indicates that the watershed exhibits variations in elevation ranging from the minimum elevation of *-27* m to the maximum elevation of *49* m above mean sea level. The elevation-frequency distribution indicates the percentage area occupied under different elevation classes within the watershed. The percentage of watershed area below specific elevation levels represents the spatial distribution of low-lying regions that favour infiltration and groundwater recharge processes.

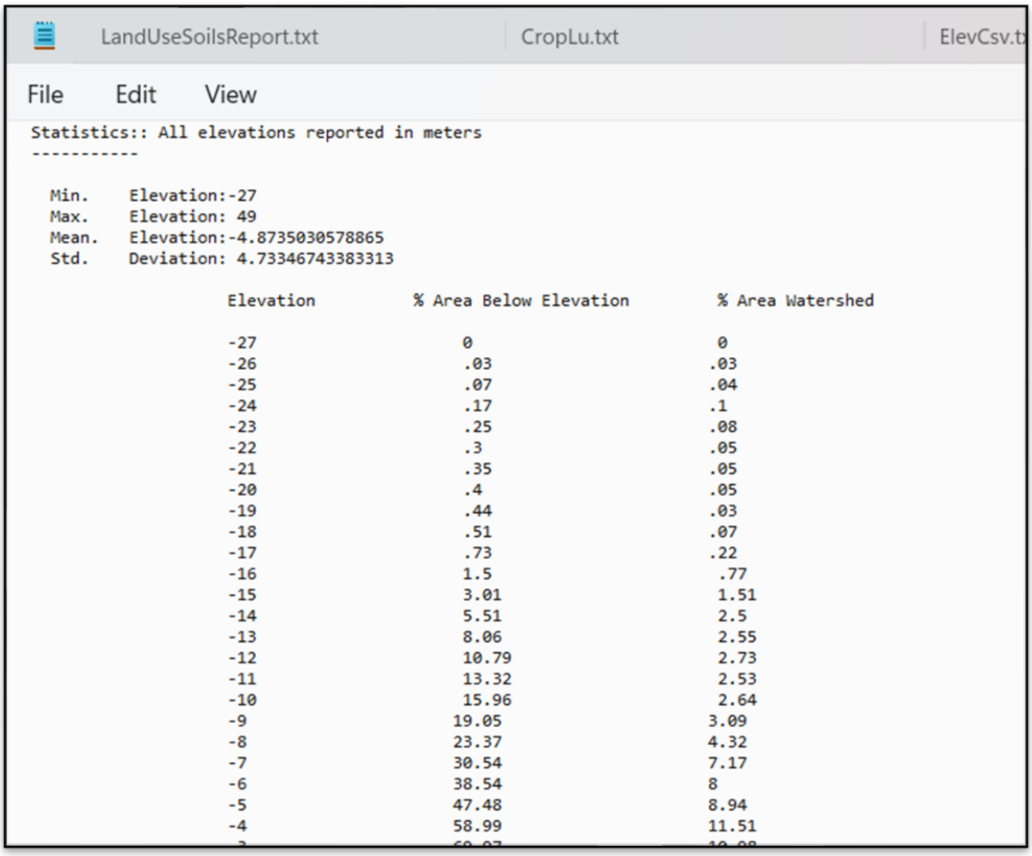

Statistics:: All elevations reported in meters

Min. Elevation:-27
Max. Elevation: 49
Mean. Elevation:-4.8735030578865
Std. Deviation: 4.73346743383313

Elevation	% Area Below Elevation	% Area Watershed
-27	0	0
-26	.03	.03
-25	.07	.04
-24	.17	.1
-23	.25	.08
-22	.3	.05
-21	.35	.05
-20	.4	.05
-19	.44	.03
-18	.51	.07
-17	.73	.22
-16	1.5	.77
-15	3.01	1.51
-14	5.51	2.5
-13	8.06	2.55
-12	10.79	2.73
-11	13.32	2.53
-10	15.96	2.64
-9	19.05	3.09
-8	23.37	4.32
-7	30.54	7.17
-6	38.54	8
-5	47.48	8.94
-4	58.99	11.51

Figure 6.7 Topographic report as generated after watershed delineation

6.4.2 HRU (Hydrologic Response Unit) formation

Hydrological Response Units (HRUs) are crucial in the SWAT model. HRU defines homogeneous areas of land use, soil, and slope, enabling accurate simulation of hydrological processes. This concept can be simply defined as follows: in a watershed, the quantity of Hydrologic Response Units (HRUs) established with a singular combination of 1) land cover, 2) soil, and 3) slope is one.

During this process, the model obtains spatial data in the form of maps, including land-use maps and soil maps, in the same specified unit (meter), format (.tiff), and projection (WGS 1984). The HRU formation process in the SWAT model was carried out through a systematic procedure involving map overlay and reclassification of land use, soil map, and slopes.

6.4.3 Maps overlay

This step involved the integration of spatial datasets, including land use/land cover, soil, and slope maps. In this process LULC maps (LULC 1985, LULC 1995, LULC 2005, and LULC 2017 maps) are uploaded to the ArcSWAT model. Reclassification is a prerequisite in SWAT to convert raw land use, soil, and slope data into standardized categories compatible with the model.

6.4.4 HRU Formation

Based on the overlay results, Hydrological Response Units (HRUs) were delineated within each sub-basin. Threshold values were applied to exclude minor land use, soil, and slope classes to reduce model complexity while maintaining accuracy. Each HRU represented a homogeneous unit with a similar hydrological response.

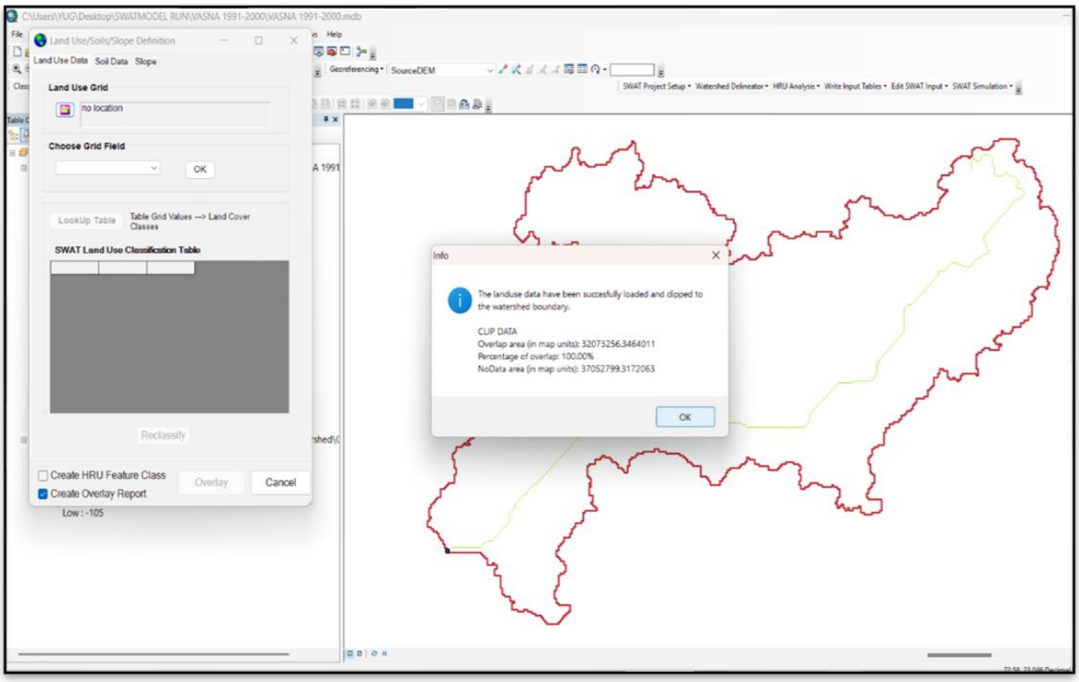

Figure 6.8 Input for land use/land cover (LULC) classification

Figure 6.8 illustrates the Land Use/Land Cover (LULC) classification layer used as a primary input dataset during the Hydrological Response Unit (HRU) formation process. Creating HRU is crucial while adding the LULC layer because the features of the land surface directly affect water movement and behaviour. The classified LULC map illustrates the spatial distribution of various land use categories within the watershed and was integrated with soil and slope layers for delineation of Hydrological Response Units (HRUs).

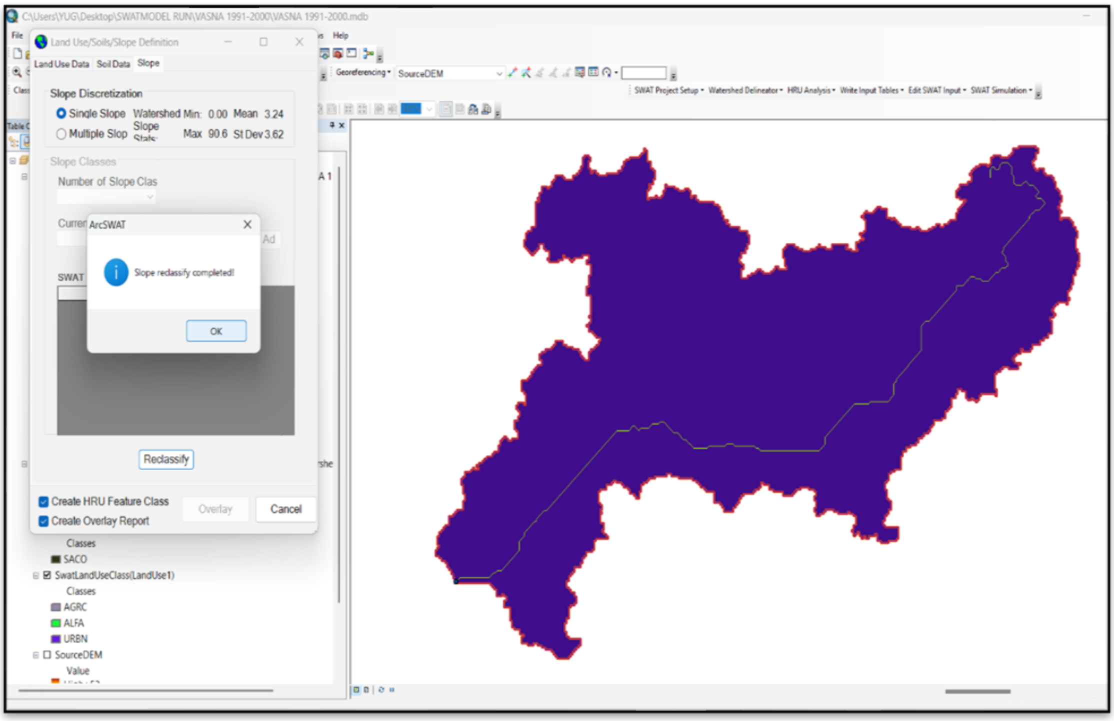

Figure 6.9 Slope classification and reclassification

Figure 6.9 illustrates the slope classification and reclassification process carried out using the SWAT framework for Hydrological Response Unit (HRU) generation. Slope is a critical topographic characteristic that affects watershed hydrology. Areas with lower slope values generally exhibit higher infiltration and groundwater recharge potential due to slower runoff movement and greater water retention capacity. On the other hand, steeper slope regions contribute to rapid runoff generation, increased flow velocity, and comparatively lower infiltration rates.

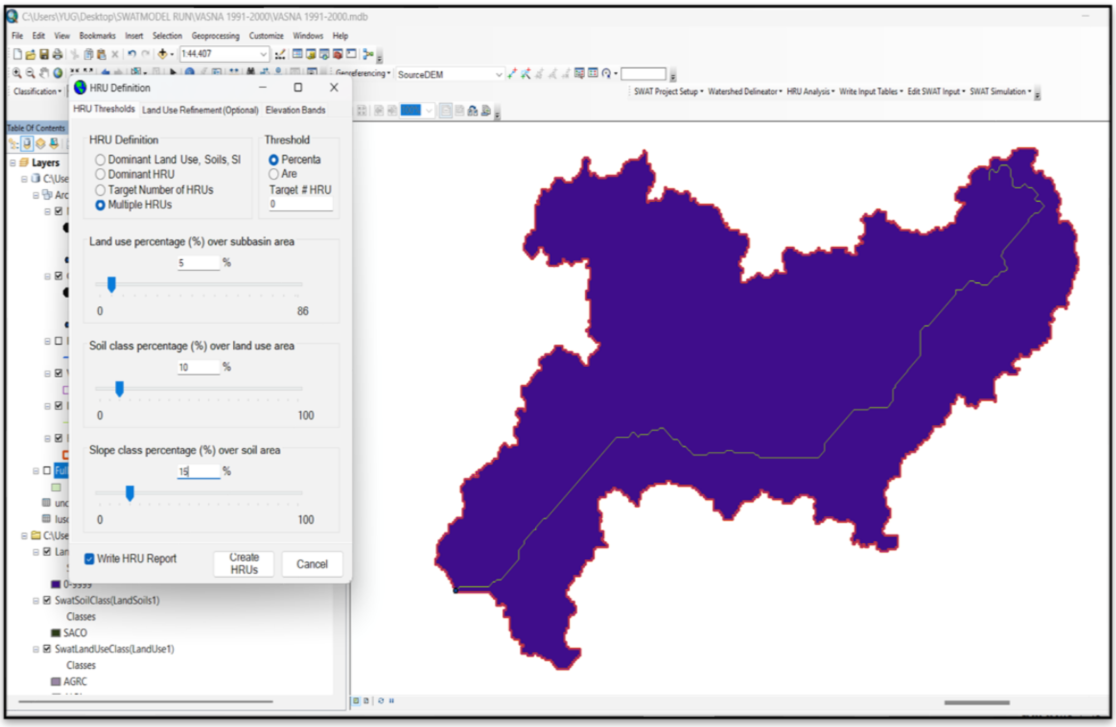

Figure 6.10 Selection of threshold values for land use, soil, and slope classes

Figure 6.10 shows percentage thresholds applied during HRU definition. The land use percentage (%) was adjusted to 5% over sub-basin area, soil class percentage (%) adjusted to 10% over land use area, and slope class percentage (%) adjusted to 15% over soil area to eliminate minor spatial units having negligible influence on watershed hydrology. The HRU definition process enabled effective representation of spatial heterogeneity associated with land surface, soil properties, and topographic variability within the study area.

The report represents the classified HRUs and their distribution is shown in *Figure 6.11*, which provides a detailed explanation of the allocation of the land, soil, and slope classes.

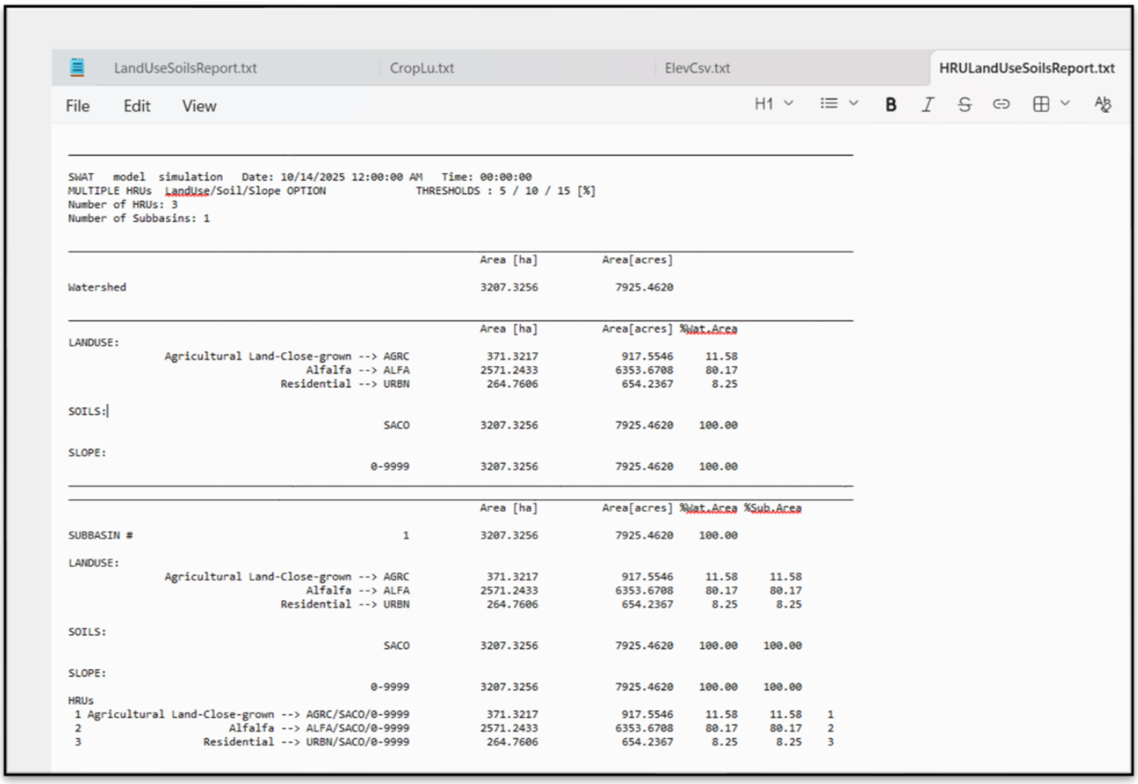


```
SWAT   model  simulation   Date: 10/14/2025 12:00:00 AM   Time: 00:00:00
MULTIPLE HRUs  LandUse/Soil/Slope OPTION            THRESHOLDS : 5 / 10 / 15 [%]
Number of HRUs: 3
Number of Subbasins: 1

                                                        Area [ha]        Area[acres]

Watershed                                               3207.3256          7925.4620

                                                        Area [ha]        Area[acres] %Wat.Area
LANDUSE:
              Agricultural Land-Close-grown --> AGRC     371.3217           917.5546     11.58
                                  Alfalfa --> ALFA      2571.2433          6353.6708     80.17
                              Residential --> URBN       264.7606           654.2367      8.25

SOILS:
                                              SACO      3207.3256          7925.4620    100.00

SLOPE:
                                            0-9999      3207.3256          7925.4620    100.00

                                                        Area [ha]        Area[acres] %Wat.Area %Sub.Area

SUBBASIN #                                       1      3207.3256          7925.4620    100.00

LANDUSE:
              Agricultural Land-Close-grown --> AGRC     371.3217           917.5546     11.58     11.58
                                  Alfalfa --> ALFA      2571.2433          6353.6708     80.17     80.17
                              Residential --> URBN       264.7606           654.2367      8.25      8.25

SOILS:
                                              SACO      3207.3256          7925.4620    100.00    100.00

SLOPE:
                                            0-9999      3207.3256          7925.4620    100.00    100.00
HRUs
 1 Agricultural Land-Close-grown --> AGRC/SACO/0-9999    371.3217           917.5546     11.58     11.58    1
 2                     Alfalfa --> ALFA/SACO/0-9999     2571.2433          6353.6708     80.17     80.17    2
 3                 Residential --> URBN/SACO/0-9999      264.7606           654.2367      8.25      8.25    3
```

Figure 6.11 HRU threshold definition (LULC, Soil, and Slope)

The report provides detailed information regarding the spatial distribution and number of HRUs formed based on unique combinations of land use, soil type, and slope classes.

6.4.5 Weather file input

This module was activated after the successful creation of Hydrological Response Units (HRUs) in the SWAT model. In this step, all required climatic inputs were incorporated into the model in a standardized format to drive hydrological simulations. In the present study, the input data included observed records of rainfall and temperature of 40 years (1981-2020) obtained from relative resources have been incorporated in the model. After successful execution of this step, the model processed the climatic inputs and generated various output files such as .hru, .rch, .sub, etc.

Figures 6.12 to 6.13 illustrate the process of incorporating weather data into the SWAT model.

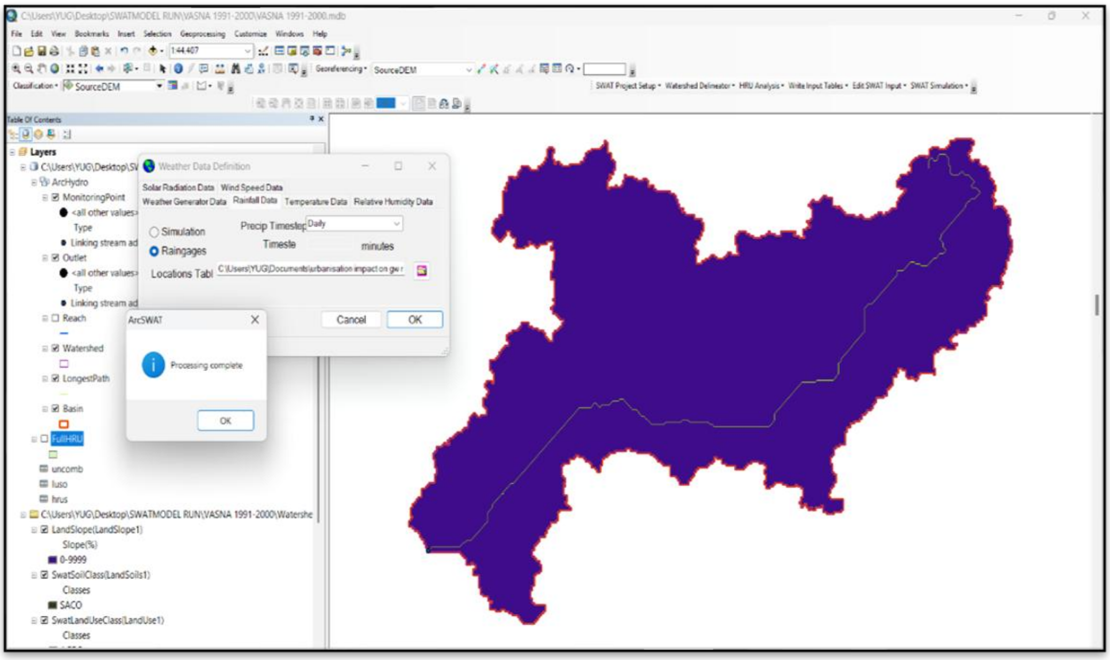

Figure 6.12 Preparation of weather input files

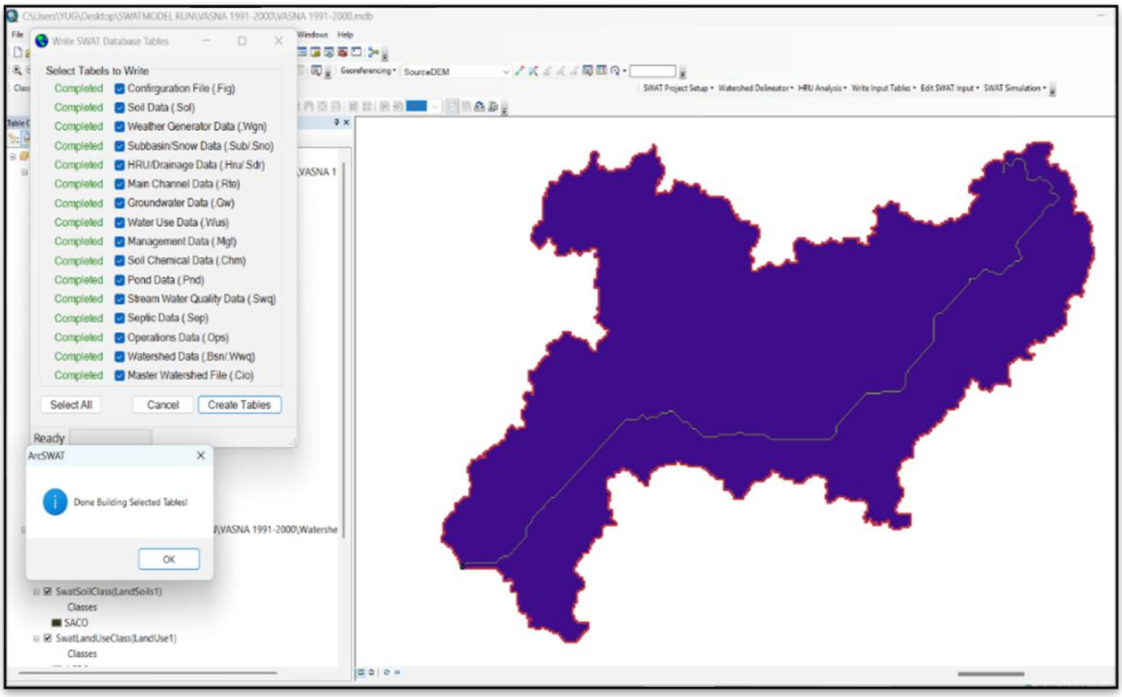

Figure 6.13 Weather generator (WGEN) file setup in SWAT

6.4.6 Model run (Simulation)

After the successful incorporation of weather data, the SWAT model simulation was executed on a daily time step for the study area. It simulated water balance components at the HRU level. A warm-up period was included to stabilize initial conditions before analysis. The simulation was carried out for a decadal period to capture long-term hydrological variability. The outputs were generated at HRU, sub-basin, and watershed levels in files such as .hru, .rch, and .sub for further analysis.

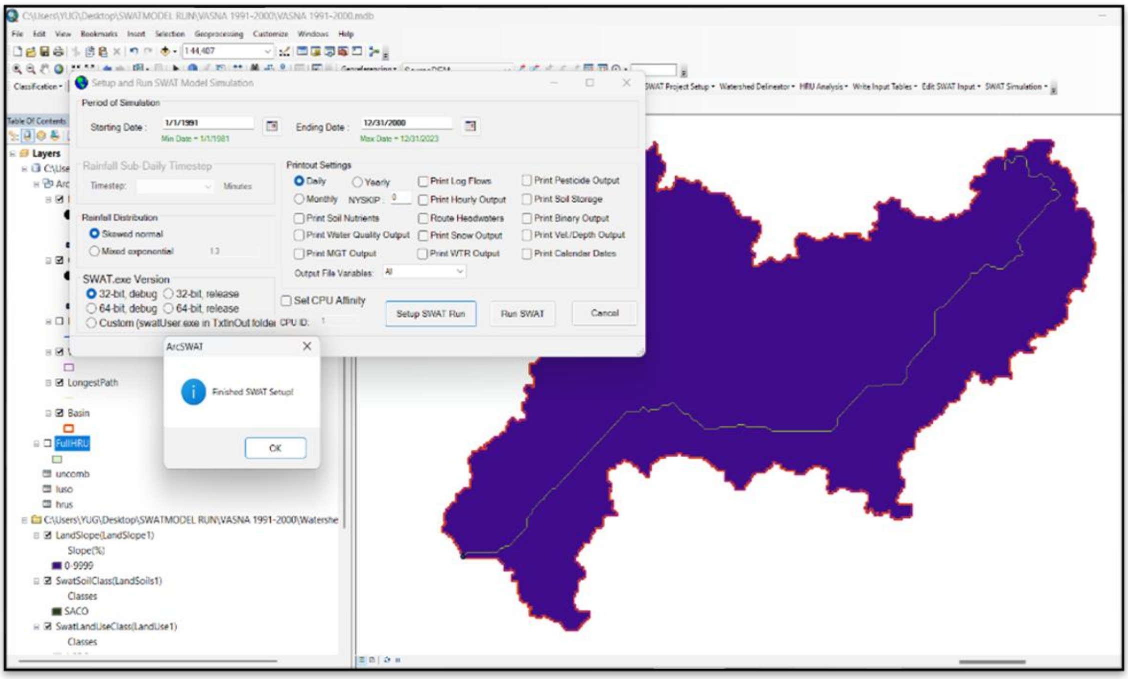

Figure 6.14 SWAT model simulation run for the delineated catchment

Figure 6.14 illustrates the execution of the SWAT model utilizing predefined input datasets, including climate, soil, and land use data, to simulate hydrological processes within the research area.

6.5 Overview of the SWAT output viewer

Numerous methods exist to visualize SWAT outputs. The SWAT output viewer is a tool used to extract, visualize, and interpret the results generated by the SWAT model. After model execution, SWAT generates multiple output files such as. hru., rch., and sub., which contain detailed hydrological information at different spatial levels. The Output Viewer provides a structured interface to access and interpret these outputs in both tabular and graphical formats. In the present study, the SWAT Output Viewer developed by Michael Yu provides the perfect presentation of the outputs for analysing model outputs in the current study. It serves as a key component in interpreting SWAT results and supporting reliable hydrological assessment and decision-making (Arnold et al., 1998; Neitsch et al., 2011).

The decadal shallow aquifer recharge was estimated using outputs from the Soil and Water Assessment Tool. The overall procedure is shown in the methodology flowchart, which outlines the stepwise process adopted in this study. The groundwater recharge variable

(GW_RCHG) was obtained from the SWAT output viewer and exported for further analysis. The data were processed and aggregated on a daily, monthly, and annual basis. Decadal recharge was computed through cumulative analysis over ten-year duration. This approach provides a systematic and reliable estimation of groundwater recharge.

Figure 6.15 illustrates the methodological framework adopted for estimation of groundwater recharge using the SWAT Output Viewer.

Initially, input datasets including Digital Elevation Model (DEM), Land Use/Land Cover (LULC), soil map, and meteorological data were collected and processed for watershed delineation and Hydrological Response Unit (HRU) generation. The delineated watershed was subsequently divided into sub-basins and HRUs that represent homogeneous combinations of land use, soil, and slope characteristics. Climatic inputs were incorporated into the SWAT model for hydrological simulation.

Following HRU generation, the SWAT model was executed to simulate major hydrological components. The calibrated model outputs were subsequently analysed using the SWAT Output Viewer to extract shallow aquifer recharge (GW_RCHG) values for different simulation periods.

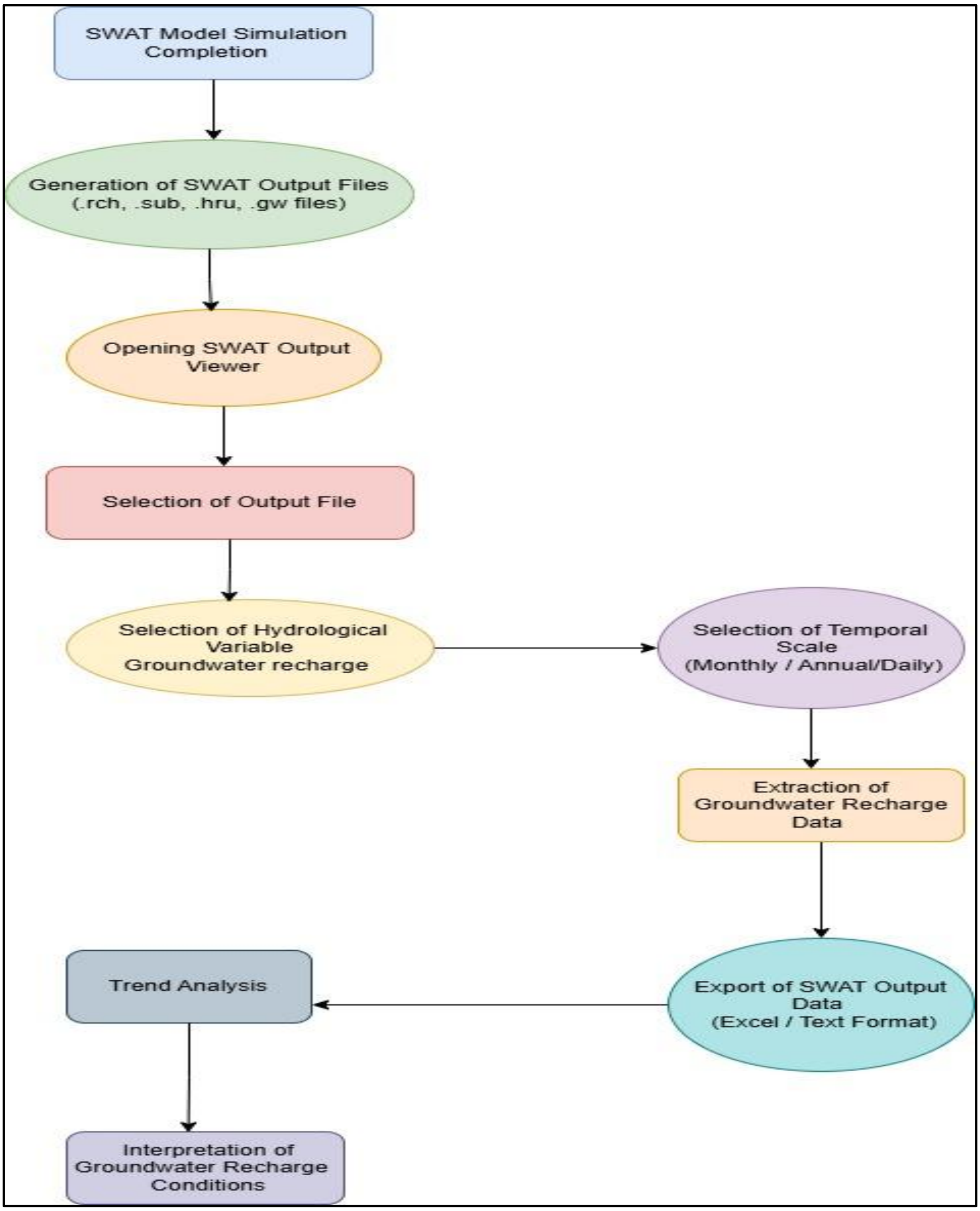

Figure 6.15 Methodological flowchart for estimating groundwater recharge using SWAT output viewer

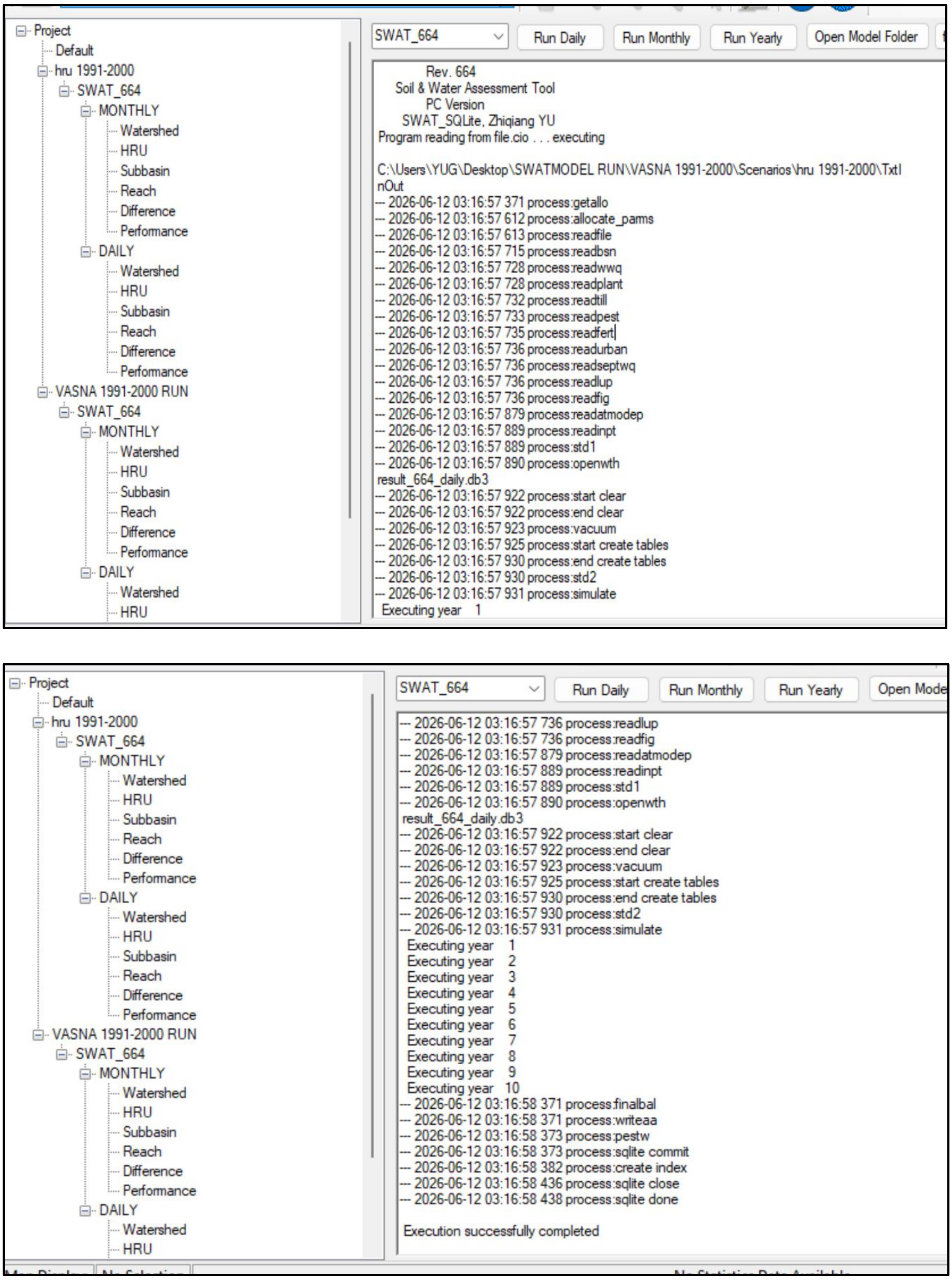

Figure 6.16 SWAT output viewer displays for selection of daily, monthly, and annual outputs

Figure 6.16 shows the SWAT output viewer interface used to visualize model results at different temporal scales, including daily, monthly, and annual outputs.

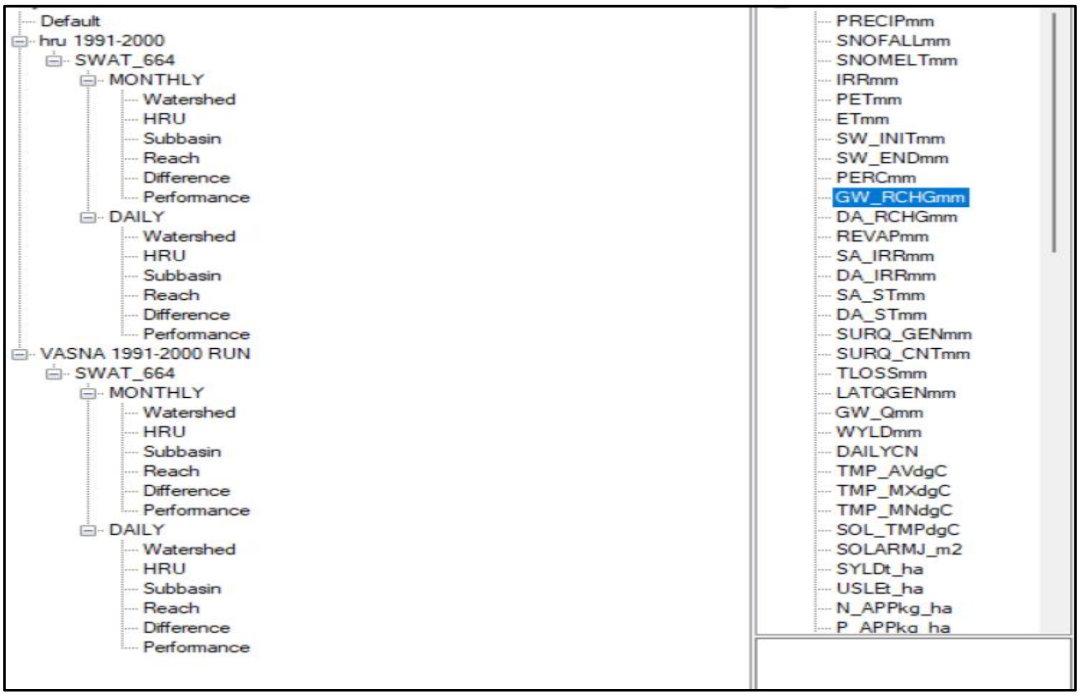

Figure 6.17 Shallow Groundwater Recharge (RECHG) Simulated using SWAT Output Viewer

Figure 6.17 represents groundwater recharge (GW_RCHG) simulated using the SWAT model, highlighting spatial variability in recharge across different hydrological response units.

The outputs generated from the SWAT output viewer give a preliminary understanding of the hydrological behaviour of the watershed system in the study area.

Although the SWAT model provides useful information regarding watershed hydrological processes, the accuracy of the simulated outputs largely depends on proper model parameterisation and input data quality. Hydrological simulations are associated with uncertainties arising from climatic inputs, watershed characteristics, and parameter interactions within the model. Therefore, it is necessary to assess the reliability and performance of the model via calibration and validation before using the simulated results for hydrological analysis and groundwater management studies.

6.6 Model calibration and validation

Calibration and validation are essential steps in hydrological modelling that evaluate the reliability and accuracy of the simulated outputs generated by the SWAT model. Hydrological simulations have uncertainties due to variability in climatic inputs, watershed characteristics, parameter interactions, and model assumptions. Therefore, the direct utilisation of simulated outputs without a statistical evaluation may affect the reliability of hydrological assessments. Calibration is performed to optimise sensitive model parameters related to surface runoff, infiltration, evapotranspiration, groundwater flow, and baseflow in order to improve the agreement between observed and simulated data. The calibration process helps in reducing uncertainties and enhancing the capability of the model to represent actual watershed conditions more realistically. The calibrated model's performance is evaluated using statistical metrics such as Nash–Sutcliffe efficiency (NSE) and coefficient of determination (R^2), which indicate the level of agreement between observed and simulated values (Moriasi et al., 2007).

After calibration, validation is carried out using an independent dataset without modifying the calibrated parameter values. The main objective of validation is to examine the predictive capability, consistency, and robustness of the model under different hydrological conditions.

In the present study, calibration and validation were conducted to establish confidence in the simulated hydrological outputs generated by the SWAT model. The observed and simulated streamflow values for Vasna Barrage were compared to evaluate model performance and reduce simulation errors.

For calibration and uncertainty analysis, the SUFI-2 (Sequential Uncertainty Fitting Version-2) algorithm available in SWAT-CUP was employed in the present study. The model is calibrated by the "Sequential Uncertainty Fitting" (SUFI-2) algorithm available as an interface with SWATCUP by entering observed streamflow data and parameter values as shown in Table 6.1. Initial parameter ranges were assigned based on literature values and model guidelines, and the algorithm then performs iterative simulations by adjusting parameter combinations within the specified ranges to minimise differences between observed and simulated streamflow values. During each iteration, model performance is evaluated using statistical indicators such as Nash–Sutcliffe efficiency (NSE) and coefficient of determination (R^2). Based on the simulation results, parameter ranges are progressively refined until satisfactory agreement between observed and simulated outputs is achieved.

The SUFI-2 algorithm also quantifies prediction uncertainty through the 95 Percent Prediction Uncertainty (95PPU), which represents the range within which most observed data are bracketed.

In this study, the observed stream flow from 2014 to 2024 for the Vasna barrage was acquired from the Ahmedabad Irrigation Division, Ahmedabad. The observed data were applied in SWAT-CUP software, where the SUFI-2 algorithm was used for calibration and validation. In SWAT-CUP, a total of 10 significant parameters that could affect the surface runoff, infiltration, evapotranspiration, groundwater flow, and baseflow were selected for simulation. The calibration of the model was done using six years of observed streamflow data for 2014-2019.

6.6.1 Sensitive parameters used for calibration

The sensitivity analysis indicated that parameters associated with surface runoff, soil moisture, groundwater recharge, and baseflow significantly influence the hydrological response of the study area. Table 6.1 shows the sensitive parameters used for calibrating the SWAT model based on extensive literature review.

The final SWAT parameters were selected based on the sensitivity analysis and calibration results obtained using the Sequential Uncertainty Fitting Version 2 (SUFI-2) algorithm within the SWAT-CUP framework. Initially, a broad range of hydrological parameters influencing surface runoff, infiltration, groundwater flow, soil moisture was considered based on previous SWAT studies and model documentation. During the sensitivity analysis, SUFI-2 quantified the influence of each parameter on streamflow simulation using the t-statistic and p-value, where parameters with higher absolute t-statistic values and lower p-values were considered more sensitive. The final parameter set was selected by considering both statistical sensitivity and hydrological significance.

Proper optimisation of these parameters is essential for reducing simulation uncertainty and improving the reliability and predictive capability of the SWAT model for hydrological assessment and groundwater recharge analysis in the study area.

Table 6.1 Sensitive parameters used for calibration of the SWAT model

Sensitivity rank	SWAT parameter name	SWAT parameter description
1	SOL_AWC	Available water capacity of the soil layer
2	REVAPMN	Minimum depth of water in the shallow aquifer (mm) for REVAP to occur.
3	RCHRG_DP	Fraction of percolation from the root zone that enters the deep aquifer.
4	CN2	SCS curve number
5	SURLAG.	Surface runoff lag time coefficient.
6	GWQMN	Threshold water depth in the shallow aquifer (mm) required before groundwater flow to the stream occurs.
7	GW_DELAY	Time lag (days) between water exiting the root zone and entering the shallow aquifer.
8	ESCO	Soil evaporation compensation coefficient
9	GW_SPYLD	Specific yield of the shallow aquifer
10	ALPHA_BF	Baseflow recession constant |

The calibration process was conducted iteratively by modifying the selected sensitive parameters until satisfactory agreement between observed and simulated streamflow was attained. The iterative optimisation process enabled reduction of model uncertainty and improved representation of watershed hydrological processes within the SWAT model framework. Table 6.2 summarizes the results of the sensitivity analysis.

Table 6.2 Global sensitivity analysis values of all 10 critical parameters of the study area

Parameter Name	t-Stat	P-Value
2:V__ALPHA_BF.gw	-0.018375769	0.985432773
8:R__GW_SPYLD.gw	0.081407845	0.935533968
7:R__ESCO.hru	-0.334069285	0.740117076
3:V__GW_DELAY.gw	-0.939265666	0.353375553
4:V__GWQMN.gw	1.013346122	0.317140672
6:R__SURLAG.bsn	-1.117079802	0.270795037
1:R__CN2.mgt	-1.132558866	0.264314762
5:R__RCHRG_DP.gw	-1.522083755	0.136055843
9:R__REVAPMN.gw	2.004924359	0.051947649
10:R__SOL_AWC(..).sol	29.970298898	0.000000000

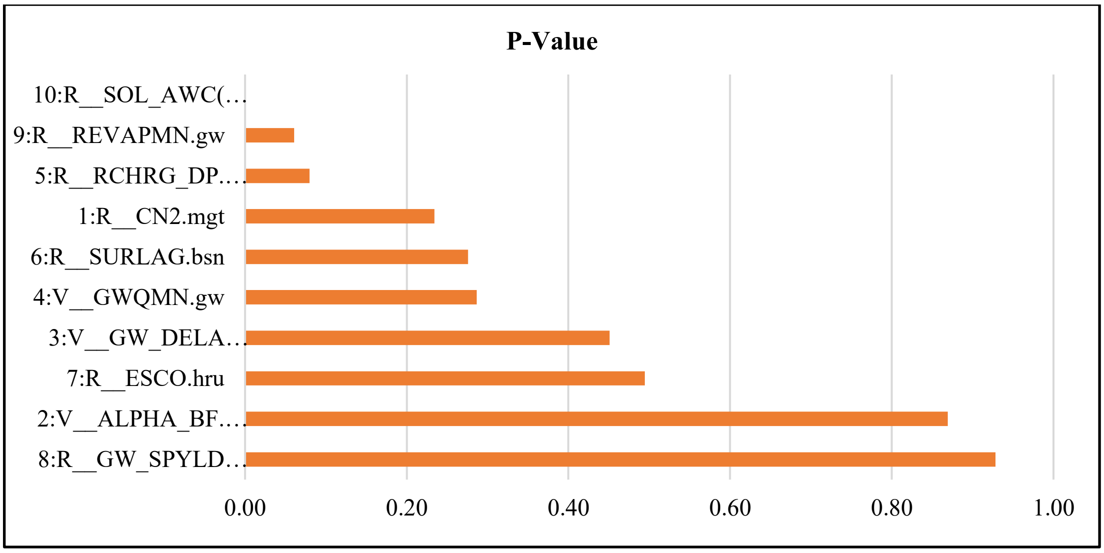

Figure 6.18 Evaluation of parameter significance based on P-values obtained from SUFI-2 analysis

Figure 6.18 represents the statistical significance of sensitive SWAT parameters based on p-values obtained during global sensitivity analysis using the SUFI-2 algorithm. Parameters having lower p-values are considered statistically more significant in influencing hydrological simulation within the watershed. The identified significant parameters were further utilised during the calibration process for optimisation of the SWAT model.

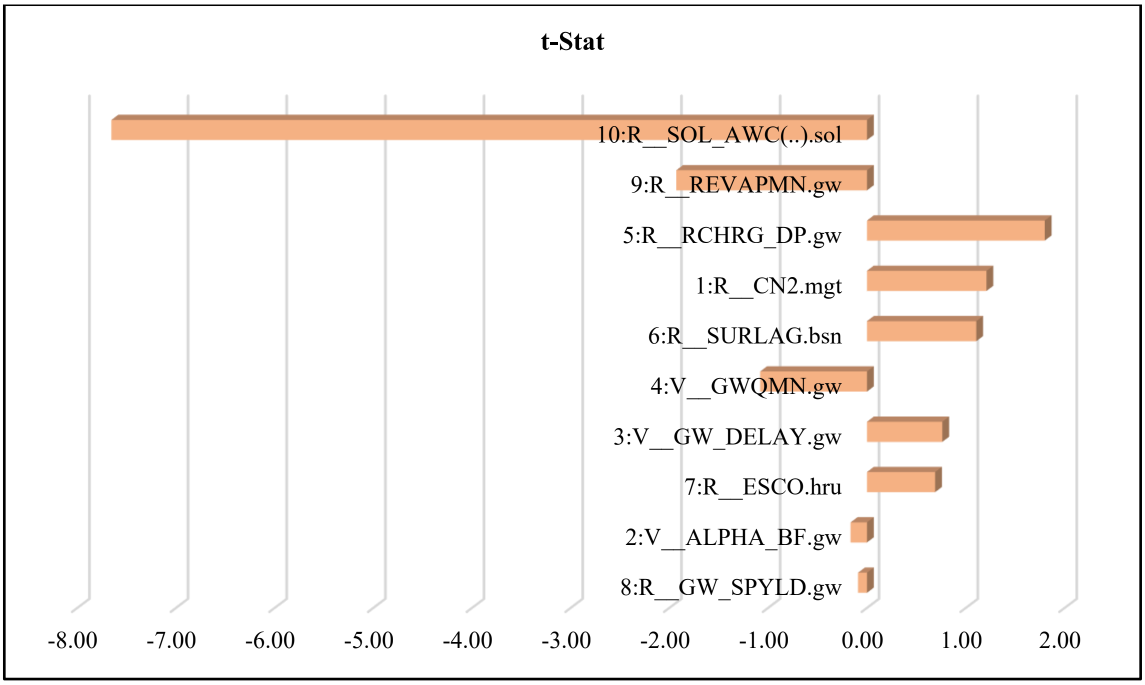

Figure 6.19 Global sensitivity analysis of SWAT parameters utilising T-stat values

Figure 6.19 shows how important different SWAT parameters are, based on t-stat values from the SUFI-2 sensitivity analysis. Parameters exhibiting higher absolute t-stat values indicate greater influence on streamflow simulation and watershed hydrological response.

The calibration is performed on a daily basis between the years 2014 and 2019. *Figure 6.20* represents SWAT-CUP output results at outlet number 50 (flow-out-50), which shows the Vasna barrage.

Table

outlets1

FID	Shape *	OBJECTID	POINTID	GRID_CODE	Xpr	Ypr	Lat	Long_	Elev	Name	Type	Subbasin	HydroID	OutletID
9	Point	10	10	10	219423.3072	2582826.0164	23.331016	72.25616	0		L	10	400010	100010
10	Point	11	11	11	191846.197	2581859.4583	23.317343	71.986948	0		L	11	400011	100011
11	Point	12	12	12	191846.197	2581829.2534	23.317071	71.986954	0		L	12	400012	100012
12	Point	13	13	13	181334.8779	2577328.7173	23.274468	71.885239	0		L	13	400013	100013
13	Point	14	14	14	187255.0461	2576150.7247	23.26498	71.943283	0		L	14	400014	100014
14	Point	15	15	15	194051.1576	2574912.3221	23.255088	72.009886	0		L	15	400015	100015
15	Point	16	16	16	194051.1576	2574882.1172	23.254815	72.009892	0		L	16	400016	100016
16	Point	17	17	17	192842.96	2574761.2974	23.2535	71.998121	0		L	17	400017	100017
17	Point	18	18	18	193779.3132	2574247.8134	23.249043	72.007366	0		L	18	400018	100018
18	Point	19	24	24	192510.7057	2570290.9663	23.213113	71.995781	0		L	24	400019	100019
19	Point	20	19	19	200605.6296	2569747.2774	23.209698	72.074896	0		L	19	400020	100020
20	Point	21	20	20	200635.8345	2569717.0724	23.209431	72.075196	0		L	20	400021	100021
21	Point	22	21	21	212053.3018	2568992.1539	23.204926	72.186777	0		L	21	400022	100022
22	Point	23	22	22	197947.5949	2567934.981	23.192864	72.049312	0		L	22	400023	100023
23	Point	24	23	23	197947.5949	2567904.776	23.192592	72.049318	0		L	23	400024	100024
24	Point	25	25	25	200031.7357	2559991.0818	23.12158	72.071211	0		L	25	400025	100025
25	Point	26	26	26	200061.9407	2559991.0818	23.121585	72.071505	0		L	26	400026	100026
26	Point	27	27	27	187104.0214	2559326.5731	23.113192	71.945261	0		L	27	400027	100027
27	Point	28	28	28	187134.2264	2559326.5731	23.113198	71.945555	0		L	28	400028	100028
28	Point	29	29	29	184113.7324	2557725.7113	23.098184	71.91643	0		L	29	400029	100029
29	Point	30	30	30	198642.3085	2557212.2273	23.096258	72.058205	0		L	30	400030	100030
30	Point	31	31	31	198642.3085	2557182.0224	23.095986	72.058211	0		L	31	400031	100031
31	Point	32	32	32	244674.637	2556638.3335	23.098813	72.507301	0		L	32	400032	100032
32	Point	33	34	34	254853.7017	2555399.9309	23.089174	72.606808	0		L	34	400033	100033
33	Point	34	33	33	196739.3973	2554523.9877	23.07166	72.04018	0		L	33	400034	100034
34	Point	35	36	36	196769.6022	2554523.9877	23.071665	72.040475	0		L	36	400035	100035
35	Point	36	42	42	254098.5782	2554403.1679	23.080066	72.599601	0		L	42	400036	100036
36	Point	37	35	35	254128.7832	2554403.1679	23.08007	72.599895	0		L	35	400037	100037
37	Point	38	37	37	193900.1329	2553587.6345	23.062691	72.012685	0		L	37	400038	100038
38	Point	39	38	38	241925.9874	2553497.0197	23.070038	72.481015	0		L	38	400039	100039
39	Point	40	39	39	188674.6783	2552983.5357	23.05627	71.961865	0		L	39	400040	100040
40	Point	41	40	40	195047.9206	2552832.511	23.056091	72.024024	0		L	40	400041	100041
41	Point	42	41	41	252256.0769	2551926.3628	23.057438	72.582027	0		L	41	400042	100042
42	Point	43	43	43	252256.0769	2551896.1579	23.057165	72.582032	0		L	43	400043	100043
43	Point	44	44	44	204894.7311	2547727.8762	23.011816	72.121002	0		L	44	400044	100044
44	Point	45	45	45	204924.936	2547727.8762	23.011822	72.121296	0		L	45	400045	100045
45	Point	46	46	46	217278.7564	2547395.6218	23.010969	72.241769	0		L	46	400046	100046
46	Point	47	47	47	217308.9614	2547395.6218	23.010974	72.242063	0		L	47	400047	100047
47	Point	48	48	48	201270.1383	2544586.5624	22.98283	72.086285	0		L	48	400048	100048
48	Point	49	49	49	201300.3432	2544586.5624	22.982835	72.086579	0		L	49	400049	100049
49	Point	50	50	50	248873.1236	2544465.7427	22.989596	72.55025	0		L	50	400050	100050
50	Point	51	51	51	248933.5335	2544465.7427	22.989605	72.550839	0		L	51	400051	100051
51	Point	52	52	52	214741.5415	2544254.3081	22.982193	72.21762	0		L	52	400052	100052
52	Point	53	53	53	214771.7464	2544254.3081	22.982198	72.217914	0		L	53	400053	100053
53	Point	54	54	54	264911.9467	2543861.6439	22.986485	72.706701	0		L	54	400054	100054
54	Point	55	57	57	264911.9467	2543831.4389	22.986213	72.706706	0		L	57	400055	100055
55	Point	56	55	55	263341.2899	2543378.3648	22.981901	72.691463	0		L	55	400056	100056
56	Point	57	56	56	263371.4948	2543378.3648	22.981905	72.691758	0		L	56	400057	100057
57	Point	58	58	58	214348.8773	2542290.987	22.964411	72.214156	0		L	58	400058	100058
58	Point	59	59	59	214379.0822	2542290.987	22.964416	72.214451	0		L	59	400059	100059
59	Point	60	60	60	272795.4361	2541988.9376	22.970675	72.783836	0		L	60	400060	100060

1 (1 out of 268 Selected)

outlets1

Figure 6.20 Location of the Vasna Barrage used for calibration and validation of the SWAT model

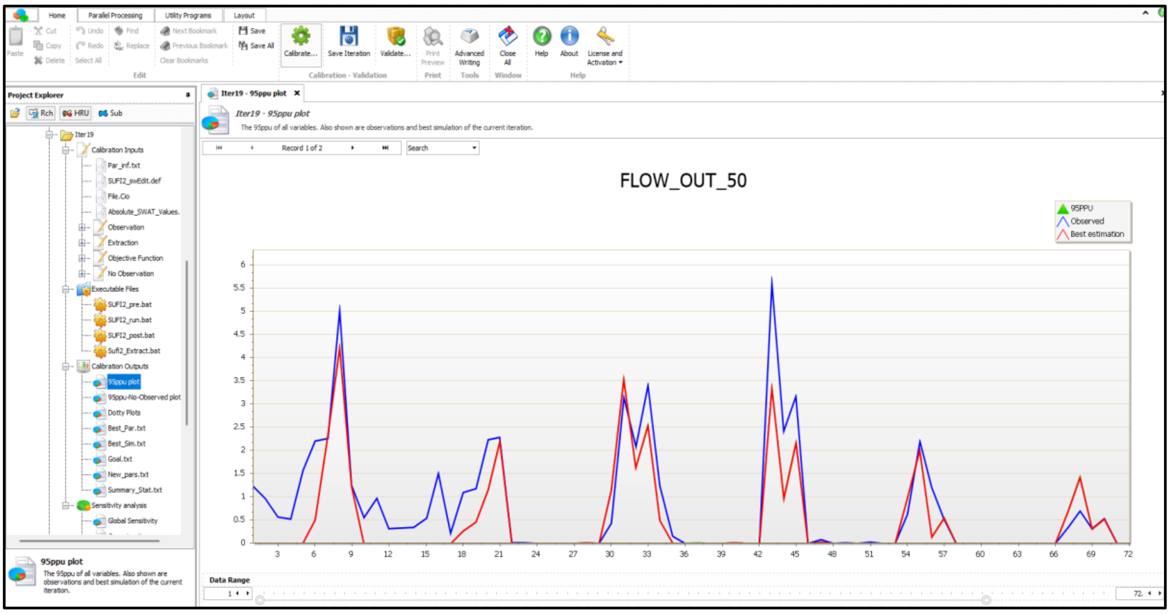

Figure 6.21 SWATCUP calibration results

Figure 6.21 shows the 95 Percent Prediction Uncertainty (95PPU) graph that was created after calibrating the SWAT model with the SUFI-2 algorithm. The graph illustrates the comparison between observed and simulated streamflow along with the uncertainty band generated during the calibration process. It can be observed that the majority of the observed streamflow values fall within the 95PPU range, indicating satisfactory model performance and acceptable prediction uncertainty.

Table 6.3 shows the best absolute values, which are edited in ARCSWAT for getting calibrated model output.

Table 6.3 Absolute values of sensitive parameters after calibration

Sensitivity rank	SWAT parameter name	SWAT parameter description	Unit	Range	Absolute value
1	SOL_AWC	Available water capacity of the soil layer	mm	0-1	0.45
2	REVAPMN	Minimum depth of water in the shallow aquifer (mm) for REVAP to occur.	mm	0-800	280
3	RCHRG_DP	Fraction of percolation from the root zone that enters the deep aquifer.	---	0-1.30	0.897
4	CN2	SCS curve Number	------	35-98	53.27
5	SURLAG.	Surface runoff lag time coefficient.	days	0-24	15.61
6	GWQMN	Threshold water depth in the shallow aquifer (mm) required before groundwater flow to the stream occurs.	mm	0-5000	150.00
7	GW_DELAY	Time lag (days) between water exiting the root zone and entering the shallow aquifer.	days	0-500	375.00
8	ESCO	Soil evaporation compensation coefficient	--------	0-1	0.01
9	GW_SPYLD	Specific yield of the shallow aquifer	------	0-600	390.00
10	ALPHA_BF	Baseflow recession constant |	Day^{-1}	0-1	0.30

The performance of the SWAT model during calibration was assessed by coefficient of determination (R^2) and the Nash–Sutcliffe efficiency (NSE) for the study area. The calibration results indicate that the model exhibited satisfactory performance, with a R^2 value of **0.79**, signifying strong correlation between observed and simulated streamflow.

The NSE value obtained during calibration was **0.74** demonstrating commendable model efficiency. The model is validated for the next five years (2020-2024) and showed satisfactory performance with an R^2 value of **0.72** and NSE value of **0.70**, indicating good agreement between observed and simulated data.

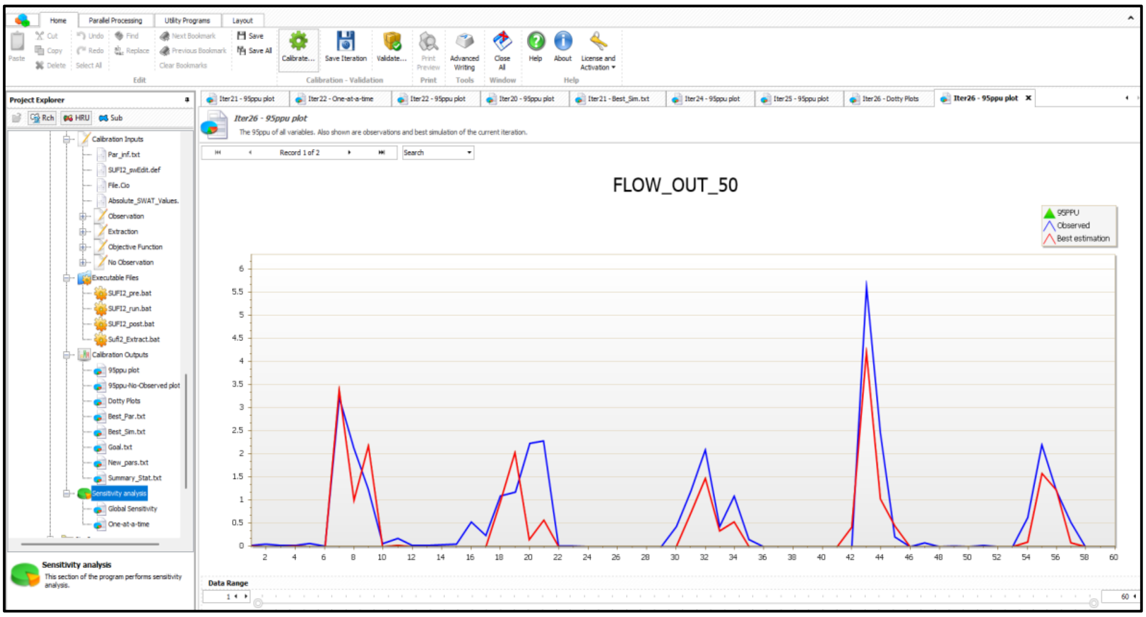

Figure 6.22 SWATCUP validation results

The SWAT model executed again for validation by altering the values of all sensitive over the years 2020 and 2024. During this process, observed streamflow data for the period 2020 to 2024 were compared with simulated streamflow generated by the calibrated SWAT model. Table 6.4 represents the summary results of calibration output as well as validation output, R^2 and NSE, indicating good agreement between observed and simulated data.

Table 6.4 Final summary of calibration and validation results in SWAT-CUP

Iteration	R^2	**NSE**
Calibration	0.79	0.74
Validation	0.72	0.70

After completing calibration and validation, the calibrated parameter values were added to the ArcSWAT model and then the model was run again for each decade to maintain consistency and stability in subsequent simulations.

6.6.2 Model Uncertainty and Challenges

During the development, calibration, and validation of the SWAT model, several practical challenges were encountered. Initially, the model execution was unsuccessful because of inconsistencies in the preparation of the input datasets. These issues were resolved by carefully reviewing, correcting, and converting all spatial and climatic datasets into formats compatible with the SWAT model. The climatic datasets were also verified for missing records, unit consistency, and continuous time series before model execution. During DEM preprocessing, an error occurred because the DEM was not initially projected to the required coordinate system. This issue was corrected by reprojecting the DEM to WGS 1984 UTM Zone 43N, after which watershed delineation and model setup were successfully completed. Furthermore, the initial simulations using the default SWAT parameter values did not satisfactorily reproduce the observed streamflow. Therefore, sensitivity analysis was performed to identify the most influential parameters, which were subsequently calibrated using the SUFI-2 algorithm in SWAT-CUP. Several calibration iterations were required to progressively refine the parameter ranges until satisfactory agreement between the observed and simulated streamflow was achieved, as indicated by acceptable values of R^2 and NSE. These steps reduced model uncertainty and improved the reliability of the simulated groundwater recharge results.

6.6.3 Model run after calibration and validation

After successful calibration and validation, the SWAT model was executed again using the optimized parameter set for the study area. The model was run for the selected decadal period to simulate long-term hydrological processes under consistent conditions.

Figures 6.23 to 6.29 show the parameter editing interface where key hydrological parameters were modified based on calibration results. The figure shows the model run initiation and execution process after parameter modification. This helps in verifying that the model was successfully re-run with updated inputs for the selected decadal period.

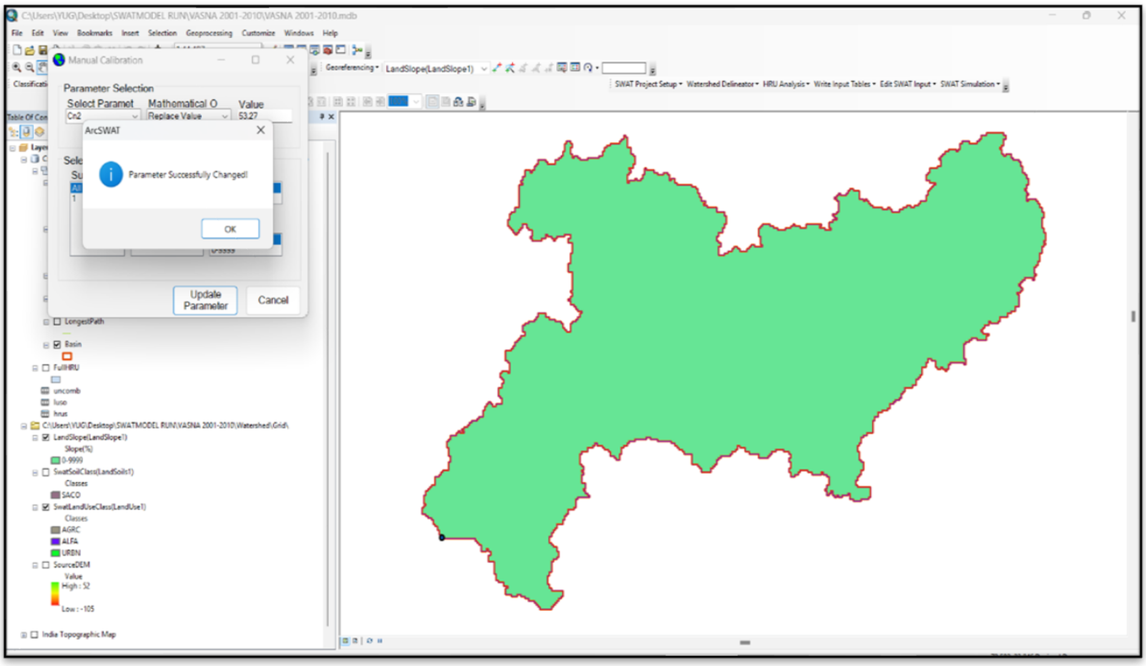

Figure 6.23 Curve number (CN2) parameter input used for calibrated SWAT model simulation

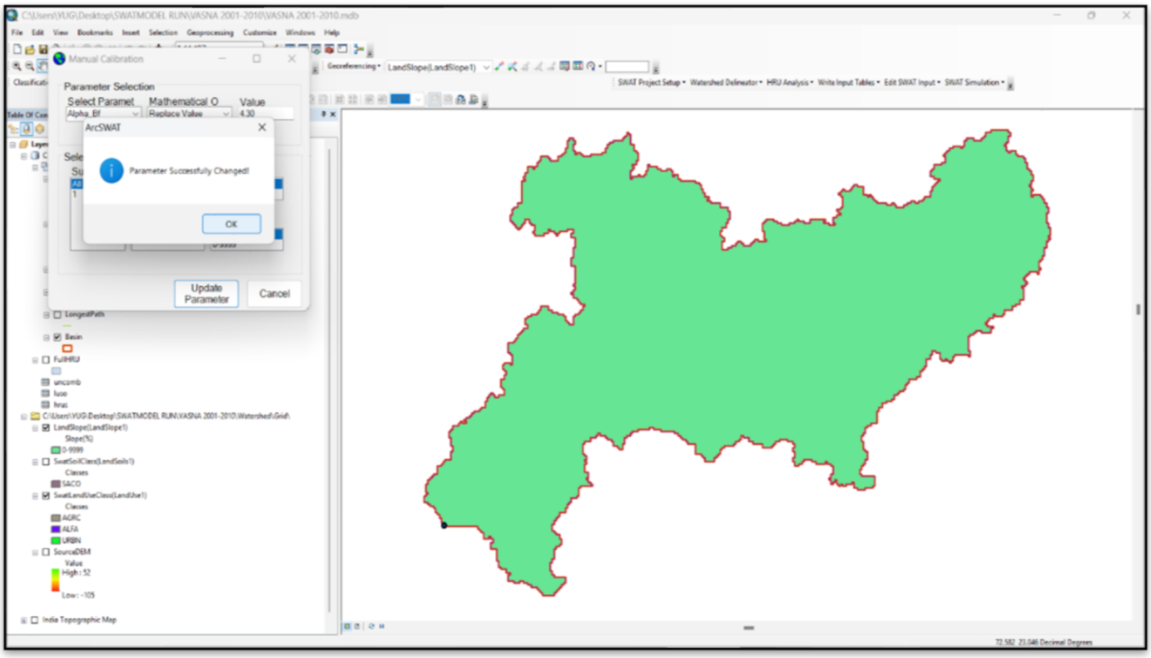

Figure 6.24 Baseflow Alpha factor (ALPHA_BF) parameter input for calibrated SWAT model execution

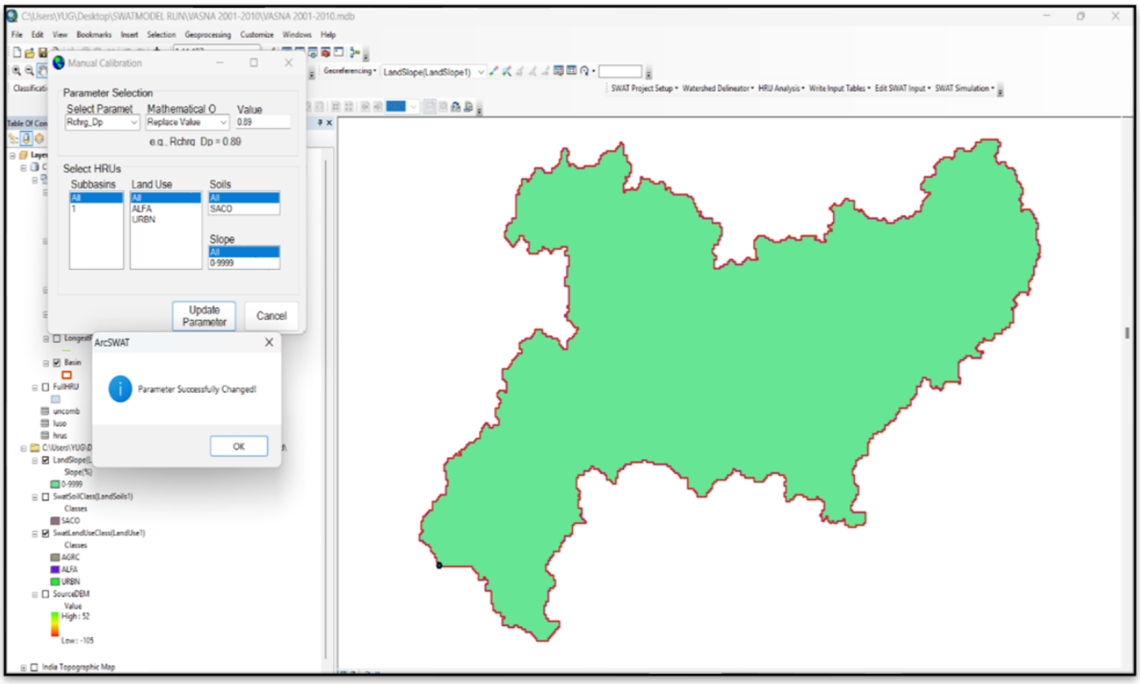

Figure 6.25 RCHG-DP parameter input for calibrated SWAT model execution

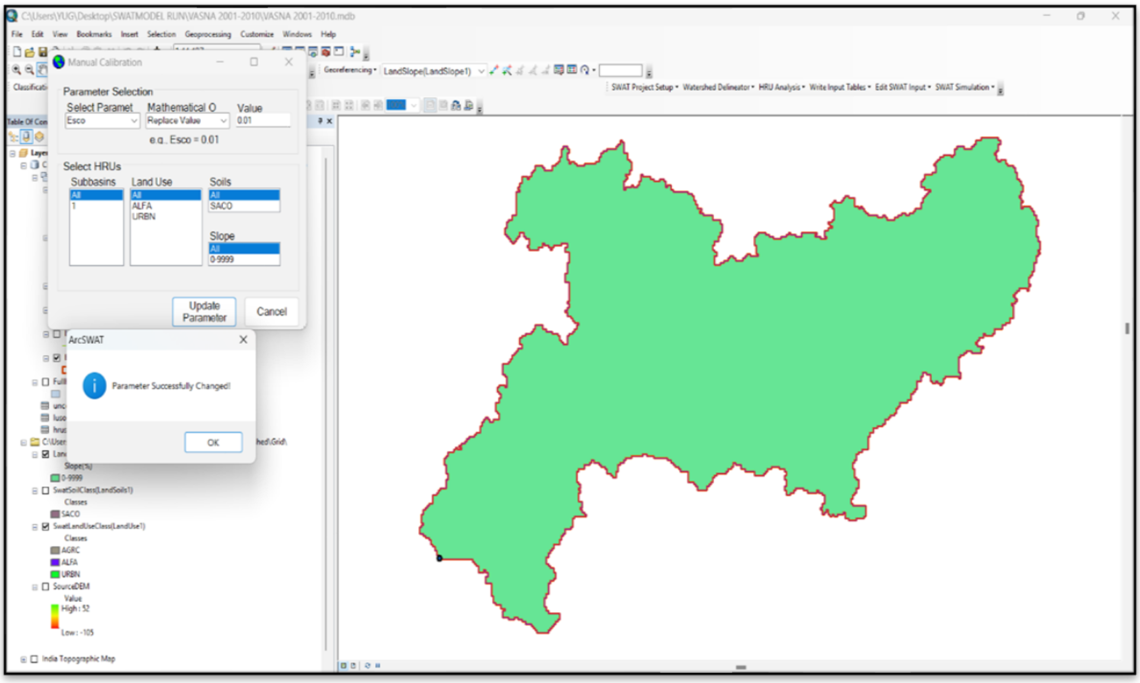

Figure 6.26 Soil evaporation compensation factor (ESCO) parameter input for calibrated model run

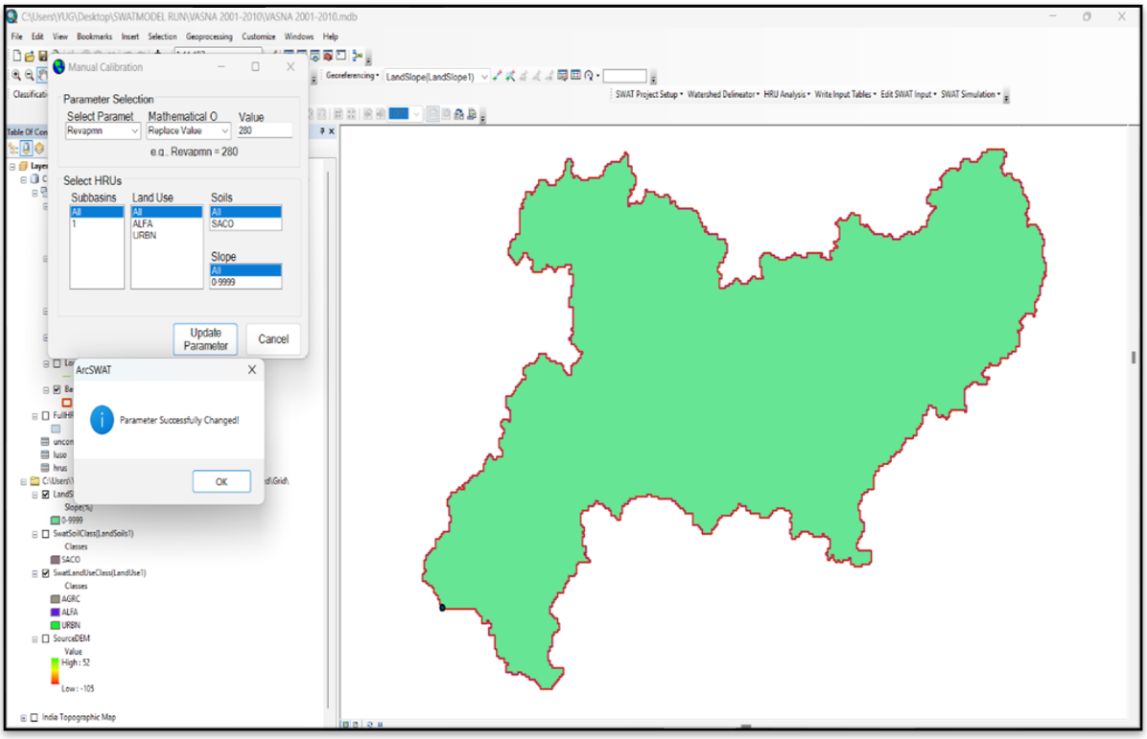

Figure 6.27 Threshold depth of water in shallow aquifer (REVAPMN) used in SWAT simulation

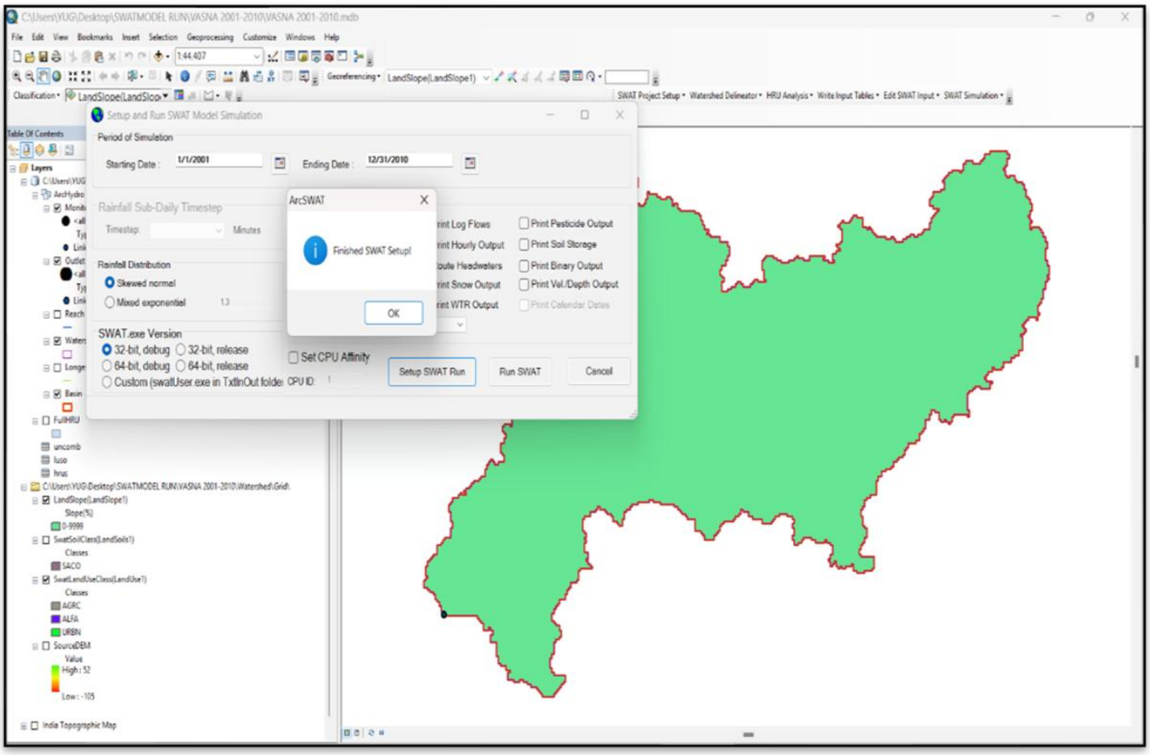

Figure 6.28 Simulation period setup for final SWAT model execution using calibrated sensitive parameters

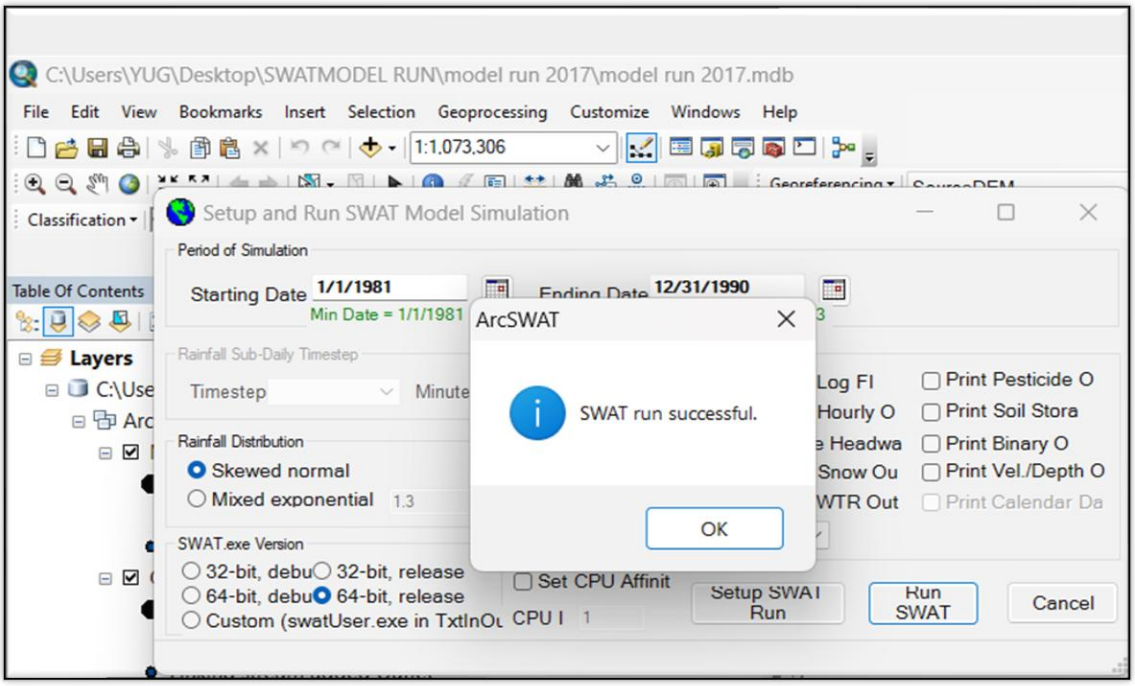

Figure 6.29 Successful SWAT model execution using calibrated and validated hydrological parameters

The hydrological cycle diagram was generated using the SWAT output viewer after re-execution of the SWAT model with calibrated parameters. The diagram represents key water balance components simulated by the model. This representation was prepared for each decadal period to illustrate the distribution and movement of water within the watershed under updated model conditions. *Figures 6.30 to 6.33* represent the decadal hydrological cycle based on SWAT model outputs.

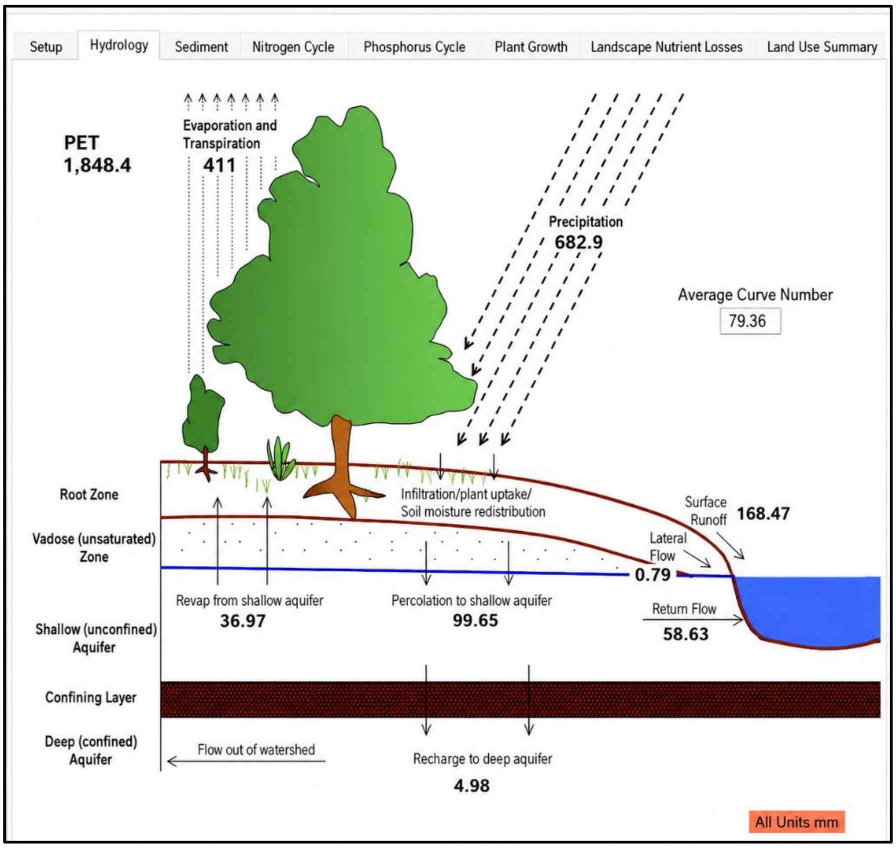

Figure 6.30 SWAT's schematic representation of the Hydrological for LULC 1985

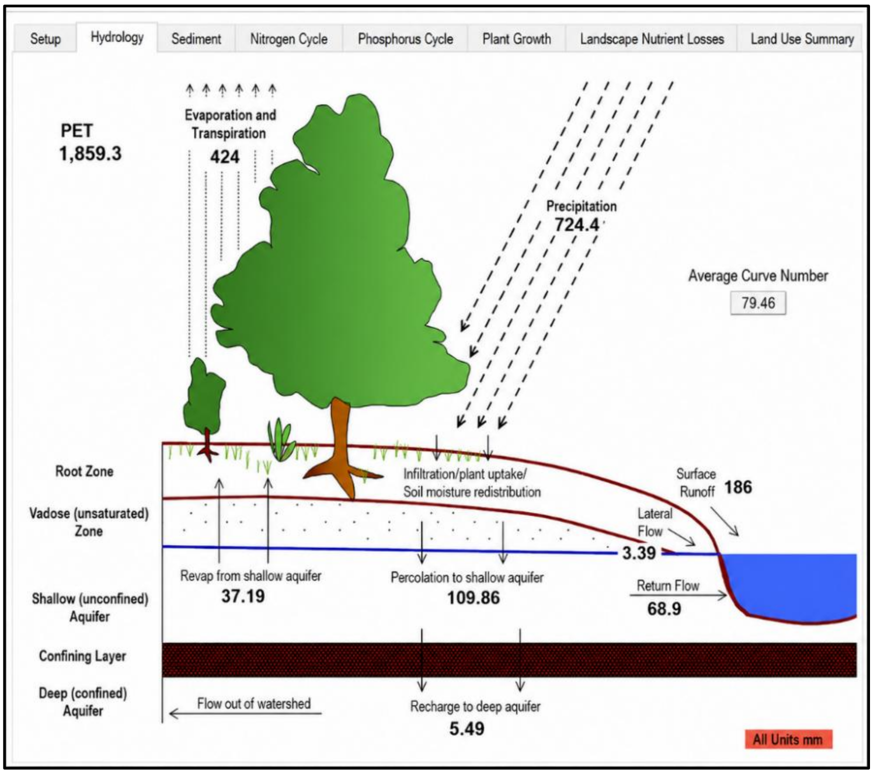

Figure 6.31 SWAT's schematic representation of the Hydrological cycle for LULC 1995

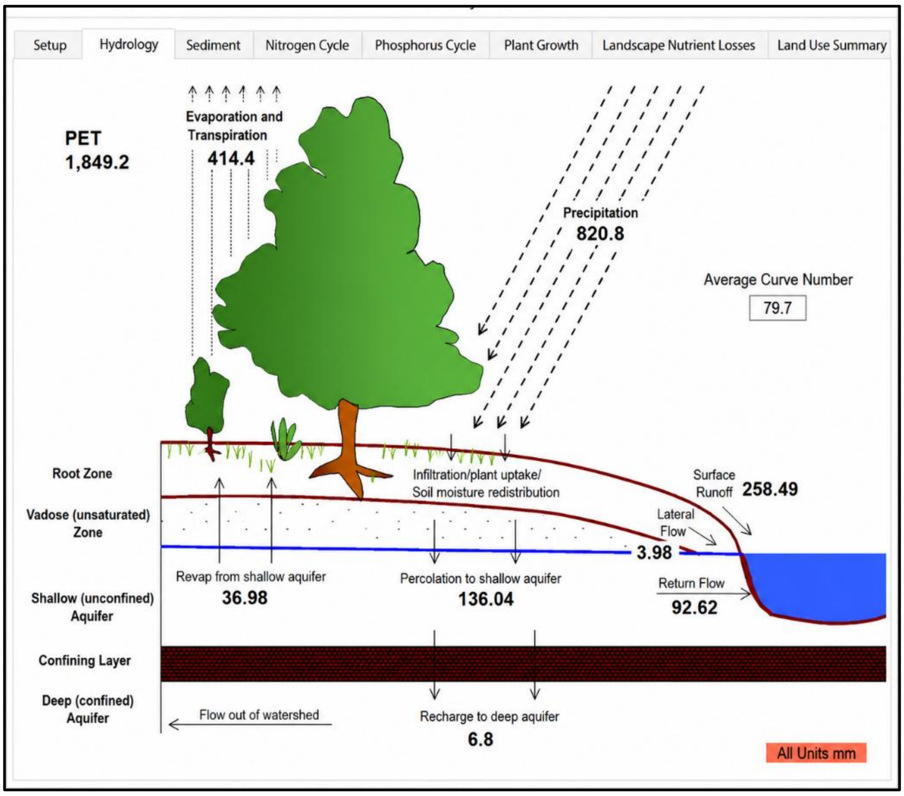

Figure 6.32 SWAT's schematic representation of the Hydrological cycle for LULC 2005

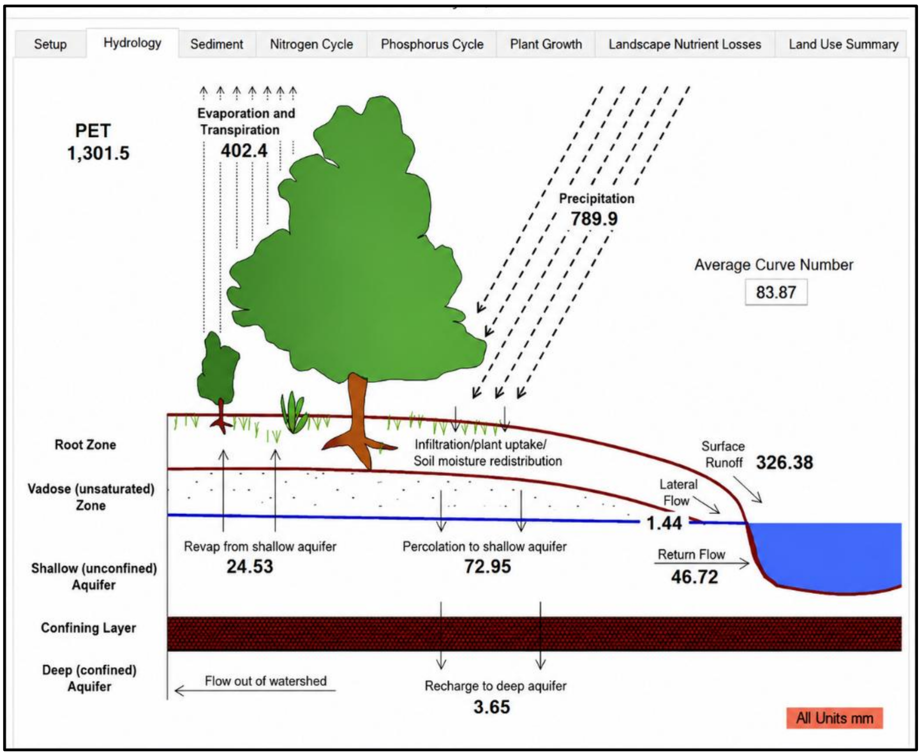

Figure 6.33 SWAT's schematic representation of the Hydrological cycle for LULC 2017

The hydrological cycle output represents the distribution and interaction of key watershed hydrological components, including precipitation, surface runoff, infiltration, evapotranspiration, percolation, groundwater recharge, and lateral flow within the study area. The decadal hydrological cycle analysis generated from the SWAT output viewer provides an understanding of long-term watershed hydrology and groundwater recharge dynamics within the study area.

Table 6.5 Year-wise groundwater recharge estimated from SWAT model

Year	GW RCHG mm	Precipitation (mm/year)
1981	102.0888	925.02
1982	90.1979	597.36
1983	262.4477	1013.03
1984	72.81089	718.94
1985	49.20824	578.46
1986	50.58208	347.51
1987	40.281	237.14
1988	222.5478	870.96
1989	92.18565	614.61
1990	132.8494	922.16
1991	38.1856	383.85
1992	72.75645	578.39
1993	29.80535	619.1
1994	254.6381	1007.58
1995	38.407	444.35
1996	79.56738	688.9
1997	111.6949	856.08
1998	111.6044	733.24
1999	44.12913	540.15
2000	87.82534	560.56
2001	98.56507	661.41
2002	40.92457	382.65
2003	108.2123	782.86
2004	137.5074	772.3
2005	198.5682	1078.19
2006	204.8231	1069.58
2007	237.6148	1101.68
2008	91.98349	785.83
2009	52.0349	367.8
2010	256.1118	1120.68
2011	221.076	980.74
2012	43.94848	551.23
2013	185.3698	824.22
2014	122.859	777.78
2015	52.20904	482.12
2016	48.2031	471.24
2017	94.01003	770.75
2018	41.46814	417.9
2019	89.70292	902.92
2020	116.0086	760.45

Following the analysis of the hydrological cycle, groundwater recharge values were extracted using the SWAT output viewer. The output viewer was utilized to access .hru files, from which recharge values corresponding to each hydrological response unit (HRU) were obtained.

The year-wise groundwater recharge values were estimated by aggregating recharge outputs from all hydrological response units (HRUs) for the study area. Daily recharge values obtained from the SWAT model were summed and converted into annual totals to represent year-wise groundwater recharge.

Table 6.5 represents annual groundwater recharge values for the selected study period, reflecting the combined effect of climatic conditions and land use characteristics.

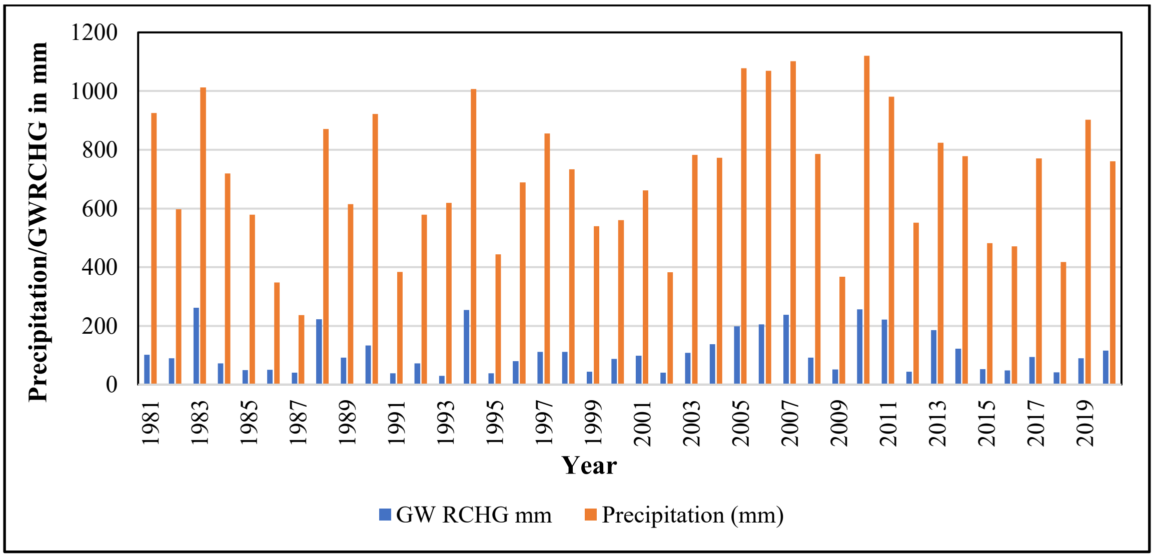

Figure 6.34 Comparative analysis of precipitation and groundwater recharge

Figure 6.34 illustrates the comparative variation between annual precipitation and simulated groundwater recharge (GW_RCHG) for the period 1981–2020 within the study area. The relationship between precipitation and groundwater recharge varied throughout the study period. In several years, comparatively high precipitation did not correspond to equivalent increases in groundwater recharge, which may be attributed to increasing urbanisation expansion of impervious surfaces, surface runoff generation, and changing land use characteristics within the watershed. Similarly, lower recharge values during certain periods indicate reduced infiltration potential and altered hydrological response of the watershed.

To understand the long-term effect of climatic variability and urbanisation on groundwater recharge dynamics within the study area, a comparative decadal analysis of precipitation, simulated groundwater recharge (GW_RCHG), and built-up area was carried out.

Table 6.6 Decadal variation in SWAT simulated precipitation, groundwater recharge, and built-up area

Decade	Average annual precipitation (mm)	Average annual groundwater recharge (mm)	% Groundwater recharge	% Baseline change	Built-up area (%)
1981–1990	682.9	99.65	14.59	-	1.6
1991–2000	724.4	109.86	15.16	0.58	3.2
2001–2010	820.8	136.04	16.57	1.98	3.3
2011–2020	789.9	72.95	9.23	5.36	7.2

The decadal analysis indicates substantial variation in hydrological conditions and urban growth throughout the study period. The built-up area increased consistently, from 1.6% to 7.2% in the most recent decade, reflecting rapid urbanisation within the study area. Although precipitation exhibited comparatively higher values during 2011-2020, groundwater recharge declined considerably during the most recent decade even under moderate rainfall conditions. analyses suggest the marginal increase in groundwater recharge was 0.58% during 1991-2000 and 1.98% increase during 2001-2010 with the baseline period (1981-1990) due to a relatively higher amount of rainfall, and during 2011-2020 groundwater recharge declined by 5.36% relative to the baseline due to rapid urbanisation.

Figure 6.35 illustrates the relationship between climatic variability, urbanisation, and groundwater recharge dynamics in the watershed. The graph indicates that precipitation exhibited fluctuating behaviour across different decades, whereas built-up areas showed a continuous increasing trend due to progressive urban expansion and land use transformation.

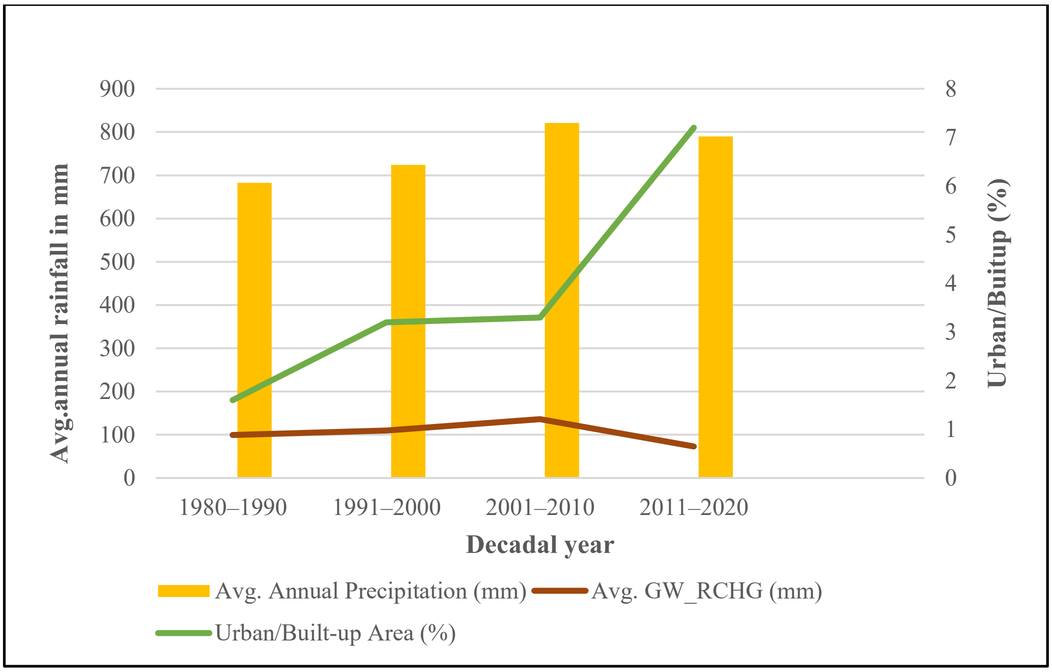

Figure 6.35 Decadal variation of precipitation, groundwater recharge (GW_RCHG) and Built-up area in the study area.

To further understand the temporal behaviour and long-term variability of groundwater recharge and precipitation within the study area, trend analysis was carried out using the Mann–Kendall (M–K) test. Although graphical and comparative analyses provide preliminary understanding of variations in hydrological parameters, statistical trend analysis is essential to determine whether the observed changes exhibit a significant increasing or decreasing trend over time.

6.7 Trend analysis of groundwater recharge

The trend analysis of groundwater recharge was carried out after extracting recharge values from the SWAT output viewer. The recharge data obtained from SWAT outputs were organized into a time series and analysed using the Mann–Kendall (M–K) test to identify long-term trends and represented in *Table 6.7.*

Positive Z-values represent increasing recharge trends, whereas negative Z-values indicate declining groundwater recharge conditions. The month-wise trend analysis further highlights seasonal variability in groundwater recharge processes. Variations in Z-values among different months indicate uneven temporal distribution of recharge influenced by rainfall intensity, land surface characteristics, evapotranspiration, etc.

Table 6.7 Mann-Kendall trend values for groundwater recharge

Month	1981-1990		1991-2000		2001-2010		2011-2020	
	Z	trend	Z	trend	Z	trend	Z	trend
January	0.27	+ve	1.43	+ve	1.18	+ve	0.89	+ve
February	0.09	+ve	1.35	+ve	1.18	+ve	0.27	+ve
March	0.27	+ve	1.35	+ve	1.18	+ve	-0.27	-ve
April	0.27	+ve	1.35	+ve	1.18	+ve	-0.27	-ve
May	0.27	+ve	1.35	+ve	1.18	+ve	0.18	+ve
June	0.27	+ve	1.43	+ve	1.18	+ve	-0.27	-ve
July	0.27	+ve	-0.09	-ve	-0.36	-ve	-0.81	-ve
August	-0.89	-ve	-1.25	-ve	0.54	+ve	-0.36	-ve
September	0.54	+ve	-0.36	-ve	1.43	+ve	-1.07	-ve
October	0.72	+ve	-0.18	-ve	1.25	+ve	-0.89	-ve
November	0.54	+ve	0.72	+ve	1.25	+ve	-0.89	-ve
December	0.27	+ve	0.72	+ve	1.25	+ve	-0.89	-ve
Monsoon	-0.36	-ve	-0.72	-ve	1.25	+ve	-0.72	-ve
Premonsoon	0.27	+ve	1.35	+ve	1.18	+ve	-0.89	-ve
Post Monsoon	0.54	+ve	-0.18	-ve	1.25	+ve	-0.89	-ve
Winter	0.54	+ve	0.54	+ve	1.25	+ve	-0.72	-ve

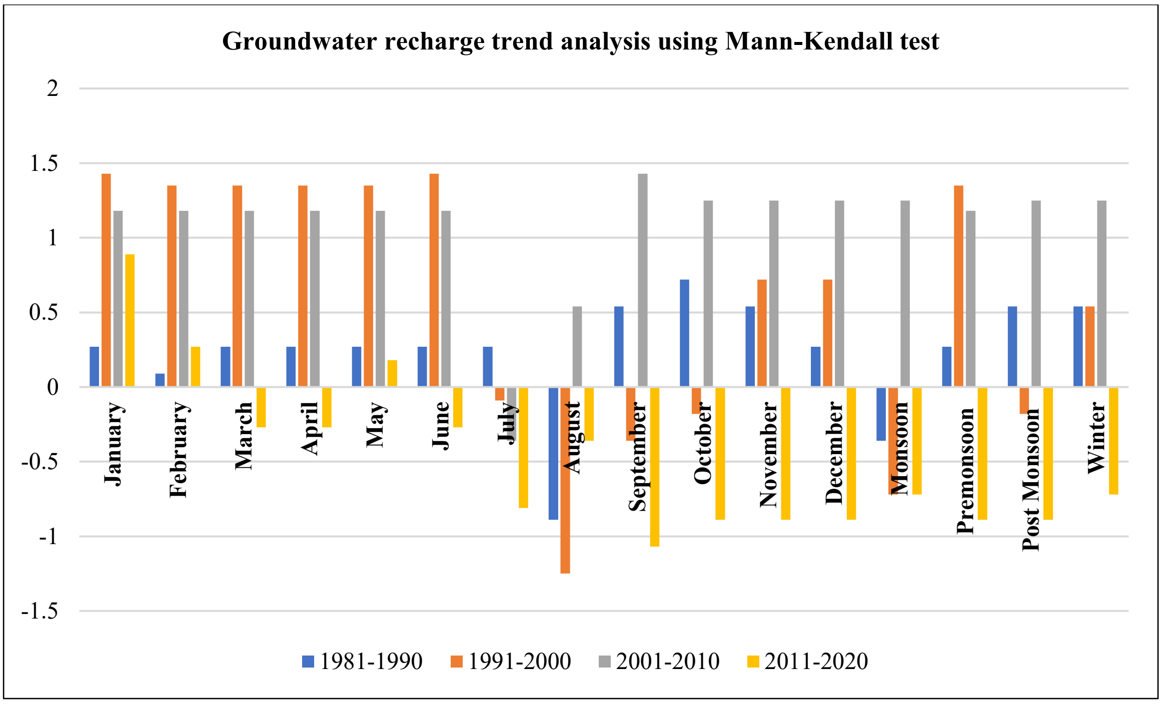

Figure 6.36 Groundwater recharge trend analysis using Mann-Kendall test

Figure 6.36 illustrates the temporal trend of simulated groundwater recharge (GW_RCHG) within the study area obtained through Mann–Kendall trend analysis. The graphical representation provides a clear understanding of long-term variations in shallow aquifer recharge under changing climatic conditions during the analysis period.

6.8 Summary of trend analysis

1981–1990

Monthly Trend: The monthly Z-values are almost uniformly positive but small, around ***0.27***. This suggests a very weak or negligible increasing trend in monthly recharge value.

Seasonal Trend: The Monsoon ***(-0.36)*** and Post Monsoon ***(0.54)*** periods show a negligible trend, while the pre-monsoon ***(0.27***) and Winter ***(0.54)*** periods also indicate a very weak positive trend.

1991-2000

Most of the months show a strong positive Z-statistic around ***1.35 to 1.45***, suggesting a strong increasing trend in recharge; July ***(-0.09)*** and August ***(-1.25)*** show a decreasing trend.

Seasonal Trend: The pre-monsoon ***(1.35)*** and monsoon ***(0.54)*** seasons show an increasing trend, while post-monsoon ***(-0.18)*** shows a weak decreasing trend. The overall decadal trend appears mostly positive but mixed.

2001-2010

Monthly Trend: This decade is characterized by a generally strong positive Z-statistic, with most months registering ***1.18 or 1.25***. This indicates a pronounced increasing trend in groundwater recharge across the year.
Seasonal Trend: All key seasons, monsoon ***(1.25)***, pre-monsoon ***(1.18)***, and post-monsoon ***(1.25)*** exhibit a clear, strong increasing trend.
2011-2020
This decade shows a dramatic shift to negative Z-statistics. Key recharge months like September ***(-1.07)***, October ***(-1.07)***, November ***(-0.89)***, and December ***(-0.89)*** all show a strong decreasing trend. The negative values for many months, including August ***(-0.81)***, indicate a significant, widespread decline in groundwater recharge.
Seasonal Trend: This sharp decline is reflected in the seasonal results: monsoon ***(-0.72)***, pre-monsoon ***(-0.89)***, and post-monsoon ***(-0.89)*** all show a strong negative Z-statistic.

Although the historical trend analysis provides valuable insight into past and present groundwater recharge behaviour within the study area, assessment of future hydrological conditions is equally essential for sustainable groundwater resource management. The Mann–Kendall trend analysis performed on historical precipitation and groundwater recharge datasets indicates temporal variability and possible changes in recharge conditions associated with climatic variability and urbanisation. However, historical analysis alone cannot fully explain the potential future response of watershed hydrology under changing climate scenarios.

Therefore, to further evaluate the future behaviour of groundwater recharge and hydrological processes, climate change forecasting using CMIP6 climate model projections was incorporated in the present study.

6.9 Simulation using forecasting scenarios

Simulations are performed under forecast scenarios to evaluate the potential future effects of urbanisation and climate variability on groundwater recharge in Ahmedabad. Climate projections are derived from the Coupled Model Intercomparison Project Phase 6 (CMIP6) framework, which provides state-of-the-art global climate model outputs for various greenhouse gas levels. Bias-corrected climate data used in this study were sourced from the Inter-Sectoral Impact Model Intercomparison Project (ISIMIP) to support hydrological modelling (Lange, 2019; Frieler et al., 2017).

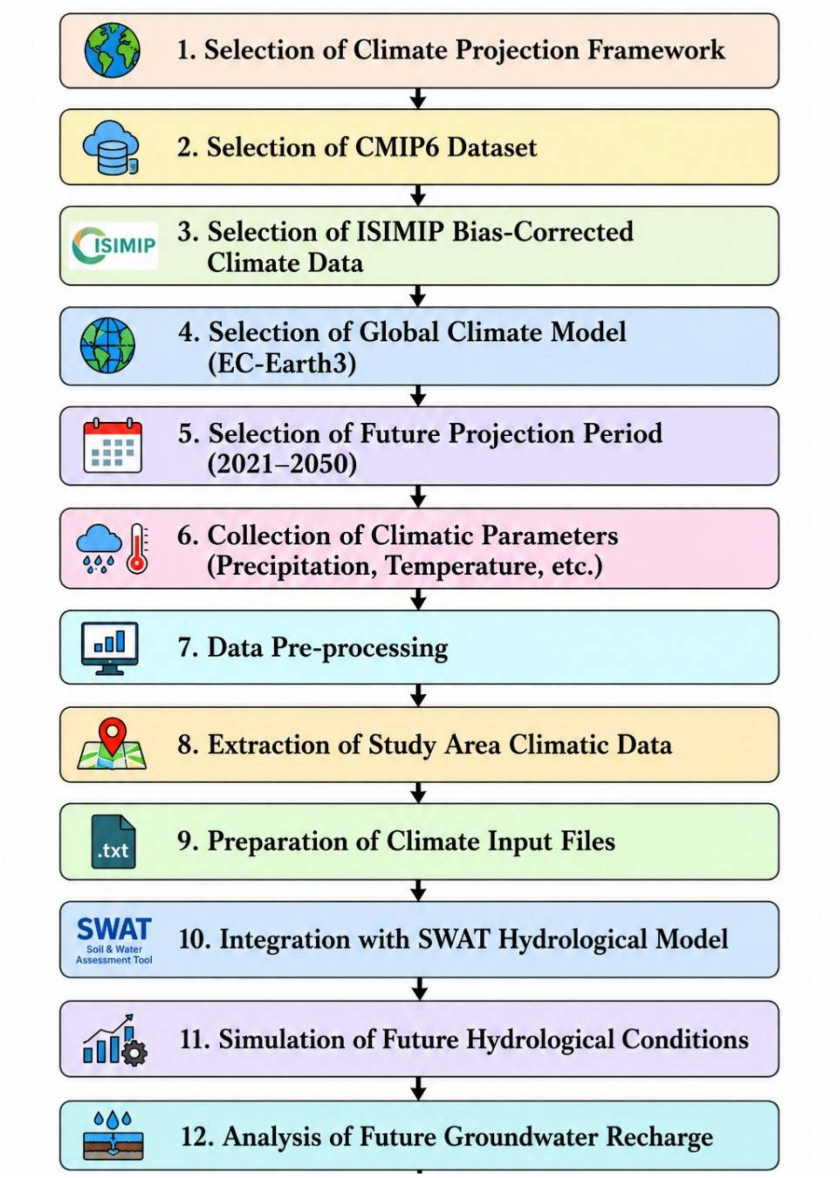

Figure 6.37 Methodological framework for CMIP6 ISIMIP EC-Earth3 climate projection and groundwater recharge assessment

Figure 6.37 illustrates the methodology employed for hydrological assessment and future climate projection. CMIP6 climate datasets are chosen, ISIMIP bias-corrected EC-Earth3 climatic variables are extracted and pre-processed, SWAT-compatible climate inputs are prepared, and future hydrological conditions are simulated.

The Inter-Sectoral Impact Model Intercomparison Project's standardized framework, especially the ISIMIP3b protocol used in the present study's climate forecasts to guarantee scientific consistency. In order to reduce the systematic biases, present in the raw Global Climate Model (GCM) outputs, the climate forcing datasets were obtained from the Coupled Model Intercomparison Project Phase 6 and then bias-adjusted within the ISIMIP framework using reference observational datasets like W5E5 (Frieler et al., 2017; Lange, 2019). The EC-Earth3 General Circulation Model (GCM) was used in this study because it is widely available across the range of SSP scenarios used in future projections (Pimonsree, S., Kamworapan, S., Gheewala, S. H., Thongbhakdi, A., & Prueksakorn, K. 2023).

Standardized ISIMIP variables were chosen for temperature and rainfall analysis based on their abbreviations. The variables "tas" and "pr" were used to measure near-surface air temperature and precipitation, respectively. These datasets were downloaded under appropriate SSP scenarios and bias-adjusted climatic forcing (sometimes denoted by "w5e5" in filenames). SSP370 is a useful scenario for comprehending possible effects of climate change on hydrology and water resources and predicts steady increases in future rainfall and temperature throughout South Asia. (South Asian climate forecasts with bias correction from Coupled Model Intercomparison Project-6, Mishra,2023). Among the common file formats were the following:

tas_day_EC-Earth3_w5e5_ssp370_global_2021_2050.nc

pr_day_EC-Earth3_w5e5_ssp370_global_2021_2050.nc

All datasets were provided in NetCDF format with ISIMIP standards.

Spatial subsetting was performed to extract the grid corresponding to Ahmedabad using latitude–longitude. It is required to convert temperature and precipitation in the required unit, i.e., temperature values were converted from Kelvin to degrees Celsius and precipitation from kg m^{-2} s^{-1} to mm/day. 1 kg m^{-2} is equivalent to 1 mm of water depth; the conversion to mm/day was performed by multiplying by the number of seconds in a day (86,400 seconds), as shown below:

$$P_{mm/day} = P_{kg\,m^{-2}\,s^{-1}} \times 86400 \qquad 6.1$$

After downloading and converting, the above required data model validation was performed by comparing historical ISIMIP datasets (1981–2020) derived from EC-Earth3 with observed climate data. Statistical evaluation was carried out using the coefficient of determination (R^2), which quantifies the agreement between observed and simulated datasets (Wilks, 2011). R^2 values are shown *in Fig. 6-38, Fig. 6-39 and Fig.6-40* for both temperature and rainfall, providing a robust measure of model performance. Higher R^2 values for average rainfall, Tmax, and Tmin are 0.96, 0.94 and 0.97, respectively, which indicate stronger agreement and increased confidence in the applicability of EC-Earth3 for regional climate projections.

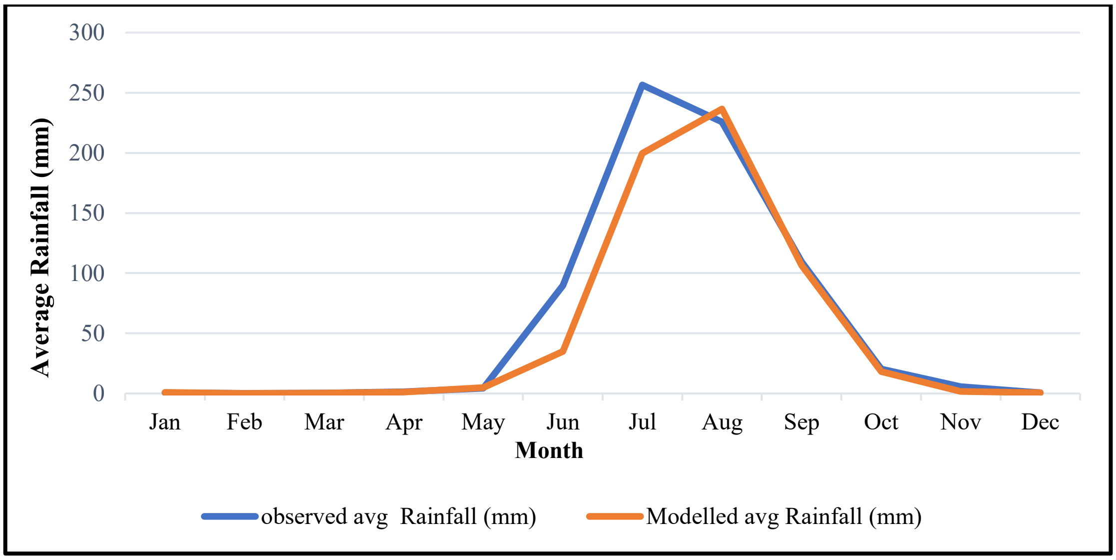

Figure 6.38 Comparison between observed and modelled monthly rainfall (1981-2020)

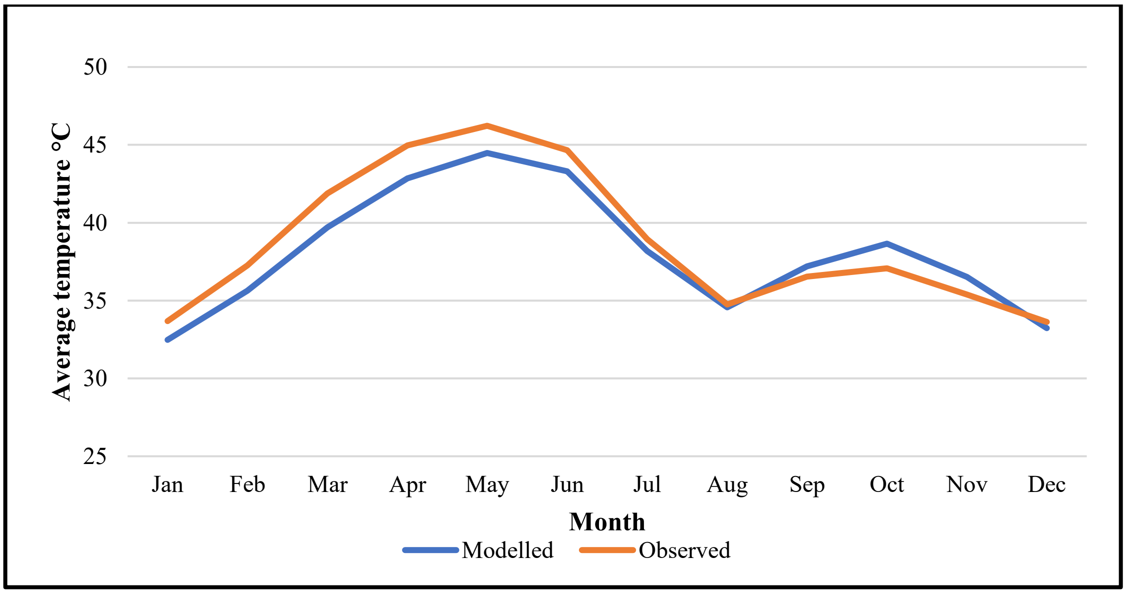

Figure 6.39 Comparison between observed and modelled monthly Tmax (1981-2020)

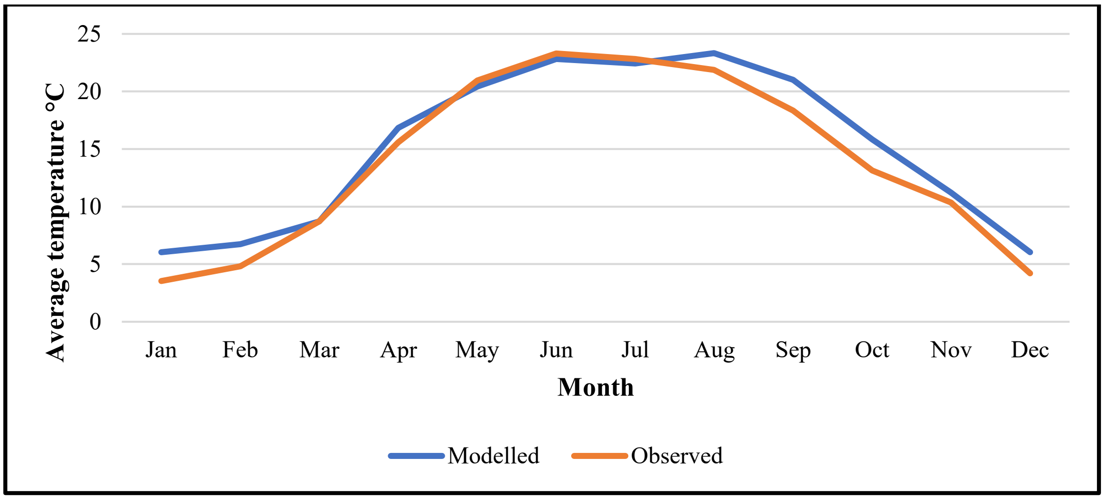

Figure 6.40 Comparison between observed and modelled monthly Tmin (1981-2020)

Following the successful validation of historical simulations (1981–2020) against observed datasets, the next phase of the study focused on the analysis of future climate projections for the period 2021–2050. The first step in the post-validation phase involved the extraction of future datasets (2021–2050) for the selected variables. These datasets were converted as previously explained.

The data were then processed into SWAT-compatible weather input formats, including daily time series for precipitation and temperature. Subsequently, the prepared datasets were integrated into the SWAT model, and simulations were carried out for the future period (2021–2050) using calibrated parameters.

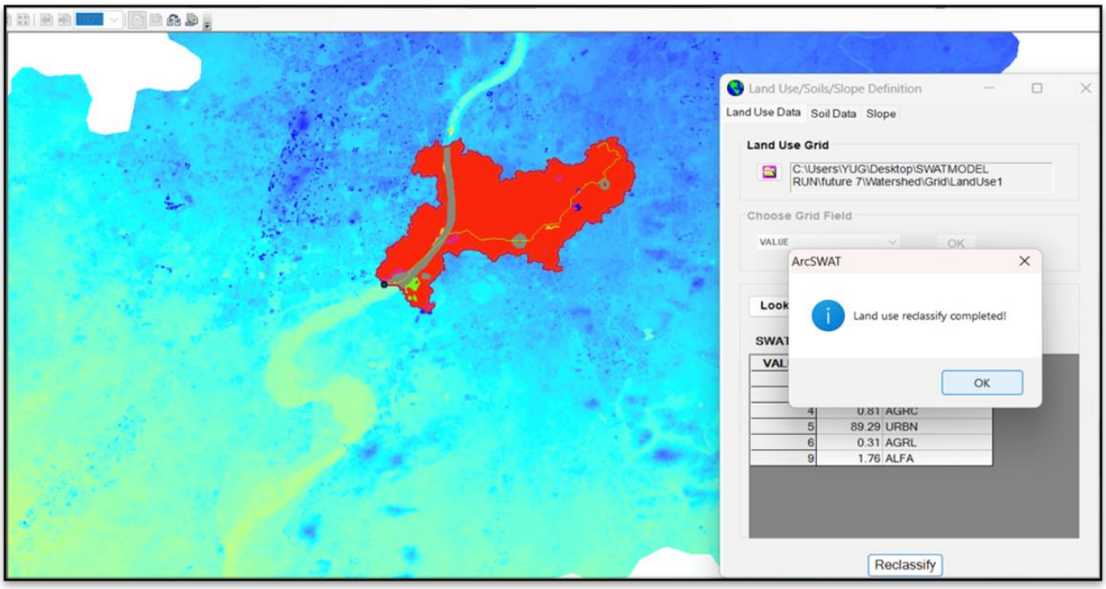

Figure 6.41 Input of LULC data into the SWAT model for future Hydrological simulation

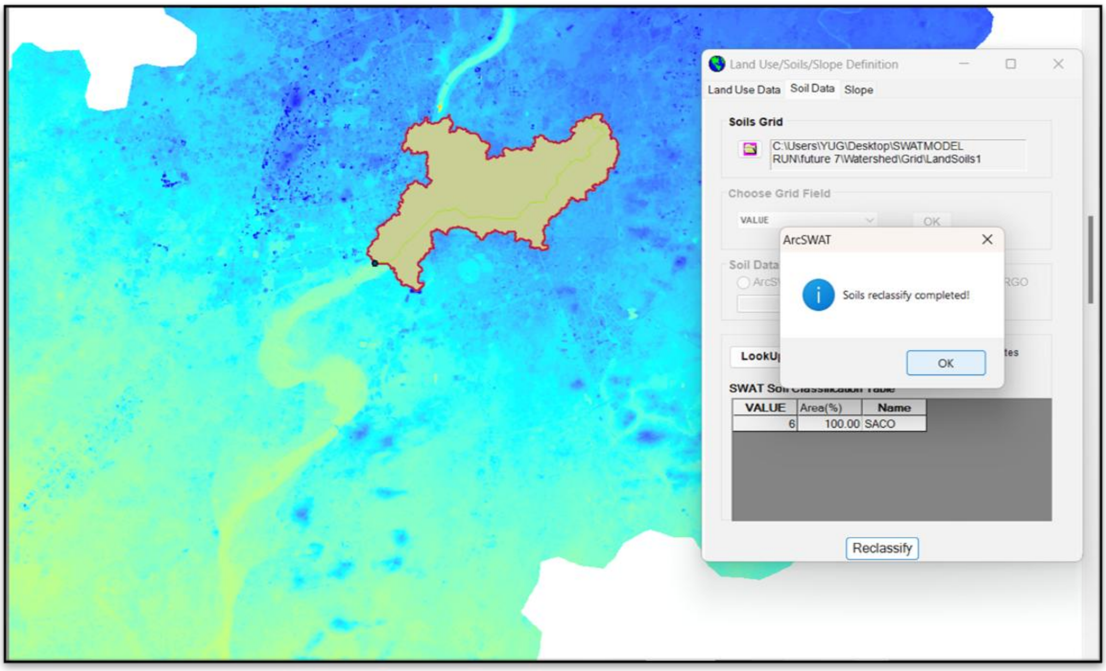

Figure 6.42 Input of soil parameter data into the SWAT model for future Hydrological simulation

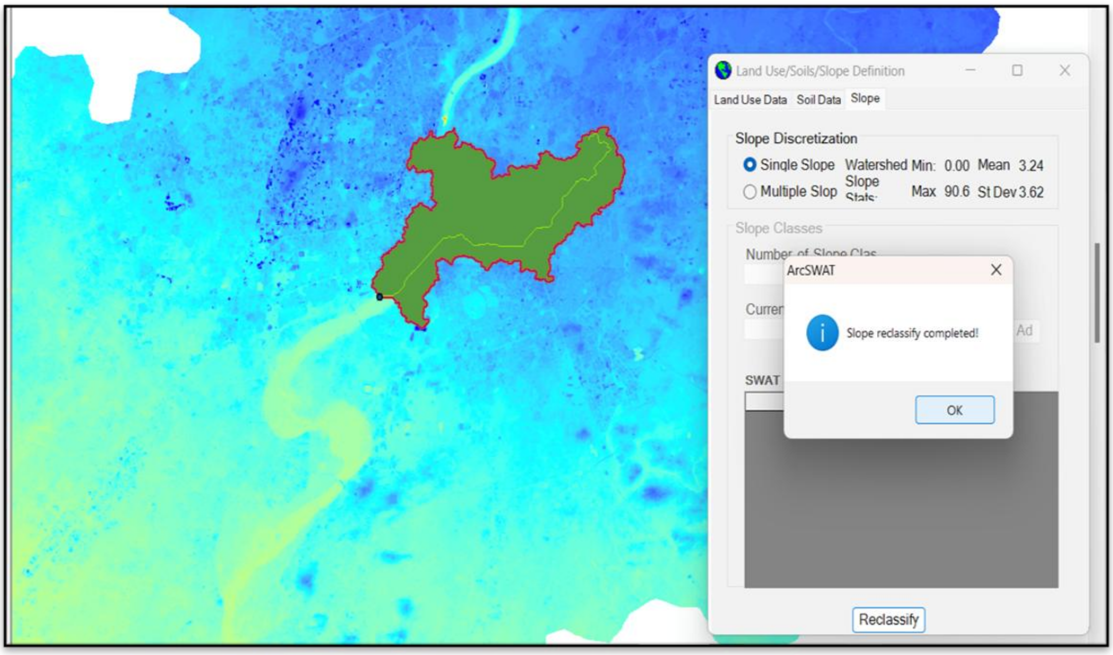

Figure 6.43 Input of slope classification data into The SWAT model for future Hydrological simulation

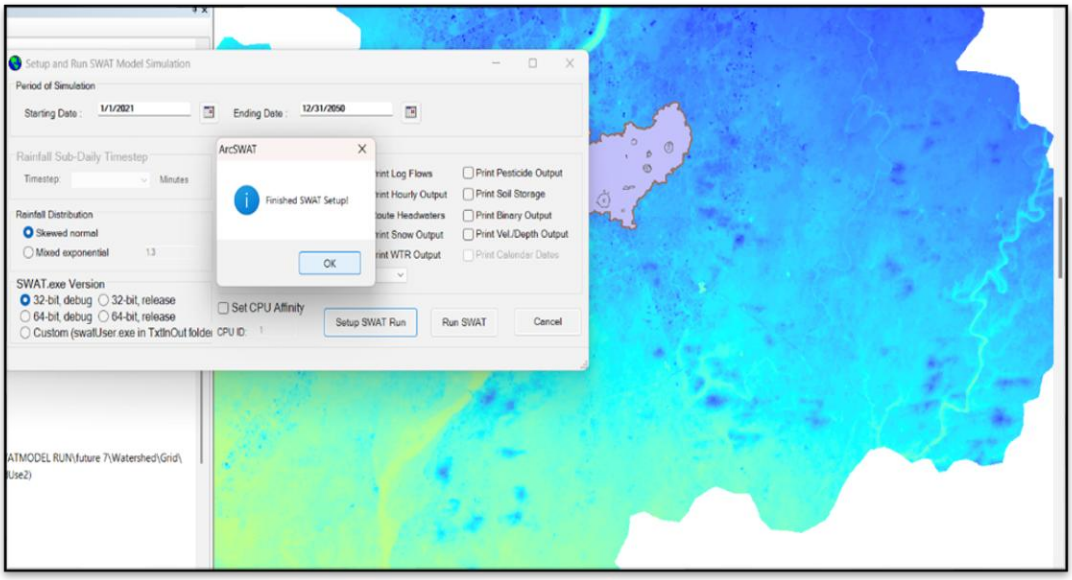

Figure 6.44 Successful execution of future SWAT model simulation for the period 2021–2050

Figure 6.44 illustrates the successful execution of the SWAT model for future hydrological simulation during the period 2021–2050.

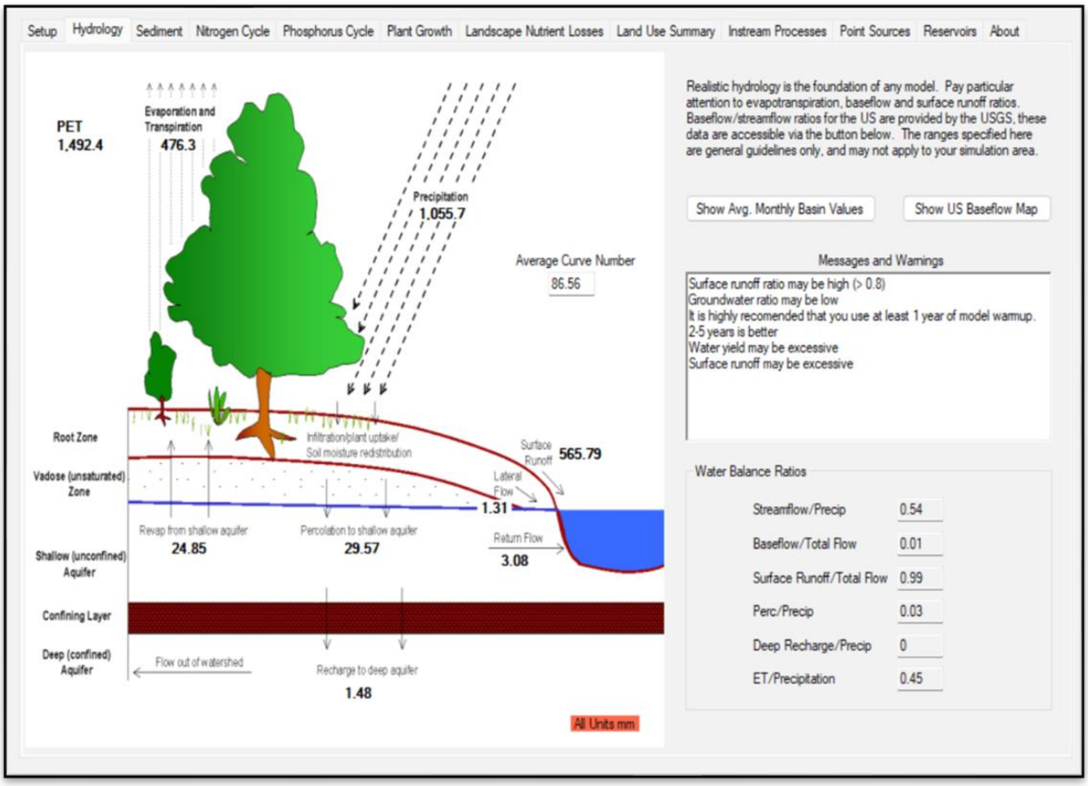

Figure 6.45Projected Hydrological cycle (2021–2050) derived from SWAT model outputs

Figure 6.45 illustrates the projected hydrological cycle for the period 2021–2050 based on SWAT model simulations. The successful model run generated simulated outputs for assessment of future precipitation variability and shallow aquifer recharge within the study area. Table 6.8 shows comparison of baseline and projected groundwater recharge, which decreases up to 11.79% by 2050.

Table 6.8 Comparison of baseline and projected groundwater recharge

Period	Precipitation (mm)	Groundwater recharge (mm)	Recharge change (%)
1981-1990 (baseline)	682.9	99.65	-
2021-2050	1055.7	29.57	11.79%

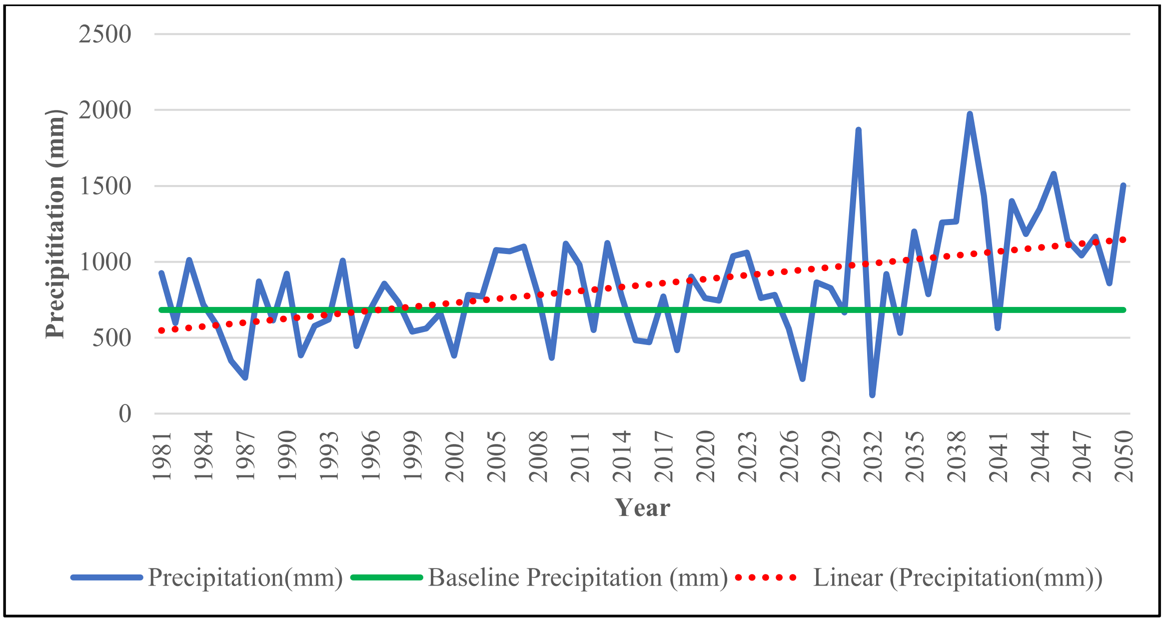

Figure 6.46 Long-Term Annual Rainfall Trend and Projection (1981–2050)

Figure 6.46 illustrates the Long-Term Annual Rainfall Trend and Projection (1981–2050), which helps in understanding the pattern and fluctuation of rainfall over the future period. The fluctuations observed in the projected rainfall pattern indicate possible variations in future climatic conditions and rainfall distribution within the watershed. Years such as 2031, 2039, and 2045 exhibit comparatively higher rainfall magnitudes, whereas lower rainfall conditions are observed during years such as 1987,2027 and 2032.

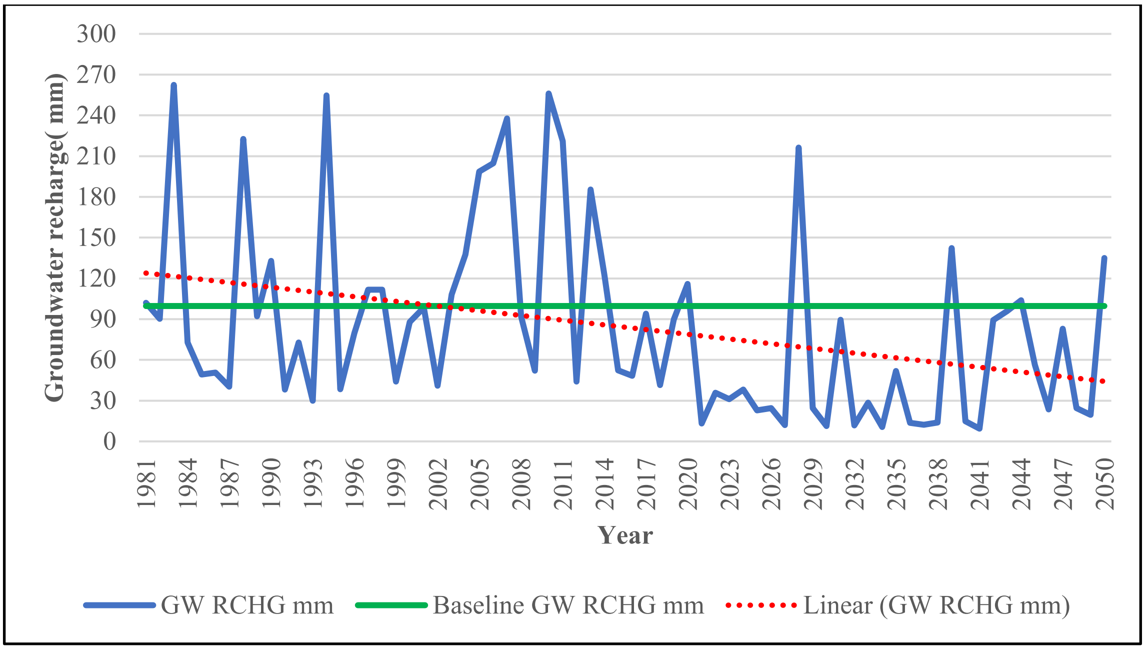

Figure 6.47 Long-Term Groundwater Trend and Projection (1981–2050)

Figure 6.47 illustrates Long-Term Groundwater Trend and Projection (1981–2050) derived from SWAT model outputs.

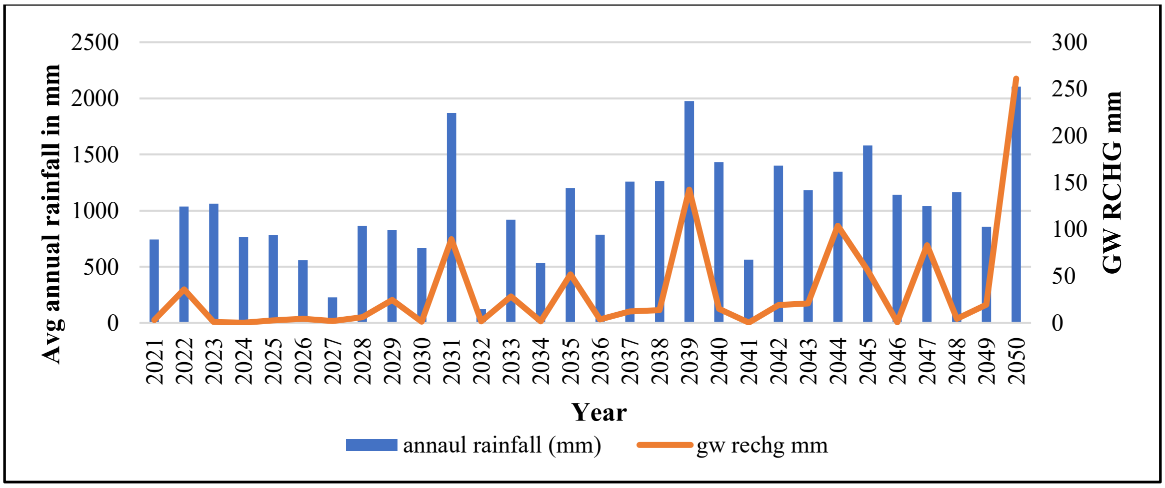

Figure 6.48 Comparative analysis of groundwater recharge and precipitation (2021–2050)

Figure 6.48 presents a comparative analysis of projected groundwater recharge and precipitation for the period 2021–2050 of the study area. The graph represents the relationship between future precipitation patterns and the corresponding groundwater recharge behaviour simulated using the SWAT model under projected climatic conditions. Higher recharge values are particularly observed during years such as 2031, 2039, 2044, 2047, and 2050, which correspond with relatively high annual precipitation conditions. Conversely, years with lower rainfall magnitudes exhibit comparatively reduced recharge values, indicating the strong dependence of groundwater recharge on precipitation variability.

However, the fluctuations observed in recharge behaviour also indicate the influence of watershed characteristics, infiltration capacity, land use conditions, and surface runoff generation on aquifer replenishment processes.

6.10 Summary

Present study uses the Soil and Water Assessment Tool (SWAT), a semi-distributed, physically-based model created by the USDA Agricultural Research Service. The model was set up for the Vasna Barrage catchment.

The model was calibrated for the period 2014–2019 and validated for 2020–2024 using observed streamflow data at the Vasna barrage outlet. The Sequential Uncertainty Fitting (SUFI-2) algorithm in SWAT-CUP was used to calibrate the model, focusing on ten important groundwater parameters. The calibration achieved a Nash-Sutcliffe Efficiency (NSE) of ***0.74*** and a coefficient of determination (R^2) of ***0.79***, while validation achieved NSE of ***0.70*** and R^2 of ***0.72*** showing satisfactory model performance. The sensitive parameter values obtained after calibration were summarized in ***Table 6.3.***

Following calibration and validation, the model was run for the historical period 1981–2020 to simulate decadal groundwater recharge. The results showed that with precipitation of 682.9 mm (1981–1990), 724.4 mm (1991–2000), 820.8 mm (2001–2010), and 789.9 mm (2011–2020), groundwater recharge shows 99.65 mm (1981–1990), 109.86 mm (1991–2000), 136.04 mm (2001–2010), and 72.95 mm (2011–2020) in the same period. In the most recent decade (2011–2020), despite high precipitation of 789.9 mm, groundwater recharge decreased to ***72.95*** mm, reflecting a decline of ***5.36%*** from the baseline period (1981–1990). This decline cannot be explained by rainfall variability and is directly attributable to the expansion of the impervious built-up area identified in the LULC change detection.

The CMIP6 EC-Earth3 model was selected for future climate projections, based on its high performance in simulating Indian climatic conditions ($R^2 = 0.96$ for rainfall, 0.94 for Tmax, and 0.97 for Tmin). Bias-corrected data from the ISIMIP3b framework were used under the SSP3-7.0 (medium-high emission) scenario. The projected climate data up to 2050 were incorporated into the calibrated SWAT model while holding LULC constant at the 2017 level to isolate the effect of climate change. The findings suggest that under SSP3-7.0, the mean annual groundwater recharge is projected to decrease by ***11.79%*** by 2050. This decline occurs despite projected increases in total annual rainfall because rainfall is expected to become more intense but less frequent, leading to higher surface runoff, reduced infiltration opportunity, and increased evapotranspiration demand due to pre-monsoon warming.

These findings provide a strong quantitative basis for prioritizing artificial recharge interventions, protecting high-recharge zones, and implementing water-sensitive urban planning in the Ahmedabad district.

CHAPTER 7
RESULTS AND DISCUSSIONS

7.1 Results

The present study evaluates the impacts of land use/land cover (LULC) changes and urbanization on groundwater recharge potential and watershed hydrological behaviour through geospatial and hydrological modelling techniques. The analysis was carried out to assess the influence of changing land cover conditions, increasing built-up areas, and urban expansion on groundwater recharge dynamics within the study area.

The study commences with a trend analysis of meteorological variables (precipitation and temperature) from 1981 to 2020, employing the Mann–Kendall test and Sen's slope method on monthly, yearly, and seasonal rainfall data. The non-parametric Mann-Kendall (M-K) test presented in ***Table 4.2*** conducted a trend analysis over a span of 40 years. Predominantly positive Z values for most months, including the monsoon **(Z = 0.87)** and yearly ***(Z = 0.81)*** periods, indicating a general upward trend in rainfall, although negative Z values in certain months and during winter reflect slight downward trends.

The trend analysis presented in ***Table 4.1*** indicated a clear seasonal pattern for maximum temperature. Positive trends between ***0.74*** and ***1.21*** were noted from February to May, signifying warming throughout the late winter and pre-monsoon phase. Conversely, negative trends of ***–0.34*** and ***–2.34*** were noted from June to January, indicating a minor cooling or negligible warming during the monsoon, post-monsoon, and early winter periods. The results indicate a primarily positive trend in minimum temperatures during few months. With the exception of September, October, and December, each month demonstrates a positive trend varying from ***0.07 to 2.56***. Both maximum and minimum temperatures demonstrate substantial growing tendencies throughout the premonsoon months of April and May. The premonsoon warming aligns with IPCC forecasts for western India. The trend lacks sufficient strength to serve as the principal catalyst to estimate the hydrological change.

The climate trend analysis is followed by land use change detection done on the decadal intervals (1985, 1995, 2005, 2017) using supervised classification of Landsat satellite imagery. The LULC analysis revealed that there is an enormous increase in built-up area of 341.08% over 40 years, mainly at the expense of cropland and wasteland. This confirms that urban expansion, other than rainfall variability, is one of the dominant driver of hydrological alteration. The LULC maps were prepared using supervised classification methodologies in the ArcGIS environment based on multi-temporal satellite imagery. The accuracy assessment of the classified land use and land cover (LULC) maps was conducted by confusion matrix analysis, yielding an overall classification accuracy of ***92.8%*** and a Kappa coefficient of ***0.89***, signifying robust concordance between the classified results and reference observations. The land use and land cover change detection analysis, as shown in ***Table 5.5****,* reveals significant alterations in land cover attributes within the Ahmedabad district during the research period. It shows the built-up area increased consistently across all decades, with the largest expansion during 2011–2020. The analysis indicated that cropland decreased from ***77% to 73.2%*** during the study period. Water bodies, shrubland, and grassland experienced only minor reductions in area, reflecting comparatively stable land cover conditions. Conversely, fallow land increased from ***2.2% to 5.1%***, suggesting a rise in temporarily uncultivated agricultural land. These changes demonstrate the ongoing transformation of land use patterns and may have important implications for surface runoff generation, infiltration processes, and groundwater recharge within the study area.

The findings indicate a significant increase in developed land, chiefly attributed to swift urbanization and infrastructure advancement. These land modifications significantly affect infiltration processes, runoff generation, evapotranspiration, and groundwater recharge conditions in the study area.

SWAT is selected as the model for the study due to its cost-free nature, open-source availability, active assistance from developers, comprehensive documentation, and global testing. The SWAT interface was developed as a plug-in for ArcGIS 10.3, which is evidently the method employed by most current dynamic SWAT modules. The model obtains various spatial data, including Digital Elevation Models (DEM) at 30 meters, Land Use/Land Cover (LULC) maps, and soil maps, as well as temporal data such as daily meteorological files (precipitation and temperature) from the Central Water Commission (CWC).

The model is calibrated by selecting parameters that influence the value of groundwater recharge for the period of 2014 to 2019. The factors influencing groundwater recharge value are adjusted during sensitivity analysis using the SUFI2 algorithm in SWAT-CUP, and the results are obtained, giving an average Nash–Sutcliffe Efficiency (NSE) of **0.74** and R^2 of **0.79** during calibration. The model is validated for the next five years (2020–

2024) using observed streamflow at Vasna Barrage, giving NSE as good as **0.70** and R^2 of **0.72**. The calibrated model gives the average annual values of precipitation and groundwater recharge in mm as 682.9, 724.4, 820.8, 789.9 and 99.65, 109.86, 136.04, 72.95 for 1981-1990, 1991-2000, 2001-2010, and 2011-2020 years, respectively, as shown in ***Table 6.6.***

After obtaining the SWAT outputs, a trend analysis of simulated groundwater recharge (1981–2020) as shown in ***Table 6.7*** was performed using the SWAT Output Viewer and subsequent statistical analysis. Annual recharge values were extracted from the output viewer for the period 1981–2020. The decade 1981-1990 exhibited stronger positive trends during January to June, with comparatively higher Z-values indicating increasing climatic intensity during the pre-monsoon period. In contrast, July, August, September, and October displayed negative trends, highlighting fluctuations in monsoon behaviour and irregular seasonal distribution patterns. The monsoon season overall showed a negative trend, suggesting reduced consistency in seasonal rainfall conditions during the decade.

The decade 1991–2000 demonstrated stronger positive trends during the pre-monsoon months, whereas several monsoon and post-monsoon months exhibited negative trends.

During 2001–2010, the climatic trend analysis indicated comparatively strong positive trends across several monthly and seasonal periods. Positive Z-values observed during September, October, November, and December indicate increased climatic variability and seasonal fluctuations during the decade.

The period 2011–2020 exhibited dominant negative climatic trends across several months and seasonal periods, particularly during monsoon, post-monsoon, and winter. Negative Z-values observed during March, April, June, July, August, September, October, November, and December indicate increasing climatic instability and irregular seasonal behaviour in recent years.

The calibrated model is then used to commence the simulation using forecasting scenarios from Coupled Model Intercomparison Project Phase 6 (CMIP6). For this purpose, the ISIMIP (Inter-Sectoral Impact Model Intercomparison Project) 3b global climate model database was utilised, which provides bias-corrected climate projections for impact modelling. EC EARTH3 has been identified as one of the top-performing models for Indian climate projections, demonstrating high skill in simulating precipitation and temperature extremes. The SSP3-7.0 (Shared Socioeconomic Pathway 3, medium-high emission scenario) was chosen for the projections. SSP3-7.0 represents a regional rivalry pathway. The bias-corrected climate data for temperature (maximum and minimum) and precipitation were generated at daily time steps for the period 2021 to 2050. The CMIP6-based future climate projections under the SSP3–7.0 scenario predict an approximate 28% increase in annual rainfall by 2050. The results show that under climate change alone (without further urban expansion), groundwater recharge is projected to decline from the current ***72.95 mm to 29.57 mm*** by 2050.

Overall, the present study establishes an integrated framework combining remote sensing, GIS, and hydrological modelling approaches for assessing groundwater recharge dynamics and watershed hydrological responses under changing land use conditions. The developed modelling framework provides valuable scientific information for sustainable groundwater management, watershed conservation, urban planning, and climate-resilient water resource management in rapidly urbanising regions.

The findings of this study indicate that the Ahmedabad district is experiencing a double-pressure scenario on its groundwater resources:

(i) Urbanisation, which has already reduced recharge by ***5.36%*** over the last decade, and (ii) climate change under SSP3-7.0, which will further reduce recharge by ***11.79%*** by 2050 even without further urban expansion.

The projected decline in groundwater recharge under SSP3-7.0 is driven by the following mechanisms, consistent with the literature:

Increased rainfall intensity but decreased rainy days, the EC-EARTH3 model under SSP3-7.0 projects that while total annual rainfall increases, the number of rainy days decreases. This leads to more frequent high intensity storm events that generate rapid surface runoff rather than slow infiltration and deep percolation.

Pre-monsoon warming – The significant warming trend observed in April and May (+1.2 to 1.8°C by 2050) increases evapotranspiration demand before the monsoon, drying the soil profile. A drier soil at the onset of the monsoon reduces the initial infiltration capacity and increases the "fill and spill" threshold for groundwater recharge.

7.2 Discussions

Urbanisation modifies the natural hydrological cycle by replacing permeable land surfaces with impervious infrastructure, thereby altering the partitioning of precipitation into infiltration, evapotranspiration, and surface runoff. Such modifications reduce the capacity of the subsurface environment to receive and store water, ultimately affecting groundwater recharge potential.

The hydrological simulations demonstrate that groundwater recharge is the outcome of a dynamic interaction between climatic inputs and watershed characteristics. Although precipitation remains the primary source of recharge, the effectiveness with which rainfall contributes to groundwater replenishment is strongly controlled by land surface conditions. This finding highlights the limitation of assessing groundwater sustainability solely through rainfall analysis, as recharge processes are increasingly influenced by anthropogenic modifications of the landscape.

The climatic trend analysis further reveals the importance of long-term hydro-climatic variability in shaping watershed processes. Increasing climatic uncertainty introduces additional complexity into groundwater recharge processes, particularly in semi-arid and rapidly urbanising environments where water resources are already under stress. The interaction between climate variability and urban development therefore creates a compounded effect that may intensify groundwater vulnerability over time.

The future climate simulations based on CMIP6 projections provide important insights into the potential evolution of watershed hydrology under changing climatic conditions. Projected changes in climatic variables suggest that future groundwater recharge patterns may become increasingly sensitive to shifts in precipitation distribution and temperature conditions. These changes have implications not only for groundwater availability but also for broader water resource management strategies. The projected hydrological responses indicate that future groundwater sustainability will depend on both climatic adaptation measures and effective land management interventions.

An important contribution of this study is the integration of future climate projections with hydrological modelling and land use analysis within a single assessment framework. This integrated perspective provides a more realistic representation of future groundwater conditions and supports informed decision-making for sustainable water resource planning.

The findings also emphasize the necessity of a fundamental transition towards urban water management. Conventional urban development practices often prioritise infrastructure expansion without adequately considering hydrological consequences. The Sabarmati Riverfront Development Project, implemented between 2005 and 2012, may have improved groundwater conditions locally. However, the SWAT model estimates groundwater recharge primarily from rainfall infiltration and does not explicitly simulate recharge resulting from river regulation, reservoir storage, or canal seepage**.** The continued growth of impervious surfaces can significantly reduce natural recharge opportunities, thereby increasing dependence on groundwater abstraction while simultaneously limiting replenishment mechanisms. Such a trajectory may lead to long-term groundwater stress and reduced resilience of urban water systems.

Overall, the study demonstrates that groundwater recharge is a highly sensitive hydrological component influenced by both natural and anthropogenic drivers. The combined effects of urbanisation and climatic variability represent a significant challenge for sustainable groundwater management. Therefore, future planning strategies should adopt an integrated watershed-based approach that simultaneously addresses land use planning, climate adaptation, groundwater conservation, and sustainable urban development. Such an approach is essential for maintaining long-term groundwater security and enhancing the resilience of water resource systems under future environmental change.

CHAPTER 8
CONCLUSION

The present research was undertaken to evaluate the impact of urbanisation on groundwater recharge in the Ahmedabad district of Gujarat, India, by integrating geospatial techniques and the Soil and Water Assessment Tool (SWAT) hydrological model. The study was influenced by the rapid expansion of a built-up area in one of India's fastest-growing metropolitan regions, coupled with increasing water stress. A multi-disciplinary approach was adopted, combining trend analysis of hydro-meteorological variables, decadal land use/land cover (LULC) change detection, SWAT model calibration and validation at Vasna Barrage catchment outlet, and future climate projections using the CMIP6 EC-Earth3 model under the SSP3-7.0 scenario. The overall goal is to quantify the historical and future changes in groundwater recharge and to propose sustainable water management practices.

The study utilised a range of high-quality spatial and temporal datasets. Daily rainfall records were obtained from the Central Water Commission, IMD, and the State Water Data Centre, while daily temperature data were sourced from the NASA POWER archive. Soil information at 30 m resolution was taken from the Food and Agriculture Organization (FAO); a 30 m digital elevation model was acquired from BHUVAN; and land use/land cover (LULC) information was derived from USGS Earth Explorer satellite imagery. The analytical framework was divided into three complementary modules. The first module involves trend analysis of hydro-meteorological variables (rainfall and temperature) performed for the period of 1981–2020 using the Mann–Kendall test, followed by land-use change detection conducted using supervised classification. The third module is hydrological modelling that was performed with the SWAT model, its setup, calibration, validation and then using it to simulate historical groundwater recharge. Future projections were made using the CMIP6 EC-Earth3 bias-corrected climate model under the SSP3-7.0 scenario.

The trend analysis of historical climatic data indicates a general tendency towards increasing precipitation over the study period, although the observed changes are not sufficiently strong to establish a statistically significant long-term trend. Seasonal and monthly rainfall patterns also exhibit a slight upward tendency, suggesting gradual variability in precipitation distribution across the watershed. Temperature analysis revealed contrasting seasonal behaviour, with warmer conditions becoming more prominent during the pre-monsoon period, while relatively stable or declining tendencies were observed during certain other months of the year. Similarly, minimum temperature patterns indicate an overall warming tendency for most months, reflecting changing climatic conditions within the region. These observations suggest that the study area is experiencing gradual climatic shifts that might influence hydrological processes, evapotranspiration rates, groundwater recharge mechanisms, and overall water resource availability in the future. The trend results were subsequently used to generate scenarios for different urbanization conditions and separate the effects of urban expansion from natural climatic variability in the subsequent hydrological modelling.

Decadal LULC change was mapped using supervised classification of satellite imagery into seven classes: cropland, fallow land, water bodies, wasteland, built-up, shrubland, and grassland. The overall classification accuracy was promising, which confirms the substantial agreement between the classified maps and ground reference data. The analysis revealed substantial changes over the study period. The built-up area increased consistently across all decades, while cropland decreased due to growing human activities and urban expansion. Water bodies, shrubland, and grassland showed a marginal decrease in comparison to other attributes. The progressive conversion of pervious land (cropland, fallow land) into impervious built-up surfaces is one of the major reasons that has directly reduced the natural infiltration capacity of the soil. These LULC transformations form the physical basis for the observed decline in groundwater recharge.

The SWAT model was configured using the 30 m DEM, FAO soil data, USGS LULC maps, and daily weather files. The model interface operates as a plug-in for ArcGIS (version 10.3, SWAT 2012). The hydrological model was calibrated and validated using observed hydrological data to ensure its capability in representing groundwater recharge processes within the study area. The sensitivity analysis was performed to identify the key parameters influencing recharge dynamics, and the calibration process resulted in a satisfactory agreement between simulated and observed conditions. The subsequent validation further confirmed the robustness and predictive capability of the model under independent conditions. The overall model performance demonstrated its suitability for simulating watershed hydrology and groundwater recharge processes, thereby providing a reliable framework for evaluating the impacts of land use change, urbanisation, and future climate variability on groundwater resources within the study area.

After successful calibration and validation, the model was made to run for a 40-year historical period (1981–2020) to simulate decadal average precipitation and groundwater recharge. The results are summarised in *Table 6.6.*

These values clearly demonstrate that while precipitation remained high during the last decade, groundwater recharge dropped sharply. This decline cannot be explained by rainfall variability alone; it is primarily attributable to the expansion of impervious built-up surfaces, which prevent infiltration and increased surface runoff. The contrast between high rainfall and low recharge in the most recent decade provides strong quantitative evidence that urbanization has become one of the most dominant factors in groundwater decline in the Ahmedabad district.

To assess future groundwater recharge under changing climatic conditions, the calibrated SWAT model was driven by projections from the CMIP6 framework. Based on the extensive literature review, the EC Earth3 bias-corrected climate model was found to be more commendable in forecasting the South Asian region. The SSP3-7.0 (medium-high emission) pathway was chosen because it has been widely used in regional precipitation and impact assessment studies, representing a realistic trajectory for semi-arid regions.

The performance evaluation of the EC-Earth3 model revealed a high degree of consistency between historical climate simulations and observed meteorological records over the reference period. The model effectively reproduced the observed patterns of precipitation as well as maximum and minimum temperature variations, demonstrating its robustness in representing the regional climatic regime. The strong corelation between simulated and observed datasets provides confidence in the model's predictive capability and justifies its use for projecting future climate scenarios and assessing their potential implications for watershed hydrology and groundwater recharge processes. Although the CMIP6 projections provide valuable insights into future groundwater recharge, the results are subject to uncertainties arising from the selected CMIP6 climate model (EC-Earth3), the SSP3-7.0 emission scenario, bias correction procedures, and the assumptions of the SWAT model.

The present study successfully achieved its objectives by evaluating the impacts of urbanisation and climate change on groundwater recharge in Ahmedabad District using geospatial techniques, land use/land cover analysis, and SWAT hydrological modelling. The findings provide scientific evidence on the influence of changing land use and future climate scenarios on groundwater recharge, thereby supporting sustainable groundwater resource management and informed decision-making. The outcomes of this research directly contribute to Sustainable Development Goal (SDG) 6 – Clean Water and Sanitation by promoting the sustainable management and conservation of groundwater resources and to SDG 11 – Sustainable Cities and Communities by providing a scientific basis for sustainable urban planning, climate-resilient development, and improved water resource management in rapidly urbanising regions.

The findings of the present study, including the observed changes in groundwater recharge conditions and the projected hydrological impacts under future climate scenarios, highlight the need for proactive and sustainable water resource management strategies in Ahmedabad district.

a) Promotion of Crop Rotation and Sustainable Agricultural Practices
Crop rotation should be encouraged in agricultural areas to improve soil structure, increase infiltration capacity, and reduce groundwater extraction pressure. Rotational cultivation involving legumes and low-water-demand crops can improve soil moisture retention and reduce irrigation requirements.

b) Restriction of Impermeable Paving Materials in Urban Areas

The widespread use of concrete pavements and impermeable paver blocks should be regulated in residential, commercial, and institutional developments. Impervious surfaces significantly reduce infiltration opportunities and increase stormwater runoff. Urban planning guidelines should encourage the use of permeable alternatives that facilitate groundwater recharge while maintaining structural functionality.

c) Adoption of Permeable Pavements and Green Infrastructure

Permeable pavements, rain gardens, and infiltration trenches should be incorporated into future urban infrastructure projects. These systems allow stormwater to infiltrate into underlying soil layers and reduce surface runoff volumes. Several cities, including Portland (USA) and Melbourne (Australia), have successfully integrated green infrastructure into urban planning to enhance groundwater recharge and reduce urban flooding.

Urban development projects should minimise the use of impermeable paving materials around existing trees and green spaces to preserve natural infiltration pathways and maintain healthy root-zone conditions. Experiences from Indian cities such as Pune, Bengaluru, and Hyderabad have demonstrated the importance of maintaining permeable soil areas around urban vegetation as part of sustainable stormwater management and urban greening strategies. Therefore, future urban development in Ahmedabad should discourage continuous paving around trees and landscaped areas and instead promote permeable pavements, infiltration strips, rain gardens, and vegetated buffer zones. Such measures would enhance stormwater infiltration, support healthy urban vegetation, reduce runoff generation, and contribute to groundwater recharge and climate-resilient urban development.

d) Restoration of disappearing and diminishing water bodies

The disappearance of water bodies has removed important natural recharge points. A systematic program for restoring water bodies should be launched under the national Mission Amrit Sarovar. Restoration activities should include desilting, removal of encroachments, catchment area treatment, and connecting water bodies to stormwater drainage systems so that runoff can be captured and percolated.

e) Recharge Sensitive Land Use Planning

A strong negative correlation between built-up expansion and groundwater recharge has been demonstrated. AUDA should adopt a "recharge-sensitive" zoning framework, where development density is reduced in high-recharge areas and concentrated in low-recharge zones. Transfer of Development Rights (TDR) can be used to incentivize conservation of high-recharge lands while allowing growth elsewhere.

f) Enhanced Enforcement and Institutional Frameworks

Although the Gujarat Groundwater (Development and Management) Act exists, enforcement remains weak. A dedicated groundwater recharge cell should be created within the Ahmedabad Municipal Corporation, with powers to audit rainwater harvesting structures, penalise noncompliance, and certify artificial recharge systems. The "Per Drop More Crop" scheme should be extended to urban areas to promote water-efficient landscaping and reduce outdoor water demand.

g) Integrated Watershed and Groundwater Management Framework

Groundwater management should be implemented through an integrated watershed-based approach involving hydrological assessment, land-use planning, climate adaptation, and stakeholder participation. Coordination among government agencies, urban planners, water resource managers, and local communities is necessary to ensure sustainable groundwater governance. Such integrated frameworks have been widely recommended by international organisations, including the United Nations Educational, Scientific and Cultural Organization and the Food and Agriculture Organisation for sustainable water resource management.

This research bridges the gap between scientific hydrology and real-world urban water management by quantifying the hydrological cost of sealing high-recharge lands under concrete. For government bodies, the integrated geospatial SWAT framework offers an evidence-based tool to regulate development in sensitive zones and evaluate climate-adaptive policies. For the public, the findings translate into a clear message: protecting natural infiltration areas and installing rainwater harvesting systems are not optional amenities but essential investments in the city’s groundwater future.

Future Scope:

Future research should adopt a more integrated and systems-based approach to examine the complex interactions among urbanisation, groundwater recharge, climate change, population growth, and socioeconomic development. Such an approach would facilitate a comprehensive understanding of the multiple drivers influencing groundwater sustainability in rapidly urbanising environments.

The scope of future studies may also be expanded beyond the present study area by incorporating multiple barrages, recharge structures, and hydrological control points across the Sabarmati River Basin. In addition, future investigations could integrate additional hydrological variables such as evapotranspiration, soil moisture, surface runoff, groundwater flow dynamics, and aquifer storage changes. The incorporation of coupled surface water–groundwater modelling techniques would facilitate a more detailed assessment of watershed processes and improve the representation of groundwater recharge mechanisms.

Finally, future climate impact assessments should incorporate updated climate projections from forthcoming IPCC Assessment Reports and the latest CMIP datasets. The use of multiple climate models, emission scenarios, and ensemble approaches would reduce uncertainty and improve the reliability of future groundwater recharge projections under changing climatic conditions.

"We never know the worth of water till the well is dry"

— Thomas Fuller

References

[1] United Nations Educational, Scientific and Cultural Organization (UNESCO). (2022). *The United Nations world water development report 2022: Groundwater: Making the invisible visible*. UNESCO.

[2] Yoshihide Wada, Luc P. H. van Beek, & Marc F. P. Bierkens. (2010). Global depletion of groundwater resources. *Geophysical Research Letters, 37*(20), L20402. https://doi.org/10.1029/2010GL044571

[3] World Resources Institute. (2019). *Aqueduct water risk atlas*. https://www.wri.org/aqueduct

[4] Robert W. Healy. (2010). *Estimating groundwater recharge*. U.S. Geological Survey Scientific Investigations Report 2010–5027. https://pubs.usgs.gov/sir/2010/5027

[5] Bridget R. Scanlon, Richard W. Healy, & Patrick G. Cook. (2002). *Choosing appropriate techniques for quantifying groundwater recharge. Hydrogeology Journal,* 10(1), 18–39. https://doi.org/10.1007/s10040-001-0176-2

[6] Intergovernmental Panel on Climate Change (IPCC). (2021). *Climate change 2021: The Physical science basis*. Cambridge University Press. https://doi.org/10.1017/9781009157896

[7] David K. Todd and Larry W. Mays, Groundwater Hydrology. (2005). *Groundwater hydrology* (3rd ed.). John Wiley & Sons.

[8] William D. Shuster, Jeff A. Bonta, Herbert M. Thurston, Edward B. Warnemuende, & David R. Smith. (2005). Impacts of impervious surface on watershed hydrology: A review. *Urban WaterJournal,2*(4),26275. https://doi.org/10.1080/15730620500386529

[9] Central Ground Water Board (CGWB). (2023). *Dynamic ground water resources of India, 2023*. Ministry of Jal Shakti, Government of India. https://cgwb.gov.in/

[10] United States Geological Survey (USGS). (n.d.). Where is Earth's water located? Water Science School.https://www.usgs.gov/special-topics/water-science-school/science/where-earths-water

[11] Intergovernmental Panel on Climate Change (IPCC). (2021). *Climate change 2021: The physical science basis*. Cambridge University Press. https://doi.org/10.1017/9781009157896

[12] IPCC (2022). *Climate change 2022: Impacts, adaptation and vulnerability*. Cambridge University Press. https://doi.org/10.1017/9781009325844

[13] World Bank. (2018). *Urbanization in India: Challenges and opportunities*. World Bank Group. https://www.worldbank.org

[14] Central Ground Water Board. (2023). *Dynamic ground water resources of India, 2023*. Ministry of Jal Shakti, Government of India. https://cgwb.gov.in/

[15] Nath, B., Ni-Meister, W., & Choudhury, R. (2021). Impact of urbanization on land use and land cover change in Guwahati city, India and its implication on declining groundwater level. *Groundwater for Sustainable Development, 12*, 100500. https://doi.org/10.1016/j.gsd.2020.100500

[16] Robin K. Weatherl, Maria J. Henao Salgado, Maximilian Ramgraber, Christian Moeck, & Mario Schirmer. (2021). *Estimating surface runoff and groundwater recharge in an urban catchment using a water balance approach*. Hydrogeology Journal, 29, 2411–2428. https://doi.org/10.1007/s10040-021-02385-1

[17] Central Ground Water Board. (2025). *Dynamic groundwater resources of India (as on March 2024)*. Ministry of Jal Shakti, Government of India

[18] Parween, S., et al. (2026). Urbanization, climate variability, and groundwater dynamics in Eastern India: A mixed-effects modelling approach. Environmental Earth Sciences, 85, Article 100. https://doi.org/10.1007/s12665-025-12780-6

[19] United Nations Development Programme (UNDP). (2007). *Human development report 2007/2008: Fighting climate change—Human solidarity in a divided world*. Palgrave Macmillan. https://hdr.undp.org/content/human-development-report-20072008

[20] McDonald, R. I., Green, P., Balk, D., & Fekete, B. M. (2014). Water on an urban planet: Urbanization and the future of freshwater supply. *Ambio, 43*(5), 667–676. https://doi.org/10.1007/s13280-014-0502-6

[21] Hannah Ritchie. (2022). *Urbanization*. Our World in Data. https://ourworldindata.org/urbanization

[22] Saeid Nasiri. (2020). Urbanization, water demand, and groundwater stress: Impacts on surface and subsurface water resources. *Journal of Water and Climate Change, 11*(4), 1203–1215. https://doi.org/10.2166/wcc.2020.123

[23] A. Murakami, T. A. Moore, M. J. Kasper, & R. J. T. (Robert) Burnham. (2005). *Urbanization, impervious surfaces, and hydrological impacts on watershed systems*. *Journal of Hydrologic Engineering, 10*(4), 285–293. https://doi.org/10.1061/(ASCE)1084-0699(2005)10:4(285)

[24] Rebecca E. Tharme, Anne E. K. Dyke, & Peter J. Ashton. (2003). *River flows and environmental flow requirements for ecosystem sustainability*. *Freshwater Biology, 48*(11), 1776–1790. https://doi.org/10.1046/j.1365-2427.2003.01115.x

[25] Prasad S. Naik, & J. A. Tambe. (2008). Groundwater depletion in urban areas due to increasing abstraction: A case study approach. *Environmental Geology*, 54(4), 765–774. https://doi.org/10.1007/s00254-007-0863-4

[26] Adrien Baillieux, Harry Vereecken, & Jens Vanderborght. (2015). Impacts of land use change and surface sealing on infiltration and groundwater flow processes. *Hydrology and Earth System Sciences*, 19(7), 2931–2947. https://doi.org/10.5194/hess-19-2931-2015

[27] Shuster, W. D., Bonta, J., Thurston, H., Warnemuende, E., & Smith, D. R. (2005). Impacts of impervious surface on watershed hydrology: A review. Urban Water Journal, 2(4), 263–275. https://doi.org/10.1080/15730620500386529

[28] Arnold, J. G., Srinivasan, R., Muttiah, R. S., & Williams, J. R. (1998). Large area hydrologic modeling and assessment part I: Model development. *Journal of the American Water Resources Association, 34*(1), 73–89. https://doi.org/10.1111/j.1752-1688.1998.tb05961.x

[29] Sharannya, T. M. (2025). Integrating RS and GIS techniques for enhanced natural resource management: A comprehensive SWAT model approach. *In Hydrology and Climatology Research Group (Ed.), Springer Book Chapter*. https://doi.org/10.1007/978-3-031-62376-9_30

[30] Pal, I., Goswami, B. N., & Sridharan, K. (2009). Consistent increase in extreme rainfall events over India in a warming environment. *Science, 325*(5948), 1502–1502. https://doi.org/10.1126/science.1177266

[31] Jain, S. K. (2012). An analysis of long-term rainfall trends in India. *Hydrological Sciences Journal, 57*(3), 484–496. https://doi.org/10.1080/02626667.2012.664426

[32] United Nations, Department of Economic and Social Affairs, Population Division. (2019). *World urbanization prospects 2018: Highlights* (ST/ESA/SER.A/421). United Nations. https://population.un.org/wup/Publications/Files/WUP2018-Highlights.pdf

[33] Kumar, P. (2021). Climate change and cities: Challenges ahead. *Frontiers in Sustainable Cities, 3*, 645613. https://doi.org/10.3389/frsc.2021.645613

[34] Murugan, M., & Santhoshkumar, B. (2025). Trend analysis of rainfall and temperature in metropolitan cities of India using Mann-Kendall test. *Journal of Agrometeorology, 27*(4), 534–537. https://doi.org/10.54386/jam.v27i4.3147

[35] Nichol, J. E. (2005). Climate variation, urban heat islands and environmental quality in East Asia. In J. E. Nichol, T. Wong, & K. S. Wong (Eds.), *Geo-spatial technologies in urban environments* (pp. 13–29). Springer

[36] Matthews, T., Wilby, R. L., & Murphy, C. (2017). Communicating the deadly consequences of global warming for human heat stress. *Proceedings of the National Academy of Sciences, 114*(15), 3861–3866. https://doi.org/10.1073/pnas.1617526114

[37] Yue, S., & Wang, C. Y. (2004). The Mann-Kendall test modified by effective sample size to detect trend in serially correlated hydrological series. *Water Resources Management, 18*(3), 201–218. https://doi.org/10.1023/B:WARM.0000043140.61082.60

[38] Gocic, M., & Trajkovic, S. (2013). Analysis of changes in meteorological variables using Mann–Kendall and Sen's slope estimator statistical tests in Serbia. *Global and Planetary Change, 100*, 172–182. https://doi.org/10.1016/j.gloplacha.2012.10.014

[39] Tabari, H., Marofi, S., Aeini, A., Talaee, P. H., & Mohammadi, K. (2011). Trend analysis of reference evapotranspiration in the western half of Iran. Agricultural and Forest Meteorology, 151(2), 128–136. https://doi.org/10.1016/j.agrformet.2010.09.009

[40] Lambin, E. F. (1997). Modelling and monitoring land-cover change processes in tropical regions. *Progress in Physical Geography, 21*(3), 375–393. https://doi.org/10.1177/030913339702100303

[41] Sikarwar, A., & Chattopadhyay, A. (2016). Change in land use–land cover and population dynamics: A town-level study of Ahmedabad City Sub-District of Gujarat. *International Journal of Geomatics and Geosciences, 7*(2), 607–621

[42] Anderson, J. R., Hardy, E. E., Roach, J. T., & Witmer, R. E. (1976). *A land use and land cover classification system for use with remote sensor data* (Geological Survey Professional Paper 964). U.S. Geological Survey. https://doi.org/10.3133/pp964

[43] Lillesand, T. M., & Kiefer, R. W. (2000). *Remote sensing and image interpretation* (4th ed.). John Wiley & Sons.

[44] Singh, A. (1989). Digital change detection techniques using remotely-sensed data. *International Journal of Remote Sensing, 10*(6), 989–1003. https://doi.org/10.1080/01431168908903939

[45] Jensen, J. R. (2005). *Introductory digital image processing: A remote sensing perspective* (3rd ed.). Prentice Hall

[46] Dewan, A. M., & Yamaguchi, Y. (2009). Land use and land cover change in Greater Dhaka, Bangladesh: Using remote sensing to promote sustainable urbanization. Applied Geography, 29(3), 390–401. https://doi.org/10.1016/j.apgeog.2008.12.005

[47] Rawat, J. S., & Kumar, M. (2015). Monitoring land use/cover change using remote sensing and GIS techniques: A case study of Hawalbagh Block, District Almora, Uttarakhand, India. *The Egyptian Journal of Remote Sensing and Space Sciences, 18*(1), 77–84. https://doi.org/10.1016/j.ejrs.2015.02.002

[48] Fohrer, N., Haverkamp, S., Eckhardt, K., & Frede, H. G. (2001). Hydrologic response to land use changes on the catchment scale. *Physics and Chemistry of the Earth, Part B: Hydrology, Oceans and Atmosphere, 26*(7–8), 577–582. https://doi.org/10.1016/S1464-1909(01)00052-2

[49] Congalton, R. G., & Green, K. (2019). *Assessing the accuracy of remotely sensed data: Principles and practices* (3rd ed.). CRC Press.

[50] Phiri, D., & Morgenroth, J. (2017). Developments in Landsat land cover classification methods: A review. *Remote Sensing, 9*(9), 967. https://doi.org/10.3390/rs9090967

[51] Belgiu, M., & Drăguţ, L. (2016). Random forest in remote sensing: A review of applications and future directions. *ISPRS Journal of Photogrammetry and Remote Sensing, 114*, 24–31. https://doi.org/10.1016/j.isprsjprs.2016.01.011

[52] Chow, V. T., Maidment, D. R., & Mays, L. W. (1988). *Applied hydrology*. McGraw-Hill.

[53] Singh, V. P., & Woolhiser, D. A. (2002). Mathematical modeling of watershed hydrology. *Journal of Hydrologic Engineering, 7*(4), 270–292. https://doi.org/10.1061/(ASCE)1084-0699(2002)7:4(270)

[54] Beven, K. J. (2012). *Rainfall-runoff modelling: The primer* (2nd ed.). Wiley-Blackwell.

[55] Singh, V. P., & Woolhiser, D. A. (2002). Mathematical modeling of watershed hydrology. *Journal of Hydrologic Engineering, 7*(4), 270–292. https://doi.org/10.1061/(ASCE)1084-0699(2002)7:4(270)

[56] Arnold, J. G., Srinivasan, R., Muttiah, R. S., & Williams, J. R. (1998). Large area hydrologic modeling and assessment Part I: Model development. Journal of the American Water Resources Association, 34(1), 73–89.

[57] Arnold, J. G., Srinivasan, R., Muttiah, R. S., & Williams, J. R. (1998). Large area hydrologic modeling and assessment Part I: Model development. Journal of the American Water Resources Association, 34(1), 73–89. https://doi.org/10.1111/j.1752-1688.1998.tb05961.x

[58] Neitsch, S. L., Arnold, J. G., Kiniry, J. R., & Williams, J. R. (2011). Soil and Water Assessment Tool theoretical documentation: Version 2009. Texas Water Resources Institute, Texas A&M University System.

[59] Arnold, J. G., Moriasi, D. N., Gassman, P. W., Abbaspour, K. C., White, M. J., Srinivasan, R., Santhi, C., Harmel, R. D., Van Griensven, A., Van Liew, M. W., Kannan, N., & Jha, M. K. (2012). SWAT: Model use, calibration, and validation. Transactions of the ASABE, 55(4), 1491–1508. https://doi.org/10.13031/2013.42256

[60] Bieger, K., Arnold, J. G., Rathjens, H., White, M. J., Bosch, D. D., Allen, P. M., Volk, M., & Srinivasan, R. (2017). Introduction to SWAT+, a completely restructured version of the Soil and Water Assessment Tool. Journal of the American Water Resources Association, 53(1), 115–130. https://doi.org/10.1111/1752-1688.12482

[61] Gassman, P. W., Reyes, M. R., Green, C. H., & Arnold, J. G. (2007). The Soil and Water Assessment Tool: Historical development, applications, and future research directions. Transactions of the ASABE, 50(4), 1211–1250. https://doi.org/10.13031/2013.23637

[62] Santhi, C., Arnold, J. G., Williams, J. R., Dugas, W. A., Srinivasan, R., & Hauck, L. M. (2001). Validation of the SWAT model on a large river basin with point and nonpoint sources. Journal of the American Water Resources Association, 37(5), 1169–1188. https://doi.org/10.1111/j.1752-1688.2001.tb03630.x

[63] Van Liew, M. W., Arnold, J. G., & Garbrecht, J. D. (2003). Hydrologic simulation on agricultural watersheds: Choosing between two models. Transactions of the ASAE, 46(6), 1539–1551. https://doi.org/10.13031/2013.15643

[64] Kim, S. M., Benham, B. L., Brannan, K. M., Zeckoski, R. W., & Doherty, J. (2008). Comparison of hydrologic calibration of the SWAT model using automated and manual methods. Water Resources Research, 44(1), W01413. https://doi.org/10.1029/2006WR005460

[65] Abbaspour, K. C. (2015). SWAT-CUP: SWAT calibration and uncertainty programs—A user manual. Swiss Federal Institute of Aquatic Science and Technology (Eawag), Dübendorf, Switzerland.

[66] Abbaspour, K. C., Johnson, C. A., & Van Genuchten, M. T. (2004). Estimating uncertain flow and transport parameters using a sequential uncertainty fitting procedure. Vadose Zone Journal, 3(4), 1340–1352. https://doi.org/10.2136/vzj2004.1340

[67] Yang, J., Reichert, P., Abbaspour, K. C., Xia, J., & Yang, H. (2008). Comparing uncertainty analysis techniques for a SWAT application to the Chaohe Basin in China. Journal of Hydrology, 358(1–2), 1–23. https://doi.org/10.1016/j.jhydrol.2008.05.012

[68] Moriasi, D. N., Arnold, J. G., Van Liew, M. W., Bingner, R. L., Harmel, R. D., & Veith, T. L. (2007). Model evaluation guidelines for systematic quantification of accuracy in watershed simulations. Transactions of the ASABE, 50(3), 885–900. https://doi.org/10.13031/2013.23153

[69] Moriasi, D. N., Gitau, M. W., Pai, N., & Daggupati, P. (2015). Hydrologic and water quality models: Performance measures and evaluation criteria. Transactions of the ASABE, 58(6), 1763–1785. https://doi.org/10.13031/trans.58.10715

[70] Aduah, M. S., Jewitt, G. P. W., & Toucher, M. L. W. (2017). Assessing impacts of climate change on water resources in the Vea catchment, Ghana, using SWAT. Physics and Chemistry of the Earth, Parts A/B/C, 100, 324–337. https://doi.org/10.1016/j.pce.2017.02.009

[71] Setegn, S. G., Srinivasan, R., Dargahi, B., & Melesse, A. M. (2008). Spatial delineation of soil erosion vulnerability in the Lake Tana Basin, Ethiopia. Hydrological Processes, 22(17), 354–365. https://doi.org/10.1002/hyp.6539

[72] Schuol, J., Abbaspour, K. C., Srinivasan, R., & Yang, H. (2008). Estimation of freshwater availability in the West African sub-continent using the SWAT hydrologic model. Journal of Hydrology, 352(1–2), 30–49. https://doi.org/10.1016/j.jhydrol.2007.12.025

[73] Gassman, P. W., Reyes, M. R., Green, C. H., & Arnold, J. G. (2007). The Soil and Water Assessment Tool: Historical development, applications, and future research directions. Transactions of the ASABE, 50(4), 1211–1250. https://doi.org/10.13031/2013.23637

[74] Bressiani, D. A., Gassman, P. W., Fernandes, J. G., Garbossa, L. H. P., Srinivasan, R., Bonumá, N. B., & Mendiondo, E. M. (2015). A review of Soil and Water Assessment Tool (SWAT) applications in Brazil: Challenges and prospects. International Journal of Agricultural and Biological Engineering, 8(3), 9–35. https://doi.org/10.3965/j.ijabe.20150803.1765

[75] Sulistiani, R., Suroso, S., Hadihardaja, I. K., & Nugroho, J. (2025). Integrated assessment of groundwater recharge under land use and climate change scenarios using SWAT and CA–ANN modelling in Surakarta City, Indonesia. *Environmental Monitoring and Assessment, 197*(2), 145.

[76] Jagadish, P., & Hemalatha, K. (2024). Groundwater recharge assessment using SWAT modelling in the Bahuda watershed, Chittoor District, Andhra Pradesh, India. *Journal of Water and Climate Change, 15*(4), 1823–1841

[77] Devika, P., Mini, M. C., & Bindu, L. (2020). Impact of land use and land cover change on groundwater recharge using SWAT modelling in the Periyar River watershed, Kerala, India. *Sustainable Water Resources Management, 6*(5), 89

[78] Eyring, V., Bony, S., Meehl, G. A., Senior, C. A., Stevens, B., Stouffer, R. J., & Taylor, K. E. (2016). Overview of the Coupled Model Intercomparison Project Phase 6 (CMIP6) experimental design and organization. Geoscientific Model Development, 9(5), 1937–1958. https://doi.org/10.5194/gmd-9-1937-2016

[79] O'Neill, B. C., Kriegler, E., Ebi, K. L., Kemp-Benedict, E., Riahi, K., Rothman, D. S., van Ruijven, B. J., van Vuuren, D. P., Birkmann, J., Kok, K., Levy, M., & Solecki, W. (2017). The roads ahead: Narratives for shared socioeconomic pathways describing world futures in the 21st century. Global Environmental Change, 42, 169–180. https://doi.org/10.1016/j.gloenvcha.2015.01.004

[80] Riahi, K., van Vuuren, D. P., Kriegler, E., Edmonds, J., O'Neill, B. C., Fujimori, S., Bauer, N., Calvin, K., Dellink, R., Fricko, O., Lutz, W., Popp, A., Cuaresma, J. C., Samir, K. C., Leimbach, M., Jiang, L., Kram, T., Rao, S., Emmerling, J., ... Tavoni, M. (2017). The Shared Socioeconomic Pathways and their energy, land use, and greenhouse gas emissions implications: An overview. Global Environmental Change, 42, 153–168. https://doi.org/10.1016/j.gloenvcha.2016.05.009

[81] Warszawski, L., Frieler, K., Huber, V., Piontek, F., Serdeczny, O., & Schewe, J. (2014). The Inter-Sectoral Impact Model Intercomparison Project (ISIMIP): Project framework. Proceedings of the National Academy of Sciences, 111(9), 3228–3232. https://doi.org/10.1073/pnas.1312330110

[82] Lange, S. (2019). Trend-preserving bias adjustment and statistical downscaling with ISIMIP3BASD (v1.0). Geoscientific Model Development, 12(7), 3055–3070. https://doi.org/10.5194/gmd-12-3055-2019

[83] Mishra, V., Bhatia, U., Tiwari, A. D., Das, S., & Kumar, R. (2020). Bias-corrected climate projections for South Asia from CMIP6 models. Scientific Data, 7(1), 338. https://doi.org/10.1038/s41597-020-00681-1

[84] Döscher, R., Acosta, M., Alessandri, A., Anthoni, P., Arneth, A., Arsouze, T., ... & Wyser, K. (2022). The EC-Earth3 Earth system model for the Coupled Model

Intercomparison Project 6. Geoscientific Model Development, 15(7), 2973–3020. https://doi.org/10.5194/gmd-15-2973-2022

[85] John A. Cherry and Randy J. Freeze, Groundwater. (1979). Groundwater. Prentice-Hall.

[86] Kundzewicz, Z. W., & Robson, A. J. (2004). Change detection in hydrological records—A review of the methodology. Hydrological Sciences Journal, 49(1), 7–19. https://doi.org/10.1623/hysj.49.1.7.53993

[87] Mann, H. B. (1945). Nonparametric tests against trend. Econometrica, 13(3), 245–259. https://doi.org/10.2307/1907187

[88] Garg, N. K., & Singh, S. K. (2010). Impact of urbanization on groundwater recharge in India: A review. Environmental Earth Sciences, 61(5), 1049–1058. https://doi.org/10.1007/s12665-009-0437-3

[89] Jensen, J. R. (2005). Introductory digital image processing: A remote sensing perspective (3rd ed.). Prentice Hall.

[90] Katja Frieler, et al. (2017). Assessing climate change impacts and risks in the ISIMIP framework. ISIMIP. https://www.isimip.org

[91] Stefan Lange. (2019). Trend-preserving bias adjustment and statistical downscaling with ISIMIP3BASD (Version 1.0). ISIMIP. https://doi.org/10.5194/gmd-12-3055-2019

[92] Suphorn Pimonsree, Suwit Kamworapan, Sutheera H. Gheewala, Anong Thongbhakdi, & Kanchana Prueksakorn. (2023). Application of EC-Earth3 general circulation model under Shared Socioeconomic Pathways (SSPs) for climate projection studies. *Sustainability, 15*(3), 1–18.

[93] Vimal Mishra. (2023). *South Asian climate forecasts with bias correction from Coupled Model Intercomparison Project Phase 6 (CMIP6) under SSP3-7.0 scenario*. Indian Institute of Technology Gandhinagar.

Publications

1. Groundwater Infiltration Trends in the Major Basin of Ahmedabad District, Gujarat, India by Chaitali Bhavsar; Dr. Mahendrasinh S. Gadhavi in International Journal of Innovative Science and Research Technology, Volume 10, Issue 11, November – 2025, ISSN No: -2456-2165, https://doi.org/10.38124/ijisrt/25nov102

2. Impact Assessment of Land Use Change Detection on the Environment of Ahmedabad District, Gujarat, India using Supervised Classification in GIS By Chaitali Bhavsar, Dr. Mahendrasinh S.Gadhavi, Dr. Mohdzuned M. Shaikh, Turkish Journal of Engineering – 2025, 9*(4)*, 823-830, DOI: https://doi.org/10.31127/tuje.1605134

LIST OF APPENDICES

Appendix A: Rainfall trend analysis

Outputs

FIGURE

< Previous Time Series

Next Time Series >

Monsoon Rainfall

TsNumber	1
Name	Rainfall in mm
Years	1981 - 2020
n	40
Test S	
Test Z	0.87
Signific.	
Q	1.88E+00
Qmin99	-5.24E+00
Qmax99	1.10E+01
Qmin95	-2.94E+00
Qmax95	8.35E+00
B	5.59E+02
Bmin99	6.93E+02
Bmax99	3.38E+02
Bmin95	6.52E+02
Bmax95	4.03E+02

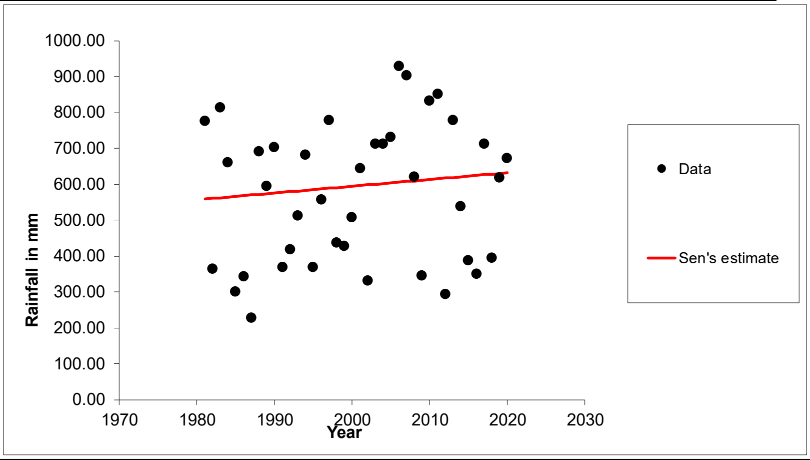

Chart options

☑ show 99 % confidence interval

☑ show 95 % confidence interval

☑ show residuals

Update chart outlook

Equation of the lines:

f(year) = Q*(year-firstDataYear) + B

FirstDataYear= 1981

Point values for the chart

Year	Data	Sen's estin	99 % conf. m	99 % conf. m	95 % conf. m	95 % conf. m	Residual
1981	776.88	558.77	693.27	338.10	651.84	403.40	218.11
1982	363.13	560.65	688.03	349.10	648.91	411.75	-197.52
1983	813.46	562.53	682.79	360.10	645.97	420.10	250.93
1984	659.53	564.41	677.55	371.10	643.03	428.44	95.12
1985	301.22	566.29	672.31	382.10	640.09	436.79	-265.07
1986	343.80	568.17	667.07	393.10	637.15	445.14	-224.37
1987	228.25	570.05	661.83	404.10	634.21	453.49	-341.80
1988	689.87	571.93	656.59	415.10	631.27	461.83	117.94
1989	593.75	573.80	651.35	426.10	628.33	470.18	19.95
1990	703.00	575.68	646.11	437.09	625.39	478.53	127.32
1991	369.04	577.56	640.87	448.09	622.46	486.87	-208.52
1992	419.14	579.44	635.63	459.09	619.52	495.22	-160.30
1993	511.69	581.32	630.39	470.09	616.58	503.57	-69.63
1994	682.06	583.20	625.15	481.09	613.64	511.92	98.86
1995	367.59	585.08	619.91	492.09	610.70	520.26	-217.49
1996	557.04	586.96	614.67	503.09	607.76	528.61	-29.92
1997	779.19	588.83	609.43	514.09	604.82	536.96	190.36
1998	437.91	590.71	604.19	525.09	601.88	545.31	-152.80
1999	426.75	592.59	598.95	536.09	598.95	553.65	-165.84
2000	507.89	594.47	593.70	547.09	596.01	562.00	-86.58
2001	643.02	596.35	588.46	558.08	593.07	570.35	46.67
2002	331.48	598.23	583.22	569.08	590.13	578.70	-266.75
2003	712.40	600.11	577.98	580.08	587.19	587.04	112.29
2004	711.34	601.99	572.74	591.08	584.25	595.39	109.35
2005	730.02	603.87	567.50	602.08	581.31	603.74	126.15
2006	929.03	605.74	562.26	613.08	578.37	612.09	323.29
2007	903.82	607.62	557.02	624.08	575.43	620.43	296.20
2008	621.05	609.50	551.78	635.08	572.50	628.78	11.55
2009	344.60	611.38	546.54	646.08	569.56	637.13	-266.78
2010	832.03	613.26	541.30	657.08	566.62	645.48	218.77
2011	850.90	615.14	536.06	668.08	563.68	653.82	235.76
2012	292.52	617.02	530.82	679.07	560.74	662.17	-324.50
2013	778.06	618.90	525.58	690.07	557.80	670.52	159.16
2014	538.36	620.77	520.34	701.07	554.86	678.87	-82.41
2015	388.07	622.65	515.10	712.07	551.92	687.21	-234.58
2016	350.45	624.53	509.86	723.07	548.98	695.56	-274.08
2017	711.64	626.41	504.62	734.07	546.05	703.91	85.23
2018	393.72	628.29	499.38	745.07	543.11	712.26	-234.57
2019	618.62	630.17	494.14	756.07	540.17	720.60	-11.55
2020	672.66	632.05	488.90	767.07	537.23	728.95	40.61

FIGURE

Premonsoon rainfall

< Previous Time Series | Next Time Series >

TsNumber	1
Name	Rainfall in mm
Years	1981 - 2020
n	40
Test S	
Test Z	0.22
Signific.	
Q	0.00E+00
Qmin99	-6.50E-02
Qmax99	9.11E-02
Qmin95	-3.98E-02
Qmax95	5.49E-02
B	1.36E+00
Bmin99	2.84E+00
Bmax99	-3.00E-01
Bmin95	2.22E+00
Bmax95	4.17E-01

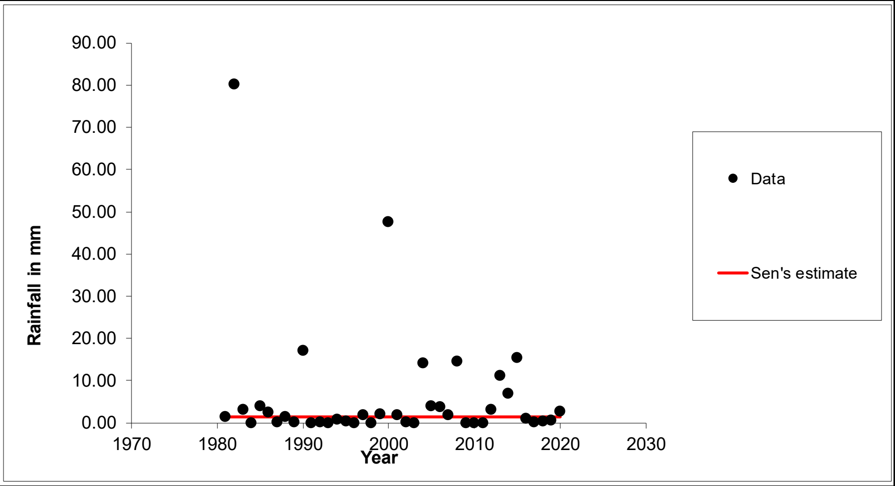

Chart options

☑ show 99 % confidence interval

☑ show 95 % confidence interval

☑ show residuals

Update chart outlook

Equation of the lines:

f(year) = Q*(year-firstDataYear) + B

FirstDataYear= 1981

Point values for the chart

Year	Data	Sen's estin	99 % conf. n	99 % conf. n	95 % conf. n	95 % conf. n	Residual
1981	1.30	1.36	2.84	-0.30	2.22	0.42	-0.06
1982	80.13	1.36	2.78	-0.21	2.18	0.47	78.77
1983	3.14	1.36	2.71	-0.12	2.14	0.53	1.78
1984	0.00	1.36	2.65	-0.03	2.10	0.58	-1.36
1985	3.94	1.36	2.58	0.06	2.06	0.64	2.58
1986	2.44	1.36	2.52	0.16	2.02	0.69	1.08
1987	0.22	1.36	2.45	0.25	1.98	0.75	-1.14
1988	1.42	1.36	2.39	0.34	1.94	0.80	0.06
1989	0.07	1.36	2.32	0.43	1.90	0.86	-1.29
1990	17.07	1.36	2.26	0.52	1.86	0.91	15.71
1991	0.00	1.36	2.19	0.61	1.82	0.97	-1.36
1992	0.04	1.36	2.13	0.70	1.78	1.02	-1.32
1993	0.00	1.36	2.06	0.79	1.74	1.08	-1.36
1994	0.69	1.36	2.00	0.88	1.70	1.13	-0.67
1995	0.40	1.36	1.93	0.98	1.66	1.19	-0.96
1996	0.00	1.36	1.87	1.07	1.62	1.24	-1.36
1997	1.92	1.36	1.80	1.16	1.58	1.29	0.56
1998	0.00	1.36	1.74	1.25	1.54	1.35	-1.36
1999	2.05	1.36	1.67	1.34	1.50	1.40	0.69
2000	47.56	1.36	1.61	1.43	1.46	1.46	46.20
2001	1.87	1.36	1.54	1.52	1.42	1.51	0.51
2002	0.03	1.36	1.48	1.61	1.38	1.57	-1.33
2003	0.01	1.36	1.41	1.70	1.34	1.62	-1.35
2004	14.16	1.36	1.35	1.79	1.30	1.68	12.80
2005	3.90	1.36	1.28	1.89	1.26	1.73	2.54
2006	3.66	1.36	1.22	1.98	1.22	1.79	2.30
2007	1.77	1.36	1.15	2.07	1.18	1.84	0.41
2008	14.63	1.36	1.09	2.16	1.14	1.90	13.27
2009	0.01	1.36	1.02	2.25	1.10	1.95	-1.35
2010	0.00	1.36	0.96	2.34	1.06	2.01	-1.36
2011	0.00	1.36	0.89	2.43	1.02	2.06	-1.36
2012	3.04	1.36	0.83	2.52	0.98	2.12	1.68
2013	11.05	1.36	0.76	2.61	0.94	2.17	9.69
2014	6.89	1.36	0.70	2.71	0.90	2.23	5.53
2015	15.47	1.36	0.63	2.80	0.86	2.28	14.11
2016	1.08	1.36	0.57	2.89	0.82	2.34	-0.28
2017	0.10	1.36	0.50	2.98	0.78	2.39	-1.26
2018	0.26	1.36	0.44	3.07	0.75	2.45	-1.10
2019	0.45	1.36	0.37	3.16	0.71	2.50	-0.91
2020	2.63	1.36	0.31	3.25	0.67	2.56	1.27

FIGURE

< Previous Time Series

Next Time Series >

Post monsoon rainfall

TsNumber	1
Name	Rainfall in mm
Years	1981 - 2020
n	40
Test S	
Test Z	-0.40
Signific.	
Q	-2.26E-02
Qmin99	-8.07E-01
Qmax99	2.73E-01
Qmin95	-4.48E-01
Qmax95	1.55E-01
B	5.83E+00
Bmin99	2.72E+01
Bmax99	3.17E-01
Bmin95	1.63E+01
Bmax95	2.26E+00

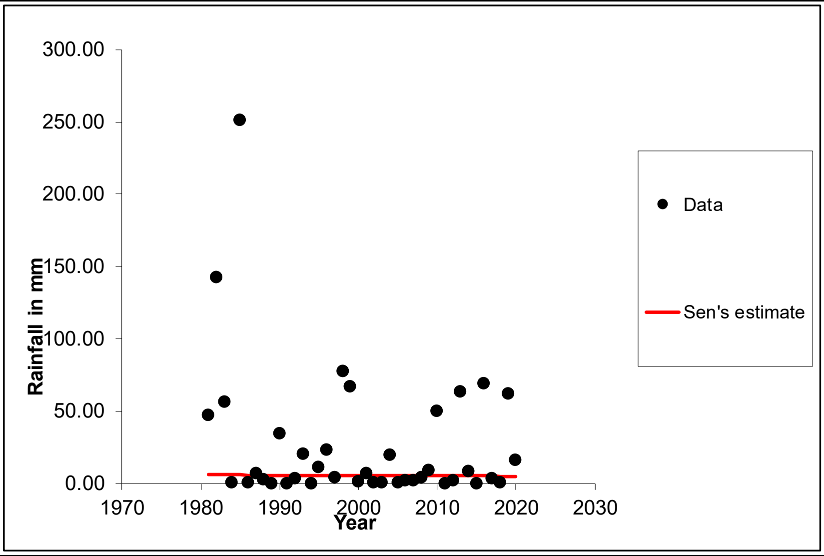

Chart options

show 99 % confidence interval

show 95 % confidence interval

show residuals

Update chart outlook

Equation of the lines:

f(year) = Q*(year-firstDataYear) + B

FirstDataYear= 1981

Point values for the chart

Year	Data	Sen's estin	99 % conf. m	99 % conf. m	95 % conf. m	95 % conf. m	Residual
1981	47.08	5.83	27.17	0.32	16.32	2.26	41.25
1982	142.69	5.81	26.36	0.59	15.87	2.42	136.88
1983	56.34	5.79	25.56	0.86	15.43	2.57	50.55
1984	0.75	5.77	24.75	1.14	14.98	2.73	-5.02
1985	250.83	5.74	23.94	1.41	14.53	2.88	245.09
1986	0.13	5.72	23.14	1.68	14.08	3.04	-5.59
1987	6.92	5.70	22.33	1.96	13.63	3.19	1.22
1988	2.41	5.68	21.52	2.23	13.18	3.35	-3.27
1989	0.01	5.65	20.72	2.50	12.74	3.50	-5.64
1990	34.09	5.63	19.91	2.78	12.29	3.66	28.46
1991	0.00	5.61	19.10	3.05	11.84	3.81	-5.61
1992	3.14	5.59	18.30	3.32	11.39	3.97	-2.45
1993	19.92	5.56	17.49	3.59	10.94	4.12	14.36
1994	0.00	5.54	16.68	3.87	10.50	4.28	-5.54
1995	11.31	5.52	15.88	4.14	10.05	4.43	5.79
1996	23.06	5.49	15.07	4.41	9.60	4.59	17.57
1997	4.25	5.47	14.26	4.69	9.15	4.74	-1.22
1998	77.45	5.45	13.46	4.96	8.70	4.90	72.00
1999	67.13	5.43	12.65	5.23	8.25	5.05	61.70
2000	1.35	5.40	11.84	5.51	7.81	5.21	-4.05
2001	6.67	5.38	11.04	5.78	7.36	5.36	1.29
2002	0.20	5.36	10.23	6.05	6.91	5.52	-5.16
2003	0.15	5.34	9.42	6.32	6.46	5.67	-5.19
2004	19.74	5.31	8.61	6.60	6.01	5.83	14.43
2005	0.25	5.29	7.81	6.87	5.57	5.98	-5.04
2006	2.10	5.27	7.00	7.14	5.12	6.14	-3.17
2007	1.49	5.25	6.19	7.42	4.67	6.29	-3.76
2008	3.66	5.22	5.39	7.69	4.22	6.45	-1.56
2009	9.05	5.20	4.58	7.96	3.77	6.60	3.85
2010	49.75	5.18	3.77	8.24	3.32	6.76	44.57
2011	0.00	5.16	2.97	8.51	2.88	6.91	-5.16
2012	1.86	5.13	2.16	8.78	2.43	7.07	-3.27
2013	63.19	5.11	1.35	9.06	1.98	7.22	58.08
2014	7.87	5.09	0.55	9.33	1.53	7.38	2.78
2015	0.04	5.07	-0.26	9.60	1.08	7.53	-5.03
2016	68.57	5.04	-1.07	9.87	0.64	7.69	63.53
2017	3.11	5.02	-1.87	10.15	0.19	7.84	-1.91
2018	0.30	5.00	-2.68	10.42	-0.26	8.00	-4.70
2019	61.90	4.98	-3.49	10.69	-0.71	8.15	56.92
2020	15.81	4.95	-4.29	10.97	-1.16	8.31	10.86

FIGURE | < Previous Time Series | Next Time Series >

Winter rainfall

TsNumber	1
Name	Rainfall in mm
Years	1981 - 2020
n	40
Test S	
Test Z	-0.22
Signific.	
Q	0.00E+00
Qmin99	-2.31E-02
Qmax99	2.96E-02
Qmin95	-1.67E-02
Qmax95	1.36E-02
B	4.20E-01
Bmin99	7.89E-01
Bmax99	-3.73E-02
Bmin95	6.40E-01
Bmax95	2.09E-01

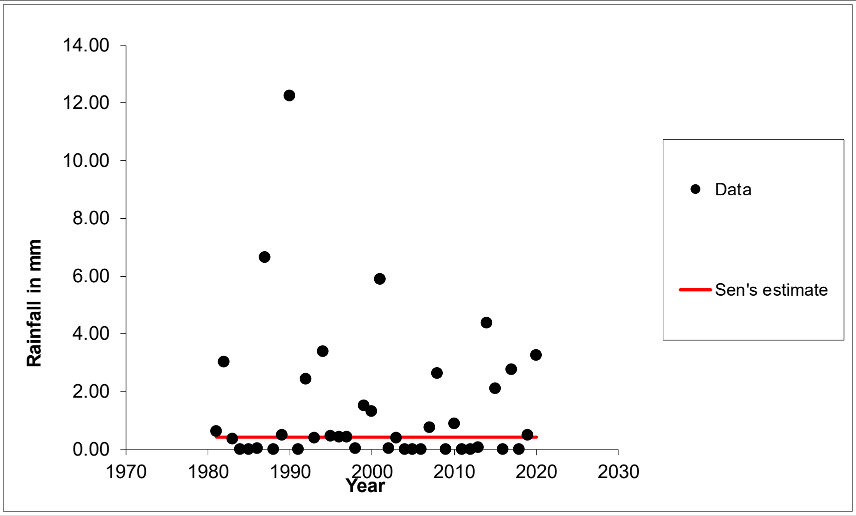

Chart options

- [x] show 99 % confidence interval
- [x] show 95 % confidence interval
- [x] show residuals

Update chart outlook

Equation of the lines:
f(year) = Q*(year-firstDataYear) + B
FirstDataYear= 1981

Point values for the chart

Year	Data	Sen's estim	99 % conf. m	99 % conf. m	95 % conf. m	95 % conf. m	Residual
1981	0.62	0.42	0.79	-0.04	0.64	0.21	0.20
1982	3.02	0.42	0.77	-0.01	0.62	0.22	2.60
1983	0.36	0.42	0.74	0.02	0.61	0.24	-0.06
1984	0.00	0.42	0.72	0.05	0.59	0.25	-0.42
1985	0.00	0.42	0.70	0.08	0.57	0.26	-0.42
1986	0.02	0.42	0.67	0.11	0.56	0.28	-0.40
1987	6.64	0.42	0.65	0.14	0.54	0.29	6.22
1988	0.00	0.42	0.63	0.17	0.52	0.30	-0.42
1989	0.47	0.42	0.60	0.20	0.51	0.32	0.05
1990	12.24	0.42	0.58	0.23	0.49	0.33	11.82
1991	0.00	0.42	0.56	0.26	0.47	0.35	-0.42
1992	2.43	0.42	0.54	0.29	0.46	0.36	2.01
1993	0.37	0.42	0.51	0.32	0.44	0.37	-0.05
1994	3.37	0.42	0.49	0.35	0.42	0.39	2.95
1995	0.45	0.42	0.47	0.38	0.41	0.40	0.03
1996	0.41	0.42	0.44	0.41	0.39	0.41	-0.01
1997	0.43	0.42	0.42	0.44	0.37	0.43	0.01
1998	0.02	0.42	0.40	0.47	0.36	0.44	-0.40
1999	1.50	0.42	0.37	0.50	0.34	0.45	1.08
2000	1.30	0.42	0.35	0.53	0.32	0.47	0.88
2001	5.88	0.42	0.33	0.56	0.31	0.48	5.46
2002	0.01	0.42	0.30	0.58	0.29	0.50	-0.41
2003	0.38	0.42	0.28	0.61	0.27	0.51	-0.04
2004	0.00	0.42	0.26	0.64	0.26	0.52	-0.42
2005	0.00	0.42	0.24	0.67	0.24	0.54	-0.42
2006	0.00	0.42	0.21	0.70	0.22	0.55	-0.42
2007	0.73	0.42	0.19	0.73	0.21	0.56	0.31
2008	2.61	0.42	0.17	0.76	0.19	0.58	2.19
2009	0.00	0.42	0.14	0.79	0.17	0.59	-0.42
2010	0.87	0.42	0.12	0.82	0.16	0.60	0.45
2011	0.00	0.42	0.10	0.85	0.14	0.62	-0.42
2012	0.00	0.42	0.07	0.88	0.12	0.63	-0.42
2013	0.04	0.42	0.05	0.91	0.11	0.65	-0.38
2014	4.37	0.42	0.03	0.94	0.09	0.66	3.95
2015	2.11	0.42	0.00	0.97	0.07	0.67	1.69
2016	0.00	0.42	-0.02	1.00	0.06	0.69	-0.42
2017	2.77	0.42	-0.04	1.03	0.04	0.70	2.35
2018	0.00	0.42	-0.07	1.06	0.02	0.71	-0.42
2019	0.47	0.42	-0.09	1.09	0.00	0.73	0.05
2020	3.26	0.42	-0.11	1.12	-0.01	0.74	2.84

FIGURE

January

< Previous Time Series

Next Time Series >

TsNumber	1
Name	Rainfall in mm
Years	1981 - 2020
n	40
Test S	
Test Z	-1.06
Signific.	
Q	0.00E+00
Qmin99	-7.69E-04
Qmax99	0.00E+00
Qmin95	-3.85E-04
Qmax95	0.00E+00
B	0.00E+00
Bmin99	2.42E-02
Bmax99	0.00E+00
Bmin95	1.31E-02
Bmax95	0.00E+00

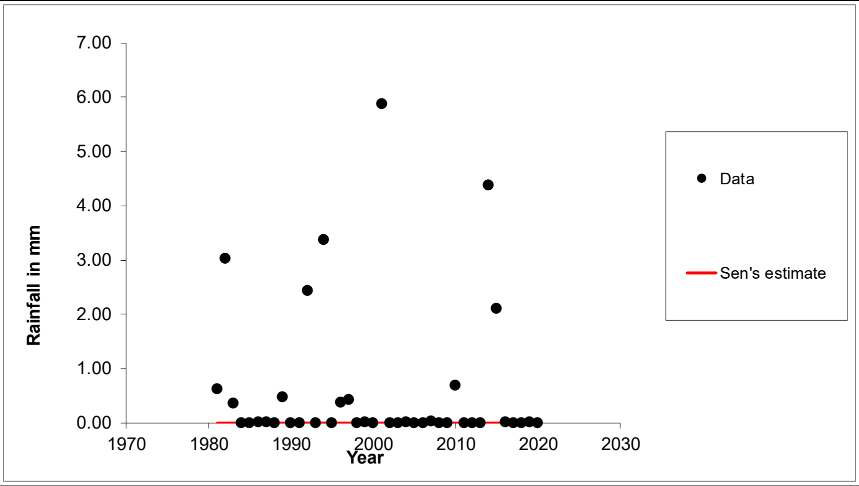

Chart options

☑ show 99 % confidence interval

☑ show 95 % confidence interval

☑ show residuals

Update chart outlook

Equation of the lines:

f(year) = Q*(year-firstDataYear) + B

FirstDataYear= 1981

Point values for the chart

Year	Data	Sen's estin	99 % conf. m	99 % conf. m	95 % conf. m	95 % conf. m	Residual
1981	0.62	0.00	0.02	0.00	0.01	0.00	0.62
1982	3.02	0.00	0.02	0.00	0.01	0.00	3.02
1983	0.36	0.00	0.02	0.00	0.01	0.00	0.36
1984	0.00	0.00	0.02	0.00	0.01	0.00	0.00
1985	0.00	0.00	0.02	0.00	0.01	0.00	0.00
1986	0.01	0.00	0.02	0.00	0.01	0.00	0.01
1987	0.01	0.00	0.02	0.00	0.01	0.00	0.01
1988	0.00	0.00	0.02	0.00	0.01	0.00	0.00
1989	0.47	0.00	0.02	0.00	0.01	0.00	0.47
1990	0.00	0.00	0.02	0.00	0.01	0.00	0.00
1991	0.00	0.00	0.02	0.00	0.01	0.00	0.00
1992	2.43	0.00	0.02	0.00	0.01	0.00	2.43
1993	0.00	0.00	0.02	0.00	0.01	0.00	0.00
1994	3.37	0.00	0.01	0.00	0.01	0.00	3.37
1995	0.00	0.00	0.01	0.00	0.01	0.00	0.00
1996	0.37	0.00	0.01	0.00	0.01	0.00	0.37
1997	0.42	0.00	0.01	0.00	0.01	0.00	0.42
1998	0.00	0.00	0.01	0.00	0.01	0.00	0.00
1999	0.01	0.00	0.01	0.00	0.01	0.00	0.01
2000	0.00	0.00	0.01	0.00	0.01	0.00	0.00
2001	5.88	0.00	0.01	0.00	0.01	0.00	5.88
2002	0.00	0.00	0.01	0.00	0.01	0.00	0.00
2003	0.00	0.00	0.01	0.00	0.00	0.00	0.00
2004	0.01	0.00	0.01	0.00	0.00	0.00	0.01
2005	0.00	0.00	0.01	0.00	0.00	0.00	0.00
2006	0.00	0.00	0.01	0.00	0.00	0.00	0.00
2007	0.02	0.00	0.00	0.00	0.00	0.00	0.02
2008	0.00	0.00	0.00	0.00	0.00	0.00	0.00
2009	0.00	0.00	0.00	0.00	0.00	0.00	0.00
2010	0.68	0.00	0.00	0.00	0.00	0.00	0.68
2011	0.00	0.00	0.00	0.00	0.00	0.00	0.00
2012	0.00	0.00	0.00	0.00	0.00	0.00	0.00
2013	0.00	0.00	0.00	0.00	0.00	0.00	0.00
2014	4.37	0.00	0.00	0.00	0.00	0.00	4.37
2015	2.11	0.00	0.00	0.00	0.00	0.00	2.11
2016	0.01	0.00	0.00	0.00	0.00	0.00	0.01
2017	0.00	0.00	0.00	0.00	0.00	0.00	0.00
2018	0.00	0.00	0.00	0.00	0.00	0.00	0.00
2019	0.01	0.00	-0.01	0.00	0.00	0.00	0.01
2020	0.00	0.00	-0.01	0.00	0.00	0.00	0.00

FIGURE

February

< Previous Time Series | Next Time Series >

TsNumber	1
Name	Rainfall in mm
Years	1981 - 2020
n	40
Test S	
Test Z	-0.43
Signific.	
Q	0.00E+00
Qmin99	0.00E+00
Qmax99	0.00E+00
Qmin95	0.00E+00
Qmax95	0.00E+00
B	0.00E+00
Bmin99	0.00E+00
Bmax99	0.00E+00
Bmin95	0.00E+00
Bmax95	0.00E+00

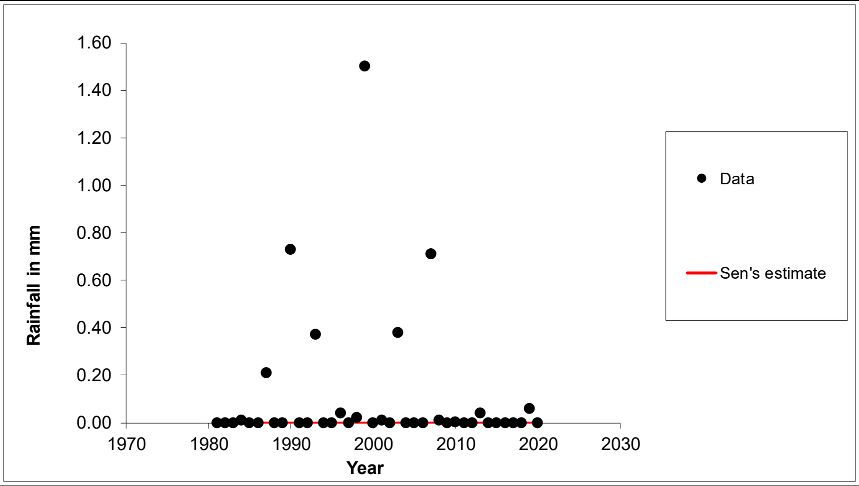

Chart options

- [x] show 99 % confidence interval
- [x] show 95 % confidence interval
- [x] show residuals

Update chart outlook

Equation of the lines:
f(year) = Q*(year-firstDataYear) + B
FirstDataYear= 1981

Point values for the chart

Year	Data	Sen's estin	99 % conf. m	99 % conf. m	95 % conf. m	95 % conf. m	Residual
1981	0.00	0.00	0.00	0.00	0.00	0.00	0.00
1982	0.00	0.00	0.00	0.00	0.00	0.00	0.00
1983	0.00	0.00	0.00	0.00	0.00	0.00	0.00
1984	0.01	0.00	0.00	0.00	0.00	0.00	0.01
1985	0.00	0.00	0.00	0.00	0.00	0.00	0.00
1986	0.00	0.00	0.00	0.00	0.00	0.00	0.00
1987	0.21	0.00	0.00	0.00	0.00	0.00	0.21
1988	0.00	0.00	0.00	0.00	0.00	0.00	0.00
1989	0.00	0.00	0.00	0.00	0.00	0.00	0.00
1990	0.73	0.00	0.00	0.00	0.00	0.00	0.73
1991	0.00	0.00	0.00	0.00	0.00	0.00	0.00
1992	0.00	0.00	0.00	0.00	0.00	0.00	0.00
1993	0.37	0.00	0.00	0.00	0.00	0.00	0.37
1994	0.00	0.00	0.00	0.00	0.00	0.00	0.00
1995	0.00	0.00	0.00	0.00	0.00	0.00	0.00
1996	0.04	0.00	0.00	0.00	0.00	0.00	0.04
1997	0.00	0.00	0.00	0.00	0.00	0.00	0.00
1998	0.02	0.00	0.00	0.00	0.00	0.00	0.02
1999	1.50	0.00	0.00	0.00	0.00	0.00	1.50
2000	0.00	0.00	0.00	0.00	0.00	0.00	0.00
2001	0.01	0.00	0.00	0.00	0.00	0.00	0.01
2002	0.00	0.00	0.00	0.00	0.00	0.00	0.00
2003	0.38	0.00	0.00	0.00	0.00	0.00	0.38
2004	0.00	0.00	0.00	0.00	0.00	0.00	0.00
2005	0.00	0.00	0.00	0.00	0.00	0.00	0.00
2006	0.00	0.00	0.00	0.00	0.00	0.00	0.00
2007	0.71	0.00	0.00	0.00	0.00	0.00	0.71
2008	0.01	0.00	0.00	0.00	0.00	0.00	0.01
2009	0.00	0.00	0.00	0.00	0.00	0.00	0.00
2010	0.00	0.00	0.00	0.00	0.00	0.00	0.00
2011	0.00	0.00	0.00	0.00	0.00	0.00	0.00
2012	0.00	0.00	0.00	0.00	0.00	0.00	0.00
2013	0.04	0.00	0.00	0.00	0.00	0.00	0.04
2014	0.00	0.00	0.00	0.00	0.00	0.00	0.00
2015	0.00	0.00	0.00	0.00	0.00	0.00	0.00
2016	0.00	0.00	0.00	0.00	0.00	0.00	0.00
2017	0.00	0.00	0.00	0.00	0.00	0.00	0.00
2018	0.00	0.00	0.00	0.00	0.00	0.00	0.00
2019	0.06	0.00	0.00	0.00	0.00	0.00	0.06
2020	0.00	0.00	0.00	0.00	0.00	0.00	0.00

FIGURE

March

< Previous Time Series | Next Time Series >

TsNumber	1
Name	Rainfall in mm
Years	1981 - 2020
n	40
Test S	
Test Z	0.31
Signific.	
Q	0.00E+00
Qmin99	0.00E+00
Qmax99	0.00E+00
Qmin95	0.00E+00
Qmax95	0.00E+00
B	0.00E+00
Bmin99	0.00E+00
Bmax99	0.00E+00
Bmin95	0.00E+00
Bmax95	0.00E+00

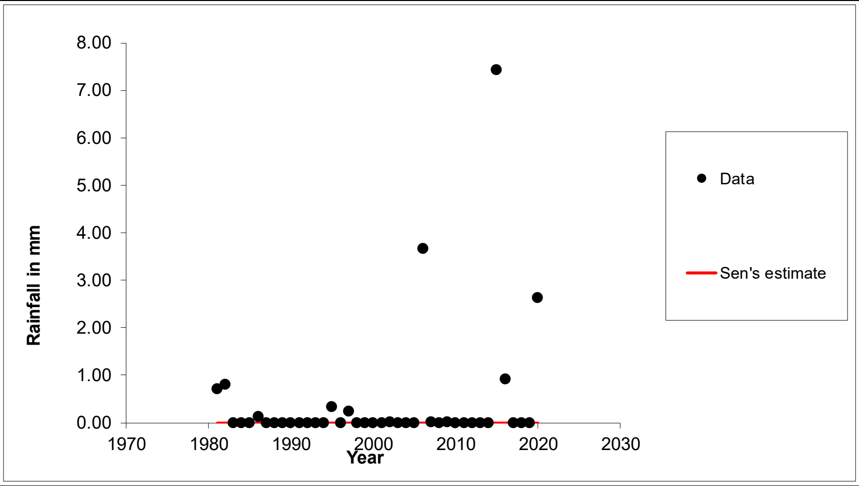

Chart options

- [x] show 99 % confidence interval
- [x] show 95 % confidence interval
- [x] show residuals

Update chart outlook

Equation of the lines:
f(year) = Q*(year-firstDataYear) + B
FirstDataYear= 1981

Point values for the chart

Year	Data	Sen's estin	99 % conf. m	99 % conf. m	95 % conf. m	95 % conf. m	Residual
1981	0.71	0.00	0.00	0.00	0.00	0.00	0.71
1982	0.81	0.00	0.00	0.00	0.00	0.00	0.81
1983	0.00	0.00	0.00	0.00	0.00	0.00	0.00
1984	0.00	0.00	0.00	0.00	0.00	0.00	0.00
1985	0.00	0.00	0.00	0.00	0.00	0.00	0.00
1986	0.12	0.00	0.00	0.00	0.00	0.00	0.12
1987	0.00	0.00	0.00	0.00	0.00	0.00	0.00
1988	0.00	0.00	0.00	0.00	0.00	0.00	0.00
1989	0.00	0.00	0.00	0.00	0.00	0.00	0.00
1990	0.00	0.00	0.00	0.00	0.00	0.00	0.00
1991	0.00	0.00	0.00	0.00	0.00	0.00	0.00
1992	0.00	0.00	0.00	0.00	0.00	0.00	0.00
1993	0.00	0.00	0.00	0.00	0.00	0.00	0.00
1994	0.00	0.00	0.00	0.00	0.00	0.00	0.00
1995	0.34	0.00	0.00	0.00	0.00	0.00	0.34
1996	0.00	0.00	0.00	0.00	0.00	0.00	0.00
1997	0.23	0.00	0.00	0.00	0.00	0.00	0.23
1998	0.00	0.00	0.00	0.00	0.00	0.00	0.00
1999	0.00	0.00	0.00	0.00	0.00	0.00	0.00
2000	0.00	0.00	0.00	0.00	0.00	0.00	0.00
2001	0.00	0.00	0.00	0.00	0.00	0.00	0.00
2002	0.02	0.00	0.00	0.00	0.00	0.00	0.02
2003	0.00	0.00	0.00	0.00	0.00	0.00	0.00
2004	0.00	0.00	0.00	0.00	0.00	0.00	0.00
2005	0.00	0.00	0.00	0.00	0.00	0.00	0.00
2006	3.66	0.00	0.00	0.00	0.00	0.00	3.66
2007	0.01	0.00	0.00	0.00	0.00	0.00	0.01
2008	0.00	0.00	0.00	0.00	0.00	0.00	0.00
2009	0.01	0.00	0.00	0.00	0.00	0.00	0.01
2010	0.00	0.00	0.00	0.00	0.00	0.00	0.00
2011	0.00	0.00	0.00	0.00	0.00	0.00	0.00
2012	0.00	0.00	0.00	0.00	0.00	0.00	0.00
2013	0.00	0.00	0.00	0.00	0.00	0.00	0.00
2014	0.00	0.00	0.00	0.00	0.00	0.00	0.00
2015	7.43	0.00	0.00	0.00	0.00	0.00	7.43
2016	0.91	0.00	0.00	0.00	0.00	0.00	0.91
2017	0.00	0.00	0.00	0.00	0.00	0.00	0.00
2018	0.00	0.00	0.00	0.00	0.00	0.00	0.00
2019	0.00	0.00	0.00	0.00	0.00	0.00	0.00
2020	2.62	0.00	0.00	0.00	0.00	0.00	2.62

FIGURE

April

< Previous Time Series | Next Time Series >

TsNumber	1
Name	Rainfall in mm
Years	1981 - 2020
n	40
Test S	
Test Z	0.13
Signific.	
Q	0.00E+00
Qmin99	0.00E+00
Qmax99	2.61E-03
Qmin95	0.00E+00
Qmax95	0.00E+00
B	0.00E+00
Bmin99	0.00E+00
Bmax99	-1.17E-02
Bmin95	0.00E+00
Bmax95	0.00E+00

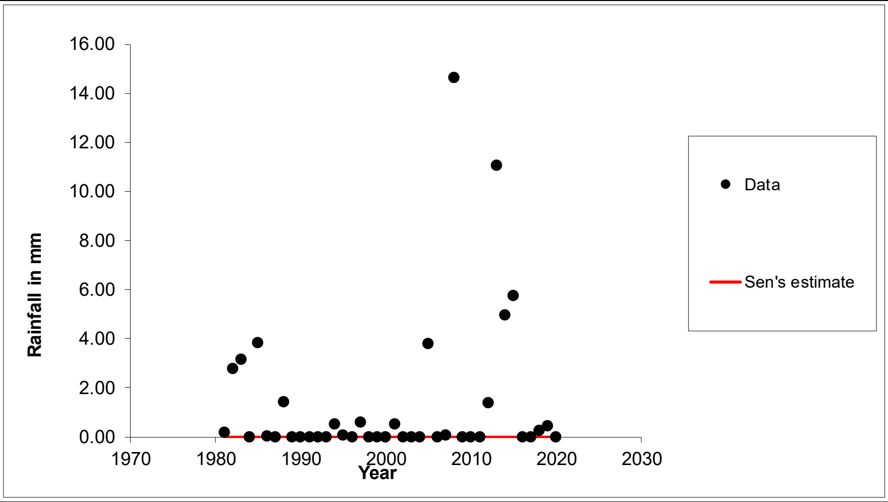

Chart options

- [x] show 99 % confidence interval
- [x] show 95 % confidence interval
- [x] show residuals

Update chart outlook

Equation of the lines:
f(year) = Q*(year-firstDataYear) + B
FirstDataYear= 1981

Point values for the chart

Year	Data	Sen's estin	99 % conf. m	99 % conf. m	95 % conf. m	95 % conf. m	Residual
1981	0.17	0.00	0.00	-0.01	0.00	0.00	0.17
1982	2.76	0.00	0.00	-0.01	0.00	0.00	2.76
1983	3.14	0.00	0.00	-0.01	0.00	0.00	3.14
1984	0.00	0.00	0.00	0.00	0.00	0.00	0.00
1985	3.83	0.00	0.00	0.00	0.00	0.00	3.83
1986	0.01	0.00	0.00	0.00	0.00	0.00	0.01
1987	0.00	0.00	0.00	0.00	0.00	0.00	0.00
1988	1.42	0.00	0.00	0.01	0.00	0.00	1.42
1989	0.00	0.00	0.00	0.01	0.00	0.00	0.00
1990	0.00	0.00	0.00	0.01	0.00	0.00	0.00
1991	0.00	0.00	0.00	0.01	0.00	0.00	0.00
1992	0.00	0.00	0.00	0.02	0.00	0.00	0.00
1993	0.00	0.00	0.00	0.02	0.00	0.00	0.00
1994	0.51	0.00	0.00	0.02	0.00	0.00	0.51
1995	0.06	0.00	0.00	0.02	0.00	0.00	0.06
1996	0.00	0.00	0.00	0.03	0.00	0.00	0.00
1997	0.58	0.00	0.00	0.03	0.00	0.00	0.58
1998	0.00	0.00	0.00	0.03	0.00	0.00	0.00
1999	0.00	0.00	0.00	0.04	0.00	0.00	0.00
2000	0.00	0.00	0.00	0.04	0.00	0.00	0.00
2001	0.53	0.00	0.00	0.04	0.00	0.00	0.53
2002	0.00	0.00	0.00	0.04	0.00	0.00	0.00
2003	0.00	0.00	0.00	0.05	0.00	0.00	0.00
2004	0.00	0.00	0.00	0.05	0.00	0.00	0.00
2005	3.80	0.00	0.00	0.05	0.00	0.00	3.80
2006	0.00	0.00	0.00	0.05	0.00	0.00	0.00
2007	0.06	0.00	0.00	0.06	0.00	0.00	0.06
2008	14.63	0.00	0.00	0.06	0.00	0.00	14.63
2009	0.00	0.00	0.00	0.06	0.00	0.00	0.00
2010	0.00	0.00	0.00	0.06	0.00	0.00	0.00
2011	0.00	0.00	0.00	0.07	0.00	0.00	0.00
2012	1.38	0.00	0.00	0.07	0.00	0.00	1.38
2013	11.05	0.00	0.00	0.07	0.00	0.00	11.05
2014	4.96	0.00	0.00	0.07	0.00	0.00	4.96
2015	5.73	0.00	0.00	0.08	0.00	0.00	5.73
2016	0.00	0.00	0.00	0.08	0.00	0.00	0.00
2017	0.00	0.00	0.00	0.08	0.00	0.00	0.00
2018	0.26	0.00	0.00	0.08	0.00	0.00	0.26
2019	0.43	0.00	0.00	0.09	0.00	0.00	0.43
2020	0.00	0.00	0.00	0.09	0.00	0.00	0.00

FIGURE

May

< Previous Time Series | Next Time Series >

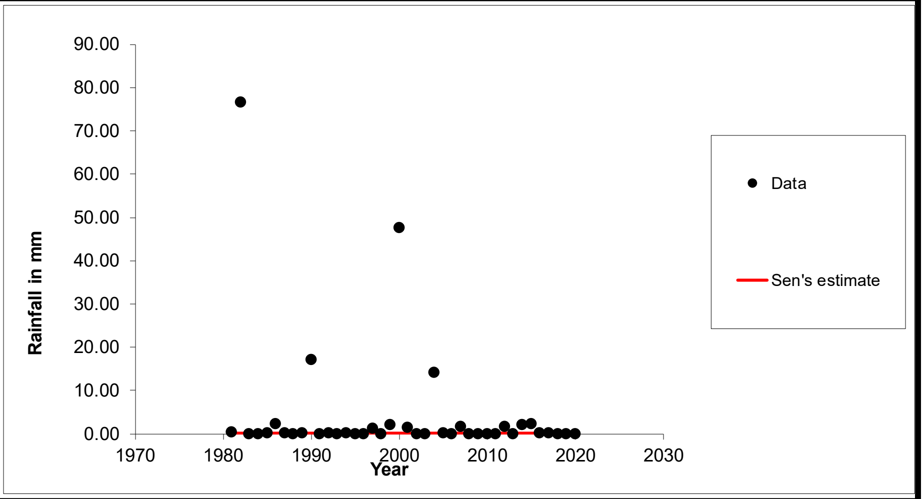

TsNumber	1
Name	Rainfall in mm
Years	1981 - 2020
n	40
Test S	
Test Z	-0.54
Signific.	
Q	0.00E+00
Qmin99	-9.74E-03
Qmax99	1.00E-03
Qmin95	-5.11E-03
Qmax95	3.63E-04
B	5.50E-02
Bmin99	3.09E-01
Bmax99	4.55E-02
Bmin95	1.99E-01
Bmax95	5.16E-02

Chart options

- [x] show 99 % confidence interval
- [x] show 95 % confidence interval
- [x] show residuals

Update chart outlook

Equation of the lines:
f(year) = Q*(year-firstDataYear) + B
FirstDataYear= 1981

Point values for the chart

Year	Data	Sen's estin	99 % conf. m	99 % conf. m	95 % conf. m	95 % conf. m	Residual
1981	0.42	0.06	0.31	0.05	0.20	0.05	0.37
1982	76.56	0.06	0.30	0.05	0.19	0.05	76.51
1983	0.00	0.06	0.29	0.05	0.19	0.05	-0.06
1984	0.00	0.06	0.28	0.05	0.18	0.05	-0.06
1985	0.11	0.06	0.27	0.05	0.18	0.05	0.06
1986	2.31	0.06	0.26	0.05	0.17	0.05	2.26
1987	0.22	0.06	0.25	0.05	0.17	0.05	0.17
1988	0.00	0.06	0.24	0.05	0.16	0.05	-0.06
1989	0.07	0.06	0.23	0.05	0.16	0.05	0.02
1990	17.07	0.06	0.22	0.05	0.15	0.05	17.02
1991	0.00	0.06	0.21	0.06	0.15	0.06	-0.06
1992	0.04	0.06	0.20	0.06	0.14	0.06	-0.02
1993	0.00	0.06	0.19	0.06	0.14	0.06	-0.06
1994	0.18	0.06	0.18	0.06	0.13	0.06	0.13
1995	0.00	0.06	0.17	0.06	0.13	0.06	-0.06
1996	0.00	0.06	0.16	0.06	0.12	0.06	-0.06
1997	1.11	0.06	0.15	0.06	0.12	0.06	1.06
1998	0.00	0.06	0.14	0.06	0.11	0.06	-0.06
1999	2.05	0.06	0.13	0.06	0.11	0.06	2.00
2000	47.56	0.06	0.12	0.06	0.10	0.06	47.51
2001	1.34	0.06	0.11	0.07	0.10	0.06	1.29
2002	0.01	0.06	0.10	0.07	0.09	0.06	-0.05
2003	0.01	0.06	0.09	0.07	0.09	0.06	-0.05
2004	14.16	0.06	0.09	0.07	0.08	0.06	14.11
2005	0.10	0.06	0.08	0.07	0.08	0.06	0.05
2006	0.00	0.06	0.07	0.07	0.07	0.06	-0.06
2007	1.70	0.06	0.06	0.07	0.07	0.06	1.65
2008	0.00	0.06	0.05	0.07	0.06	0.06	-0.06
2009	0.00	0.06	0.04	0.07	0.06	0.06	-0.06
2010	0.00	0.06	0.03	0.07	0.05	0.06	-0.06
2011	0.00	0.06	0.02	0.08	0.05	0.06	-0.06
2012	1.66	0.06	0.01	0.08	0.04	0.06	1.61
2013	0.00	0.06	0.00	0.08	0.04	0.06	-0.06
2014	1.93	0.06	-0.01	0.08	0.03	0.06	1.88
2015	2.31	0.06	-0.02	0.08	0.03	0.06	2.26
2016	0.17	0.06	-0.03	0.08	0.02	0.06	0.12
2017	0.10	0.06	-0.04	0.08	0.02	0.06	0.05
2018	0.00	0.06	-0.05	0.08	0.01	0.06	-0.06
2019	0.02	0.06	-0.06	0.08	0.00	0.07	-0.04
2020	0.01	0.06	-0.07	0.08	0.00	0.07	-0.05

FIGURE

June

< Previous Time Series | Next Time Series >

TsNumber	1
Name	Rainfall in mm
Years	1981 - 2020
n	40
Test S	
Test Z	0.36
Signific.	
Q	2.16E-01
Qmin99	-1.64E+00
Qmax99	2.69E+00
Qmin95	-1.08E+00
Qmax95	2.03E+00
B	7.74E+01
Bmin99	1.15E+02
Bmax99	3.35E+01
Bmin95	1.03E+02
Bmax95	4.57E+01

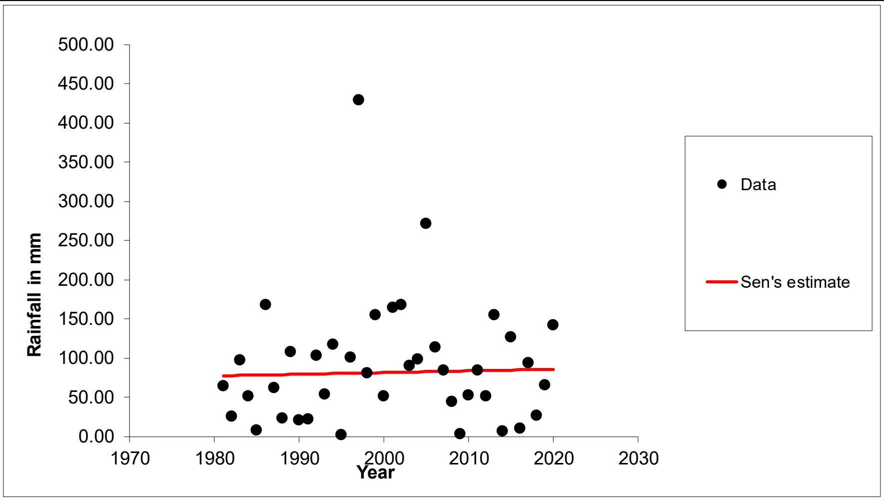

Chart options

show 99 % confidence interval

show 95 % confidence interval

show residuals

Update chart outlook

Equation of the lines:

f(year) = Q*(year-firstDataYear) + B

FirstDataYear= 1981

Point values for the chart

Year	Data	Sen's estin	99 % conf. m	99 % conf. m	95 % conf. m	95 % conf. m	Residual
1981	63.80	77.43	114.86	33.51	102.98	45.67	-13.63
1982	25.90	77.64	113.22	36.19	101.90	47.69	-51.74
1983	97.64	77.86	111.58	38.88	100.83	49.72	19.78
1984	51.41	78.07	109.93	41.57	99.75	51.74	-26.66
1985	8.29	78.29	108.29	44.25	98.67	53.77	-70.00
1986	167.74	78.50	106.65	46.94	97.60	55.79	89.24
1987	62.44	78.72	105.01	49.63	96.52	57.82	-16.28
1988	22.51	78.94	103.36	52.31	95.44	59.84	-56.43
1989	107.41	79.15	101.72	55.00	94.37	61.87	28.26
1990	20.82	79.37	100.08	57.69	93.29	63.89	-58.55
1991	21.39	79.58	98.44	60.38	92.21	65.92	-58.19
1992	102.54	79.80	96.79	63.06	91.13	67.94	22.74
1993	53.42	80.02	95.15	65.75	90.06	69.97	-26.60
1994	117.54	80.23	93.51	68.44	88.98	71.99	37.31
1995	1.93	80.45	91.87	71.12	87.90	74.02	-78.52
1996	100.77	80.66	90.22	73.81	86.83	76.04	20.11
1997	428.95	80.88	88.58	76.50	85.75	78.07	348.07
1998	81.25	81.10	86.94	79.18	84.67	80.09	0.15
1999	154.84	81.31	85.30	81.87	83.59	82.12	73.53
2000	51.65	81.53	83.65	84.56	82.52	84.14	-29.88
2001	164.31	81.74	82.01	87.24	81.44	86.17	82.57
2002	168.32	81.96	80.37	89.93	80.36	88.19	86.36
2003	90.55	82.18	78.73	92.62	79.29	90.22	8.37
2004	98.40	82.39	77.08	95.30	78.21	92.24	16.01
2005	271.06	82.61	75.44	97.99	77.13	94.27	188.45
2006	113.40	82.82	73.80	100.68	76.05	96.29	30.58
2007	84.35	83.04	72.15	103.36	74.98	98.32	1.31
2008	44.65	83.26	70.51	106.05	73.90	100.34	-38.61
2009	2.59	83.47	68.87	108.74	72.82	102.37	-80.88
2010	52.86	83.69	67.23	111.42	71.75	104.39	-30.83
2011	83.75	83.90	65.58	114.11	70.67	106.42	-0.15
2012	50.90	84.12	63.94	116.80	69.59	108.44	-33.22
2013	154.86	84.34	62.30	119.49	68.51	110.47	70.52
2014	6.87	84.55	60.66	122.17	67.44	112.49	-77.68
2015	127.16	84.77	59.01	124.86	66.36	114.52	42.39
2016	10.45	84.98	57.37	127.55	65.28	116.55	-74.53
2017	93.47	85.20	55.73	130.23	64.21	118.57	8.27
2018	26.62	85.42	54.09	132.92	63.13	120.60	-58.80
2019	65.24	85.63	52.44	135.61	62.05	122.62	-20.39
2020	141.75	85.85	50.80	138.29	60.98	124.65	55.90

FIGURE

July

< Previous Time Series

Next Time Series >

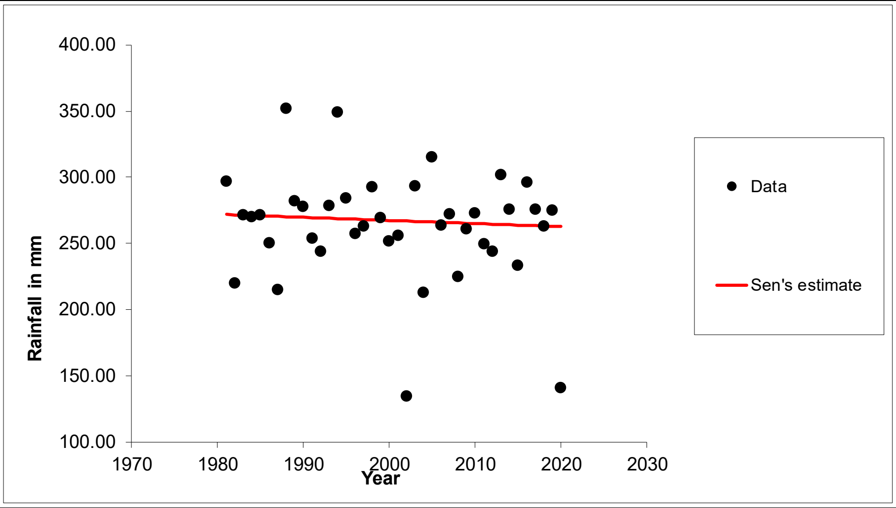

TsNumber	1
Name	Rainfall in mm
Years	1981 - 2020
n	40
Test S	
Test Z	-0.50
Signific.	
Q	-2.39E-01
Qmin99	-1.64E+00
Qmax99	9.05E-01
Qmin95	-1.16E+00
Qmax95	6.73E-01
B	2.72E+02
Bmin99	2.96E+02
Bmax99	2.46E+02
Bmin95	2.89E+02
Bmax95	2.52E+02

Chart options

- ☑ show 99 % confidence interval
- ☑ show 95 % confidence interval
- ☑ show residuals

Update chart outlook

Equation of the lines:

f(year) = Q*(year-firstDataYear) + B

FirstDataYear= 1981

Point values for the chart

Year	Data	Sen's estin	99 % conf. m	99 % conf. m	95 % conf. m	95 % conf. m	Residual
1981	296.80	271.82	296.04	245.70	288.99	251.86	24.98
1982	220.08	271.58	294.40	246.61	287.83	252.54	-51.50
1983	271.40	271.34	292.76	247.51	286.67	253.21	0.06
1984	269.54	271.10	291.12	248.42	285.51	253.88	-1.56
1985	271.47	270.87	289.48	249.32	284.35	254.56	0.60
1986	250.38	270.63	287.83	250.23	283.19	255.23	-20.25
1987	214.97	270.39	286.19	251.13	282.02	255.90	-55.42
1988	351.89	270.15	284.55	252.04	280.86	256.58	81.74
1989	282.15	269.91	282.91	252.95	279.70	257.25	12.24
1990	277.80	269.67	281.27	253.85	278.54	257.92	8.13
1991	253.90	269.43	279.63	254.76	277.38	258.59	-15.53
1992	244.08	269.19	277.99	255.66	276.22	259.27	-25.11
1993	278.24	268.95	276.35	256.57	275.06	259.94	9.29
1994	348.80	268.71	274.71	257.47	273.90	260.61	80.09
1995	284.05	268.47	273.07	258.38	272.74	261.29	15.58
1996	257.14	268.24	271.43	259.28	271.58	261.96	-11.10
1997	263.13	268.00	269.79	260.19	270.42	262.63	-4.87
1998	292.41	267.76	268.15	261.09	269.26	263.30	24.65
1999	268.84	267.52	266.51	262.00	268.10	263.98	1.32
2000	251.70	267.28	264.87	262.91	266.94	264.65	-15.58
2001	255.65	267.04	263.23	263.81	265.78	265.32	-11.39
2002	134.10	266.80	261.59	264.72	264.62	266.00	-132.70
2003	293.42	266.56	259.95	265.62	263.45	266.67	26.86
2004	212.58	266.32	258.31	266.53	262.29	267.34	-53.74
2005	315.40	266.08	256.67	267.43	261.13	268.01	49.32
2006	263.38	265.85	255.03	268.34	259.97	268.69	-2.47
2007	272.28	265.61	253.39	269.24	258.81	269.36	6.67
2008	224.95	265.37	251.75	270.15	257.65	270.03	-40.42
2009	261.03	265.13	250.11	271.05	256.49	270.71	-4.10
2010	272.51	264.89	248.47	271.96	255.33	271.38	7.62
2011	249.11	264.65	246.83	272.86	254.17	272.05	-15.54
2012	243.88	264.41	245.19	273.77	253.01	272.72	-20.53
2013	301.62	264.17	243.55	274.68	251.85	273.40	37.45
2014	275.43	263.93	241.91	275.58	250.69	274.07	11.50
2015	233.11	263.69	240.27	276.49	249.53	274.74	-30.58
2016	296.18	263.45	238.63	277.39	248.37	275.42	32.73
2017	275.59	263.22	236.99	278.30	247.21	276.09	12.37
2018	262.92	262.98	235.35	279.20	246.04	276.76	-0.06
2019	274.99	262.74	233.71	280.11	244.88	277.43	12.25
2020	140.33	262.50	232.07	281.01	243.72	278.11	-122.17

FIGURE

August

< Previous Time Series | Next Time Series >

TsNumber	1
Name	Rainfall in mm
Years	1981 - 2020
n	40
Test S	
Test Z	-0.50
Signific.	
Q	-2.39E-01
Qmin99	-1.64E+00
Qmax99	9.05E-01
Qmin95	-1.16E+00
Qmax95	6.73E-01
B	2.72E+02
Bmin99	2.96E+02
Bmax99	2.46E+02
Bmin95	2.89E+02
Bmax95	2.52E+02

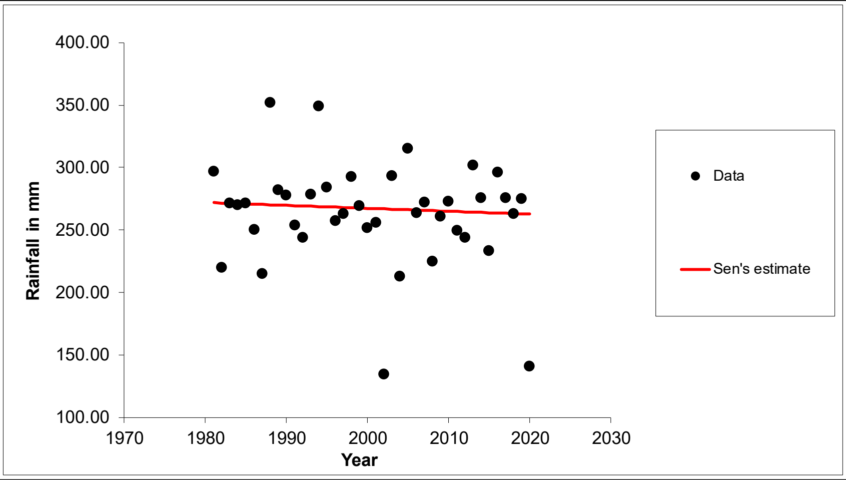

Chart options

- [x] show 99 % confidence interval
- [x] show 95 % confidence interval
- [x] show residuals

Update chart outlook

Equation of the lines:
f(year) = Q*(year-firstDataYear) + B
FirstDataYear= 1981

Point values for the chart

Year	Data	Sen's estin	99 % conf. m	99 % conf. m	95 % conf. m	95 % conf. m	Residual
1981	296.80	271.82	296.04	245.70	288.99	251.86	24.98
1982	220.08	271.58	294.40	246.61	287.83	252.54	-51.50
1983	271.40	271.34	292.76	247.51	286.67	253.21	0.06
1984	269.54	271.10	291.12	248.42	285.51	253.88	-1.56
1985	271.47	270.87	289.48	249.32	284.35	254.56	0.60
1986	250.38	270.63	287.83	250.23	283.19	255.23	-20.25
1987	214.97	270.39	286.19	251.13	282.02	255.90	-55.42
1988	351.89	270.15	284.55	252.04	280.86	256.58	81.74
1989	282.15	269.91	282.91	252.95	279.70	257.25	12.24
1990	277.80	269.67	281.27	253.85	278.54	257.92	8.13
1991	253.90	269.43	279.63	254.76	277.38	258.59	-15.53
1992	244.08	269.19	277.99	255.66	276.22	259.27	-25.11
1993	278.24	268.95	276.35	256.57	275.06	259.94	9.29
1994	348.80	268.71	274.71	257.47	273.90	260.61	80.09
1995	284.05	268.47	273.07	258.38	272.74	261.29	15.58
1996	257.14	268.24	271.43	259.28	271.58	261.96	-11.10
1997	263.13	268.00	269.79	260.19	270.42	262.63	-4.87
1998	292.41	267.76	268.15	261.09	269.26	263.30	24.65
1999	268.84	267.52	266.51	262.00	268.10	263.98	1.32
2000	251.70	267.28	264.87	262.91	266.94	264.65	-15.58
2001	255.65	267.04	263.23	263.81	265.78	265.32	-11.39
2002	134.10	266.80	261.59	264.72	264.62	266.00	-132.70
2003	293.42	266.56	259.95	265.62	263.45	266.67	26.86
2004	212.58	266.32	258.31	266.53	262.29	267.34	-53.74
2005	315.40	266.08	256.67	267.43	261.13	268.01	49.32
2006	263.38	265.85	255.03	268.34	259.97	268.69	-2.47
2007	272.28	265.61	253.39	269.24	258.81	269.36	6.67
2008	224.95	265.37	251.75	270.15	257.65	270.03	-40.42
2009	261.03	265.13	250.11	271.05	256.49	270.71	-4.10
2010	272.51	264.89	248.47	271.96	255.33	271.38	7.62
2011	249.11	264.65	246.83	272.86	254.17	272.05	-15.54
2012	243.88	264.41	245.19	273.77	253.01	272.72	-20.53
2013	301.62	264.17	243.55	274.68	251.85	273.40	37.45
2014	275.43	263.93	241.91	275.58	250.69	274.07	11.50
2015	233.11	263.69	240.27	276.49	249.53	274.74	-30.58
2016	296.18	263.45	238.63	277.39	248.37	275.42	32.73
2017	275.59	263.22	236.99	278.30	247.21	276.09	12.37
2018	262.92	262.98	235.35	279.20	246.04	276.76	-0.06
2019	274.99	262.74	233.71	280.11	244.88	277.43	12.25
2020	140.33	262.50	232.07	281.01	243.72	278.11	-122.17

FIGURE

September

< Previous Time Series | Next Time Series >

TsNumber	1
Name	Rainfall in mm
Years	1981 - 2020
n	40
Test S	
Test Z	1.60
Signific.	
Q	1.67E+00
Qmin99	-1.37E+00
Qmax99	5.22E+00
Qmin95	-4.52E-01
Qmax95	4.19E+00
B	4.86E+01
Bmin99	1.04E+02
Bmax99	2.39E+00
Bmin95	8.94E+01
Bmax95	6.00E+00

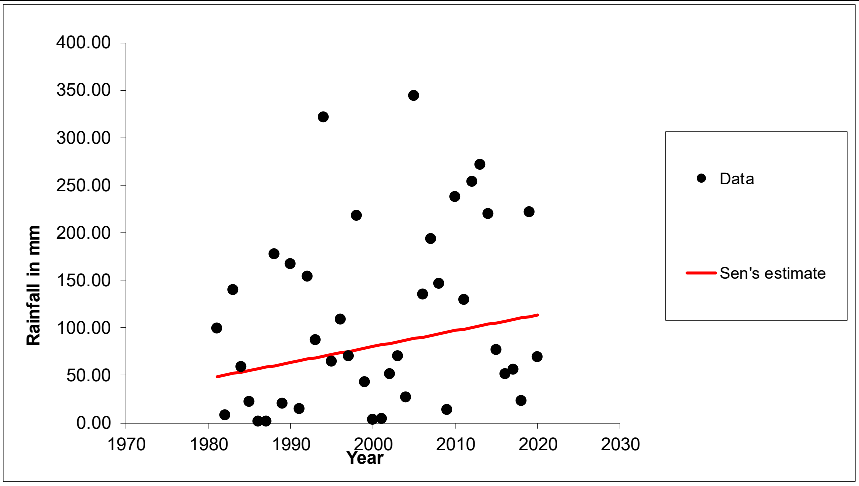

Chart options

- [x] show 99 % confidence interval
- [x] show 95 % confidence interval
- [x] show residuals

Update chart outlook

Equation of the lines:

f(year) = Q*(year-firstDataYear) + B

FirstDataYear= 1981

Point values for the chart

Year	Data	Sen's estin	99 % conf. m	99 % conf. m	95 % conf. m	95 % conf. m	Residual
1981	99.14	48.61	104.31	2.39	89.38	6.00	50.53
1982	8.40	50.28	102.94	7.61	88.93	10.20	-41.88
1983	139.74	51.95	101.57	12.82	88.48	14.39	87.79
1984	58.67	53.62	100.21	18.04	88.03	18.59	5.05
1985	22.46	55.29	98.84	23.25	87.58	22.78	-32.83
1986	1.13	56.96	97.47	28.47	87.12	26.98	-55.83
1987	1.54	58.64	96.11	33.68	86.67	31.17	-57.10
1988	177.26	60.31	94.74	38.90	86.22	35.37	116.95
1989	20.32	61.98	93.37	44.12	85.77	39.56	-41.66
1990	167.28	63.65	92.01	49.33	85.32	43.76	103.63
1991	14.81	65.32	90.64	54.55	84.86	47.95	-50.51
1992	153.65	66.99	89.27	59.76	84.41	52.14	86.66
1993	87.12	68.66	87.91	64.98	83.96	56.34	18.46
1994	321.47	70.33	86.54	70.19	83.51	60.53	251.14
1995	65.05	72.01	85.17	75.41	83.06	64.73	-6.96
1996	108.39	73.68	83.81	80.63	82.61	68.92	34.71
1997	70.30	75.35	82.44	85.84	82.15	73.12	-5.05
1998	217.85	77.02	81.08	91.06	81.70	77.31	140.83
1999	42.73	78.69	79.71	96.27	81.25	81.51	-35.96
2000	3.75	80.36	78.34	101.49	80.80	85.70	-76.61
2001	3.99	82.03	76.98	106.70	80.35	89.90	-78.04
2002	50.94	83.71	75.61	111.92	79.89	94.09	-32.77
2003	69.92	85.38	74.24	117.14	79.44	98.29	-15.46
2004	27.06	87.05	72.88	122.35	78.99	102.48	-59.99
2005	344.02	88.72	71.51	127.57	78.54	106.68	255.30
2006	134.79	90.39	70.14	132.78	78.09	110.87	44.40
2007	193.86	92.06	68.78	138.00	77.63	115.07	101.80
2008	146.49	93.73	67.41	143.21	77.18	119.26	52.76
2009	14.12	95.40	66.04	148.43	76.73	123.46	-81.28
2010	238.22	97.08	64.68	153.64	76.28	127.65	141.14
2011	129.84	98.75	63.31	158.86	75.83	131.85	31.09
2012	253.82	100.42	61.94	164.08	75.38	136.04	153.40
2013	271.89	102.09	60.58	169.29	74.92	140.24	169.80
2014	220.28	103.76	59.21	174.51	74.47	144.43	116.52
2015	76.42	105.43	57.85	179.72	74.02	148.63	-29.01
2016	51.15	107.10	56.48	184.94	73.57	152.82	-55.95
2017	55.90	108.77	55.11	190.15	73.12	157.02	-52.87
2018	23.61	110.45	53.75	195.37	72.66	161.21	-86.84
2019	221.89	112.12	52.38	200.59	72.21	165.41	109.77
2020	69.36	113.79	51.01	205.80	71.76	169.60	-44.43

FIGURE

October

< Previous Time Series | Next Time Series >

TsNumber	1
Name	Rainfall in mm
Years	1981 - 2020
n	40
Test S	
Test Z	-0.34
Signific.	
Q	-5.83E-03
Qmin99	-3.78E-01
Qmax99	8.74E-02
Qmin95	-2.24E-01
Qmax95	3.96E-02
B	2.00E+00
Bmin99	1.30E+01
Bmax99	7.08E-01
Bmin95	7.87E+00
Bmax95	1.04E+00

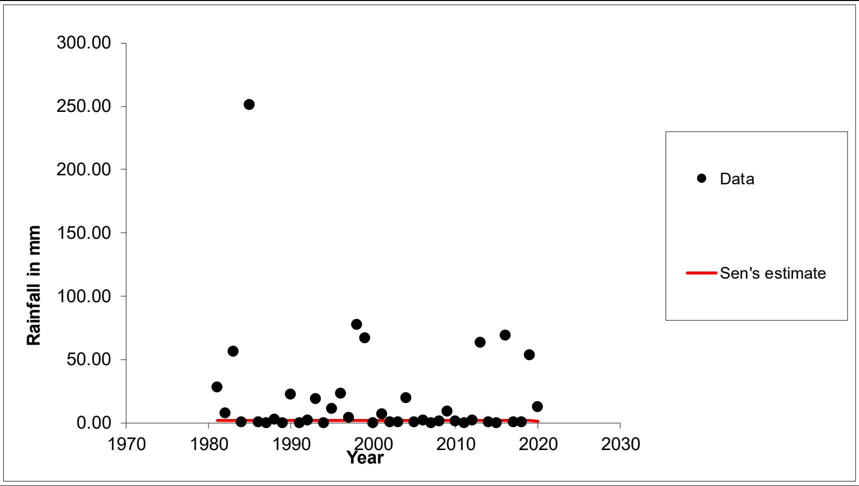

Chart options

- ☑ show 99 % confidence interval
- ☑ show 95 % confidence interval
- ☑ show residuals

Update chart outlook

Equation of the lines:

f(year) = Q*(year-firstDataYear) + B

FirstDataYear= 1981

Point values for the chart

Year	Data	Sen's estin	99 % conf. n	99 % conf. n	95 % conf. n	95 % conf. n	Residual
1981	28.31	2.00	12.96	0.71	7.87	1.04	26.31
1982	7.56	1.99	12.58	0.80	7.64	1.08	5.57
1983	56.34	1.99	12.21	0.88	7.42	1.12	54.35
1984	0.75	1.98	11.83	0.97	7.20	1.16	-1.23
1985	250.83	1.97	11.45	1.06	6.97	1.20	248.86
1986	0.12	1.97	11.07	1.15	6.75	1.24	-1.85
1987	0.00	1.96	10.69	1.23	6.52	1.28	-1.96
1988	2.41	1.96	10.31	1.32	6.30	1.32	0.45
1989	0.01	1.95	9.94	1.41	6.07	1.36	-1.94
1990	22.12	1.95	9.56	1.49	5.85	1.40	20.18
1991	0.00	1.94	9.18	1.58	5.63	1.44	-1.94
1992	1.89	1.93	8.80	1.67	5.40	1.48	-0.04
1993	18.60	1.93	8.42	1.76	5.18	1.52	16.67
1994	0.00	1.92	8.05	1.84	4.95	1.56	-1.92
1995	10.79	1.92	7.67	1.93	4.73	1.60	8.87
1996	23.06	1.91	7.29	2.02	4.50	1.64	21.15
1997	3.72	1.90	6.91	2.11	4.28	1.68	1.82
1998	77.44	1.90	6.53	2.19	4.06	1.72	75.54
1999	67.13	1.89	6.16	2.28	3.83	1.76	65.24
2000	0.05	1.89	5.78	2.37	3.61	1.80	-1.84
2001	6.67	1.88	5.40	2.46	3.38	1.84	4.79
2002	0.19	1.88	5.02	2.54	3.16	1.88	-1.69
2003	0.15	1.87	4.64	2.63	2.93	1.91	-1.72
2004	19.53	1.86	4.27	2.72	2.71	1.95	17.67
2005	0.25	1.86	3.89	2.81	2.48	1.99	-1.61
2006	1.51	1.85	3.51	2.89	2.26	2.03	-0.34
2007	0.02	1.85	3.13	2.98	2.04	2.07	-1.83
2008	0.99	1.84	2.75	3.07	1.81	2.11	-0.85
2009	8.70	1.83	2.37	3.16	1.59	2.15	6.87
2010	1.02	1.83	2.00	3.24	1.36	2.19	-0.81
2011	0.00	1.82	1.62	3.33	1.14	2.23	-1.82
2012	1.86	1.82	1.24	3.42	0.91	2.27	0.04
2013	63.19	1.81	0.86	3.51	0.69	2.31	61.38
2014	0.55	1.81	0.48	3.59	0.47	2.35	-1.26
2015	0.04	1.80	0.11	3.68	0.24	2.39	-1.76
2016	68.57	1.79	-0.27	3.77	0.02	2.43	66.78
2017	0.34	1.79	-0.65	3.86	-0.21	2.47	-1.45
2018	0.30	1.78	-1.03	3.94	-0.43	2.51	-1.48
2019	53.46	1.78	-1.41	4.03	-0.66	2.55	51.68
2020	12.55	1.77	-1.78	4.12	-0.88	2.59	10.78

FIGURE

November

< Previous Time Series | Next Time Series >

TsNumber	1
Name	Rainfall in mm
Years	1981 - 2020
n	40
Test S	
Test Z	-0.38
Signific.	
Q	0.00E+00
Qmin99	0.00E+00
Qmax99	0.00E+00
Qmin95	0.00E+00
Qmax95	0.00E+00
B	0.00E+00
Bmin99	0.00E+00
Bmax99	0.00E+00
Bmin95	0.00E+00
Bmax95	0.00E+00

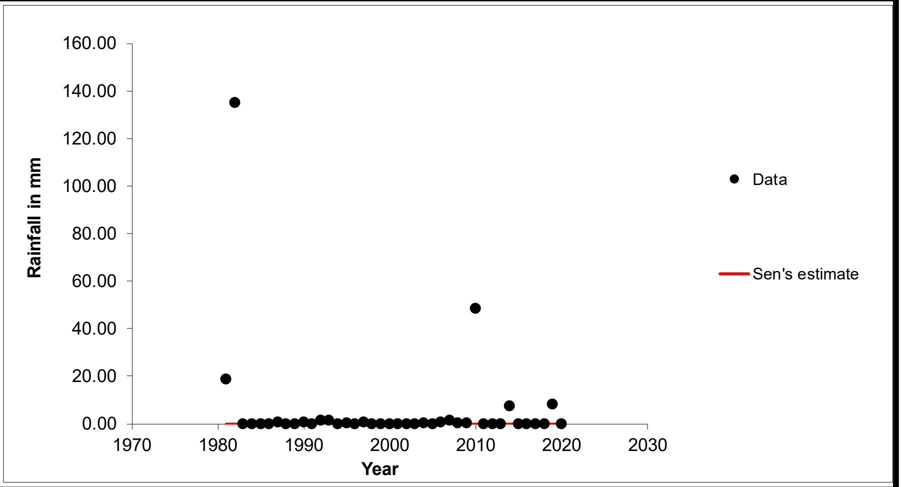

Chart options

- ☑ show 99 % confidence interval
- ☑ show 95 % confidence interval
- ☑ show residuals

Update chart outlook

Equation of the lines:

f(year) = Q*(year-firstDataYear) + B

FirstDataYear= 1981

Point values for the chart

Year	Data	Sen's estin	99 % conf. m	99 % conf. m	95 % conf. m	95 % conf. m	Residual
1981	18.77	0.00	0.00	0.00	0.00	0.00	18.77
1982	135.13	0.00	0.00	0.00	0.00	0.00	135.13
1983	0.00	0.00	0.00	0.00	0.00	0.00	0.00
1984	0.00	0.00	0.00	0.00	0.00	0.00	0.00
1985	0.00	0.00	0.00	0.00	0.00	0.00	0.00
1986	0.00	0.00	0.00	0.00	0.00	0.00	0.00
1987	0.50	0.00	0.00	0.00	0.00	0.00	0.50
1988	0.00	0.00	0.00	0.00	0.00	0.00	0.00
1989	0.00	0.00	0.00	0.00	0.00	0.00	0.00
1990	0.46	0.00	0.00	0.00	0.00	0.00	0.46
1991	0.00	0.00	0.00	0.00	0.00	0.00	0.00
1992	1.25	0.00	0.00	0.00	0.00	0.00	1.25
1993	1.32	0.00	0.00	0.00	0.00	0.00	1.32
1994	0.00	0.00	0.00	0.00	0.00	0.00	0.00
1995	0.07	0.00	0.00	0.00	0.00	0.00	0.07
1996	0.00	0.00	0.00	0.00	0.00	0.00	0.00
1997	0.52	0.00	0.00	0.00	0.00	0.00	0.52
1998	0.01	0.00	0.00	0.00	0.00	0.00	0.01
1999	0.00	0.00	0.00	0.00	0.00	0.00	0.00
2000	0.00	0.00	0.00	0.00	0.00	0.00	0.00
2001	0.00	0.00	0.00	0.00	0.00	0.00	0.00
2002	0.00	0.00	0.00	0.00	0.00	0.00	0.00
2003	0.00	0.00	0.00	0.00	0.00	0.00	0.00
2004	0.21	0.00	0.00	0.00	0.00	0.00	0.21
2005	0.00	0.00	0.00	0.00	0.00	0.00	0.00
2006	0.59	0.00	0.00	0.00	0.00	0.00	0.59
2007	1.47	0.00	0.00	0.00	0.00	0.00	1.47
2008	0.07	0.00	0.00	0.00	0.00	0.00	0.07
2009	0.35	0.00	0.00	0.00	0.00	0.00	0.35
2010	48.54	0.00	0.00	0.00	0.00	0.00	48.54
2011	0.00	0.00	0.00	0.00	0.00	0.00	0.00
2012	0.00	0.00	0.00	0.00	0.00	0.00	0.00
2013	0.00	0.00	0.00	0.00	0.00	0.00	0.00
2014	7.32	0.00	0.00	0.00	0.00	0.00	7.32
2015	0.00	0.00	0.00	0.00	0.00	0.00	0.00
2016	0.00	0.00	0.00	0.00	0.00	0.00	0.00
2017	0.00	0.00	0.00	0.00	0.00	0.00	0.00
2018	0.00	0.00	0.00	0.00	0.00	0.00	0.00
2019	8.03	0.00	0.00	0.00	0.00	0.00	8.03
2020	0.00	0.00	0.00	0.00	0.00	0.00	0.00

FIGURE

December

< Previous Time Series | Next Time Series >

TsNumber	1
Name	Rainfall in mm
Years	1981 - 2020
n	40
Test S	
Test Z	0.81
Signific.	
Q	0.00E+00
Qmin99	0.00E+00
Qmax99	3.06E-06
Qmin95	0.00E+00
Qmax95	0.00E+00
B	0.00E+00
Bmin99	0.00E+00
Bmax99	-1.07E-05
Bmin95	0.00E+00
Bmax95	0.00E+00

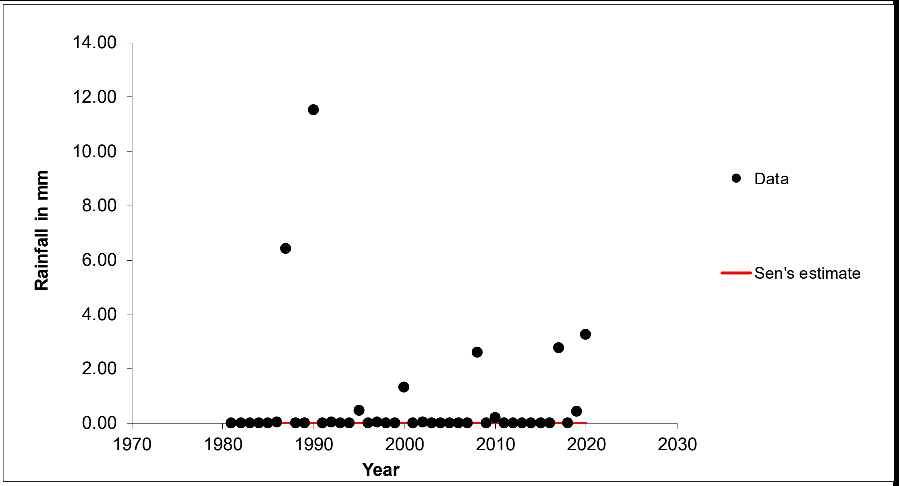

Chart options

☑ show 99 % confidence interval

☑ show 95 % confidence interval

☑ show residuals

Update chart outlook

Equation of the lines:

f(year) = Q*(year-firstDataYear) + B

FirstDataYear= 1981

Point values for the chart

Year	Data	Sen's estin	99 % conf. m	99 % conf. m	95 % conf. m	95 % conf. m	Residual
1981	0.00	0.00	0.00	0.00	0.00	0.00	0.00
1982	0.00	0.00	0.00	0.00	0.00	0.00	0.00
1983	0.00	0.00	0.00	0.00	0.00	0.00	0.00
1984	0.00	0.00	0.00	0.00	0.00	0.00	0.00
1985	0.00	0.00	0.00	0.00	0.00	0.00	0.00
1986	0.01	0.00	0.00	0.00	0.00	0.00	0.01
1987	6.42	0.00	0.00	0.00	0.00	0.00	6.42
1988	0.00	0.00	0.00	0.00	0.00	0.00	0.00
1989	0.00	0.00	0.00	0.00	0.00	0.00	0.00
1990	11.51	0.00	0.00	0.00	0.00	0.00	11.51
1991	0.00	0.00	0.00	0.00	0.00	0.00	0.00
1992	0.01	0.00	0.00	0.00	0.00	0.00	0.01
1993	0.00	0.00	0.00	0.00	0.00	0.00	0.00
1994	0.00	0.00	0.00	0.00	0.00	0.00	0.00
1995	0.45	0.00	0.00	0.00	0.00	0.00	0.45
1996	0.00	0.00	0.00	0.00	0.00	0.00	0.00
1997	0.01	0.00	0.00	0.00	0.00	0.00	0.01
1998	0.00	0.00	0.00	0.00	0.00	0.00	0.00
1999	0.00	0.00	0.00	0.00	0.00	0.00	0.00
2000	1.30	0.00	0.00	0.00	0.00	0.00	1.30
2001	0.00	0.00	0.00	0.00	0.00	0.00	0.00
2002	0.01	0.00	0.00	0.00	0.00	0.00	0.01
2003	0.00	0.00	0.00	0.00	0.00	0.00	0.00
2004	0.00	0.00	0.00	0.00	0.00	0.00	0.00
2005	0.00	0.00	0.00	0.00	0.00	0.00	0.00
2006	0.00	0.00	0.00	0.00	0.00	0.00	0.00
2007	0.00	0.00	0.00	0.00	0.00	0.00	0.00
2008	2.60	0.00	0.00	0.00	0.00	0.00	2.60
2009	0.00	0.00	0.00	0.00	0.00	0.00	0.00
2010	0.19	0.00	0.00	0.00	0.00	0.00	0.19
2011	0.00	0.00	0.00	0.00	0.00	0.00	0.00
2012	0.00	0.00	0.00	0.00	0.00	0.00	0.00
2013	0.00	0.00	0.00	0.00	0.00	0.00	0.00
2014	0.00	0.00	0.00	0.00	0.00	0.00	0.00
2015	0.00	0.00	0.00	0.00	0.00	0.00	0.00
2016	0.00	0.00	0.00	0.00	0.00	0.00	0.00
2017	2.77	0.00	0.00	0.00	0.00	0.00	2.77
2018	0.00	0.00	0.00	0.00	0.00	0.00	0.00
2019	0.41	0.00	0.00	0.00	0.00	0.00	0.41
2020	3.26	0.00	0.00	0.00	0.00	0.00	3.26

Temperature Trend Analysis

FIGURE

< Previous Time Series | Next Time Series >

AHMEDABAD April Max temp

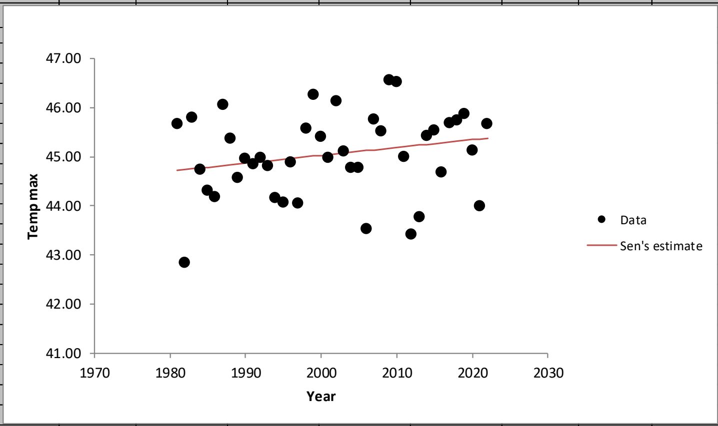

TsNumber	1
Name	Temp max
Years	1981 - 2022
n	42
Test S	
Test Z	1.21
Signific.	
Q	1.60E-02
Qmin99	-1.67E-02
Qmax99	4.14E-02
Qmin95	-9.06E-03
Qmax95	3.33E-02
B	4.47E+01
Bmin99	4.54E+01
Bmax99	4.42E+01
Bmin95	4.52E+01
Bmax95	4.44E+01

Chart options

- [ ] show 99 % confidence interval
- [ ] show 95 % confidence interval
- [ ] show residuals

Update chart outlook

Equation of the lines:

f(year) = Q*(year-firstDataYear) + B

FirstDataYear= 1981

Point values for the chart

Year	Data	Sen's estim	99 % conf. m	99 % conf. m	95 % conf. m	95 % conf. m	Residual
1981	45.66	44.72	45.39	44.20	45.21	44.40	0.94
1982	42.83	44.74	45.37	44.24	45.20	44.43	-1.91
1983	45.80	44.76	45.36	44.28	45.19	44.46	1.04
1984	44.73	44.77	45.34	44.32	45.18	44.50	-0.04
1985	44.31	44.79	45.32	44.37	45.17	44.53	-0.48
1986	44.18	44.80	45.31	44.41	45.16	44.56	-0.62
1987	46.06	44.82	45.29	44.45	45.15	44.60	1.24
1988	45.36	44.84	45.27	44.49	45.14	44.63	0.52
1989	44.57	44.85	45.26	44.53	45.13	44.66	-0.28
1990	44.95	44.87	45.24	44.57	45.13	44.70	0.08
1991	44.85	44.88	45.22	44.61	45.12	44.73	-0.03
1992	44.98	44.90	45.21	44.66	45.11	44.76	0.08
1993	44.80	44.92	45.19	44.70	45.10	44.80	-0.12
1994	44.16	44.93	45.17	44.74	45.09	44.83	-0.77
1995	44.06	44.948	45.1566667	44.7795231	45.079689	44.8616667	-0.888
1996	44.89	44.964	45.14	44.8208882	45.0706263	44.895	-0.074
1997	44.05	44.98	45.1233333	44.8622533	45.0615637	44.9283333	-0.93
1998	45.57	44.996	45.1066667	44.9036185	45.0525011	44.9616667	0.574
1999	46.26	45.012	45.09	44.9449836	45.0434384	44.995	1.248
2000	45.4	45.028	45.0733333	44.9863487	45.0343758	45.0283333	0.372
2001	44.97	45.044	45.0566667	45.0277138	45.0253132	45.0616667	-0.074
2002	46.12	45.06	45.04	45.069079	45.0162505	45.095	1.06
2003	45.11	45.076	45.0233333	45.1104441	45.0071879	45.1283333	0.034
2004	44.77	45.092	45.0066667	45.1518092	44.9981253	45.1616667	-0.322
2005	44.77	45.108	44.99	45.1931744	44.9890626	45.195	-0.338
2006	43.53	45.124	44.9733333	45.2345395	44.98	45.2283333	-1.594
2007	45.76	45.14	44.9566667	45.2759046	44.9709374	45.2616667	0.62
2008	45.52	45.156	44.94	45.3172697	44.9618747	45.295	0.364
2009	46.55	45.172	44.9233333	45.3586349	44.9528121	45.3283333	1.378
2010	46.52	45.188	44.9066667	45.4	44.9437495	45.3616667	1.332
2011	44.99	45.204	44.89	45.4413651	44.9346868	45.395	-0.214
2012	43.42	45.22	44.8733333	45.4827303	44.9256242	45.4283333	-1.8
2013	43.76	45.236	44.8566667	45.5240954	44.9165616	45.4616667	-1.476
2014	45.43	45.252	44.84	45.5654605	44.9074989	45.495	0.178
2015	45.54	45.268	44.8233333	45.6068256	44.8984363	45.5283333	0.272
2016	44.67	45.284	44.8066667	45.6481908	44.8893737	45.5616667	-0.614
2017	45.69	45.3	44.79	45.6895559	44.880311	45.595	0.39
2018	45.73	45.316	44.7733333	45.730921	44.8712484	45.6283333	0.414
2019	45.87	45.332	44.7566667	45.7722862	44.8621858	45.6616667	0.538
2020	45.13	45.348	44.74	45.8136513	44.8531231	45.695	-0.218
2021	43.98	45.364	44.7233333	45.8550164	44.8440605	45.7283333	-1.384
2022	45.66	45.38	44.7066667	45.8963815	44.8349978	45.7616667	0.28

FIGURE

< Previous Time Series | Next Time Series >

AHMEDABAD MAY Tmax

TsNumber	1
Name	Temp max
Years	1981 - 2022
n	42
Test S	
Test Z	0.16
Signific.	
Q	5.00E-03
Qmin99	-4.21E-02
Qmax99	4.95E-02
Qmin95	-3.25E-02
Qmax95	3.91E-02
B	4.63E+01
Bmin99	4.73E+01
Bmax99	4.53E+01
Bmin95	4.71E+01
Bmax95	4.55E+01

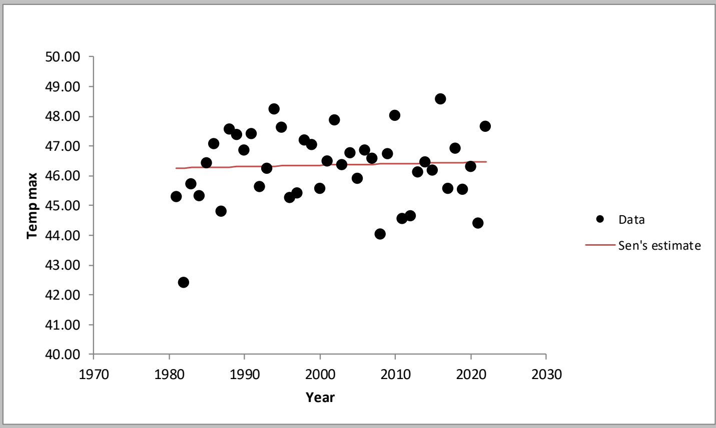

Chart options

- [ ] show 99 % confidence interval
- [ ] show 95 % confidence interval
- [ ] show residuals

Update chart outlook

Equation of the lines:
f(year) = Q*(year-firstDataYear) + B
FirstDataYear= 1981

Point values for the chart

Year	Data	Sen's estin	99 % conf. m	99 % conf. m	95 % conf. m	95 % conf. m	Residual
1981	45.29	46.26	47.31	45.29	47.15	45.53	-0.97
1982	42.40	46.27	47.26	45.34	47.11	45.57	-3.87
1983	45.73	46.27	47.22	45.39	47.08	45.60	-0.54
1984	45.32	46.28	47.18	45.43	47.05	45.64	-0.96
1985	46.41	46.28	47.14	45.48	47.02	45.68	0.13
1986	47.08	46.29	47.10	45.53	46.98	45.72	0.79
1987	44.79	46.29	47.05	45.58	46.95	45.76	-1.50
1988	47.55	46.30	47.01	45.63	46.92	45.80	1.25
1989	47.37	46.30	46.97	45.68	46.89	45.84	1.07
1990	46.84	46.31	46.93	45.73	46.85	45.88	0.53
1991	47.41	46.31	46.89	45.78	46.82	45.92	1.10
1992	45.62	46.32	46.84	45.83	46.79	45.96	-0.70
1993	46.25	46.32	46.80	45.88	46.76	46.00	-0.07
1994	48.22	46.33	46.76	45.93	46.72	46.03	1.89
1995	47.61	46.3325	46.7168588	45.979522	46.6909977	46.073991	1.2775
1996	45.25	46.3375	46.6747646	46.029044	46.6585365	46.1130919	-1.0875
1997	45.4	46.3425	46.6326705	46.0785659	46.6260753	46.1521928	-0.9425
1998	47.19	46.3475	46.5905763	46.1280879	46.5936142	46.1912937	0.8425
1999	47.03	46.3525	46.5484822	46.1776099	46.561153	46.2303946	0.6775
2000	45.58	46.3575	46.506388	46.2271319	46.5286918	46.2694955	-0.7775
2001	46.48	46.3625	46.4642939	46.2766539	46.4962306	46.3085964	0.1175
2002	47.87	46.3675	46.4221997	46.3261758	46.4637694	46.3476973	1.5025
2003	46.36	46.3725	46.3801056	46.3756978	46.4313082	46.3867982	-0.0125
2004	46.76	46.3775	46.3380114	46.4252198	46.398847	46.4258991	0.3825
2005	45.91	46.3825	46.2959173	46.4747418	46.3663858	46.465	-0.4725
2006	46.85	46.3875	46.2538231	46.5242638	46.3339247	46.5041009	0.4625
2007	46.57	46.3925	46.211729	46.5737857	46.3014635	46.5432018	0.1775
2008	44.04	46.3975	46.1696348	46.6233077	46.2690023	46.5823027	-2.3575
2009	46.72	46.4025	46.1275407	46.6728297	46.2365411	46.6214036	0.3175
2010	48.01	46.4075	46.0854465	46.7223517	46.2040799	46.6605045	1.6025
2011	44.55	46.4125	46.0433524	46.7718737	46.1716187	46.6996054	-1.8625
2012	44.63	46.4175	46.0012582	46.8213956	46.1391575	46.7387063	-1.7875
2013	46.12	46.4225	45.9591641	46.8709176	46.1066964	46.7778072	-0.3025
2014	46.44	46.4275	45.9170699	46.9204396	46.0742352	46.8169081	0.0125
2015	46.19	46.4325	45.8749758	46.9699616	46.041774	46.856009	-0.2425
2016	48.58	46.4375	45.8328816	47.0194836	46.0093128	46.8951099	2.1425
2017	45.58	46.4425	45.7907875	47.0690055	45.9768516	46.9342108	-0.8625
2018	46.91	46.4475	45.7486933	47.1185275	45.9443904	46.9733117	0.4625
2019	45.53	46.4525	45.7065992	47.1680495	45.9119292	47.0124126	-0.9225
2020	46.3	46.4575	45.664505	47.2175715	45.8794681	47.0515135	-0.1575
2021	44.4	46.4625	45.6224109	47.2670935	45.8470069	47.0906144	-2.0625
2022	47.65	46.4675	45.5803167	47.3166154	45.8145457	47.1297153	1.1825

FIGURE

< Previous Time Series | Next Time Series >

AHMEDABAD

TsNumber	1
Name	Temp max
Years	1981 - 2022
n	42
Test S	
Test Z	-0.73
Signific.	
Q	-1.76E-02
Qmin99	-7.71E-02
Qmax99	3.57E-02
Qmin95	-6.28E-02
Qmax95	2.40E-02
B	4.51E+01
Bmin99	4.64E+01
Bmax99	4.39E+01
Bmin95	4.61E+01
Bmax95	4.41E+01

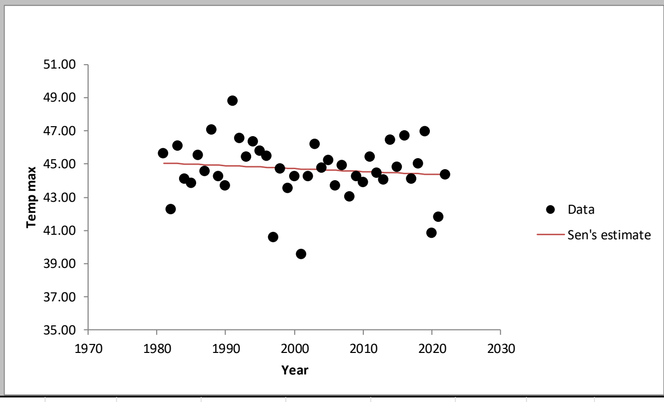

Chart options

- show 99 % confidence interval
- show 95 % confidence interval
- show residuals

Update chart outlook

Equation of the lines:
f(year) = Q*(year-firstDataYear) + B
FirstDataYear= 1981

Point values for the chart

Year	Data	Sen's estin	99 % conf. m	99 % conf. m	95 % conf. m	95 % conf. m	Residual
1981	45.65	45.06	46.39	43.94	46.12	44.07	0.59
1982	42.26	45.04	46.31	43.98	46.06	44.10	-2.78
1983	46.08	45.03	46.23	44.01	46.00	44.12	1.05
1984	44.10	45.01	46.16	44.05	45.93	44.15	-0.91
1985	43.82	44.99	46.08	44.08	45.87	44.17	-1.17
1986	45.52	44.97	46.00	44.12	45.81	44.19	0.55
1987	44.55	44.95	45.92	44.16	45.74	44.22	-0.40
1988	47.06	44.94	45.85	44.19	45.68	44.24	2.12
1989	44.24	44.92	45.77	44.23	45.62	44.27	-0.68
1990	43.69	44.90	45.69	44.26	45.56	44.29	-1.21
1991	48.78	44.88	45.62	44.30	45.49	44.31	3.90
1992	46.54	44.87	45.54	44.33	45.43	44.34	1.67
1993	45.43	44.85	45.46	44.37	45.37	44.36	0.58
1994	46.33	44.83	45.38	44.41	45.31	44.39	1.50
1995	45.77	44.814	45.3077911	44.4413943	45.2423665	44.410926	0.956
1996	45.45	44.7964	45.2306592	44.4771314	45.1795707	44.4349347	0.6536
1997	40.58	44.7788	45.1535274	44.5128686	45.1167749	44.4589434	-4.1988
1998	44.73	44.7612	45.0763955	44.5486057	45.0539791	44.4829521	-0.0312
1999	43.56	44.7436	44.9992637	44.5843429	44.9911832	44.5069608	-1.1836
2000	44.24	44.726	44.9221318	44.62008	44.9283874	44.5309695	-0.486
2001	39.54	44.7084	44.845	44.6558172	44.8655916	44.5549782	-5.1684
2002	44.26	44.6908	44.7678682	44.6915543	44.8027958	44.5789869	-0.4308
2003	46.2	44.6732	44.6907363	44.7272915	44.74	44.6029956	1.5268
2004	44.75	44.6556	44.6136045	44.7630286	44.6772042	44.6270044	0.0944
2005	45.2	44.638	44.5364726	44.7987658	44.6144084	44.6510131	0.562
2006	43.69	44.6204	44.4593408	44.8345029	44.5516126	44.6750218	-0.9304
2007	44.9	44.6028	44.3822089	44.8702401	44.4888168	44.6990305	0.2972
2008	43.04	44.5852	44.3050771	44.9059772	44.4260209	44.7230392	-1.5452
2009	44.26	44.5676	44.2279452	44.9417144	44.3632251	44.7470479	-0.3076
2010	43.89	44.55	44.1508134	44.9774515	44.3004293	44.7710566	-0.66
2011	45.44	44.5324	44.0736815	45.0131887	44.2376335	44.7950653	0.9076
2012	44.47	44.5148	43.9965497	45.0489258	44.1748377	44.819074	-0.0448
2013	44.05	44.4972	43.9194178	45.084663	44.1120419	44.8430827	-0.4472
2014	46.42	44.4796	43.842286	45.1204001	44.0492461	44.8670914	1.9404
2015	44.81	44.462	43.7651542	45.1561373	43.9864503	44.8911001	0.348
2016	46.69	44.4444	43.6880223	45.1918744	43.9236545	44.9151088	2.2456
2017	44.08	44.4268	43.6108905	45.2276116	43.8608586	44.9391175	-0.3468
2018	44.99	44.4092	43.5337586	45.2633487	43.7980628	44.9631262	0.5808
2019	46.95	44.3916	43.4566268	45.2990859	43.735267	44.9871349	2.5584
2020	40.83	44.374	43.3794949	45.334823	43.6724712	45.0111436	-3.544
2021	41.8	44.3564	43.3023631	45.3705602	43.6096754	45.0351523	-2.5564
2022	44.37	44.3388	43.2252312	45.4062973	43.5468796	45.059161	0.0312

FIGURE

< Previous Time Series | Next Time Series >

Ahmedabad Dec Tmin

TsNumber	1
Name	TMIN
Years	1981 - 2020
n	40
Test S	
Test Z	-0.50
Signific.	
Q	-1.55E-02
Qmin99	-1.02E-01
Qmax99	6.91E-02
Qmin95	-8.12E-02
Qmax95	4.46E-02
B	1.01E+01
Bmin99	1.13E+01
Bmax99	8.60E+00
Bmin95	1.07E+01
Bmax95	8.80E+00

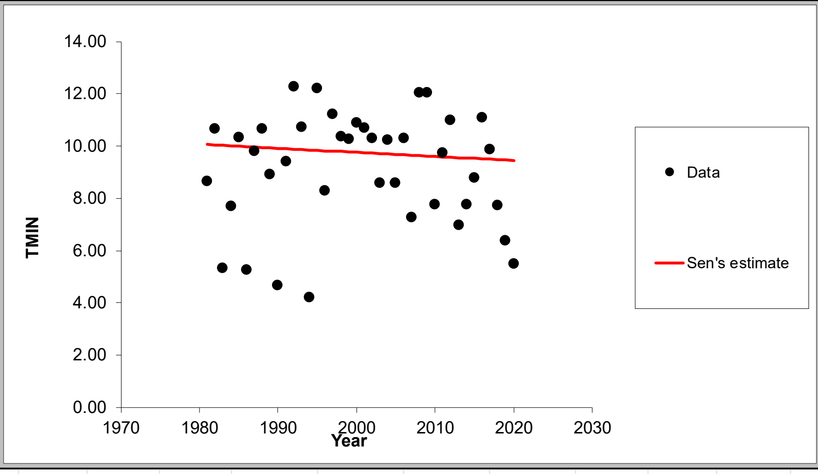

Chart options

- [x] show 99 % confidence interval
- [x] show 95 % confidence interval
- [x] show residuals

Update chart outlook

Equation of the lines:
f(year) = Q*(year-firstDataYear) + B
FirstDataYear= 1981

Point values for the chart

Year	Data	Sen's estin	99 % conf. m	99 % conf. m	95 % conf. m	95 % conf. m	Residual
1981	8.64	10.05	11.26	8.60	10.73	8.80	-1.41
1982	10.65	10.04	11.16	8.67	10.65	8.84	0.61
1983	5.33	10.02	11.06	8.74	10.57	8.89	-4.69
1984	7.69	10.01	10.95	8.81	10.49	8.93	-2.32
1985	10.34	9.99	10.85	8.88	10.41	8.98	0.35
1986	5.26	9.98	10.75	8.95	10.33	9.02	-4.72
1987	9.80	9.96	10.65	9.02	10.25	9.06	-0.16
1988	10.67	9.95	10.55	9.09	10.16	9.11	0.72
1989	8.93	9.93	10.44	9.15	10.08	9.15	-1.00
1990	4.67	9.91	10.34	9.22	10.00	9.20	-5.24
1991	9.40	9.90	10.24	9.29	9.92	9.24	-0.50
1992	12.29	9.88	10.14	9.36	9.84	9.29	2.41
1993	10.73	9.87	10.04	9.43	9.76	9.33	0.86
1994	4.21	9.85	9.93	9.50	9.68	9.38	-5.64
1995	12.20	9.84	9.83	9.57	9.60	9.42	2.36
1996	8.29	9.82	9.73	9.64	9.51	9.47	-1.53
1997	11.22	9.81	9.63	9.71	9.43	9.51	1.41
1998	10.38	9.79	9.53	9.78	9.35	9.55	0.59
1999	10.26	9.78	9.42	9.85	9.27	9.60	0.49
2000	10.90	9.76	9.32	9.91	9.19	9.64	1.14
2001	10.69	9.74	9.22	9.98	9.11	9.69	0.95
2002	10.29	9.73	9.12	10.05	9.03	9.73	0.56
2003	8.60	9.71	9.02	10.12	8.95	9.78	-1.11
2004	10.22	9.70	8.91	10.19	8.87	9.82	0.52
2005	8.59	9.68	8.81	10.26	8.78	9.87	-1.09
2006	10.30	9.67	8.71	10.33	8.70	9.91	0.63
2007	7.26	9.65	8.61	10.40	8.62	9.96	-2.39
2008	12.05	9.64	8.51	10.47	8.54	10.00	2.41
2009	12.05	9.62	8.40	10.54	8.46	10.05	2.43
2010	7.77	9.60	8.30	10.61	8.38	10.09	-1.83
2011	9.75	9.59	8.20	10.67	8.30	10.13	0.16
2012	10.98	9.57	8.10	10.74	8.22	10.18	1.41
2013	6.97	9.56	8.00	10.81	8.13	10.22	-2.59
2014	7.77	9.54	7.89	10.88	8.05	10.27	-1.77
2015	8.78	9.53	7.79	10.95	7.97	10.31	-0.75
2016	11.08	9.51	7.69	11.02	7.89	10.36	1.57
2017	9.87	9.50	7.59	11.09	7.81	10.40	0.37
2018	7.73	9.48	7.49	11.16	7.73	10.45	-1.75
2019	6.38	9.47	7.38	11.23	7.65	10.49	-3.09
2020	5.49	9.45	7.28	11.30	7.57	10.54	-3.96

FIGURE

< Previous Time Series | Next Time Series >

Jan Tmin

TsNumber	1
Name	TMIN
Years	1981 - 2020
n	40
Test S	
Test Z	0.07
Signific.	
Q	2.33E-03
Qmin99	-4.92E-02
Qmax99	5.88E-02
Qmin95	-3.70E-02
Qmax95	4.62E-02
B	7.82E+00
Bmin99	8.93E+00
Bmax99	6.93E+00
Bmin95	8.58E+00
Bmax95	7.15E+00

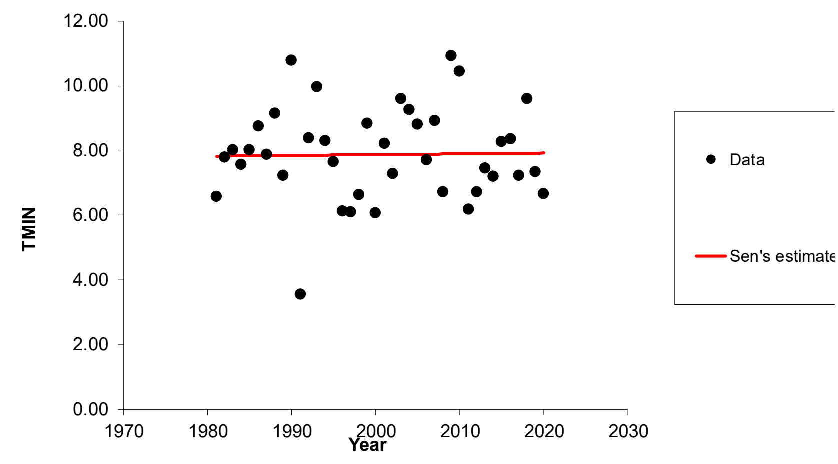

Chart options

- [x] show 99 % confidence interval
- [x] show 95 % confidence interval
- [x] show residuals

Update chart outlook

Equation of the lines:
f(year) = Q*(year-firstDataYear) + B
FirstDataYear= 1981

Point values for the chart

Year	Data	Sen's estin	99 % conf. n	99 % conf. n	95 % conf. n	95 % conf. n	Residual
1981	6.56	7.82	8.93	6.93	8.58	7.15	-1.26
1982	7.79	7.82	8.88	6.99	8.55	7.19	-0.03
1983	8.01	7.83	8.83	7.05	8.51	7.24	0.18
1984	7.55	7.83	8.78	7.11	8.47	7.28	-0.28
1985	8.01	7.83	8.73	7.17	8.43	7.33	0.18
1986	8.73	7.83	8.68	7.22	8.40	7.38	0.90
1987	7.87	7.84	8.63	7.28	8.36	7.42	0.03
1988	9.13	7.84	8.58	7.34	8.32	7.47	1.29
1989	7.23	7.84	8.53	7.40	8.29	7.51	-0.61
1990	10.77	7.84	8.48	7.46	8.25	7.56	2.93
1991	3.54	7.85	8.43	7.52	8.21	7.61	-4.31
1992	8.38	7.85	8.38	7.58	8.18	7.65	0.53
1993	9.95	7.85	8.34	7.64	8.14	7.70	2.10
1994	8.30	7.85	8.29	7.69	8.10	7.75	0.45
1995	7.65	7.85	8.24	7.75	8.06	7.79	-0.20
1996	6.12	7.86	8.19	7.81	8.03	7.84	-1.74
1997	6.10	7.86	8.14	7.87	7.99	7.88	-1.76
1998	6.62	7.86	8.09	7.93	7.95	7.93	-1.24
1999	8.84	7.86	8.04	7.99	7.92	7.98	0.98
2000	6.07	7.87	7.99	8.05	7.88	8.02	-1.80
2001	8.21	7.87	7.94	8.11	7.84	8.07	0.34
2002	7.28	7.87	7.89	8.17	7.81	8.11	-0.59
2003	9.58	7.87	7.84	8.22	7.77	8.16	1.71
2004	9.24	7.88	7.79	8.28	7.73	8.21	1.36
2005	8.81	7.88	7.74	8.34	7.69	8.25	0.93
2006	7.70	7.88	7.70	8.40	7.66	8.30	-0.18
2007	8.90	7.88	7.65	8.46	7.62	8.35	1.02
2008	6.70	7.88	7.60	8.52	7.58	8.39	-1.18
2009	10.93	7.89	7.55	8.58	7.55	8.44	3.04
2010	10.44	7.89	7.50	8.64	7.51	8.48	2.55
2011	6.18	7.89	7.45	8.69	7.47	8.53	-1.71
2012	6.70	7.89	7.40	8.75	7.44	8.58	-1.19
2013	7.44	7.90	7.35	8.81	7.40	8.62	-0.46
2014	7.18	7.90	7.30	8.87	7.36	8.67	-0.72
2015	8.26	7.90	7.25	8.93	7.33	8.71	0.36
2016	8.36	7.90	7.20	8.99	7.29	8.76	0.46
2017	7.21	7.91	7.15	9.05	7.25	8.81	-0.70
2018	9.58	7.91	7.10	9.11	7.21	8.85	1.67
2019	7.32	7.91	7.06	9.16	7.18	8.90	-0.59
2020	6.65	7.91	7.01	9.22	7.14	8.95	-1.26

Appendix B

Groundwater recharge trend analysis

FIGURE

< Previous Time Series | Next Time Series >

1981-1990

Groundwater recharge -July

TsNumber	1
Name	Groundwater recharge m3
Years	1 - 10
n	10
Test S	
Test Z	0.27
Signific.	
Q	6.87E-04
Qmin99	-2.02E+00
Qmax99	4.83E+00
Qmin95	-9.05E-03
Qmax95	1.65E+00
B	5.51E-03
Bmin99	1.11E+01
Bmax99	-1.69E+01
Bmin95	5.29E-02
Bmax95	-5.76E+00

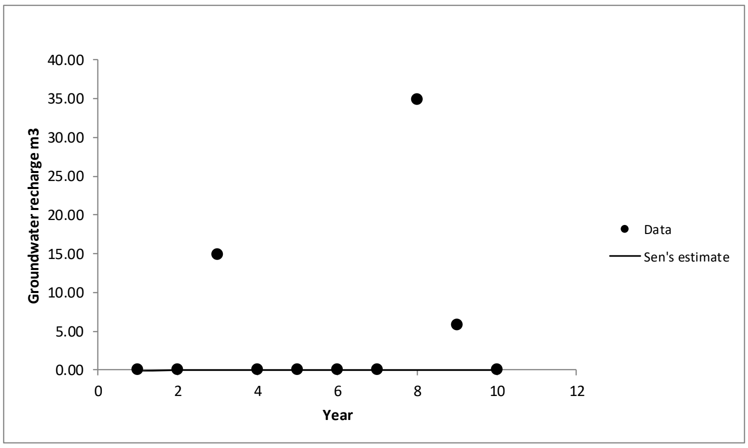

Chart options

show 99 % confidence interval

show 95 % confidence interval

show residuals

Update chart outlook

Equation of the lines:
f(year) = Q*(year-firstDataYear) + B
FirstDataYear= 1

Point values for the chart

Year	Data	Sen's estin	99 % conf. m	99 % conf. m	95 % conf. m	95 % conf. m	Residual
1	0.00	0.01	11.14	-16.88	0.05	-5.76	-0.01
2	0.01	0.01	9.11	-12.05	0.04	-4.11	0.00
3	14.85	0.01	7.09	-7.22	0.03	-2.46	14.85
4	0.02	0.01	5.06	-2.40	0.03	-0.81	0.02
5	0.00	0.01	3.04	2.43	0.02	0.84	0.00
6	0.00	0.01	1.01	7.25	0.01	2.49	-0.01
7	0.00	0.01	-1.01	12.08	0.00	4.14	-0.01
8	34.86	0.01	-3.03	16.91	-0.01	5.79	34.85
9	5.80	0.01	-5.06	21.73	-0.02	7.44	5.79
10	0.01	0.01	-7.08	26.56	-0.03	9.09	0.00

FIGURE	< Previous Time Series	Next Time Series >
1981-1990		

Groundwater recharge-August

TsNumber	1
Name	Groundwater recharge m3
Years	1 - 10
n	10
Test S	
Test Z	-0.89
Signific.	
Q	-2.61E+00
Qmin99	-8.01E+01
Qmax99	3.75E+01
Qmin95	-4.23E+01
Qmax95	1.87E+01
B	7.65E+01
Bmin99	4.41E+02
Bmax99	-8.98E+01
Bmin95	2.39E+02
Bmax95	-4.28E+01

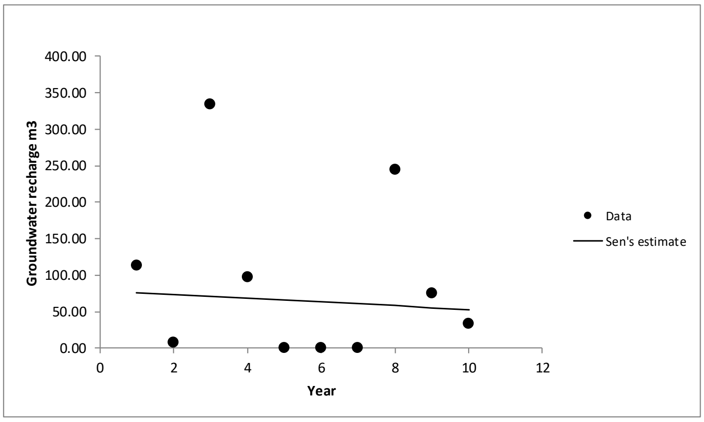

Chart options

show 99 % confidence interval

show 95 % confidence interval

show residuals

Update chart outlook

Equation of the lines:
f(year) = Q*(year-firstDataYear) + B
FirstDataYear= 1

Point values for the chart

Year	Data	Sen's estin	99 % conf. m	99 % conf. m	95 % conf. m	95 % conf. m	Residual
1	113.47	76.49	440.58	-89.83	239.34	-42.76	36.99
2	7.82	73.88	360.48	-52.33	197.02	-24.03	-66.05
3	334.23	71.27	280.37	-14.84	154.71	-5.31	262.96
4	97.87	68.66	200.26	22.66	112.40	13.42	29.20
5	0.00	66.06	120.16	60.16	70.09	32.15	-66.05
6	0.00	63.45	40.05	97.66	27.78	50.88	-63.45
7	0.00	60.84	-40.05	135.15	-14.53	69.60	-60.84
8	244.14	58.23	-120.16	172.65	-56.85	88.33	185.90
9	75.20	55.63	-200.26	210.15	-99.16	107.06	19.58
10	33.44	53.02	-280.37	247.65	-141.47	125.79	-19.58

FIGURE	< Previous Time Series	Next Time Series >
1981-1990		

Groundwater recharge-September

TsNumber	1
Name	Groundwater recharge m3
Years	1 - 10
n	10
Test S	
Test Z	0.72
Signific.	
Q	9.40E+00
Qmin99	-3.76E+01
Qmax99	4.76E+01
Qmin95	-1.79E+01
Qmax95	3.48E+01
B	5.04E+01
Bmin99	2.55E+02
Bmax99	-1.72E+02
Bmin95	1.67E+02
Bmax95	-8.83E+01

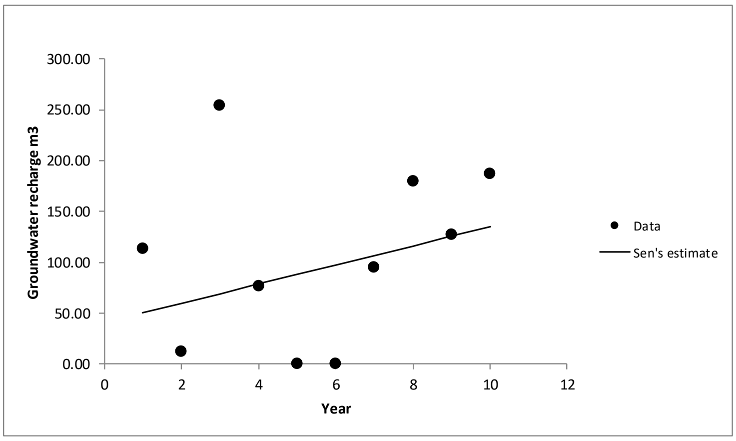

Chart options

show 99 % confidence interval

show 95 % confidence interval

show residuals

Update chart outlook

Equation of the lines:
f(year) = Q*(year-firstDataYear) + B
FirstDataYear= 1

Point values for the chart

Year	Data	Sen's estin	99 % conf. m	99 % conf. m	95 % conf. m	95 % conf. m	Residual
1	114.01	50.43	255.38	-171.62	166.62	-88.35	63.58
2	12.31	59.83	217.80	-124.05	148.76	-53.59	-47.52
3	254.74	69.23	180.21	-76.49	130.89	-18.84	185.52
4	77.19	78.62	142.62	-28.93	113.03	15.91	-1.43
5	0.00	88.02	105.03	18.63	95.17	50.66	-88.02
6	0.00	97.42	67.44	66.19	77.30	85.41	-97.42
7	95.28	106.81	29.85	113.75	59.44	120.16	-11.54
8	179.79	116.21	-7.74	161.31	41.57	154.91	63.58
9	127.04	125.61	-45.33	208.88	23.71	189.66	1.43
10	187.50	135.01	-82.92	256.44	5.84	224.41	52.50

FIGURE

1991-2000

< Previous Time Series | Next Time Series >

Groundwater recharge-July

TsNumber	1
Name	Groundwater recharge m3
Years	1 - 10
n	10
Test S	
Test Z	-0.09
Signific.	
Q	-4.37E-05
Qmin99	-8.65E+00
Qmax99	4.40E+00
Qmin95	-6.92E+00
Qmax95	2.55E-01
B	2.43E-02
Bmin99	5.56E+01
Bmax99	-1.10E+01
Bmin95	4.78E+01
Bmax95	-1.87E-01

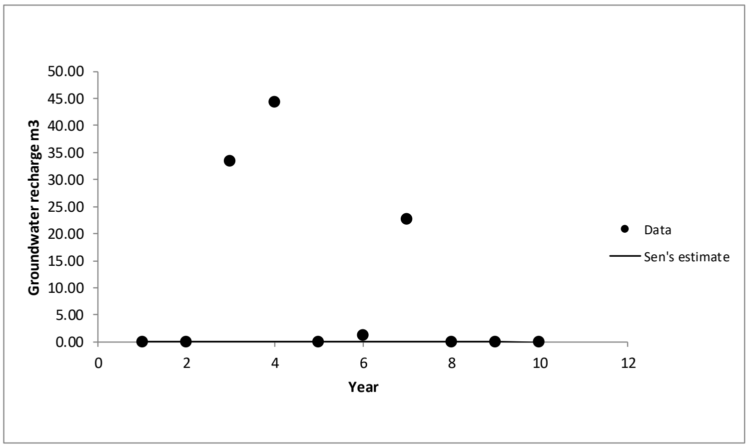

Chart options

show 99 % confidence interval

show 95 % confidence interval

show residuals

Update chart outlook

Equation of the lines:
f(year) = Q*(year-firstDataYear) + B
FirstDataYear= 1

Point values for the chart

Year	Data	Sen's estin	99 % conf. n	99 % conf. n	95 % conf. n	95 % conf. n	Residual
1	0.00	0.02	55.65	-10.98	47.84	-0.19	-0.02
2	0.00	0.02	47.00	-6.59	40.92	0.07	-0.02
3	33.42	0.02	38.34	-2.19	34.01	0.32	33.40
4	44.33	0.02	29.69	2.21	27.09	0.58	44.31
5	0.02	0.02	21.04	6.61	20.17	0.83	0.00
6	1.16	0.02	12.39	11.01	13.26	1.09	1.13
7	22.58	0.02	3.74	15.41	6.34	1.35	22.56
8	0.01	0.02	-4.91	19.80	-0.58	1.60	-0.02
9	0.02	0.02	-13.57	24.20	-7.49	1.86	0.00
10	0.00	0.02	-22.22	28.60	-14.41	2.11	-0.02

FIGURE

1991-2000

< Previous Time Series | Next Time Series >

Groundwater recharge-August

TsNumber	1
Name	Groundwater recharge m3
Years	1 - 10
n	10
Test S	
Test Z	-1.25
Signific.	
Q	-4.61E+00
Qmin99	-2.72E+01
Qmax99	1.87E+01
Qmin95	-1.76E+01
Qmax95	9.40E+00
B	4.63E+01
Bmin99	2.00E+02
Bmax99	-1.71E+01
Bmin95	1.39E+02
Bmax95	1.44E+01

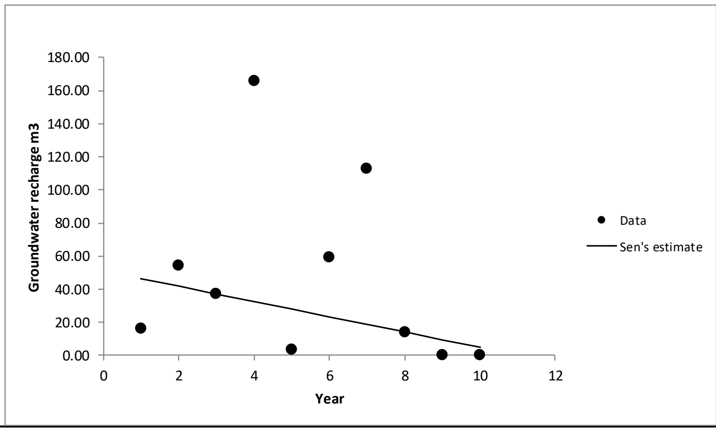

Chart options

show 99 % confidence interval

show 95 % confidence interval

show residuals

Update chart outlook

Equation of the lines:
f(year) = Q*(year-firstDataYear) + B
FirstDataYear= 1

Point values for the chart

Year	Data	Sen's estin	99 % conf. n	99 % conf. n	95 % conf. n	95 % conf. n	Residual
1	16.42	46.30	199.92	-17.06	139.01	14.45	-29.89
2	54.57	41.70	172.72	1.61	121.41	23.85	12.88
3	37.09	37.09	145.53	20.28	103.82	33.25	0.00
4	166.12	32.48	118.34	38.95	86.22	42.65	133.64
5	3.55	27.88	91.15	57.62	68.62	52.05	-24.32
6	59.48	23.27	63.96	76.29	51.03	61.45	36.21
7	112.92	18.66	36.77	94.96	33.43	70.85	94.26
8	14.06	14.06	9.58	113.63	15.83	80.25	0.00
9	0.01	9.45	-17.61	132.31	-1.77	89.65	-9.44
10	0.00	4.84	-44.81	150.98	-19.36	99.05	-4.84

FIGURE

1991-2000

< Previous Time Series | Next Time Series >

Groundwater recharge-September

TsNumber	1
Name	Groundwater recharge m3
Years	1 - 10
n	10
Test S	
Test Z	0.18
Signific.	
Q	3.58E+00
Qmin99	-5.22E+01
Qmax99	2.98E+01
Qmin95	-1.58E+01
Qmax95	2.35E+01
B	7.41E+01
Bmin99	3.91E+02
Bmax99	-4.84E+01
Bmin95	1.55E+02
Bmax95	-2.14E+01

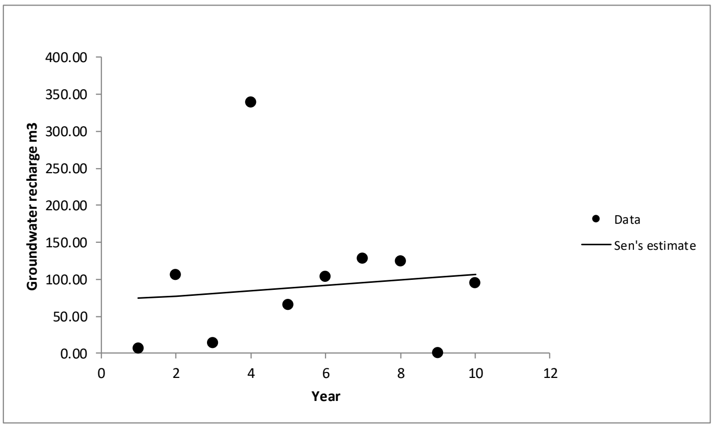

Chart options

show 99 % confidence interval

show 95 % confidence interval

show residuals

Update chart outlook

Equation of the lines:

f(year) = Q*(year-firstDataYear) + B

FirstDataYear= 1

Point values for the chart

Year	Data	Sen's estin	99 % conf. m	99 % conf. m	95 % conf. m	95 % conf. m	Residual
1	6.22	74.14	390.71	-48.40	155.37	-21.43	-67.92
2	106.09	77.72	338.54	-18.61	139.62	2.11	28.37
3	13.38	81.30	286.36	11.19	123.87	25.65	-67.92
4	338.57	84.88	234.19	40.99	108.12	49.18	253.69
5	65.84	88.46	182.01	70.79	92.37	72.72	-22.62
6	103.15	92.04	129.84	100.59	76.62	96.26	11.10
7	128.20	95.63	77.66	130.39	60.87	119.80	32.57
8	124.72	99.21	25.49	160.19	45.12	143.34	25.51
9	0.00	102.79	-26.69	189.99	29.37	166.88	-102.79
10	95.27	106.37	-78.86	219.79	13.61	190.42	-11.10

FIGURE

2001-2010

< Previous Time Series | Next Time Series >

Groundwater recharge -July

TsNumber	1
Name	Groundwater recharge m3
Years	1 - 10
n	10
Test S	
Test Z	-0.36
Signific.	
Q	-4.31E-01
Qmin99	-7.99E+00
Qmax99	1.07E+01
Qmin95	-2.45E+00
Qmax95	4.89E+00
B	8.80E+00
Bmin99	5.42E+01
Bmax99	-1.78E+01
Bmin95	2.16E+01
Bmax95	-4.41E+00

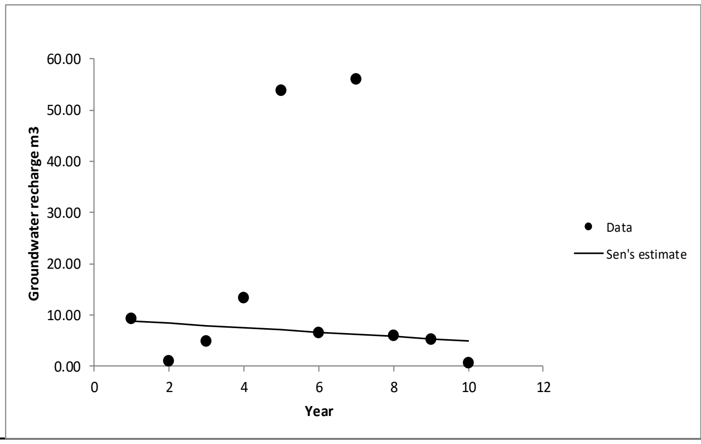

Chart options

show 99 % confidence interval

show 95 % confidence interval

show residuals

Update chart outlook

Equation of the lines:

f(year) = Q*(year-firstDataYear) + B

FirstDataYear= 1

Point values for the chart

Year	Data	Sen's estin	99 % conf. m	99 % conf. m	95 % conf. m	95 % conf. m	Residual
1	9.37	8.80	54.16	-17.78	21.59	-4.41	0.56
2	1.00	8.37	46.17	-7.05	19.15	0.49	-7.37
3	4.86	7.94	38.18	3.69	16.70	5.38	-3.08
4	13.26	7.51	30.19	14.42	14.25	10.27	5.75
5	53.85	7.08	22.20	25.16	11.81	15.16	46.78
6	6.50	6.65	14.21	35.90	9.36	20.05	-0.14
7	55.98	6.21	6.21	46.63	6.92	24.94	49.77
8	5.93	5.78	-1.78	57.37	4.47	29.83	0.14
9	5.21	5.35	-9.77	68.11	2.03	34.72	-0.14
10	0.58	4.92	-17.76	78.84	-0.42	39.61	-4.34

FIGURE

20001-2010

< Previous Time Series | Next Time Series >

Groundwater recharge-August

TsNumber	1
Name	Groundwater recharge m3
Years	1 - 10
n	10
Test S	
Test Z	0.54
Signific.	
Q	7.34E+00
Qmin99	-4.53E+01
Qmax99	5.67E+01
Qmin95	-2.85E+01
Qmax95	4.31E+01
B	1.36E+02
Bmin99	3.53E+02
Bmax99	-7.03E+01
Bmin95	2.75E+02
Bmax95	-2.34E+01

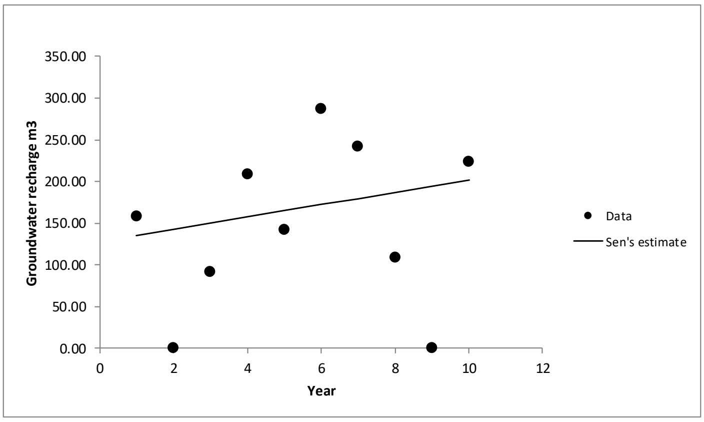

Chart options

show 99 % confidence interval

show 95 % confidence interval

show residuals

Update chart outlook

Equation of the lines:

f(year) = Q*(year-firstDataYear) + B

FirstDataYear= 1

Point values for the chart

Year	Data	Sen's estin	99 % conf. n	99 % conf. n	95 % conf. n	95 % conf. n	Residual
1	157.93	135.62	353.21	-70.30	275.44	-23.43	22.31
2	0.00	142.96	307.94	-13.65	246.90	19.68	-142.96
3	92.10	150.29	262.67	43.00	218.37	62.78	-58.20
4	208.47	157.63	217.41	99.66	189.83	105.89	50.84
5	142.66	164.97	172.14	156.31	161.29	148.99	-22.31
6	287.20	172.30	126.87	212.96	132.76	192.10	114.90
7	241.54	179.64	81.60	269.61	104.22	235.20	61.89
8	109.06	186.98	36.33	326.26	75.69	278.31	-77.92
9	0.00	194.31	-8.93	382.92	47.15	321.41	-194.31
10	223.96	201.65	-54.20	439.57	18.61	364.51	22.31

FIGURE

2001-2010

< Previous Time Series | Next Time Series >

Groundwater recharge-September

TsNumber	1
Name	Groundwater recharge m3
Years	1 - 10
n	10
Test S	
Test Z	1.43
Signific.	
Q	1.96E+01
Qmin99	-2.84E+01
Qmax99	4.54E+01
Qmin95	-9.29E+00
Qmax95	3.53E+01
B	8.96E+01
Bmin99	2.52E+02
Bmax99	-3.16E+01
Bmin95	1.77E+02
Bmax95	2.32E+01

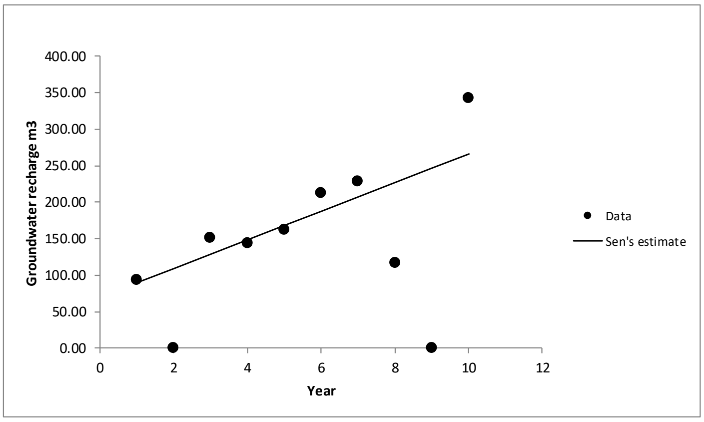

Chart options

show 99 % confidence interval

show 95 % confidence interval

show residuals

Update chart outlook

Equation of the lines:

f(year) = Q*(year-firstDataYear) + B

FirstDataYear= 1

Point values for the chart

Year	Data	Sen's estin	99 % conf. n	99 % conf. n	95 % conf. n	95 % conf. n	Residual
1	94.12	89.57	252.42	-31.61	176.93	23.18	4.55
2	0.00	109.12	224.04	13.82	167.64	58.52	-109.12
3	150.88	128.68	195.67	59.25	158.35	93.86	22.20
4	143.68	148.23	167.29	104.68	149.07	129.20	-4.55
5	162.53	167.78	138.91	150.11	139.78	164.54	-5.26
6	213.00	187.33	110.54	195.53	130.50	199.88	25.67
7	228.54	206.89	82.16	240.96	121.21	235.22	21.66
8	117.32	226.44	53.78	286.39	111.93	270.56	-109.12
9	0.00	245.99	25.40	331.82	102.64	305.90	-245.99
10	343.26	265.55	-2.97	377.25	93.36	341.24	77.71

FIGURE

2011-2020

< Previous Time Series | Next Time Series >

Groundwater recharge-July

TsNumber	1
Name	Groundwater recharge m3
Years	1 - 10
n	10
Test S	
Test Z	-0.81
Signific.	
Q	-3.26E-03
Qmin99	-1.31E+01
Qmax99	5.28E+00
Qmin95	-6.60E-01
Qmax95	9.52E-01
B	3.00E-01
Bmin99	7.83E+01
Bmax99	-1.81E+01
Bmin95	3.96E+00
Bmax95	-2.43E+00

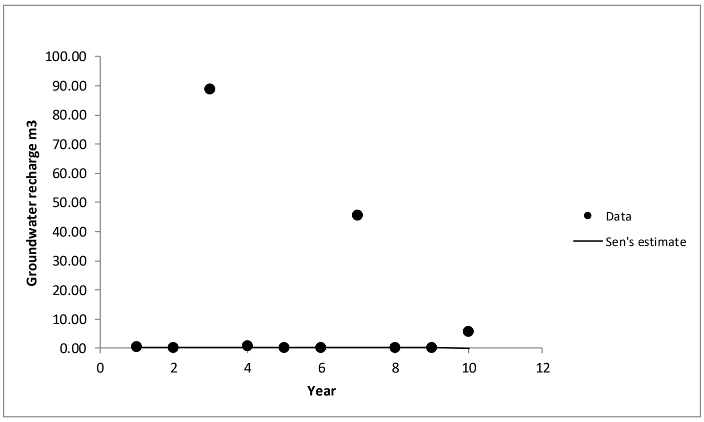

Chart options

show 99 % confidence interval

show 95 % confidence interval

show residuals

Update chart outlook

Equation of the lines:

f(year) = Q*(year-firstDataYear) + B

FirstDataYear= 1

Point values for the chart

Year	Data	Sen's estin	99 % conf. n	99 % conf. n	95 % conf. n	95 % conf. n	Residual
1	0.57	0.30	78.34	-18.06	3.96	-2.43	0.27
2	0.02	0.30	65.29	-12.78	3.30	-1.48	-0.28
3	88.78	0.29	52.23	-7.50	2.64	-0.53	88.48
4	0.83	0.29	39.17	-2.22	1.98	0.43	0.54
5	0.01	0.29	26.12	3.06	1.32	1.38	-0.27
6	0.00	0.28	13.06	8.34	0.66	2.33	-0.28
7	45.57	0.28	0.00	13.62	0.00	3.28	45.29
8	0.01	0.28	-13.05	18.91	-0.66	4.23	-0.27
9	0.00	0.27	-26.11	24.19	-1.32	5.19	-0.27
10	5.73	0.27	-39.17	29.47	-1.98	6.14	5.46

FIGURE

2011-2020

< Previous Time Series | Next Time Series >

Groundwater recharge-August

TsNumber	1
Name	Groundwater recharge m3
Years	1 - 10
n	10
Test S	
Test Z	-0.36
Signific.	
Q	-8.90E-04
Qmin99	-5.16E+01
Qmax99	4.57E+01
Qmin95	-3.76E+01
Qmax95	2.91E+01
B	5.59E+01
Bmin99	3.10E+02
Bmax99	-1.53E+02
Bmin95	2.26E+02
Bmax95	-3.65E+01

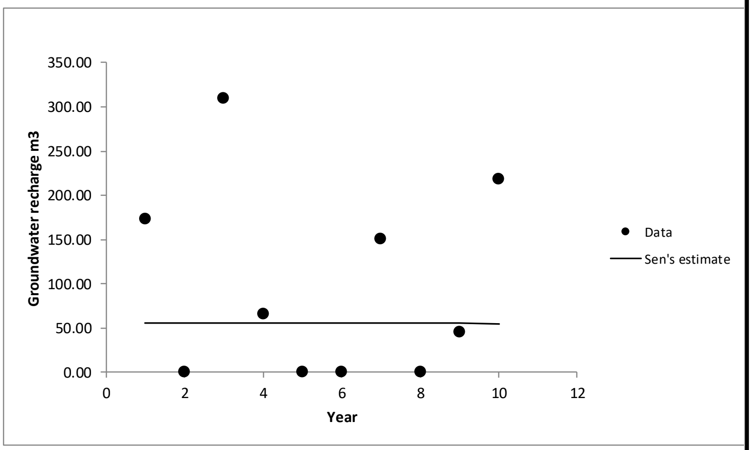

Chart options

show 99 % confidence interval

show 95 % confidence interval

show residuals

Update chart outlook

Equation of the lines:

f(year) = Q*(year-firstDataYear) + B

FirstDataYear= 1

Point values for the chart

Year	Data	Sen's estin	99 % conf. n	99 % conf. n	95 % conf. n	95 % conf. n	Residual
1	173.62	55.94	309.61	-152.98	225.64	-36.55	117.68
2	0.01	55.94	258.01	-107.30	188.04	-7.41	-55.93
3	309.44	55.94	206.41	-61.62	150.43	21.73	253.50
4	65.97	55.94	154.81	-15.95	112.82	50.87	10.03
5	0.00	55.94	103.21	29.73	75.22	80.01	-55.93
6	0.00	55.94	51.60	75.41	37.61	109.15	-55.94
7	150.81	55.94	0.00	121.08	0.00	138.29	94.87
8	0.00	55.93	-51.60	166.76	-37.61	167.43	-55.93
9	45.90	55.93	-103.20	212.44	-75.21	196.57	-10.03
10	218.29	55.93	-154.80	258.12	-112.82	225.71	162.36

FIGURE

2011-2020

< Previous Time Series   Next Time Series >

Groundwater recharge-September

TsNumber	1
Name	Groundwater recharge m3
Years	1 - 10
n	10
Test S	
Test Z	-1.07
Signific.	
Q	-1.00E+01
Qmin99	-6.42E+01
Qmax99	3.93E+01
Qmin95	-4.78E+01
Qmax95	1.54E+01
B	1.94E+02
Bmin99	3.47E+02
Bmax99	-1.20E+02
Bmin95	3.22E+02
Bmax95	4.31E+01

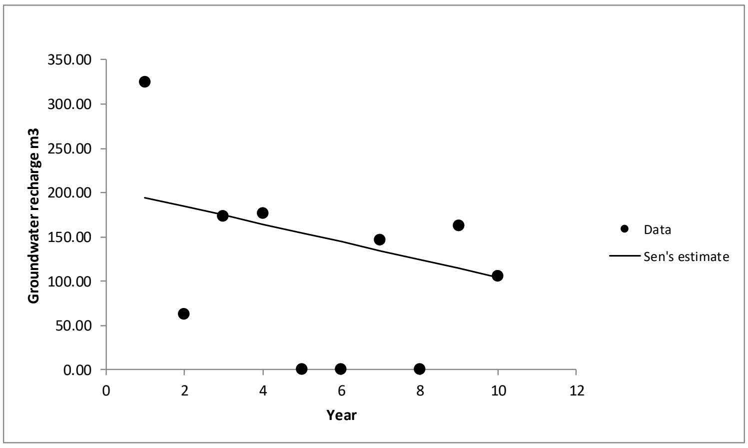

Chart options

show 99 % confidence interval

show 95 % confidence interval

show residuals

Update chart outlook

Equation of the lines:

f(year) = Q*(year-firstDataYear) + B

FirstDataYear= 1

Point values for the chart

Year	Data	Sen's estin	99 % conf. m	99 % conf. m	95 % conf. m	95 % conf. m	Residual
1	324.86	194.44	347.09	-120.15	322.40	43.12	130.42
2	62.55	184.44	282.84	-80.90	274.61	58.56	-121.88
3	173.13	174.43	218.59	-41.64	226.82	74.01	-1.30
4	176.57	164.43	154.34	-2.39	179.03	89.46	12.14
5	0.00	154.43	90.09	36.87	131.24	104.91	-154.43
6	0.00	144.43	25.85	76.12	83.45	120.35	-144.43
7	146.56	134.43	-38.40	115.38	35.67	135.80	12.14
8	0.00	124.43	-102.65	154.64	-12.12	151.25	-124.42
9	162.71	114.42	-166.90	193.89	-59.91	166.69	48.28
10	105.72	104.42	-231.14	233.15	-107.70	182.14	1.30

APPENDIX-C: Files of SWAT Run

Calibration output files from SUFI-2

FLOW_OUT_50

observed	L95PPU	U95PPU	Best_Sim	M95PPU
1.231000	0.000000	0.000000	0.000000	0.000000
0.975000	0.000000	0.000000	0.000000	0.000000
0.575000	0.000000	0.000000	0.000000	0.000000
0.523000	0.000000	0.000000	0.000000	0.000000
1.567000	0.000000	0.000000	0.000000	0.000000
2.208000	0.493629	0.501854	0.495000	0.496100
2.256000	2.329169	2.352963	2.329000	2.337960
5.132000	4.278250	4.317052	4.285000	4.293481
1.256000	1.225156	1.229541	1.228000	1.227860
0.567000	0.000000	0.000000	0.000000	0.000000
0.985000	0.000000	0.000000	0.000000	0.000000
0.325000	0.000000	0.000000	0.000000	0.000000
0.336000	0.000000	0.000000	0.000000	0.000000
0.352000	0.000000	0.000000	0.000000	0.000000
0.546000	0.000000	0.000000	0.000000	0.000000
1.545000	0.000000	0.000000	0.000000	0.000000
0.256000	0.000001	0.000001	0.000000	0.000001
1.103000	0.258119	0.262804	0.258800	0.259614
1.181000	0.454643	0.463143	0.454600	0.457506
2.235000	1.153921	1.168975	1.153000	1.158440
2.289000	2.234082	2.264176	2.234000	2.241920
0.010000	0.000955	0.001411	0.001100	0.001169

0.015000	0.000000	0.000000	0.000000	0.000000
0.000000	0.000000	0.000000	0.000000	0.000000
0.000000	0.000000	0.000000	0.000000	0.000000
0.000000	0.000000	0.000000	0.000000	0.000000
0.000000	0.000000	0.000000	0.000000	0.000000
0.000000	0.014612	0.015386	0.014600	0.014803
0.000000	0.000000	0.000000	0.000000	0.000000
0.426000	1.132083	1.149750	1.132000	1.138540
3.188000	3.601155	3.642712	3.601000	3.613040
2.123000	1.657035	1.661187	1.659000	1.658821
3.452000	2.547367	2.591230	2.570000	2.573920
1.234000	0.486162	0.492368	0.491100	0.490330
0.158000	0.000000	0.000000	0.000000	0.000000
0.000000	0.000000	0.000000	0.000000	0.000000
0.000000	0.002696	0.007094	0.003800	0.004544
0.000000	0.000000	0.000000	0.000000	0.000000
0.000000	0.000000	0.000000	0.000000	0.000000
0.000000	0.007962	0.007993	0.008000	0.007982
0.000000	0.000151	0.000151	0.000200	0.000151
0.000000	0.002031	0.002087	0.002100	0.002059
5.741000	3.430086	3.453075	3.430000	3.437120
2.458000	1.018060	1.040188	1.019000	1.023820
3.213000	2.203844	2.227976	2.211000	2.215280
0.000000	0.000000	0.000000	0.000000	0.000000
0.087500	0.017052	0.025841	0.021100	0.021997
0.000000	0.000000	0.000000	0.000000	0.000000

0.012000	0.000063	0.000218	0.000100	0.000099
0.000000	0.000000	0.000000	0.000000	0.000000
0.023400	0.002454	0.002847	0.002500	0.002537
0.000000	0.003376	0.003395	0.003400	0.003381
0.000000	0.000449	0.000449	0.000400	0.000449
0.618000	0.964936	0.973154	0.964900	0.967614
2.231000	2.046771	2.059314	2.046000	2.051260
1.210000	0.152418	0.157459	0.152400	0.154024
0.527000	0.552901	0.567515	0.554900	0.559088
0.000000	0.000000	0.000000	0.000000	0.000000
0.000000	0.000000	0.000000	0.000000	0.000000
0.000000	0.000000	0.000000	0.000000	0.000000
0.000000	0.000000	0.000000	0.000000	0.000000
0.000000	0.000000	0.000000	0.000000	0.000000
0.000000	0.000000	0.000000	0.000000	0.000000
0.000000	0.000000	0.000000	0.000000	0.000000
0.000000	0.000000	0.000000	0.000000	0.000000
0.000000	0.002493	0.002542	0.002500	0.002507
0.345000	0.687596	0.710752	0.687500	0.694486
0.714000	1.438109	1.473500	1.438000	1.447620
0.315000	0.317529	0.335682	0.322200	0.325290
0.545000	0.513451	0.538624	0.522500	0.525852
0.000000	0.000000	0.000000	0.000000	0.000000
0.000000	0.000000	0.000000	0.000000	0.000000
0.000000	0.000000	0.000000	0.000000	0.000000
0.000000	0.000000	0.000000	0.000000	0.000000

0.000000	0.000000	0.000000	0.000000	0.000000
0.000000	0.000000	0.000000	0.000000	0.000000
0.000000	0.000000	0.000000	0.000000	0.000000
1.258000	0.411737	0.418001	0.411700	0.414070
3.513000	4.251167	4.293599	4.251000	4.263680
1.012000	0.997260	1.030604	1.011000	1.015336
0.998000	0.424612	0.442467	0.434700	0.436244
0.000000	0.000000	0.000000	0.000000	0.000000
0.000000	0.000000	0.000000	0.000000	0.000000
0.000000	0.001551	0.004392	0.002600	0.003001

$R^2 = 0.79$

Nash_Sutcliffe = 0.74